Neuroradiology - Expect the Unexpected

Martina Špero
Hrvoje Vavro

Springer

Martina Špero • Hrvoje Vavro

Neuroradiology - Expect the Unexpected

Springer

Martina Špero
University Hospital Dubrava
Department of Diagnostic and
Interventional Radiology
Zagreb
Croatia

Hrvoje Vavro
University Hospital Dubrava
Department of Diagnostic and
Interventional Radiology
Zagreb
Croatia

ISBN 978-3-319-73481-1 ISBN 978-3-319-73482-8 (eBook)
https://doi.org/10.1007/978-3-319-73482-8

Library of Congress Control Number: 2018937966

Printed on acid-free paper

This Springer imprint is published by the registered company Springer International Publishing AG part of Springer Nature.
The registered company address is: Gewerbestrasse 11, 6330 Cham, Switzerland

Acknowledgements

Although we know each other from the time when we were both medical students, this book is a result of our mutual work as neuroradiologists for the past nine years. All cases presented in this book are cases from our daily work at the Department of Diagnostic and Interventional Radiology, University Hospital Dubrava in Zagreb. These cases are small but important and interesting part of our busy and fruitful work. We have more cases to present and maybe we will have another chance to do it in the future.

We would like to thank Antonella Cerri from Springer Milan who invited us and gave us a chance to prepare this book and Corinna Parravicini for assisting us in the process.

We wish to thank Boris Brkljačić, Professor of Radiology and Chairman of our Department, who gave us the chance to become neuroradiologists and always supported our work.

Special thanks to Majda Thurnher, Professor of Radiology at the University Hospital Vienna, Austria, for always being our friend and teacher and supporting us and our work.

We are deeply grateful to the closest members of our families, to our closest friends and colleagues, who always stood by us, helping us and supporting us in our private and professional life.

Contents

Part V Unusual Spine

Part VI Something Different

Abbreviations

ABC	Aneurysmal bone cyst
ADC	Apparent diffusion coefficient
AQP4	Aquaporin-4
AVM	Arteriovenous malformation
CBV	Cerebral blood volume
CFD	Cranial fibrous dysplasia
CISS	Constructive interference in steady-state
CO	Carbon monoxide
CPA	Cystic pituitary adenoma
CS	Crouzon syndrome
CSF	Cerebrospinal fluid
CT	Computed tomography
CTA	Computed tomography angiography
DSA	Digital subtraction angiography
DWI	Diffusion weighted imaging
EHD	Emergency hospital department
EMG	Electromyography
FD	Fibrous dysplasia
FLAIR	Fluid attenuation inversion recovery
FNA	Fine needle aspiration
FS	Fat suppressed
GCT	Giant cell tumour
IDH	Isocitrate dehydrogenase
IE	Intradiploic encephalocele
LMC	Leptomeningeal carcinomatosis
MRA	Magnetic resonance angiography
MRI	Magnetic resonance imaging
MRS	Magnetic resonance spectroscopy
NAA	*N*-acetylaspartate
NMO	Neuromyelitis optica
PAVF	Pulmonary arteriovenous fistula
PCNSL	Primary central nervous system lymphoma
PDL	Primary dural lymphoma
PTC	Papillary thyroid carcinoma
PVS	Perivascular space
RCC	Rathke's cleft cyst

R-CHOP	Rituximab-cyclophosphamide, doxorubicin, vincristine, prednisone
SLSC	Sphenoid lateral spontaneous cephalocele
STIR	Short tau inversion recovery
SWI	Susceptibility weighted imaging
TDL	Tumefactive demyelinating lesion
TIRM	Turbo inversion recovery magnitude
TOF	Time-of-flight
VBD	Van Buchem disease
VRT	Volume rendering technique
WHO	World Health Organisation

Part I

Most Likely Differential Diagnosis

Cerebrovascular Infarction: Oligodendroglioma

1

One morning in November 2009, a 73-year-old female was referred to the brain computed tomography scanning from emergency hospital department (EHD) due to motoric dysphasia lasting for 5 days and subjective right-sided weakness (Fig. 1.1).

It was reported as an acute ischaemic lesion by a referring radiologist, and the patient was hospitalised: during hospitalisation MRI of the brain or control brain CT has not been ordered by neurologist.

During following 16 months, patient has developed spasms of the right arm, and due to a present mild motoric dysphasia, she has again started with speech therapy. Therefore, in February 2011, neurologist referred her to the brain CT scanning as an out-hospital patient (Fig. 1.2).

At that time, it was obvious that the lesion is primary brain tumour, and MRI of the brain was performed (Fig. 1.3).

According to the described morphological characteristics on CT and MRI, we concluded it could be the case of low-grade oligodendroglioma which was confirmed histologically by stereotactic biopsy: low-grade oligodendroglioma WHO grade II.

I could say this is a case of oligodendroglioma mimicking an acute ischaemic lesion in an early tumour stage, or I could say it is obviously a case of misdiagnosed primary brain tumour. The basic CT examination was performed using old single-slice CT scanner without possibility of making adequate coronal and sagittal reconstructions that could help analysing the lesion. Patient age, clinical presentation and duration of symptoms matched together with CT finding of subcortical ill-defined hypodense lesion with narrow overlying sulci in the vascular territory of the left middle cerebral artery and therefore have probably led radiologist to report an acute ischaemic lesion. This diagnosis has also matched neurologist suspicion of an acute stroke as a working diagnosis. Probably that was the reason why neurologist did not order a MRI or a follow-up CT of the brain during the hospitalisation. The absence of restricted diffusion on the MRI, as well as the absence of changes in size, shape, density and sharpness of the lesion edges on follow-up CT scans, would alert radiologist to report that the lesion in question is not an acute ischaemic lesion, but a brain tumour.

1.1 Oligodendroglioma

Different conditions may mimic stroke; tumours may be one of the mimickers, usually gliomas and meningiomas. Anaplastic oligodendroglioma is prone to haemorrhage; therefore, those tumours may mimic haemorrhagic stroke [1]. Ischaemic stroke does not present a "great mimicker" of oligodendroglioma due to features like involvement of a specific vascular territory, diffusion

M. Špero, H. Vavro, *Neuroradiology - Expect the Unexpected*,
https://doi.org/10.1007/978-3-319-73482-8_1

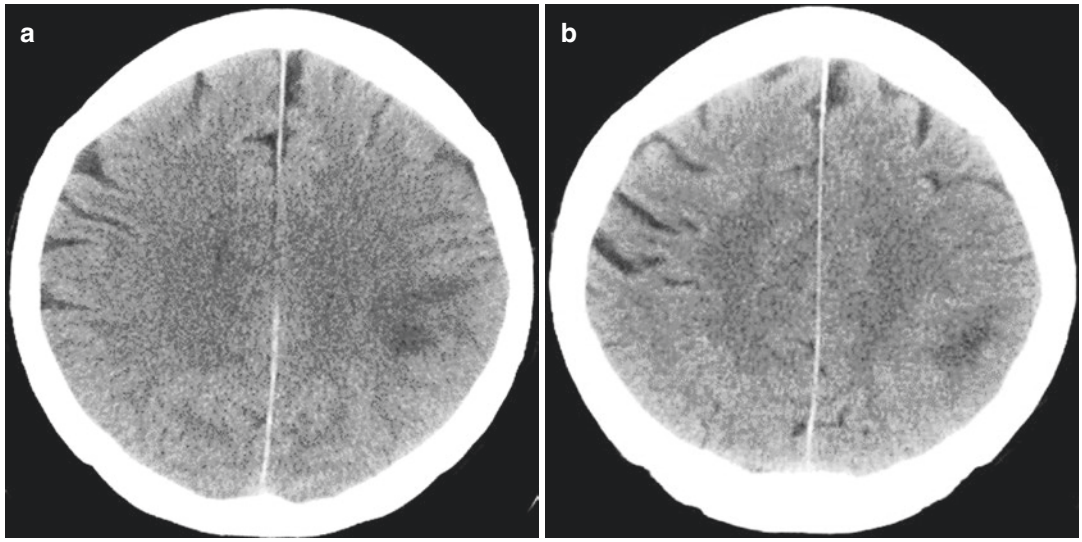

Fig. 1.1 Computed tomography of the brain, axial scan (**a**, **b**), performed at the emergency admission, revealed supratentorial subcortical hypodense lesion in the left hemisphere, involving parenchyma around the central sulcus, involving left frontal and parietal lobes. Lesion was irregularly shaped with ill-defined borders and narrowed overlying sulci

restriction or typical gyriform contrast enhancement in case of subacute ischaemia. In early stage of oligodendroglioma, if an ischaemic stroke is suspected and radiologist is not completely convinced in vascular aetiology of a lesion, MRI is mandatory to exclude one and confirm other diagnosis. It is important to reach the correct diagnosis as early as possible, due to a prompt medical treatment and subsequent better prognosis.

Oligodendrogliomas are typically slow-growing glial tumours (5–18% of all glial tumours) composed predominantly of neoplastic oligodendrocytes, most common in adults with a peak incidence in ages 35–44. Anaplastic oligodendrogliomas tend to occur in slightly older adults, ages 45–74. Although these tumours are found in both sexes, they tend to occur more often in men [2].

Genotyping of these tumours has revealed chromosomal loss of the short arm of chromosome 1 (1p) and the long arm of chromosome 19 (19q) as a genetic signature in about 60–90% of all oligodendrogliomas which has diagnostic, prognostic and predictive relevance: tumours with codeletion demonstrate improved disease-free survival and median survival and may respond better to alkylating chemotherapeutics [2, 3]. The 2016 WHO classification uses "integrated" phenotypic and genotypic parameters for CNS tumour classification and now divides oligodendrogliomas into oligodendroglioma, IDH-mutant and 1p/19q-codeleted, oligodendroglioma NOS (not otherwise specified), anaplastic oligodendroglioma IDH-mutant and 1p/19q-codeleted, anaplastic oligodendroglioma NOS, oligoastrocytoma NOS and anaplastic oligoastrocytoma NOS. In case of oligodendrogliomas, NOS categories should be rendered only in the absence of diagnostic molecular testing or in the very rare instance of a dual-genotype oligoastrocytoma [4].

The most common symptoms in oligodendroglioma clinical presentation are seizures, headaches and personality changes. Other symptoms vary due to location and size of a tumour and may include weakness, numbness or visual symptoms.

The majority of oligodendrogliomas are located supratentorially: codeleted tumours are most commonly located in the frontal, parietal and occipital lobes; intact tumours are more

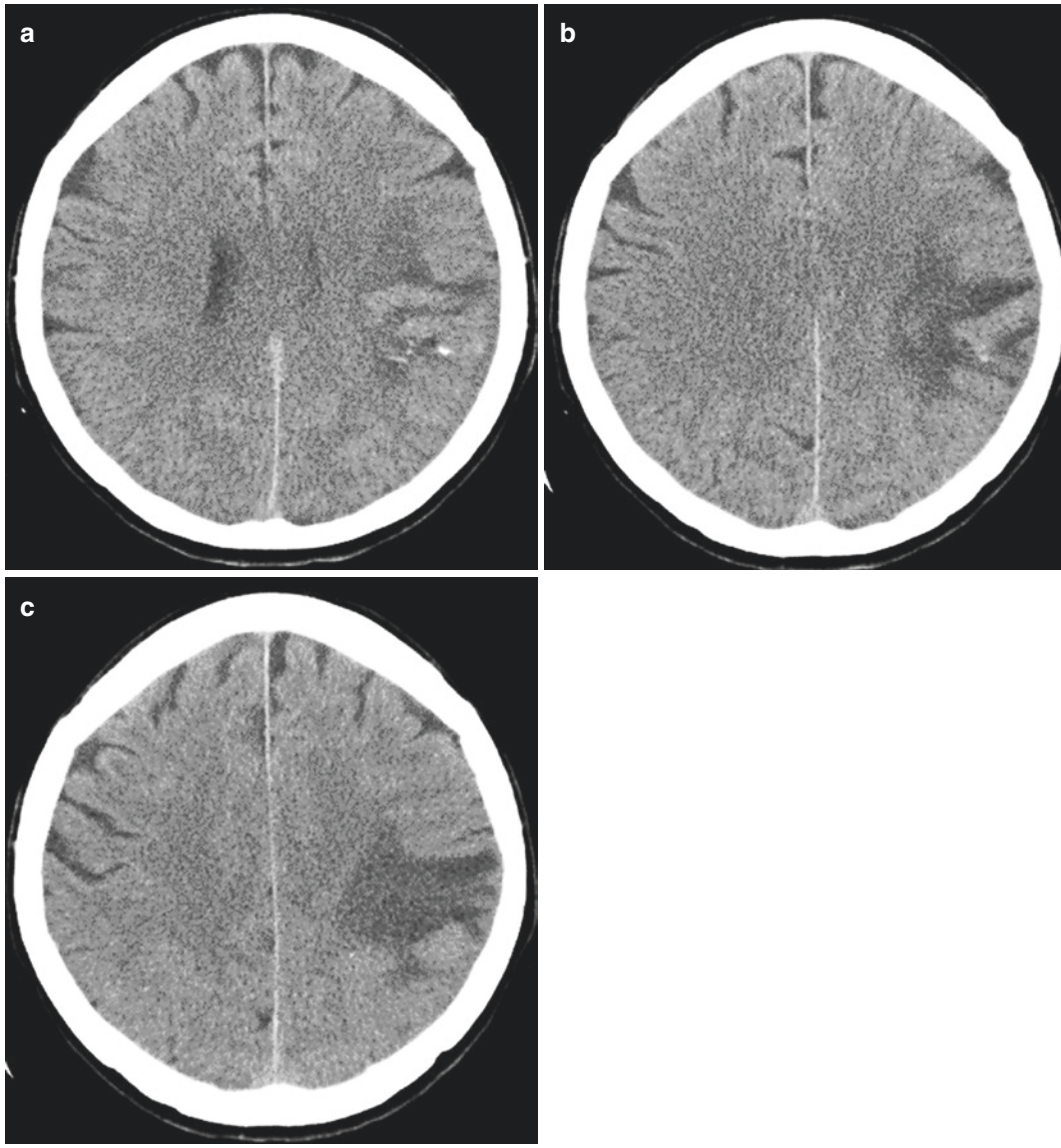

Fig. 1.2 Follow-up non-contrast computed tomography of the brain, axial scan (**a**–**c**), performed 16 months after the initial one, revealed enlargement in the size of the left frontoparietal lesion around the central sulcus, lesion involved cortical-subcortical parenchyma (**b**, **c**), it was more irregular in shape, well-circumscribed, more hypodense, with a few coarse, linear calcifications (**a**). Overlying left frontoparietal sulci were more reduced and narrowed, while adjacent part of the left lateral ventricle was compressed

likely found in the temporal, insular or temporo-insular locations. In frontal location, tumours may extend through the corpus callosum producing a "butterfly" pattern. Infratentorial involvement is very rare, but possible [2, 5].

Oligodendrogliomas are relatively well-circumscribed masses resembling low-grade diffuse astrocytoma in shape. They typically involve cortex and subcortical white matter and due to peripheral location may involve overlying skull causing focal thinning or remodelling of the bone [2, 5].

On CT scans, oligodendrogliomas are usually hypodense with coarse calcifications but, due to

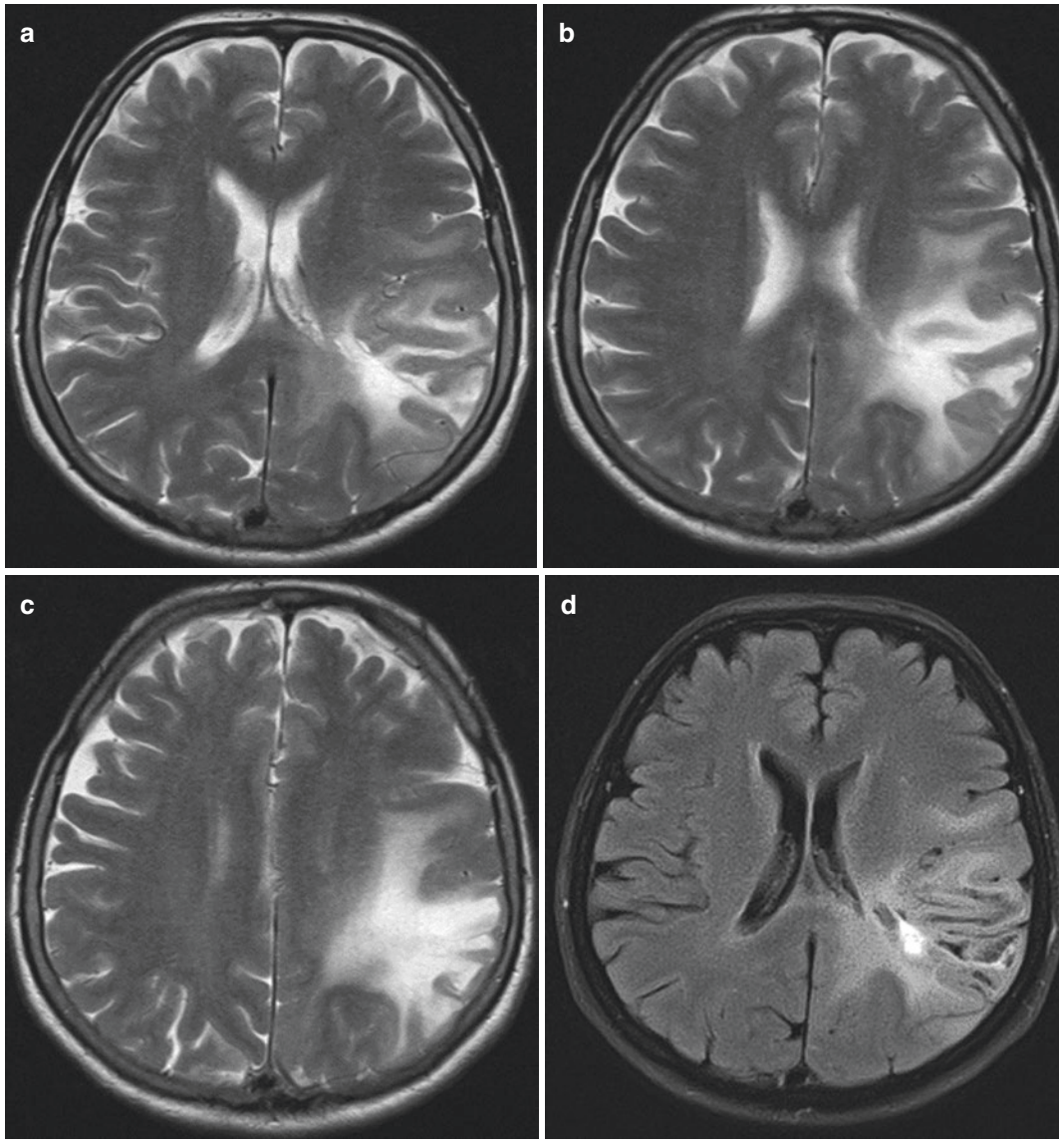

Fig. 1.3 Magnetic resonance imaging confirmed all morphological characteristics of the tumour described on CT scans: axial T2WI (**a**–**c**), axial FLAIR (**d**–**f**), axial DWI (**g**), ADC (**h**), T2*WI (**i**), axial post-contrast T1WI (**j**–**l**), and MR spectroscopy (MRS). Infiltrating, expansile tumour hyperintense on T2WI and FLAIR with moderate cystic degeneration, without restricted diffusion (**g**, **h**). Few linear calcifications were visible on T2*WI, there was no sign of haemorrhage (**i**), as well there was no surrounding vasogenic oedema. After intravenous administration of gadolinium contrast media, there was no contrast enhancement (**j**–**l**). MR spectroscopy (MRS) revealed elevated choline (Cho) and decreased n-acetylaspartate (NAA), without lactate peak (**m**)

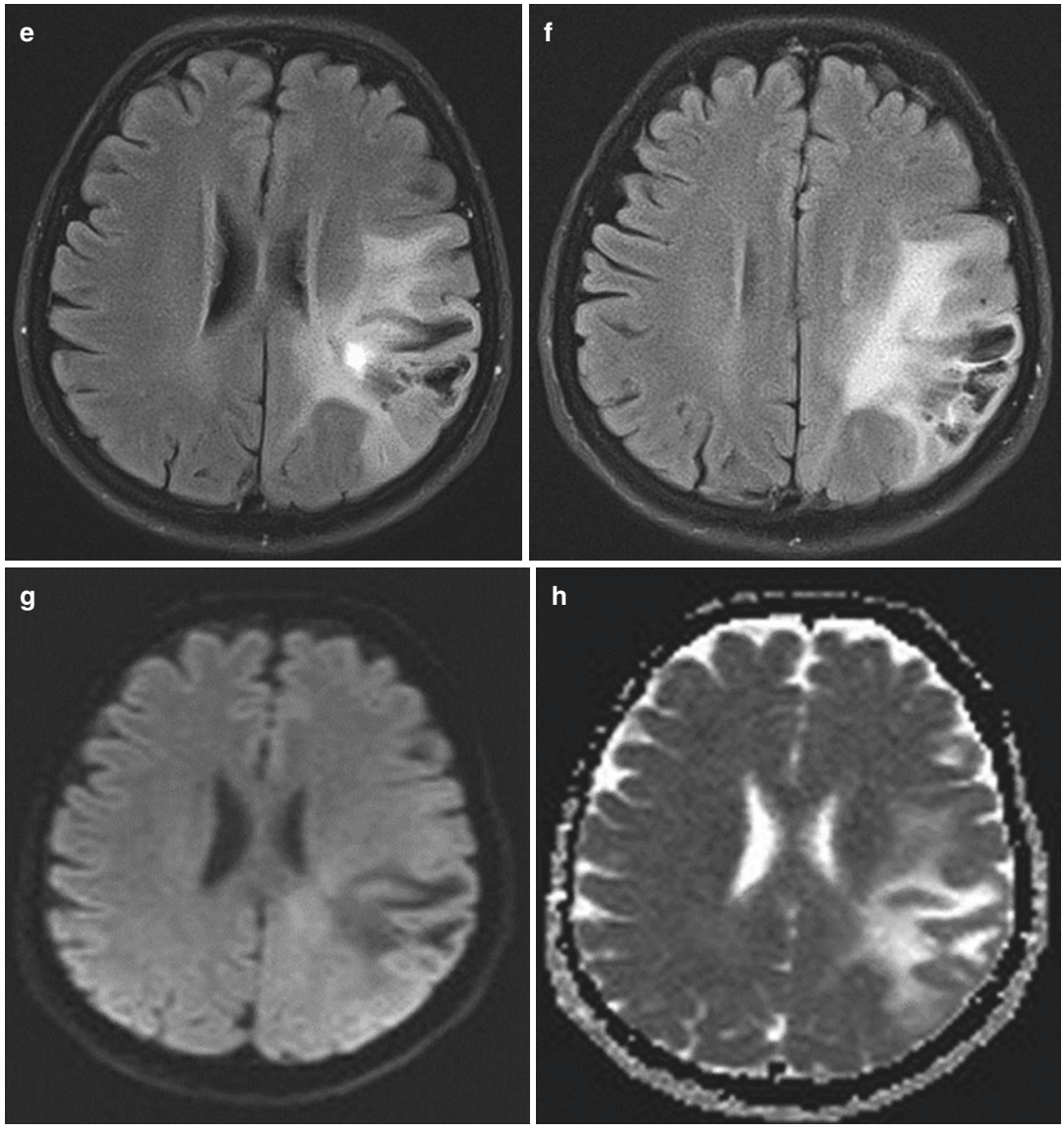

Fig. 1.3 (continued)

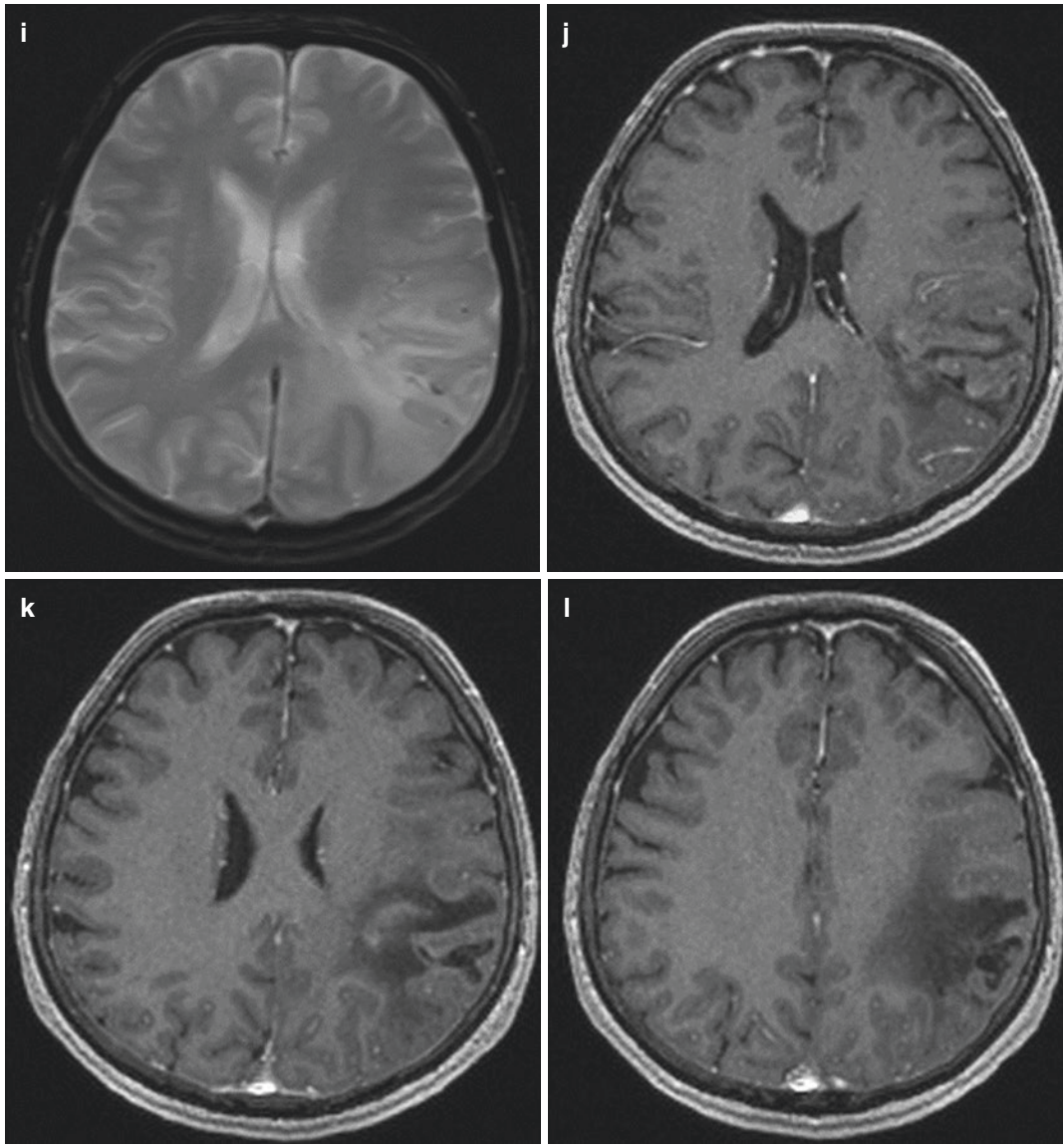

Fig. 1.3 (continued)

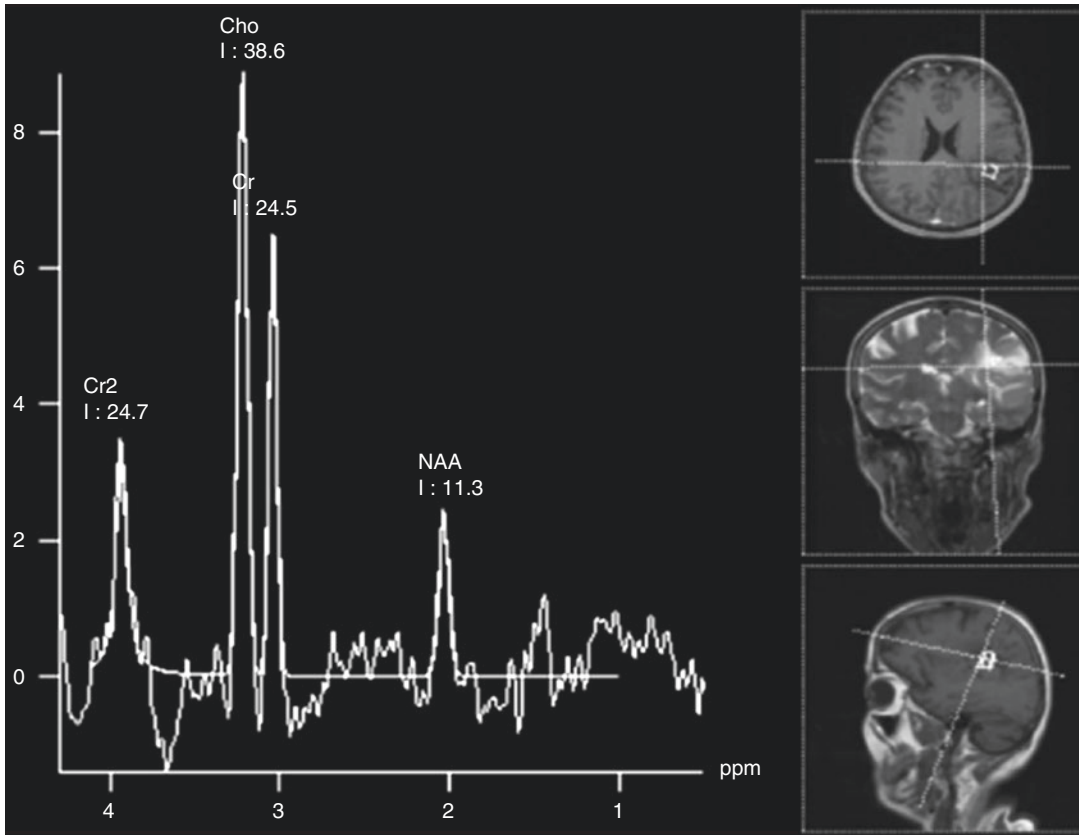

Fig. 1.3 (continued)

possible cystic degeneration or haemorrhage, could have mixed density. On MRI, these tumours are hypointense on T1WI compared to the grey matter and hyperintense on T2WI and FLAIR; calcifications may be less prominent or not visible at all. Cystic degeneration and haemorrhage may occur but are not frequent findings. Codeleted oligodendrogliomas commonly have indistinct margins, calcification and heterogeneous signal intensity in comparison to intact oligodendrogliomas [6–8]. After intravenous administration of a contrast media, oligodendroglioma generally does not enhance, but there are studies which reported "dot-like" or lacy contrast enhancement accounted to delicate branching network of capillaries producing a "honeycomb" or "chicken-wire" pattern on histopathologic evaluation [2, 5, 9]. Although anaplastic tumours tend to enhance somewhat more frequently, the presence of contrast enhancement is not a reliable imaging feature to grade oligodendroglioma.

Diffusion restriction is typically absent in oligodendroglioma, while perfusion may be moderately increased: rCBV (cerebral blood volume) is increased due to the increased microvascular density and numerous slow-flowing collateral vessels [10–12]. MR spectroscopy in oligodendroglioma shows typical spectrum with moderately elevated Cho and decreased NAA without lactate peak: the absence of lipid/lactate peak aids in differentiating oligodendroglioma from its anaplastic form, while Cho/Cr ratio threshold of 2.33 was found to distinguish high- from low-grade oligodendroglioma [5, 13].

Differential diagnosis of oligodendrogliomas includes anaplastic form or other tumours like low-grade diffuse astrocytoma; in case of intraventricular location, central neurocytoma is a differential diagnosis: distinction relies only on

immunohistochemistry or ultrastructural examination. Cerebritis and cerebral ischaemia in case of cortically located lesions, and entirely thrombosed arteriovenous malformation due to typical flow void absence and prominent gyriform calcifications, are included as possible differential diagnosis [2, 5, 13].

Surgical resection is the main form of therapy. Combination of procarbazine, lomustine and vincristine (PLC) in combination with radiotherapy is remarkable in patients with codeleted tumours.

References

1. Hatzitolios A et al (2008) Stroke and conditions that mimic it: a protocol secures a safe early recognition. Hippokratia 12(2):98–102
2. Koeller KK et al (2005) From the archives and its variants: oligodendroglioma and its variants: radiologic-pathologic correlation. Radiographics 25:1669–1688
3. Sonnen JA et al (2010) Molecular pathology: neuropathology. In: Coleman WB, Tsongalis GJ (eds) Essential Concepts in molecular pathology. Elsevier, San Diego, pp 373–398
4. Louis DN et al (2016) The 2016 World Health Organization classification of tumors of the Central Nervous System: a summary. Acta Neuropathol 131:803–820
5. Smits M (2016) Imaging of oligodendroglioma. Br J Radiol 89(1060):20150857
6. Kim JW et al (2011) Relationship between radiological characteristics and combined 1p adn 19q deletion in World Health Organization grade III oligodendroglial tumours. J Neurol Neurosurg Psyshiatry 82:224–227
7. Meyesi JF et al (2004) Imaging correlates of molecular signatures in oligodendrogliomas. Clin Cancer Res 10:4303–4306
8. Jenkinson MD et al (2006) Histological growth patterns and genotype in oligodendroglial tumours: correlation with MRI features. Brain 129(Pt 7):1884–1889
9. White ML et al (2005) Can tumor contrast enhancement be used as a criterion for differentiating tumor grades of oligodendrogliomas? AJNR Am J Neuroradiol 26:784–790
10. Law M et al (2003) Glioma grading: sensitivity, specificity, and predictive values of perfusion MR imaging and proton MR spectroscopic imaging compared with conventional MR imaging. AJNR Am J Neuroradiol 24:1989–1998
11. Khalid L et al (2012) Imaging characteristics of oligodendrogliomas that predict grade. AJNR Am J Neuroradiol 33:852–857
12. Jenkinson MD et al (2006) Cerebral blood volume, genotype and chemosensitivity in oligodendroglial tumours. Neuroradiology 48:703–713
13. Osborn A (2013) Osborn's brain imaging pathology anatomy. Amirsys, Salt Lake City, pp 494–497

2 Cerebrovascular Infarction: Primary Brain Lymphoma

A 65-year-old lady suddenly developed speech difficulties and numbness in the left arm and leg which progressed to limb weakness. She did not have any other symptoms. She was rushed to the emergency hospital unit. On examination there was no limb weakness, only central left-sided facial palsy; during examination she developed left-sided facial myoclonus, as well as myoclonus of the first and second finger of her left hand which was felt to be an epileptic seizure and promptly resolved on intravenous antiepileptic therapy. A brain CT examination was done (Fig. 2.1).

The CT report stated this was a subacute ischaemic stroke but morphologically it might differentially be in keeping with a tumour. A brain MRI exam was done the very next day (Fig. 2.2).

No carotid or vertebral artery abnormalities were found on the duplex Doppler examination.

The patient was referred to a rehabilitation facility several days later, with improved neurological status and residual mild left-sided supranuclear facial nerve paresis, mild speech impairment and a very mild left-sided hemiparesis.

There was further improvement of the patient's neurological status until it suddenly deteriorated 3 weeks later, at the rehabilitation facility. The patient was transferred back to the hospital, and a follow-up CT exam was done (Fig. 2.3).

A sample of the lesion tissue was obtained by stereotactic biopsy. The histopathology reported non-Hodgkin lymphoma of the brain, with perivascular infiltration.

The patient was transferred to the haematology department, and additional workup was done, including CT scans of the thorax, abdomen and pelvis and bone marrow biopsy, which did not reveal any other lymphoma foci.

It was concluded that the lesion was a primary brain lymphoma and chemotherapy protocol was started (Fig. 2.4).

M. Špero, H. Vavro, *Neuroradiology - Expect the Unexpected*,
https://doi.org/10.1007/978-3-319-73482-8_2

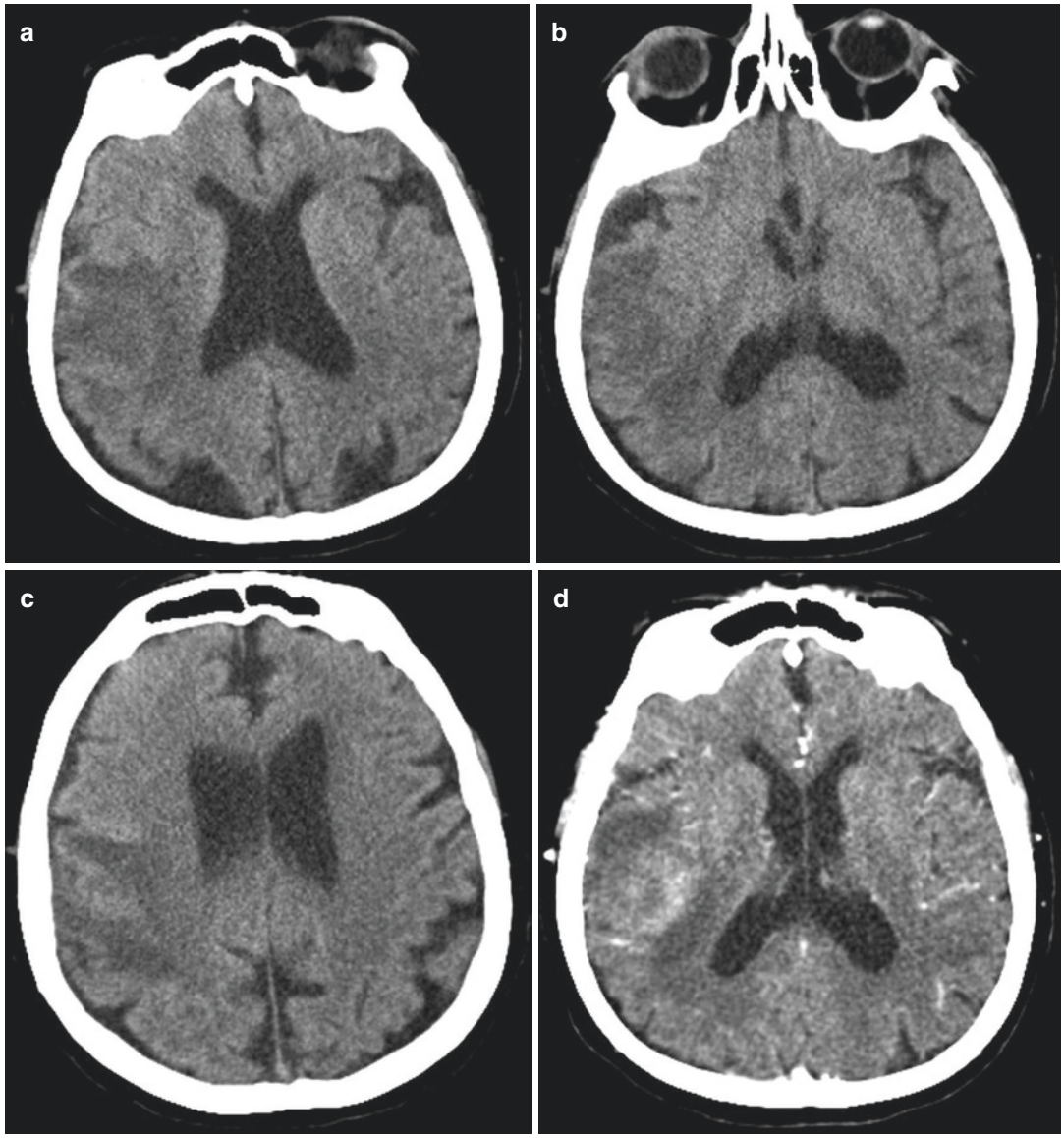

Fig. 2.1 Non-contrast- (**a**–**c**) and contrast-enhanced (**d**–**i**) CT scan of the brain showing cortical-subcortical irregular hypodensity with sulcal effacement and gyriform contrast enhancement in the right frontoparietal operculum

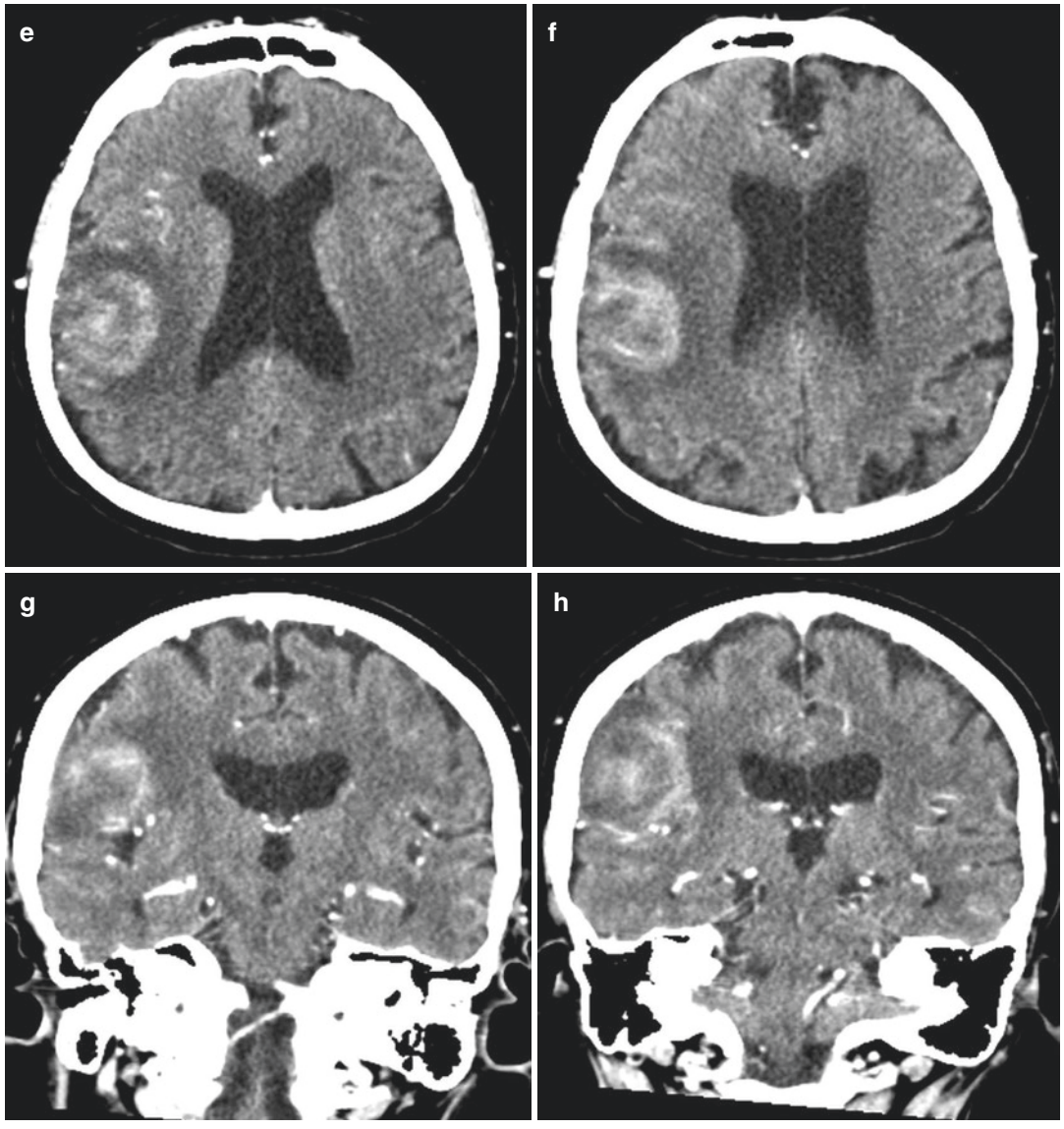

Fig. 2.1 (continued)

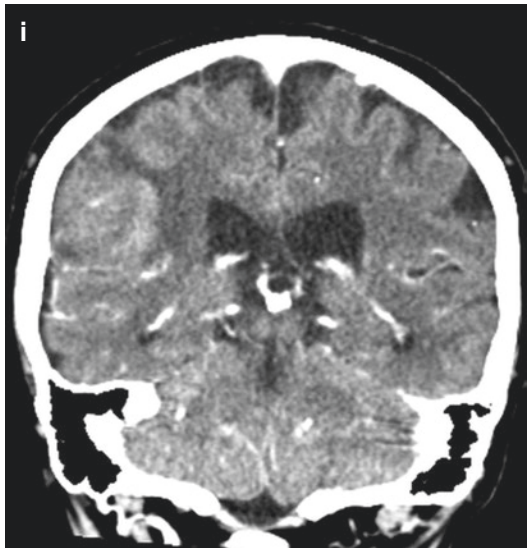

Fig. 2.1 (continued)

2.1 Primary Central Nervous System Lymphoma

Primary central nervous system lymphoma (PCNSL) is a presentation of extranodal lymphoma confined to the central nervous system. It is a relatively uncommon entity, accounting for only 1–2% of all lymphoma cases and 3–6% of all primary brain tumours. The prevalence of PCNSL is higher in immunocompromised patients—a PCNSL in an HIV-seropositive patient is an AIDS-defining condition [1]. Transplant patients are another group at risk for a PCNSL. Additionally, congenital deficiency syndromes and prolonged immunosuppressive therapy, as well as some autoimmune diseases such as Sjogren's syndrome and systemic lupus erythematosus, are reported to be risks for PCNSL development. Histologically, over 90% of PCNSL are high-grade non-Hodgkin B-cell lymphoma. Malignant cells accumulate around and within blood vessels. They mostly present as solitary (60–70%) supratentorial periventricular white matter lesions, although occurrence is possible in the cortex or deep grey matter.

In immunocompetent patients, CT appearance of a PCNSL is that of a hyperdense mass. MR imaging reveals a T1 hypointense, T2 hypointense to isointense lesion with a very low diffusion coupled with characteristic dark appearance on ADC maps—it is a hypercellular tumour with high nucleus-to-cytoplasm ratio. Both CT and MR post-contrast enhancements are typically avid and homogeneous, indicating breakdown of the blood-brain barrier. Linear enhancement along perivascular spaces is highly suggestive of PCNSL [2]. Most lesions occur in the central hemispheric or in periventricular white matter [2]. There is a propensity of PCNSL to spread through subependymal white matter, involving the periventricular regions, corpus callosum and septum pellucidum. Crossing of the corpus cal-

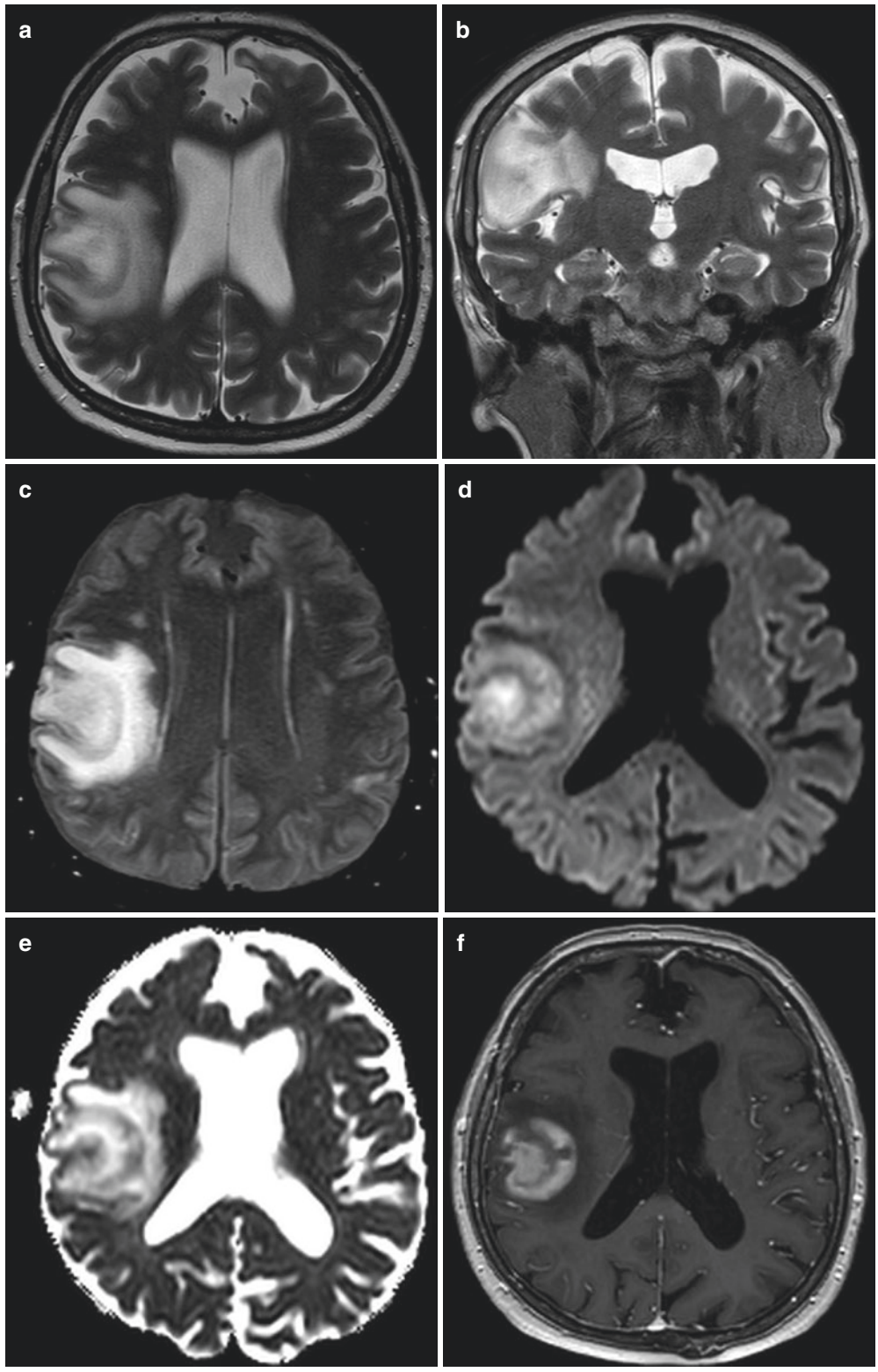

Fig. 2.2 Brain MRI exam—axial (**a**) and coronal (**b**) T2WI, axial T2-FLAIR image (**c**), axial DWI (**d**) and ADC map (**e**), post-contrast axial T1WI (**f**). The report described right-sided frontal cytotoxic cortical oedema and gyriform enhancement which was probably in keeping with acute or subacute ischaemic lesion

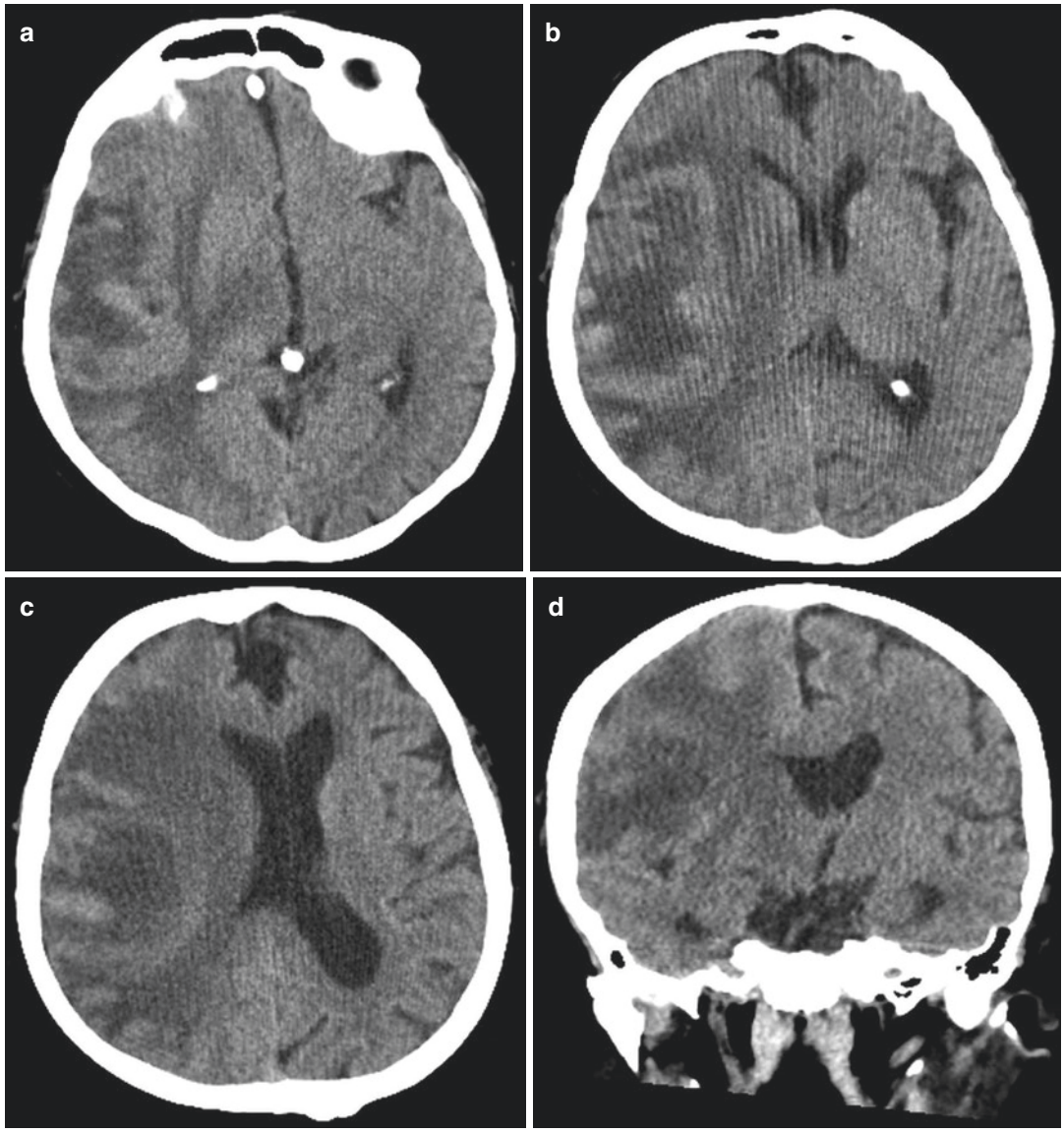

Fig. 2.3 Non-contrast and contrast-enhanced CT exam of the brain—non-contrast axial (**a**–**c**) and coronal reformatted (**d**–**f**) images. Contrast-enhanced axial (**g**, **h**) and coronal reformatted (**i**) images. There has been enlargement of the irregular intra-axial lesion in the right-sided frontal lobe, with progression of the perifocal oedema and mass effect. The findings were suggestive of a space-occupying lesion

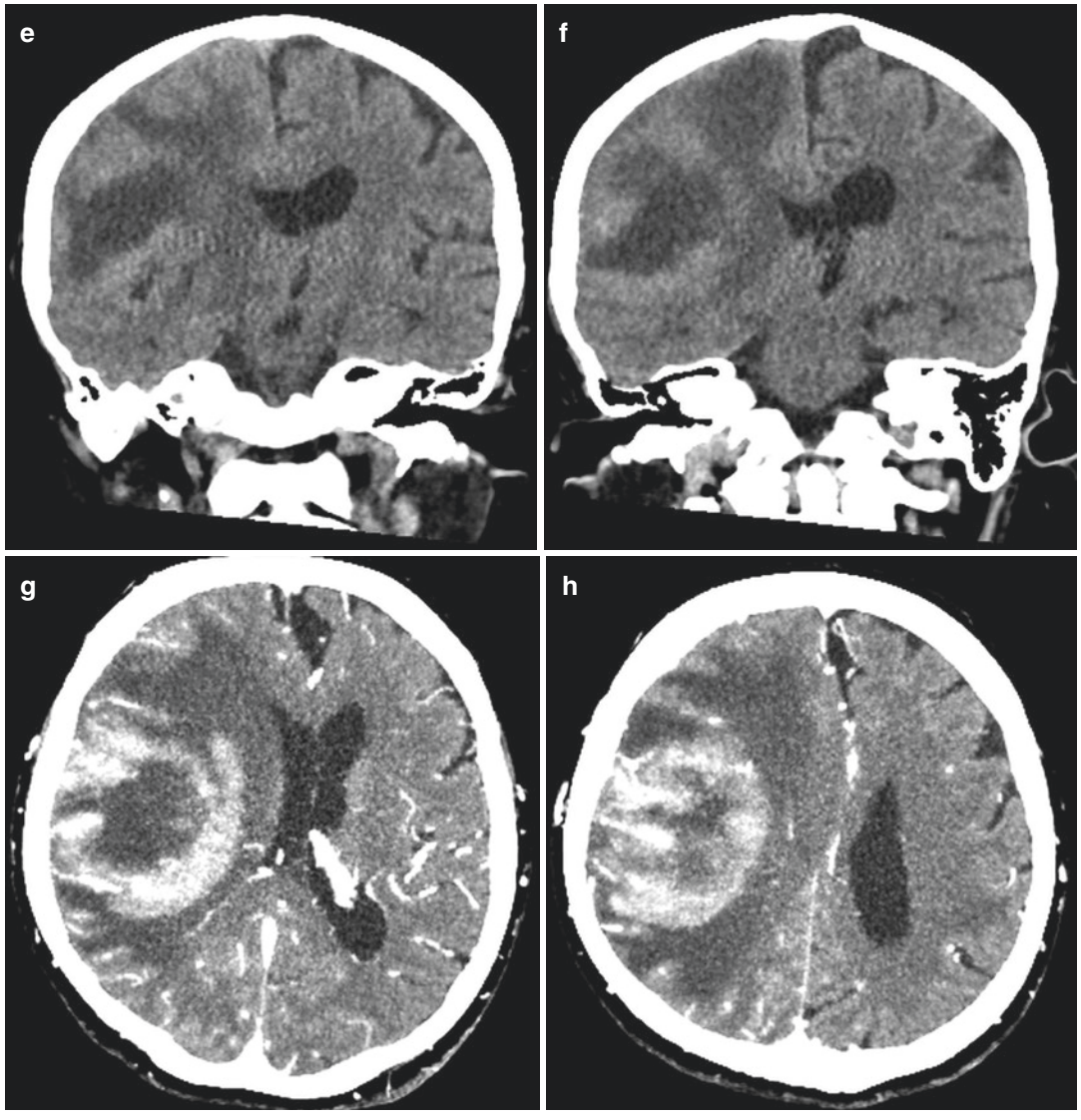

Fig. 2.3 (continued)

Fig. 2.3 (continued)

losum is not uncommon. Usually there is associated vasogenic oedema and mass effect, less prominent than in malignant gliomas or metastases. On perfusion studies, there is a very mild or absent increase in rCBV, as opposed to a very high rCBV in malignant gliomas.

Pretherapeutic ADC measurement within the contrast-enhancing tumour tissue is predictive of the clinical tumour behaviour—lower ADC values mean shorter progression-free survival and overall survival. Under treatment, ADC increase indicates favourable response to therapy [2].

In immunocompromised patients, the appearances are more of necrotic and haemorrhagic lesions, and contrast enhancement may vary or be completely absent, especially after steroid treatment [3].

Differential diagnoses include glioblastoma (usually necrotic, heterogeneous, irregularly enhancing, with very high rCBV on perfusion studies and not as low ADC values of the solid enhancing tumour), tumefactive demyelination (specific contrast enhancement pattern, minimal oedema, low rCBV), toxoplasmosis, metastatic tumour, abscess [2, 3] and stroke [2]. It is often difficult to uniequivocally differentiate PCNSL from these lesions based on characteristic MR imaging appearance only [2].

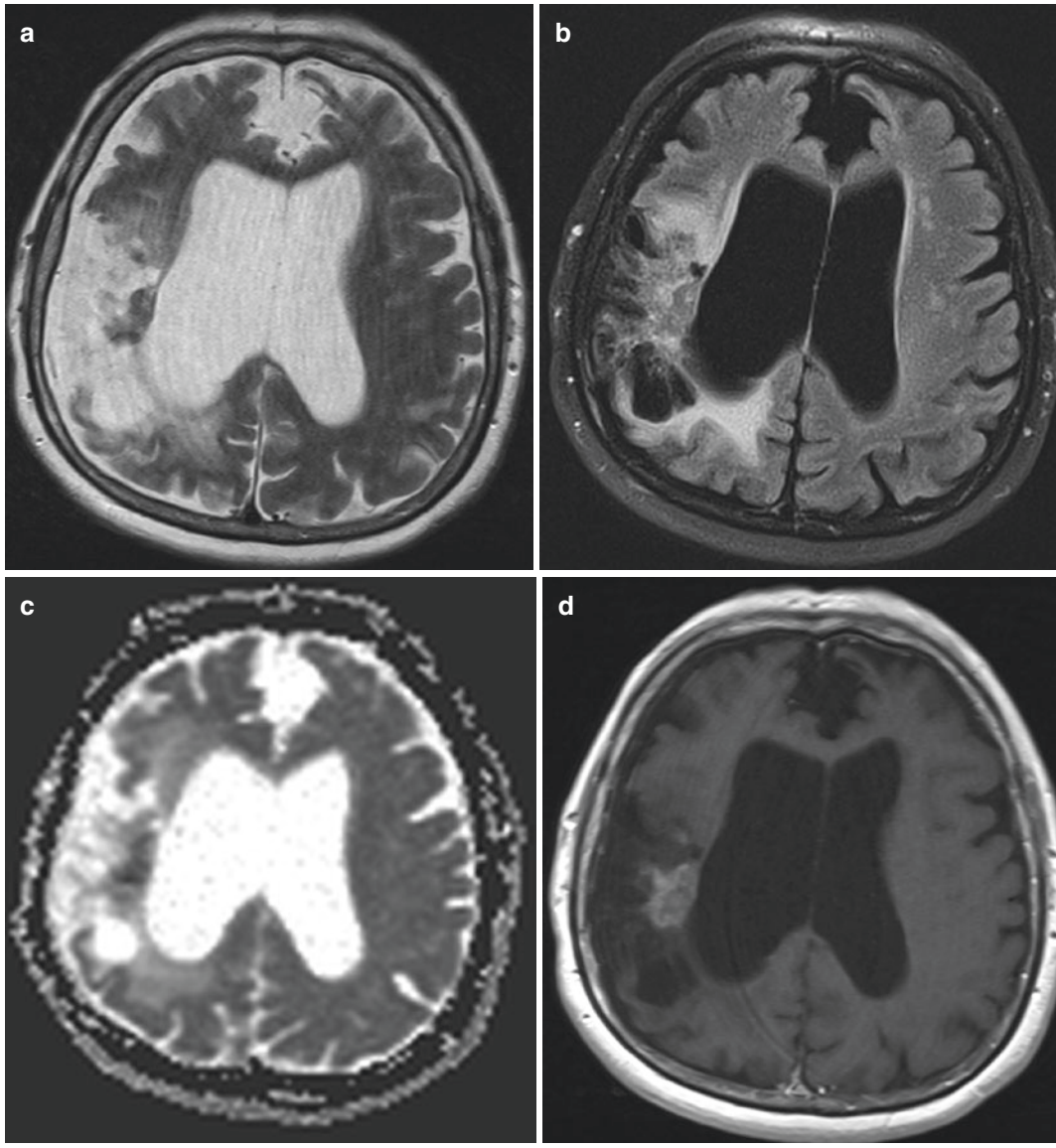

Fig. 2.4 Follow-up MRI of the brain 1 year into therapy – axial T2WI (**a**), axial T2-FLAIR (**b**), axial ADC map (**c**) and axial post-contrast T1WI (**d**). There is a residual/recurrent lymphoma adjacent to the right-sided lateral ventricle. Note the low ADC signal (**c**) of the enhancing tumour (**d**)

References

1. Newton HB, Jolesz FA (2008) Handbook of neuro-oncology neuroimaging. Academic Press, Amsterdam
2. Haldorsen IS et al (2011) Central nervous system lymphoma: characteristic findings on traditional and advanced imaging. Am J Neuroradiol 32(6):984–992. https://doi.org/10.3174/ajnr.A2171
3. Rumboldt Z et al (2010) Brain imaging with MRI and CT: an image pattern approach. Cambridge University Press, New York. https://doi.org/10.1017/CBO9781139030854

3 Cerebrovascular Infarction: Enlarged Perivascular Spaces

In November 2011, a 64-year-old male patient was referred from his neurologist, as an out-hospital patient, to perform MRI of the brain, due to general weakness with nausea lasting for a year on a daily basis. He worked as a captain of merchant overseas ships and, back then he was retired for a year, had a mild arterial hypertension in anamnesis.

Patient has enclosed MRI of the brain which he performed 5 years before in a private clinic—in year 2006, an experienced neuroradiologist reported those lesions as multiple chronic lacunar infarcts in the left cerebral peduncle. There were no changes in number, size and signal intensities of those lesions comparing two brain MRIs performed in 2006 and 2011 (Fig. 3.1). Lacunar infarctions are differential diagnosis of enlarged PVSs, but in this particular case, the diagnosis of chronic lacunar infarction reported in 2006 is a misdiagnosis. Although our patient had a mild arterial hypertension, the following facts, together with typical PVS imaging features, exclude chronic lacunar infarction as the diagnosis: there were no other vascular lesions in the rest of the brain parenchyma, cerebral peduncles are not predilection site for lacunar infarcts which are usually larger than PVSs, and chronic lacunar infarction has signal intensities that reflect gliosis.

3.1 Enlarged or Giant Perivascular Spaces

It is important not to mistake enlarged perivascular spaces (PVSs) with cerebral pathologies like cystic neoplasms or lacunar infarcts, because such diagnosis will burden a patient and probably initiate unnecessary diagnostic procedures. PVSs are "do not touch lesions" which require regular timely follow-up MR examinations, for example, the first follow-up MRI about 6 months after the basic one and, if needed, the third follow-up MRI a year after the second one, to detect any increase in size.

Perivascular spaces (PVSs) or Virchow-Robin spaces surround the walls of arteries, arterioles, veins and venules as they course from the subarachnoid space through the brain parenchyma. Those spaces represent the lymphatic drainage pathways of the brain and do not communicate directly with subarachnoid spaces [1]. Small perivascular or Virchow-Robin spaces, up to 2 mm in diameter, are common finding in the inferior basal ganglia clustering around the anterior commissure, in the centrum semiovale and in the cerebral peduncle [2].

Perivascular spaces can be moderately enlarged from 2 to 5 mm, but when measure more

M. Špero, H. Vavro, *Neuroradiology - Expect the Unexpected*,
https://doi.org/10.1007/978-3-319-73482-8_3

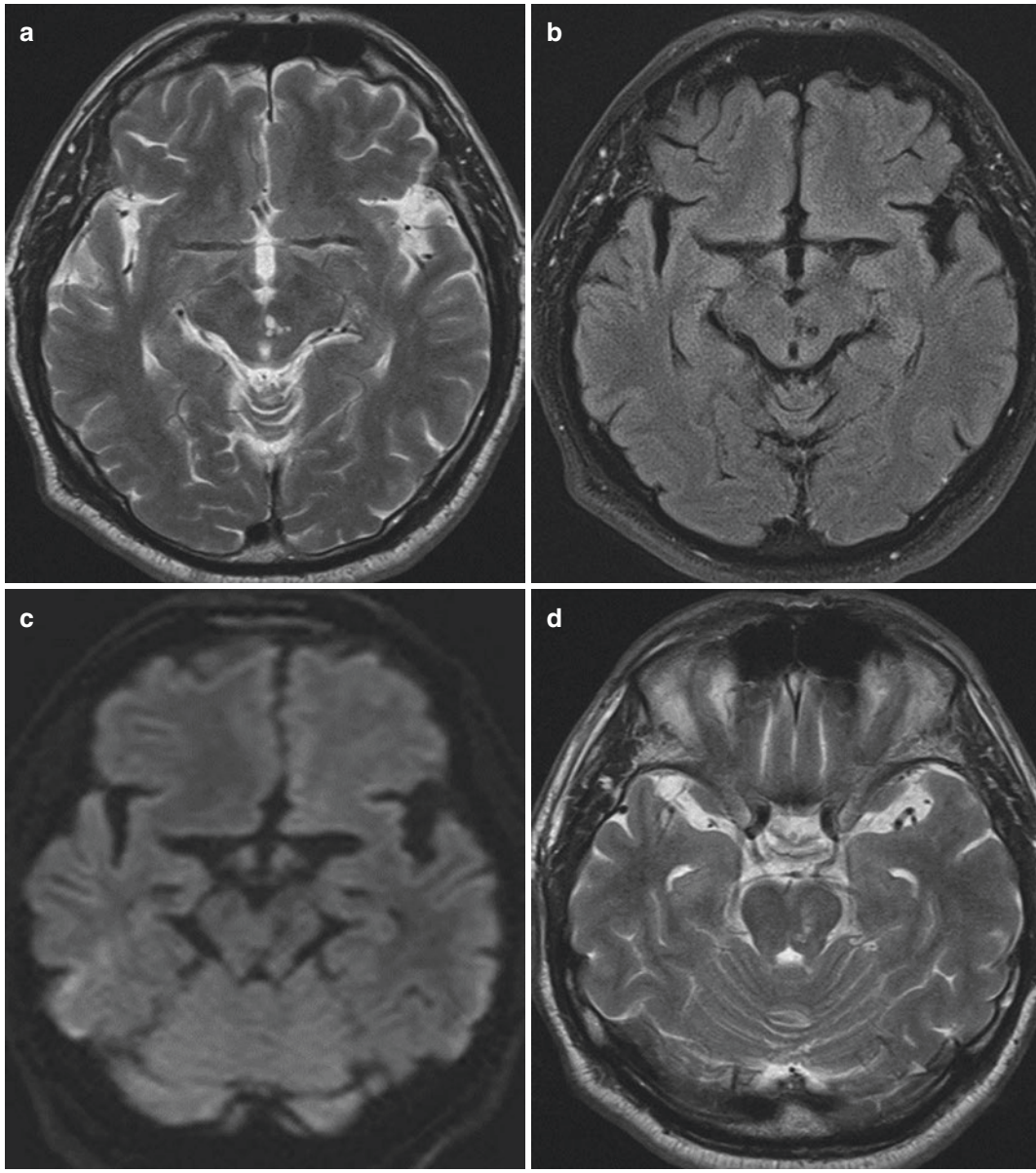

Fig. 3.1 Magnetic resonance imaging of the brain: axial (**a**, **d**) and coronal (**g**, **h**) T2WI, axial FLAIR (**b**, **e**), axial DWI (**c**) and ADC (**f**), axial T2*WI (**i**), post-contrast T1WI (**j**–**l**), revealed multiple, well defined, oval and round lesions in the left cerebral peduncle and two in the right cerebral peduncle, without mass effect. Lesion signal intensities were similar to the CSF on all sequences; there were no restricted diffusion and no contrast enhancement, while the surrounding parenchyma showed normal signal intensities on all sequences. According to the described morphological characteristics, those were reported as enlarged type III perivascular spaces (PVSs)

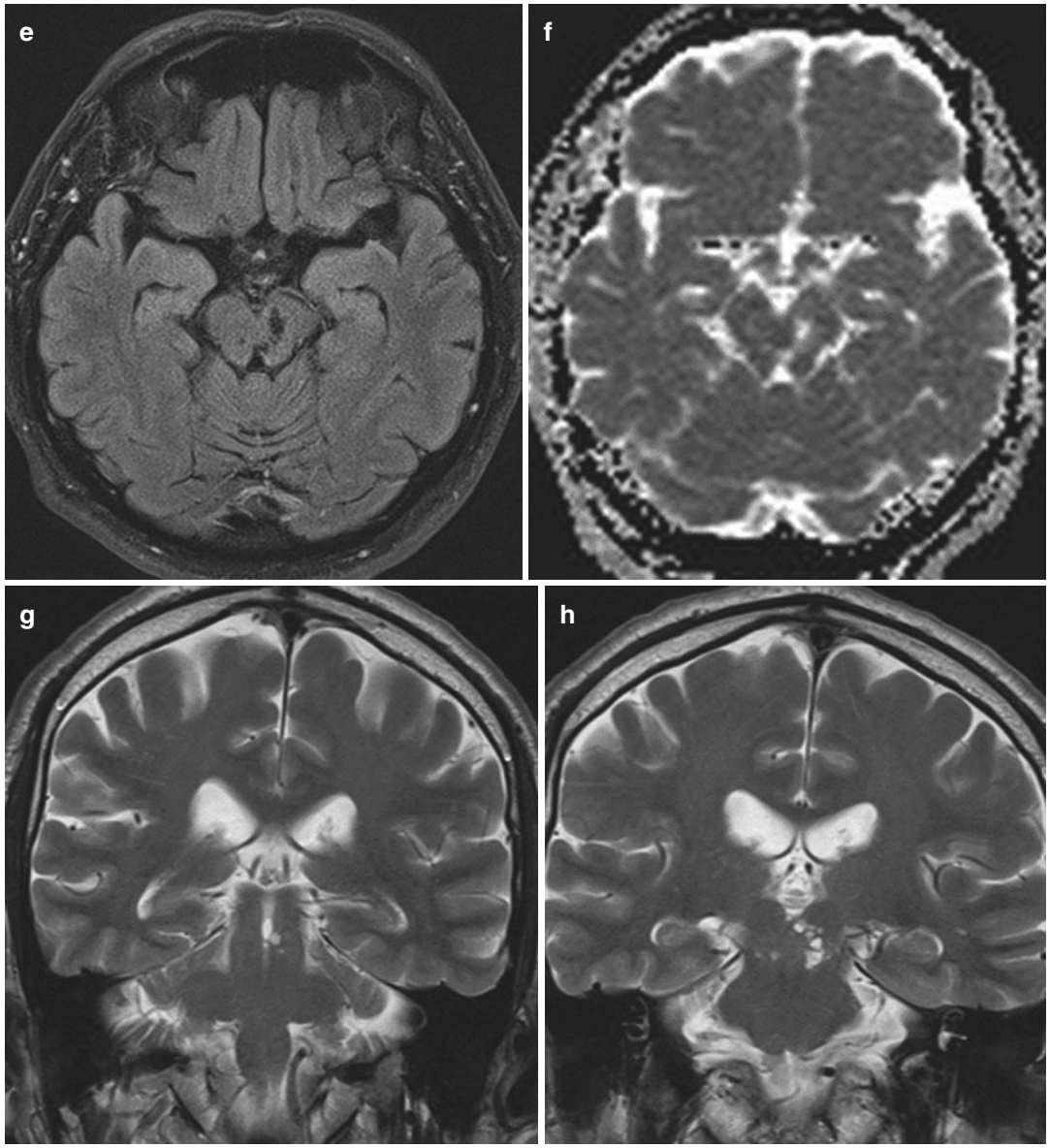

Fig. 3.1 (continued)

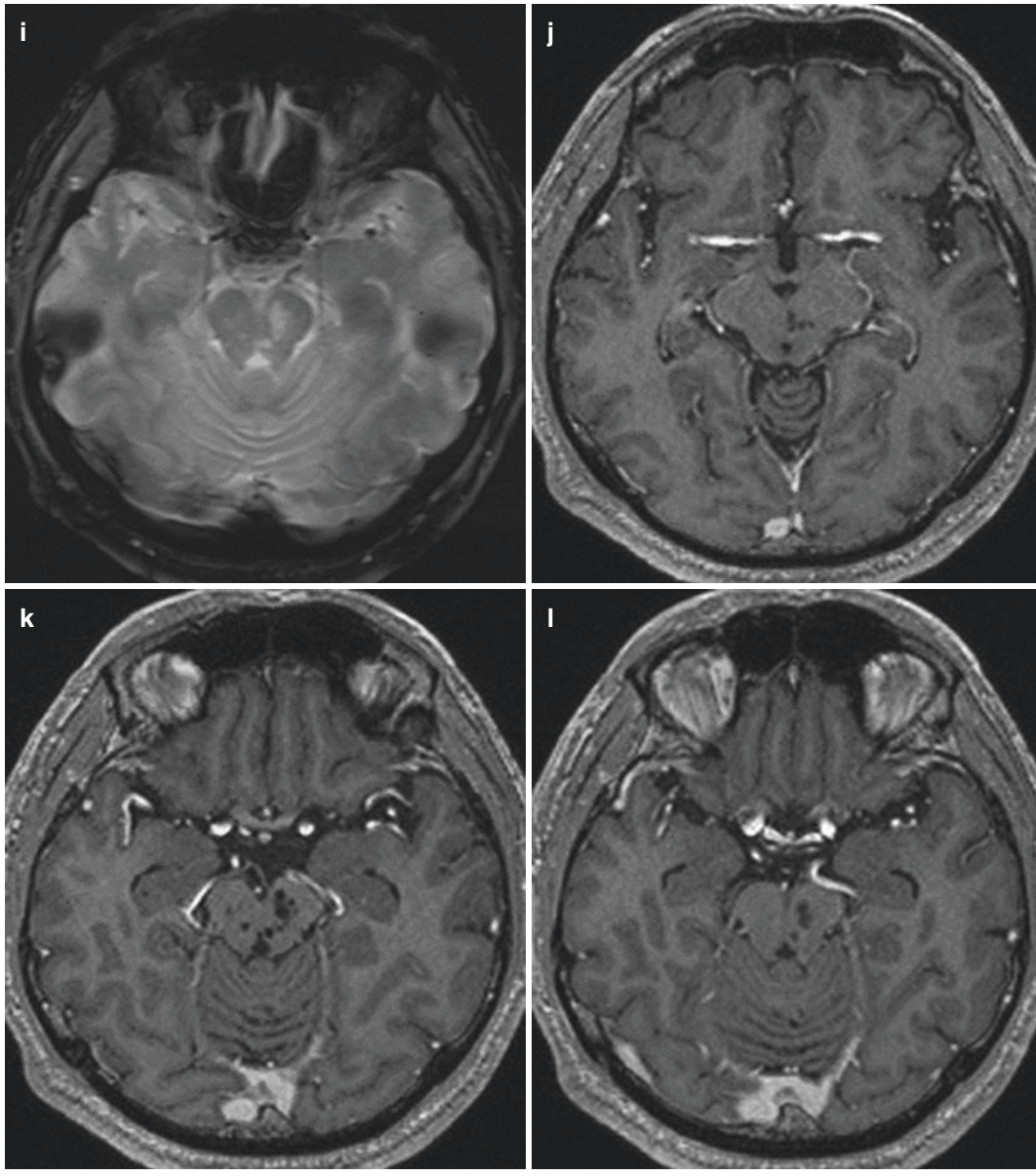

Fig. 3.1 (continued)

than 5 mm, sometimes up to 2 or 3 cm, these are termed giant PV spaces. According to typical locations, there are three types of dilated PVSs: type I appear along the lenticulostriate arteries entering the basal ganglia through the anterior perforated substance, type II are located along the paths of the perforating medullary arteries as they enter the cortical grey matter over the high convexities and extend into the white matter and the third type (III) of dilated PVSs are located in the midbrain—in the lower midbrain at the pontomesencephalic junction and in the upper midbrain at the mesencephalodiencephalic junction [1, 3]. The exact mechanism of PV spaces dilatation is still not defined, but several mechanisms are postulated.

Perivascular spaces are typically oval, round or curvilinear, with well-defined, smooth margin, and on CT are isodense to the CSF, and on MRI they visually follow signal intensities of CSF on all sequences, without contrast enhancement after its administration. When small or moderately enlarged, PVSs do not demonstrate any mass effect, and the surrounding parenchyma is of normal signal intensity [1, 3, 4]. Giant or markedly enlarged PVSs may assume bizarre cystic shapes and cause mass effect, while the surrounding parenchyma may reveal discrete T2 and FLAIR hyperintensities secondary due to gliosis or spongiosis in younger patients or due to advanced chronic ischaemic changes related to mass effect in elderly patients [3]. Alternatively, those signal intensity changes may be related to multiple tiny tightly clustered PVSs that are too small to be discriminated on the basis of current MRI findings [3].

Small or dilated PVSs are asymptomatic and are usually accidental finding on MRI of the brain performed due to symptoms which are not attributable to dilated PVSs, like headache, dizziness, dementia, visual changes, syncope, post-trauma, seizures, memory problems and poor concentration. Giant PVSs may be symptomatic when they are located at the mesencephalothalamic region where they may compress the adjacent third ventricle or Sylvian aqueduct causing hydrocephalus that requires surgical shunt surgery [1, 3].

It is important to distinguish dilated PVSs not only from cystic neoplasms or lacunar infarcts but also from other cerebral pathologies such as non-neoplastic neuroepithelial cyst, parasitic cysts, periventricular leukomalacia and mucopolysaccharidosis. Cystic neoplasms do not demonstrate signal intensity of the CSF; parasitic cysts like neurocysticercosis usually have a small scolex and enhancing cyst walls. Lacunar infarcts have clinical symptoms of stroke, on MRI have restricted diffusion if acute or show T2 and FLAIR hyperintensities in adjacent parenchyma if chronic. Differentiation between neuroepithelial cysts and enlarged PVSs can be made with certainty only by pathologic study. Patients with mucopolysaccharidosis have typical clinical features, while periventricular leukomalacia occurs in premature infants and shows loss of periventricular, predominantly periatrial white mater [1, 5].

I will end this chapter with several CT and MR images revealing giant PVSs in the right midbrain and right cerebellar hemisphere (Fig. 3.2).

In these two cases, the possibility of enlarged PVSs was not considered as possible differential diagnosis at all. Maybe it is because radiologists sometimes forget about this simple pathology or do not even take it into consideration because they think more often of other, possibly ominous, cerebral pathologies. Therefore, when you find a lesion on brain CT or MRI looking like cystic space with smooth regular margins and normal adjacent parenchyma, located along the course of cerebral vessels, isodense with CSF on CT, having similar signal intensity to CSF in all MR sequences, without contrast enhancement, with or without mass effect, recall this simple diagnosis of enlarged or giant perivascular Virchow-Robin spaces and take it into consideration as differential diagnosis; it will help you in decision-making and solving a case you have in front of you and maybe sweat about.

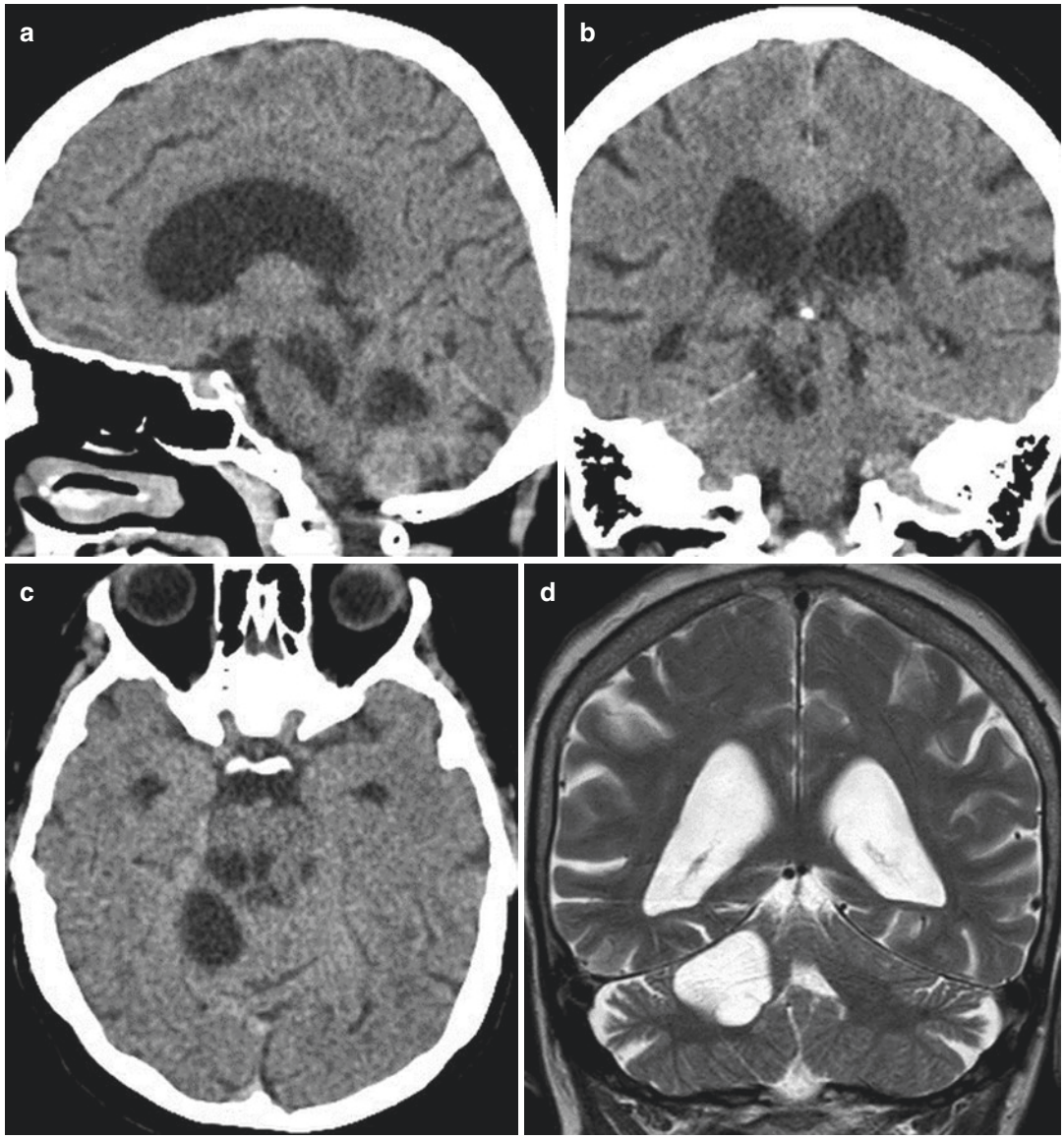

Fig. 3.2 A 75-year-old female with blurred vision on both eyes during several years. Computed tomography (axial **a**–**c**) and magnetic resonance imaging of the brain: coronal (**d**, **e**) and axial (**f**) T2WI, axial FLAIR (**g**), DWI (**h**) and ADC (**i**), pre-contrast sagittal T1WI (**j**) and post-contrast axial T1WI (**k**, **l**), revealed oval and round, well-demarcated cystic lesions in the right cerebral peduncle and upper cerebellar hemisphere showing mild mass effect, isodense with the CSF on CT scans, following signal intensities of the CSF on all MRI sequences, without restricted diffusion, without contrast enhancement on post-contrast T1 sequence, without signal intensity changes in adjacent parenchyma. She had several MRIs performed in other hospitals during the past 5 years: cystic lesions and possible cystic neoplasm without changes in size, number and radiological features on follow-up examinations were reported by radiologist in enclosed previous reports—giant perivascular spaces were never mentioned in those reports but were reported in our report due to typical location, size and described radiological features

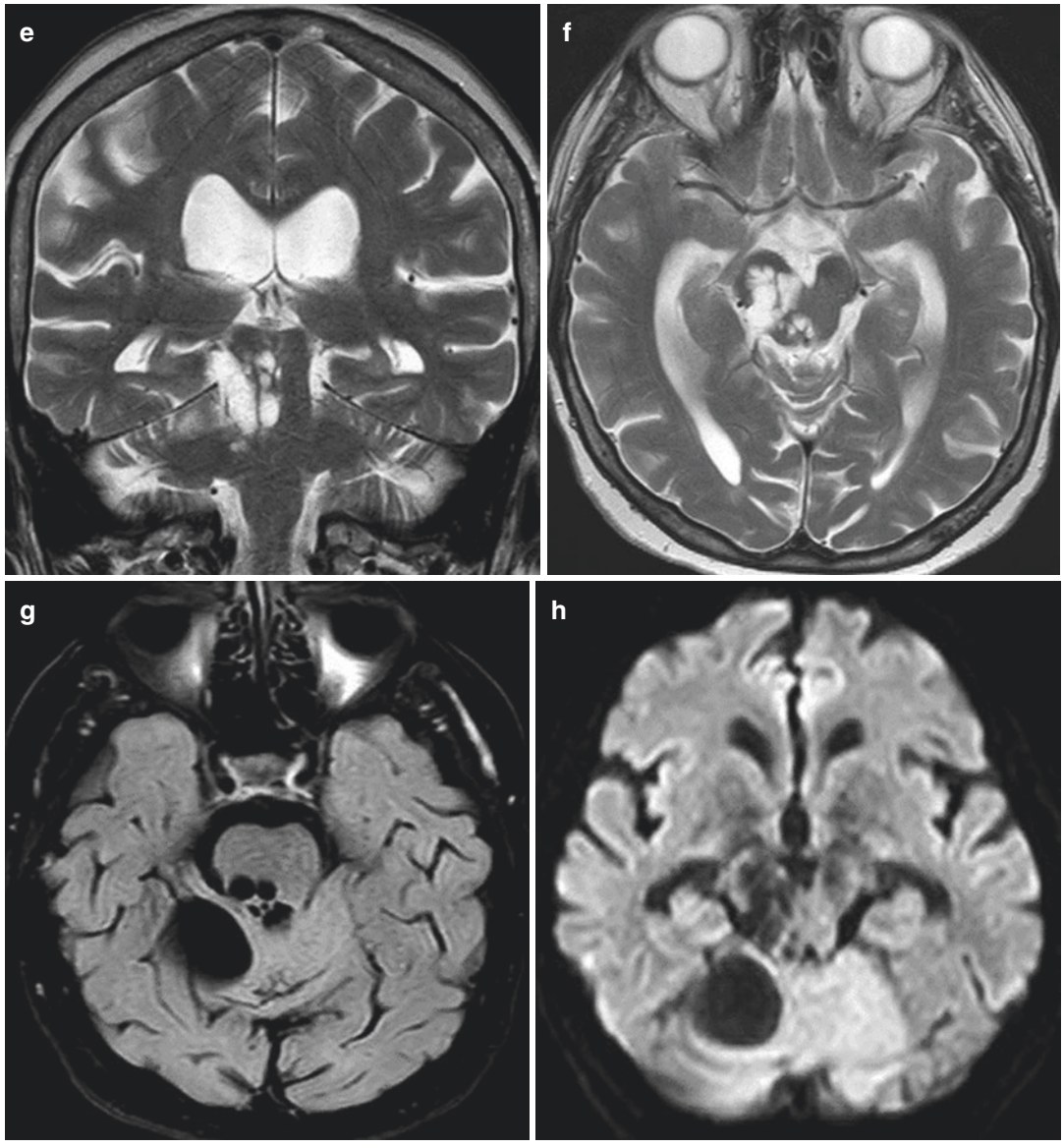

Fig. 3.2 (continued)

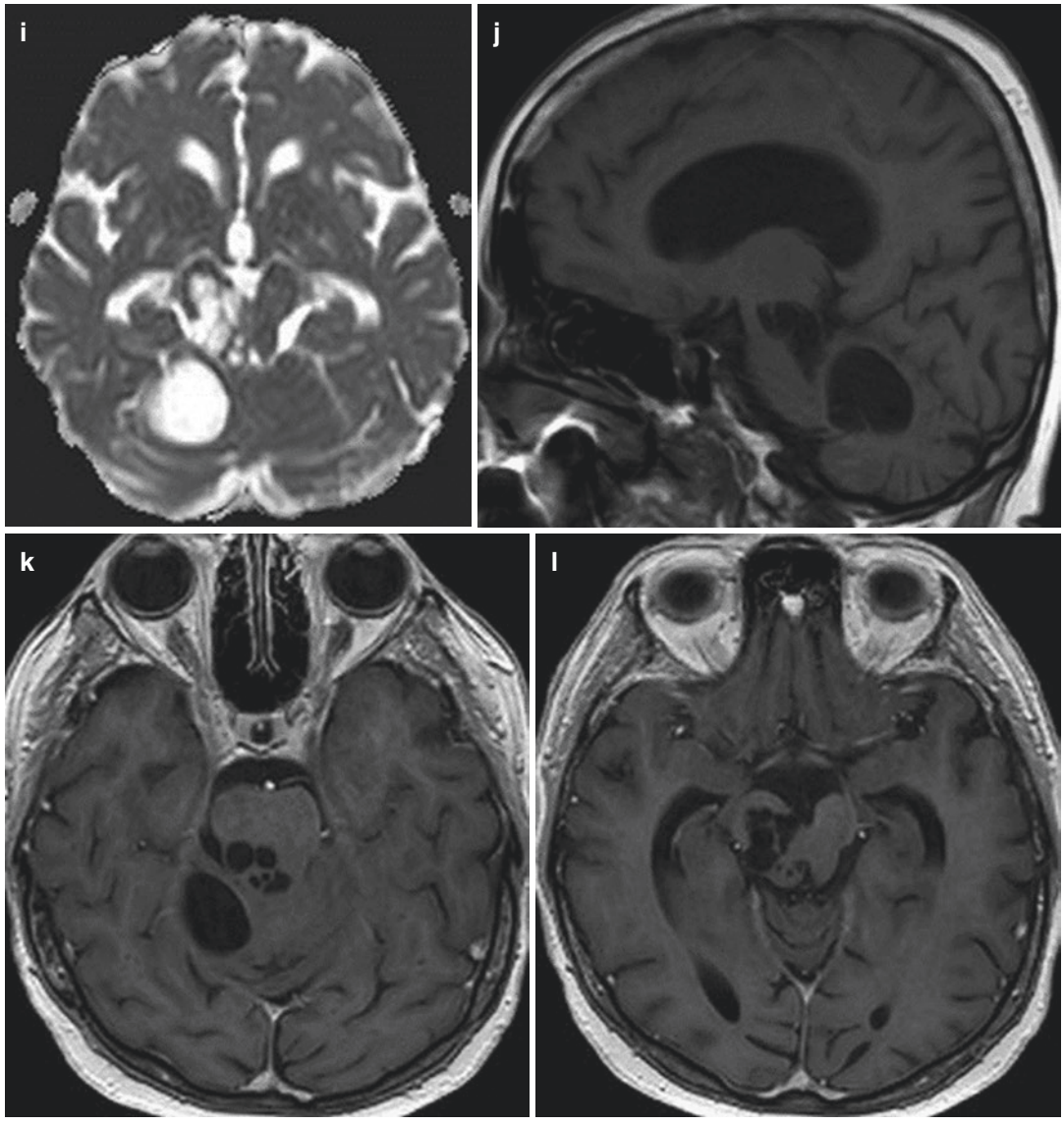

Fig. 3.2 (continued)

References

1. Kwee RM, Kvee TC (2007) Virchow-Robin spaces at MR imaging. Radiographics 27:1071–1086
2. Boukobza M, Laissy JP (2016) Unusual unilateral dilated VR spaces in the basal ganglia with mass effect: diagnosis and follow-up. Glob Imaging Insights 2(1):1–2
3. Salzman KL et al (2005) Giant tumefactive perivascular spaces. Am J Neuroradiol 26:298–305
4. Wani NA et al (2011) Giant cystic Virchow-Robin spaces with adjacent white matter signal alteration. Turk Neurosurg 21(2):235–238
5. Ahmad A et al (2014) Giant perivascular spaces: utility of MR in differentiation from other cystic lesions of the brain. JBR-BTR 97:364–365

Tumefactive Demyelination: Glioblastoma

4

At the end of November 2014, a 55-year-old male patient woke up in the morning with, as he described, face slightly distorted towards right and discrete speech disorder. During next few days, he noticed he was slightly clumsy with left hand and leg but without more pronounced motor difficulties. He was afebrile, without headache or nausea, and without previous head trauma.

He was admitted to an emergency room at a local hospital: brain CT was performed, but it was unremarkable; there were no signs of stroke, haemorrhage or tumour. Therefore, he was released from the hospital with recommendation for brain MRI. On the first day of December, brain MRI was performed in a private clinic: contrast medium was not applied for unknown reason (Fig. 4.1).

Described expansile lesion was reported as possible tumefactive demyelination lesion (TDL) or tumour, and further diagnostic work-up was recommended. Because weakness of the inferior right half of the face, right hand and leg has progressed during next 2–3 weeks, patient was admitted to a hospital, and wide diagnostic work-up has been commenced, including lumbar puncture and CT of the thorax and abdomen that did not reveal malignant process. CSF analysis did not reveal autoimmune intrathecal process; it demonstrated blood-brain barrier disruption, typical in intrathecal primary or secondary tumours. Follow-up MRI of the brain was performed at the end of December 2014, during hospitalisation (Fig. 4.2).

According to CSF analysis and described imaging features, including enlargement in short time period with development of central necrosis with hemosiderin deposits, distribution of oedema involving corticospinal tract and contrast enhancement pattern, we have reported the lesion was a primary brain tumour. Stereotactic biopsy was performed, and glioblastoma (grade IV) was confirmed. Oncologic therapy, including chemotherapy and irradiation, was conducted, but a patient died about a year after beginning of the symptoms.

4.1 Tumefactive Demyelination or Glioblastoma

Isolated cerebral mass with clinical features including acute or subacute onset, neurologic deficits and contrast enhancement, particularly ring-like or open-ring enhancement, with little mass effect and surrounding oedema should alert radiologist of possible diagnosis: TDL, brain tumour or glioblastoma?

Tumefactive demyelinating lesions (TDLs) are large (2–6 cm or larger) demyelinating lesions that usually appear as solitary supratentorial lesions with little mass effect and surrounding vasogenic oedema which are usually less conspicuous than malignancy but increase with larger lesions. They have predilection for white matter of frontal and parietal lobes but may

M. Špero, H. Vavro, *Neuroradiology - Expect the Unexpected*,
https://doi.org/10.1007/978-3-319-73482-8_4

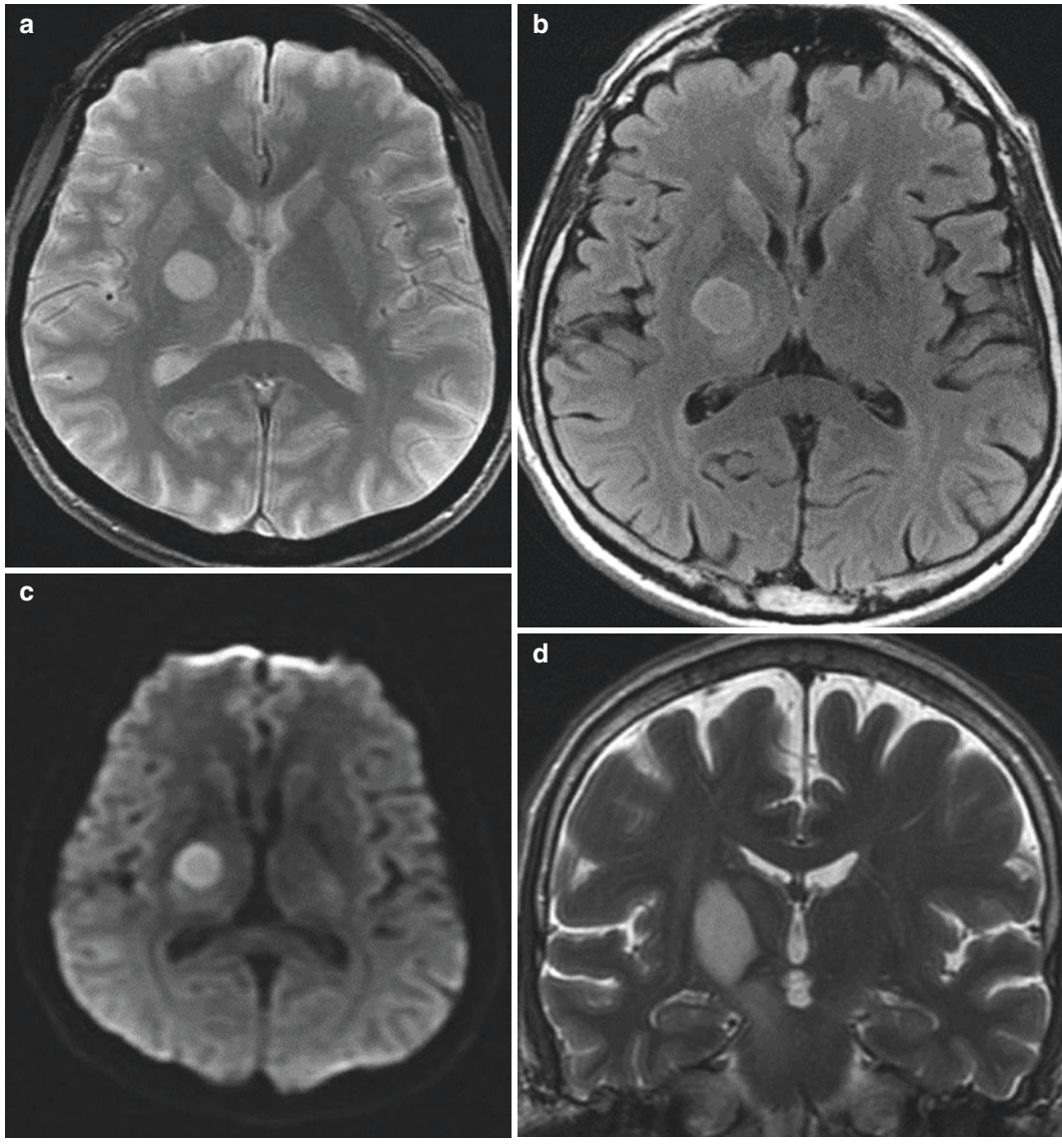

Fig. 4.1 Non-contrast MRI of the brain, axial greT2*WI (**a**), FLAIR (**b**), DWI (**c**), coronal T2WI (**d**), sagittal T1WI (**e**), axial ADC (**f**), revealed supratentorial expansile lesion, oval and well-circumscribed (16 × 16 × 27 mm) in the globus pallidus and genu of internal capsule, without surrounding vasogenic oedema, except a mild oedema coming from the inferior rim of the lesion to the right cerebral peduncle. It was hypointense on T1WI, moderately hyperintense on T2WI and FLAIR, did not show restricted diffusion. There was no central dilated vascular structure within the lesion on T2WI and greT2*WI

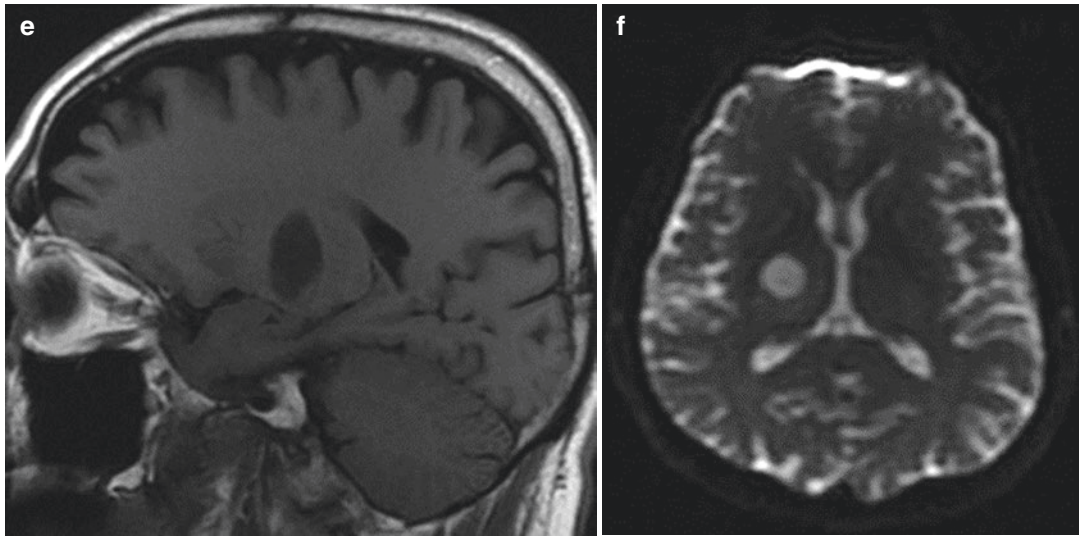

Fig. 4.1 (continued)

involve corpus callosum or basal ganglia as well [1]. Glioblastoma is the most common and most malignant brain tumour: the mortality and disability rates are among the highest. Therefore, early diagnosis and surgical treatment followed by radiation and chemotherapy are key to prolonging patient life and improving their life quality.

Clinical presentation of TDL and brain tumours includes symptoms of an increased intracranial pressure (headache and vomiting), local neurological deficits and seizures [2]. In gliomas, symptoms usually have longer duration between onset and admission (weeks to months), while in TDLs have more acute onset and shorter duration [3]. Clinical presentation and imaging characteristics of TDL overlap with brain tumours; therefore, it is not rare to misdiagnose TDL with intracranial tumours, especially gliomas. Primary brain lymphoma and metastases are other possibilities. To avoid misdiagnosis and consequently unnecessary surgery or even radiotherapy, it is important to try to distinguish TDL and brain tumour. Differentiation of TDL and brain tumours presents a diagnostic challenge; sometimes it is not possible only according to imaging features and clinical presentation—CSF analysis is more than helpful, but correct diagnosis is often made after biopsy.

Both TDL and glioblastoma may present as a well-circumscribed or ill-defined lesion. Central necrosis and cystic degeneration are typical for glioblastoma but are present in cases of severe demyelination, while signs of haemorrhage of different age are seen in glioblastoma. Peripheral diffusion restriction is present in TDL due to intramyelinic oedema in acute or subacute phase and due to hypercellular part of a tumour. Low-grade gliomas usually present as subcortical mass with little mass effect and surrounding vasogenic oedema, without contrast enhancement, while high-grade gliomas enhance and demonstrate pronounced mass effect and vasogenic oedema [2].

TDLs demonstrate ring-like or open-ring pattern of contrast enhancement: enhancing periphery represents advancing area of active inflammation, while non-enhancing core represents more chronic phase of the inflammatory process. Metastases and gliomas in certain cases may show ring-like contrast enhancement [1, 2].

Dilated vascular structure running centrally within the lesion on T2W and T2*W images probably represents dilated vein draining towards the distended subependymal veins, and is specific for TDLs, and may be used to distinguish it from gliomas [2, 4]. Perfusion studies showed decreased relative cerebral blood volume (rCBV)

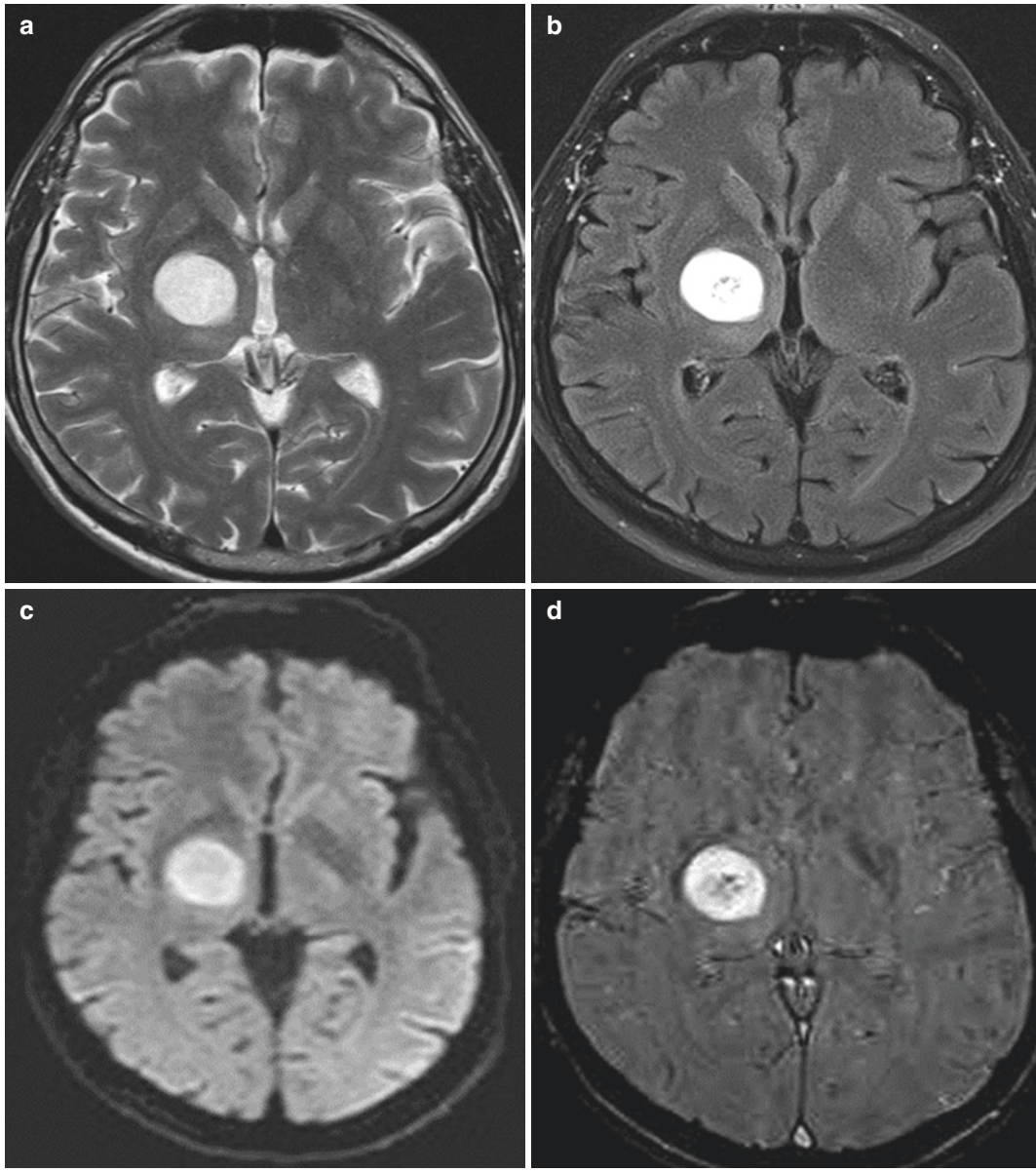

Fig. 4.2 Follow-up brain MRI performed about 4 weeks after the initial one, axial T2WI (**a**), FLAIR (**b**), DWI (**c**), axial SWI (**d**), coronal T2WI (**e**), axial ADC (**f**), sagittal T1WI (**g**), post-contrast axial T1WI (**h**), single-voxel MR spectroscopy (**i**): during 4 weeks expansile lesion (25 × 25 × 34 mm) in the right globus pallidus and genu of the internal capsule had enlarged, with central necrosis (**b**, **h**) and hemosiderin deposits (**c**). It showed intensive contrast enhancement in the rest of the lesion (**h**). Oedema in the right cerebral peduncle was more pronounced involving anterior right half of the pons (**e**). MR spectroscopy demonstrated elevated choline and moderately decreased NAA levels, and inverted lactate/lipids peak at 1.3 ppm

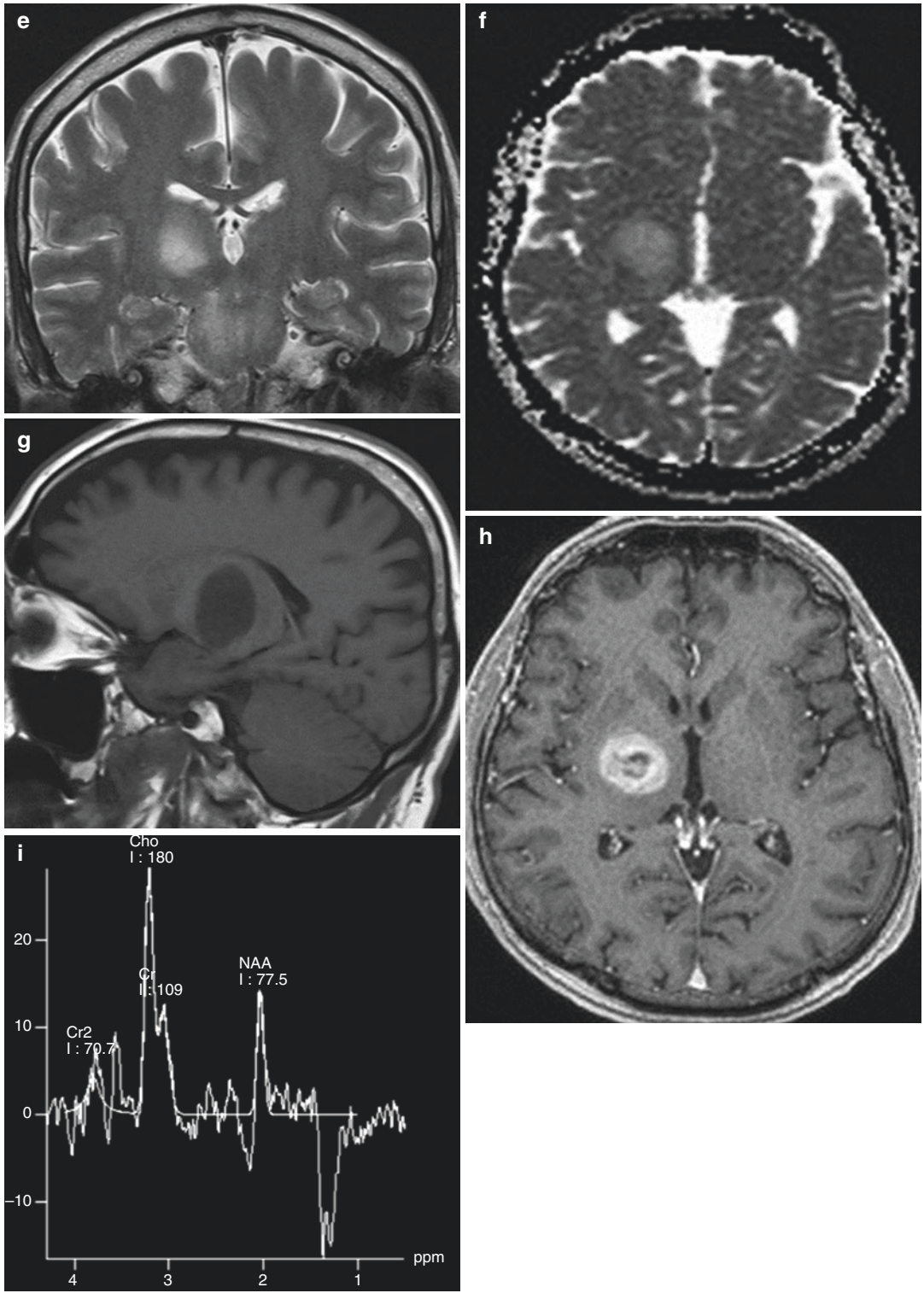

Fig. 4.2 (continued)

in TDL, while, due to vascular proliferation and tumour angiogenesis, rCBV is increased in glioblastoma compared to TDL [5].

Elevated choline level and decreased NAA levels on MR spectroscopy are typically regarded as diagnostic feature of brain tumours, with lactate/lipid signal at 1.3 ppm. In active demyelination, MRS shows increased choline and lactate levels and decreased NAA levels as well, allowing inflammatory demyelinating process to mimic malignant glioma: NAA/Cr ratios are normal or decreased due to neuronal or axonal loss concomitant with increased choline levels corresponding to glial proliferation that occurs in demyelinating plaques [6, 7].

Toh and his team suggested diffusion tensor imaging (DTI) could be helpful in differentiating TDL from high-grade gliomas by using visual inspections and quantitative analysis [8].

In our case it was important to distinguish between TDL and primary brain tumour. It was not easy: clinical presentation, lesion location and brain CT finding, together with the initial brain MRI, were more in favour of secondary TDL, although there was no central vein sing on greT2*WI or restricted diffusion due to possible intramyelinic oedema. Follow-up MRI was more in favour of tumour due to enlargement in size in short time, development of central necrosis with hemosiderin deposits. CSF analysis was more than helpful in decision making: no obvious oligoclonal band or pleocytosis confirmed our suspicion. Final confirmation was done by lesion biopsy.

References

1. Abdoli M, Freedman MS (2015) Neuro-oncology dilemma: tumour or tumefactive demyelinating lesion. Mult Scler Relat Disord 4:555–566
2. Qi W et al (2015) Cerebral tumefactive demyelinating lesions. Oncol Lett 10:1763–1768
3. Kim DS et al (2009) Distinguishing tumefactive demyelinating lesions from glioma or central nervous system lymphoma: added value of unenhanced CT compared with conventional contrast-enhanced MR imaging. Radiology 251:467–475
4. Fallah A et al (2010) Tumefactive demyelinating lesions: a diagnostic challenge. Can J Surg 53(1):69–70
5. Wang S et al (2011) Differentiation between glioblastomas, solitary brain metastases, and primary cerebral lymphomas using diffusion tensor and dynamic susceptibility contrast-enhanced MR imaging. AJNR Am J Neuroradiol 32(3):507–514
6. Oz P et al (2014) Clinical proton MR spectroscopy in central nervous system disorders. Radiology 270(3):658–679
7. Hayashi T et al (2003) Inflammatory demyelinating disease mimicking malignant glioma. J Nucl Med 44:565–569
8. Toh CH et al (2012) Differentiation of tumefactive demyelinating lesions from high-grade gliomas with the use of diffusion tensor imaging. AJNR Am J Neuroradiol 33:846–851

5 Cerebrovascular Infarction: Glioblastoma

While sitting in front of TV with his family on a calm Sunday evening, a 63-year-old man suddenly experienced what looked like tonic seizures of his left arm and face and became unresponsive for a moment or two. Afterwards he had speech difficulties and left facial droop. The patient had no previous health issues. He was immediately brought to an emergency hospital department, and a CT exam of the brain was done (Fig. 5.1).

However, the second reader was not convinced this was an ischaemic lesion, in spite of abrupt onset of symptoms. A brain MRI exam was recommended (Fig. 5.2).

The patient was immediately scheduled for a neurosurgical stereotactic tumour biopsy. The histopathological examination revealed a glioblastoma (WHO grade IV).

5.1 Glioblastoma

Glioblastoma (GB) is the most common malignant primary brain tumour in adults. It represents about 15% of all primary brain tumours and 60–75% of all astrocytomas. The most common type is IDH wild-type form, which corresponds to clinically defined primary GB [1], occurring without evidence of a lower-grade precursor tumour, with a short clinical course of approximately 3 months; mean patient age is 55 years [2, 3]. IDH-mutant type, clinically defined as secondary, is less frequent, arises from a lower-grade astrocytoma, has a longer clinical course and affects younger patients (mean age 40 years) [2, 3].

GB is frequently hypodense on CT and hyperintense in T2 MRI images. Thus, it is often difficult to assess its size on non-contrast-enhanced CT, due to the similar appearance of the perifocal vasogenic oedema. The oedema is generally infiltrative, containing tumour cells beyond the enhancement borders [4]. Post-contrast imaging almost always demonstrates thick, irregular peripheral enhancement and unenhanced central necrotic part of the lesion. Solid, enhanced portions of the tumour often show increased DWI signal and ADC hypointensity. Large haemorrhage is uncommon, but there are often T2* or SWI hypointensities representing small haemorrhagic foci. MRS features elevated choline and decreased NAA, in necrotic areas also elevated lipid and lactate peaks. A characteristic of glioblastoma perfusion imaging is markedly elevated rCBV.

In 10–20% of cases, the initial imaging studies show multifocal lesions. Spread along white matter tracts is common. True multicentric tumours are uncommon.

Seizures are not as common at presentation as in low-grade gliomas. Typically patients present with a focal neurological deficit or symptoms of increased intracranial pressure, rarely with stroke-like symptoms. However, in rare cases a sudden alteration of neurological status is caused by haemorrhage or direct vascular infiltration and subsequent acute cerebral infarct [4].

M. Špero, H. Vavro, *Neuroradiology - Expect the Unexpected*,
https://doi.org/10.1007/978-3-319-73482-8_5

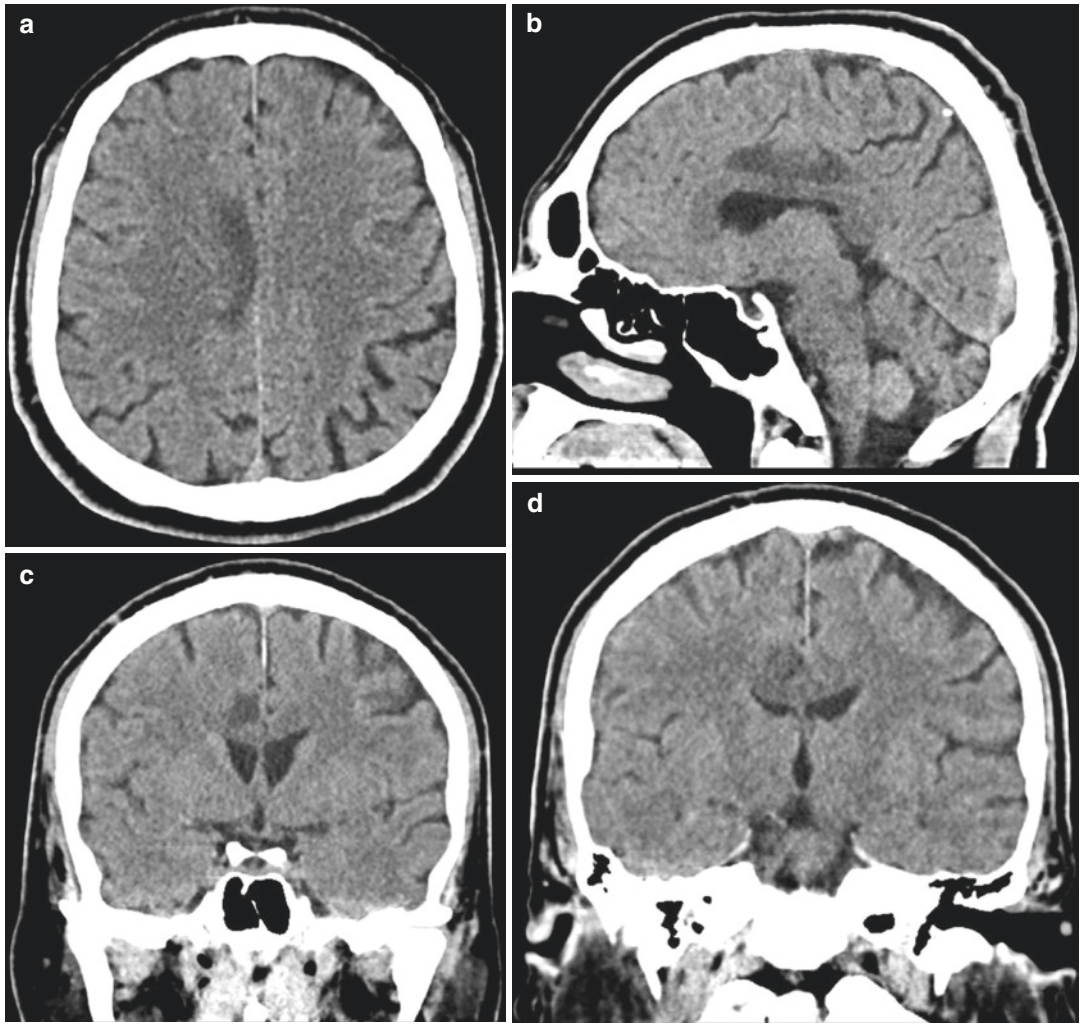

Fig. 5.1 Initial CT exam of the brain—axial image (**a**) with sagittal (**b**) and coronal (**c**, **d**) reformatted images done in an emergency setting. A hypodense lesion adjacent to the body of corpus callosum on the right (in the right cingulate gyrus) in keeping with an acute ischaemic lesion was reported

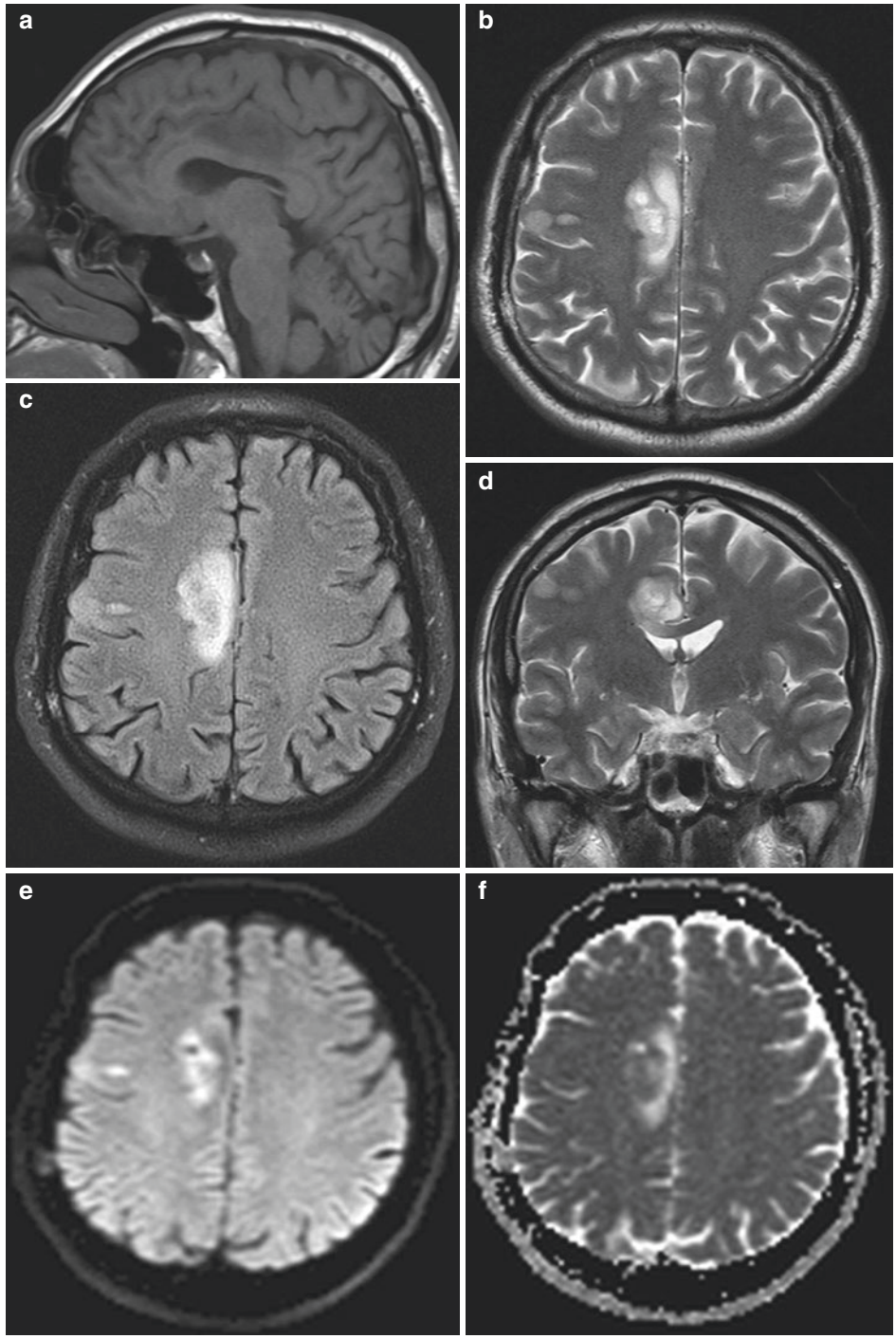

Fig. 5.2 MRI exam of the brain—sagittal T1WI (**a**), axial T2WI (**b**), axial T2-FLAIR (**c**), axial DWI (**d**), axial ADC (**e**), coronal T2WI (**f**) and post gadolinium coronal (**g**), axial (**h**) and sagittal (**i**) T1WI demonstrate a peripherally enhancing lesion within the right-sided cingulate gyrus, with perifocal oedema and mild compression of the corpus callosum. Additionally, there are two smaller enhancing lesions in the lateral basal aspect of the right precentral gyrus. The findings are suggestive of a space-occupying lesion (glioma) with two smaller satellite lesions. No features of acute ischaemia were found—the DWI and ADC signal abnormalities are subtle—in the core of the biggest lesion they are actually opposite of what would be expected in an ischaemic lesion. The peripheral DWI hyperintensities reveal the hypercellular segments of the tumour, which also enhance the most

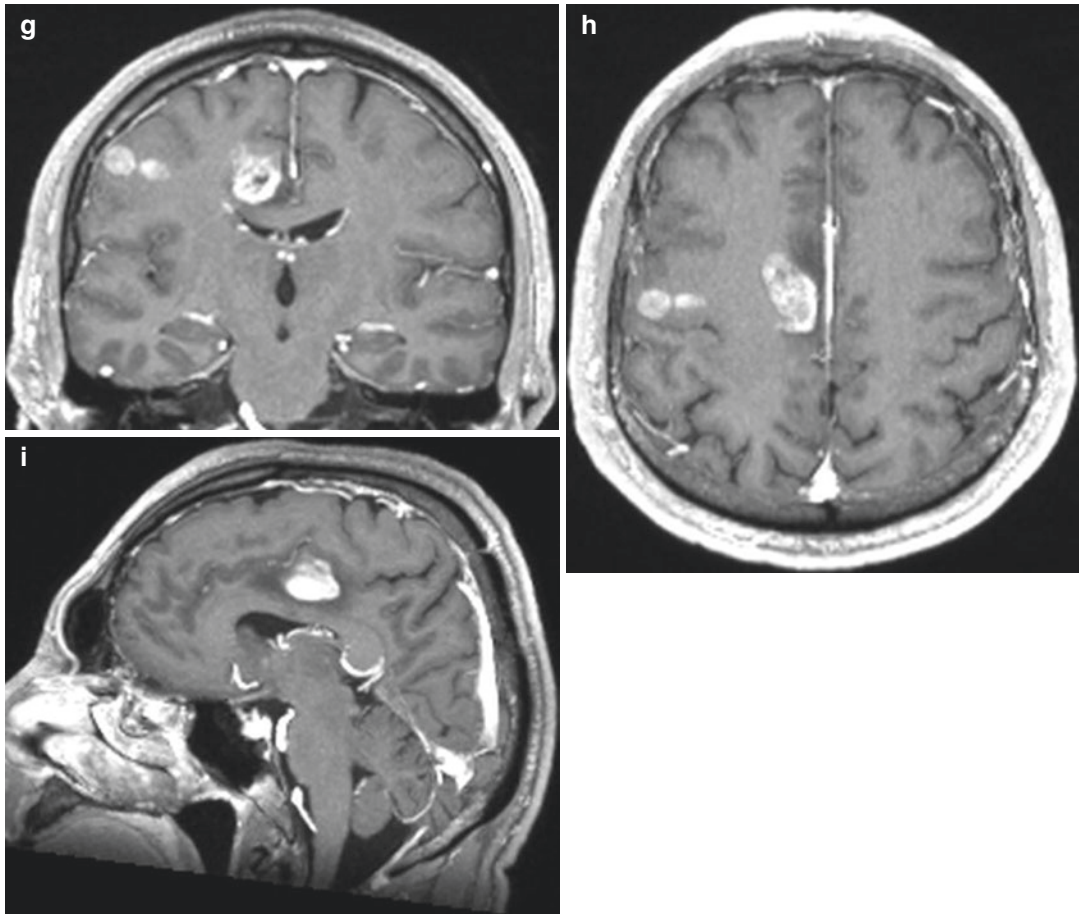

Fig. 5.2 (continued)

Differential diagnoses include metastasis, primary CNS lymphoma, tumefactive demyelinating lesion (see Chap. 4), abscess and subacute infarction.

References

1. Komori T (2017) The 2016 WHO classification of tumours of the central nervous system: the major points of revision. Neurol Med Chir 57(7):301–311. https://doi.org/10.2176/nmc.ra.2017-0010
2. Altman DA et al (2007) Best cases from the AFIP: glioblastoma multiforme. Radiographics 27(3):883–888
3. Eidel O et al (2017) Tumor infiltration in enhancing and non-enhancing parts of glioblastoma: a correlation with histopathology. PLoS One 12(1):e0169292. https://doi.org/10.1371/journal.pone.0169292
4. Pina S et al (2014) Acute ischemic stroke secondary to glioblastoma. A case report. Neuroradiol J 27(1): 85–90. https://doi.org/10.15274/NRJ-2014-10009

6 Cystic Pituitary Macroadenoma: Rathke's Cleft Cyst with Intracystic Nodule

During the spring of 2014, a 22-year-old female patient was admitted to Department of Neurology for a diagnostic work-up of right-sided headaches and menstrual cycle disturbance. Headaches occurred almost every evening for several months, while menstrual cycle was regular until June 2013: from that time periods were irregular and finally were missed. She has attributed headaches and menstrual cycle disturbance to a stress she was exposed to daily. A patient also gained weight, 6 kg in 4 months, and did not have visual field loss, and later on we found out she did not have galactorrhea.

Pituitary MRI was performed before pituitary hormone level report was finished by a biochemical laboratory (Figs. 6.1, 6.2, and 6.3).

According to the described imaging features, cystic pituitary macroadenoma (CPA) or Rathke's cleft cyst (RCC) with intracystic nodule was reported as possible diagnosis, and further endocrine work-up was recommended. Pituitary hormone level report revealed high prolactin levels, 4237 mIU/L (normal levels for women, 127–637 mIU/L). Since Rathke's cleft cyst symptoms do not include high pituitary hormone levels, it was confirmed that the lesion was a cystic pituitary macroadenoma, not a RCC with intracystic nodule. A committee of endocrinologist, neuroradiologist and neurosurgeon has chosen a medicamentous treatment as a therapeutic approach.

6.1 Cystic Pituitary Adenoma or Rathke's Cleft Cyst with Intracystic Nodule

Pituitary adenoma is a benign neoplasm that arises from the adenohypophysis and represents the most common intrasellar pathology. Imaging findings of an uncomplicated adenoma are typical, but intratumoural haemorrhage and ischemic changes in larger pituitary adenomas result in haemorrhagic and cystic changes or both, leading to various signal intensities and imaging features, wherefore it may be difficult to differentiate CPA from large RCC [1–5]. Therefore, pretreatment differentiation between these two entities remains a common issue but is important for treatment planning.

Rathke's cleft cyst is a benign epithelial cyst that originates from the embryonic remnants of Rathke's pouch and is located mainly in the midline of the pituitary gland. Typical imaging findings include intrasellar and/or suprasellar cyst of various signal intensities depending on the content of the intracystic fluid: it may follow CSF signal intensities on T1WI and T2WI, but it may be iso- to hyperintense on T1WI (Figs. 6.4c and 6.5a, b, e) due to protein, mucopolysaccharides and/or high cholesterol content [4]. It usually does not enhance, but in case of larger RCCs enhancing thin rim of compressed pituitary

M. Špero, H. Vavro, *Neuroradiology - Expect the Unexpected*,
https://doi.org/10.1007/978-3-319-73482-8_6

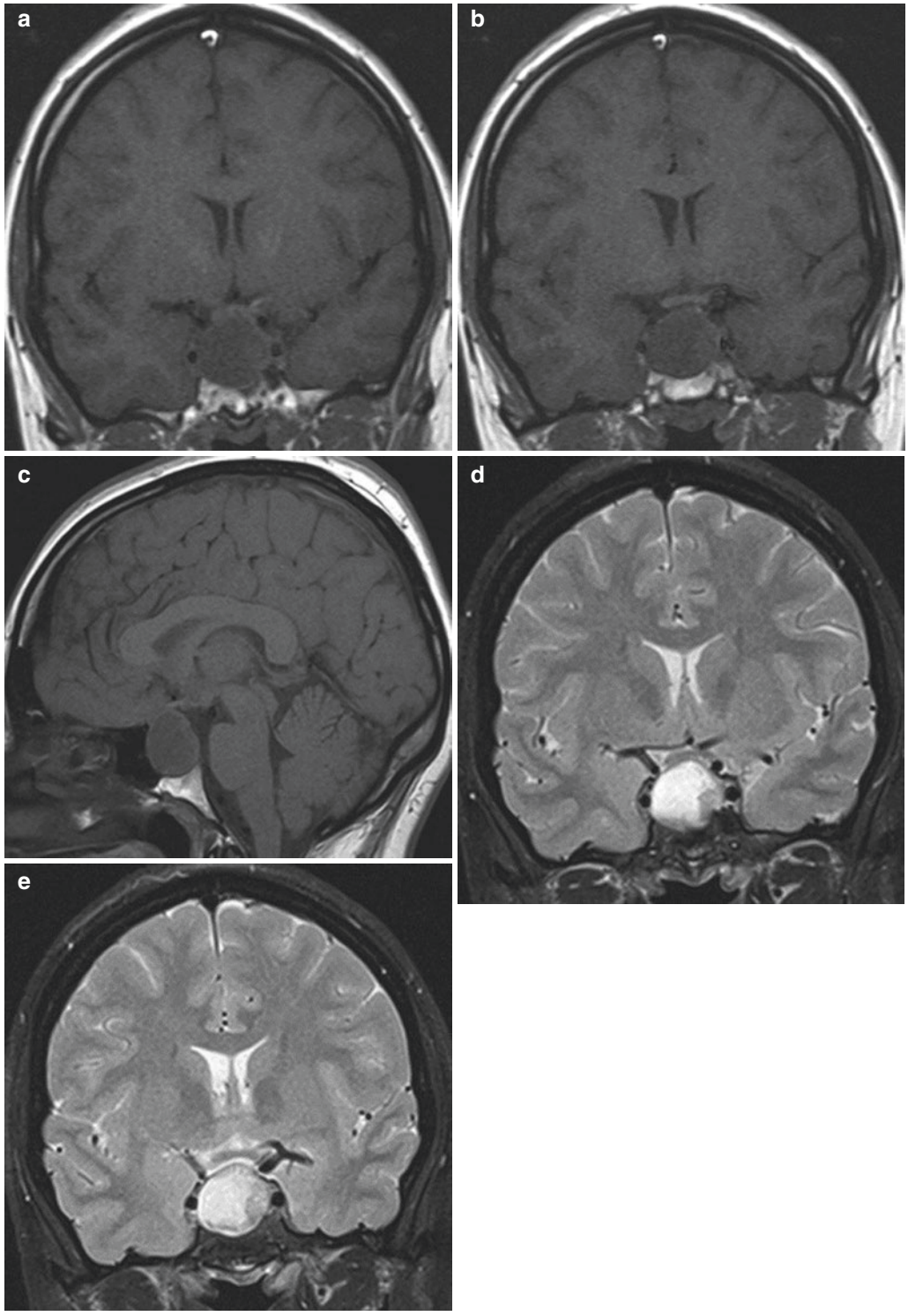

Fig. 6.1 Non-contrast pituitary MRI, coronal (**a**, **b**) and sagittal (**c**) T1WI, coronal FST2WI (**d**, **e**), revealed enlarged sella turcica due to intrasellar and suprasellar cystic lesion reaching and slightly stretching optic chiasm. The cystic lesion was hypointense on T1WI and hyperintense on T2WI: irregular structure extended inside the cystic lesion, along the inferior and left lateral cystic wall, almost isointense with the grey matter on T1WI and T2WI

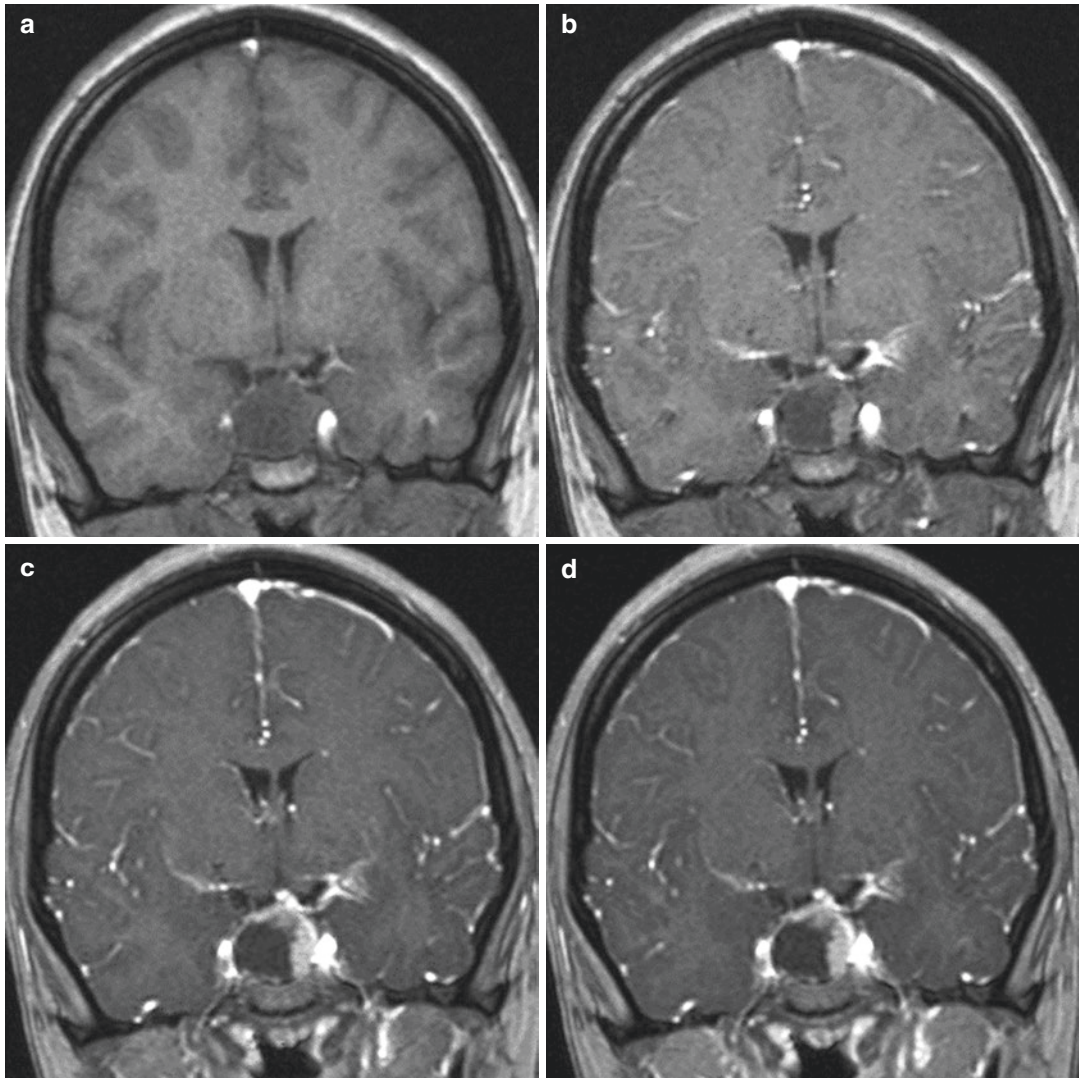

Fig. 6.2 Post-contrast pituitary MRI, dynamic post-contrast coronal T1WI (**a**–**d**): cystic lesion revealed rim enhancement, as well as the enhancement of the intracystic nodule along the inferior and left lateral cyst wall (**c**, **d**)

gland, surrounding non-enhancing cyst, mimics cyst wall enhancement (Fig. 6.4a, b). Intracystic nodule may be present (up to 75%), freely floating inside a cyst or adherent to a cyst wall, consisting of cholesterol and protein. It may be hyperintense on T1WI and iso- or hypointense on T2WI and does not enhance on post-contrast T1WI (Fig. 6.5) [1, 3, 4]. Wen et al. have reported RCC with markedly enhanced intracystic nodule: histology revealed squamous metaplasia cell debris as the main component of the enhanced nodule [4].

Functioning pituitary adenomas can cause a variety of signs and symptoms depending on the hormone they produce. Signs and symptoms of non-functioning pituitary tumours are related to their growth and the pressure they put on surrounding structures. Pituitary adenomas usually enlarge slowly over years and exhibit size change, while RCCs remain stable in dimension with time and no neoplastic transformation is reported in the literature. The majority of RCCs are asymptomatic, while symptomatic patients present with headache, pituitary dysfunction (hypopituitarism) and visual impairment [1, 3, 4].

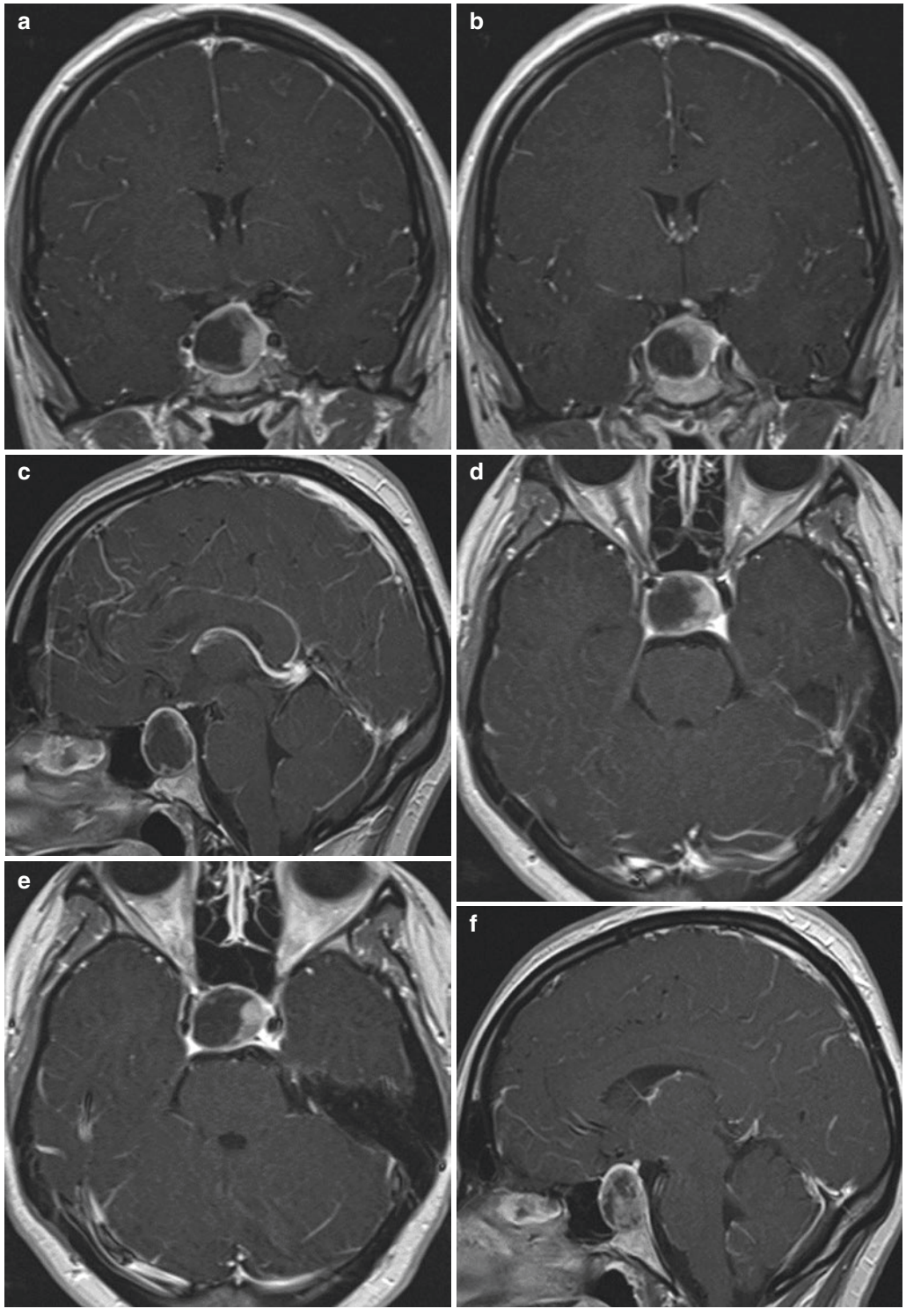

Fig. 6.3 Post-contrast pituitary MRI: post-contrast T1WI in coronal (**a**, **b**), sagittal (**c**, **f**) and axial (**d**, **e**) planes. Midline cystic pituitary lesion revealed rim enhancement, homogeneous enhancement of the intracystic nodule. Infundibulum was slightly tilted towards left. Sellar floor bulged into the sphenoid sinus. Lesion did not involve cavernous sinuses

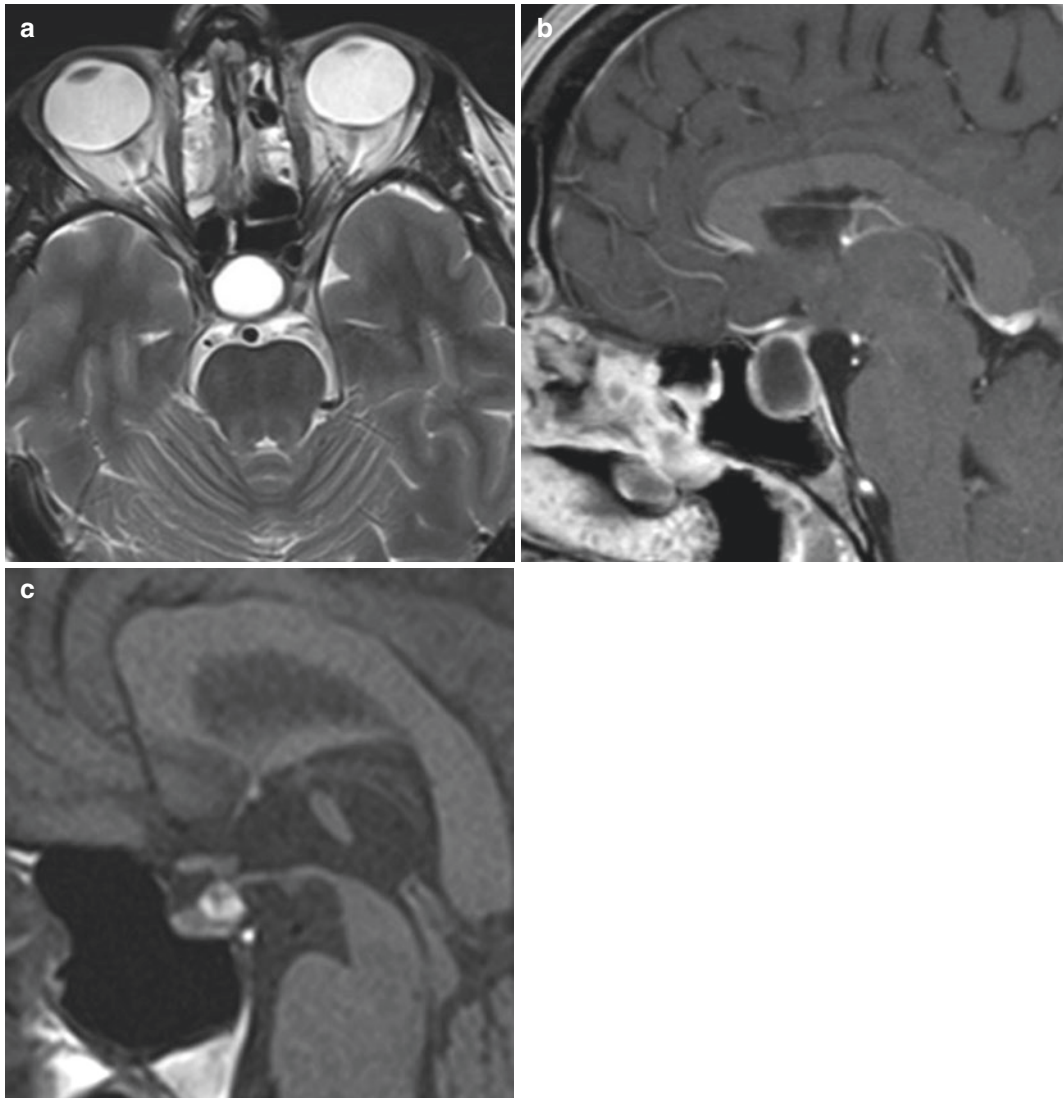

Fig. 6.4 Pituitary MRI, axial T2WI (**a**), post-contrast sagittal T1WI (**b**), pre-contrast sagittal T1WI (**c**): large Rathke's cleft cyst with enhancing thin rim of compressed pituitary gland, surrounding non-enhancing cyst, mimics cyst wall enhancement (**a**, **b**). Small Rathke's cleft cyst hyperintense on pre-contrast T1WI (**c**)

To help differentiate CPA and large RCC, different authors have developed their own models for differentiation between these two entities on the basis of MR imaging findings. For example, according to the diagnostic model reported by Park et al., the presence of fluid-fluid level, a hypointense rim on T2WI, septation and an off-midline location favoured CPA, whereas the presence of an intracystic nodule was more common with RCC [1]. Bonneville JF suggested those imaging features might be helpful, but are not strictly typical because pituitary adenomas may be on the midline, as well as RCC may be rarely in an off-midline location, while fluid-fluid level and septations are inconstant. Bonneville proposed ancillary signs for differentiating RCC and CPA: intrasellar adenomas give rise to more mass effect compared to less or even no mass effect of RCC; strict midline location, regular convex symmetric anterior surface and close contact with the posterior lobe are characteristic T1WI features of a RCC [5].

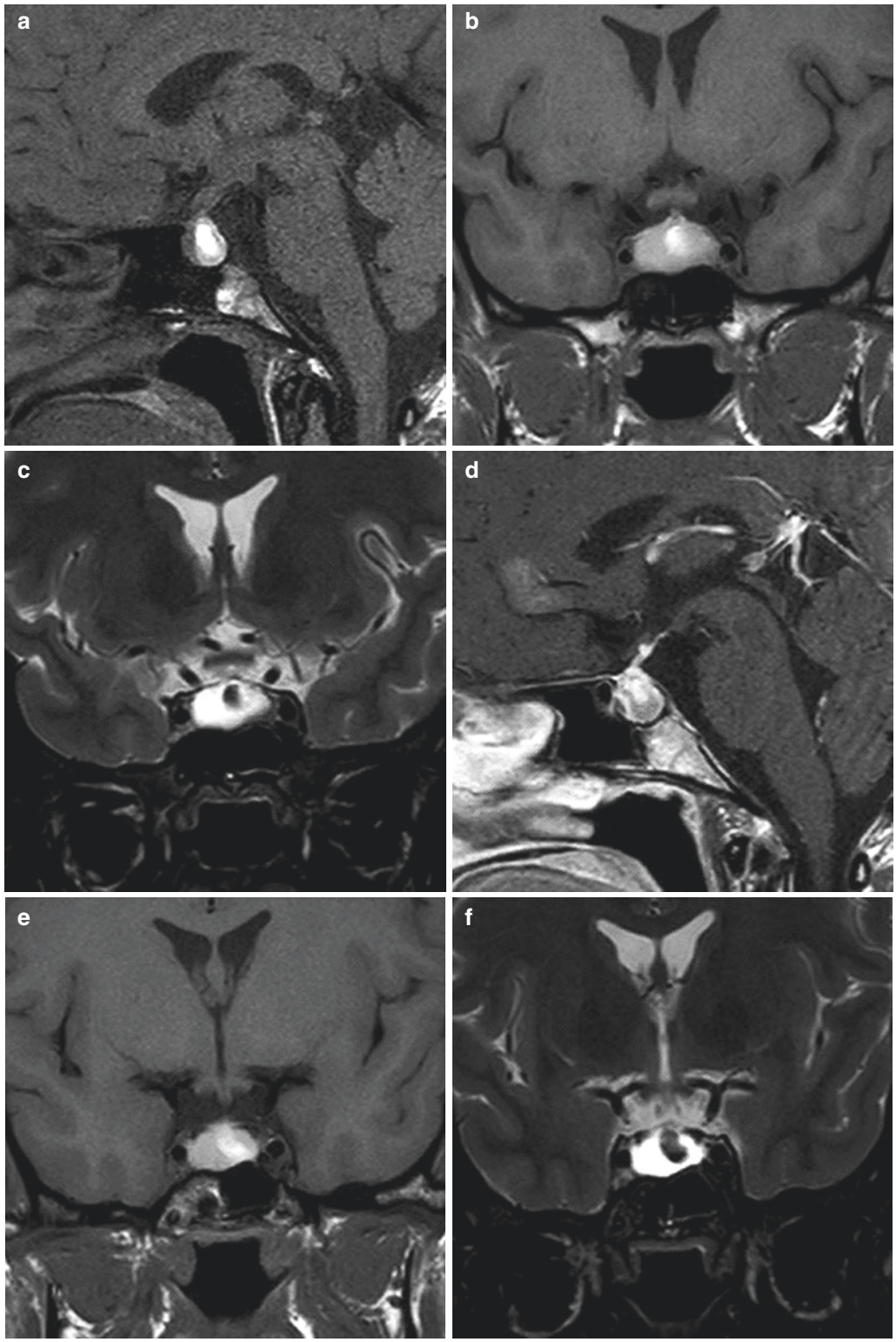

Fig. 6.5 Pituitary MRI pre-contrast sagittal T1WI (**a**), coronal T1WI (**b**, **e**), coronal T2WI (**c**, **f**), post-contrast sagittal T1WI (**d**): intrasellar Rathke's cleft cyst with intracystic nodule adherent from a cyst roof, hyperintense on T1WI (**a**, **b**, **e**), hypointense on T2WI (**c**, **f**). On post-contrast T1WI thin rim of compressed pituitary gland enhanced, intracystic nodule did not enhance. RCC content was slightly hyperintense on pre-contrast T1WI (**a**, **b**, **e**)

In case of our patient, symptoms were not specific for pituitary adenoma but have pointed out to a possible female sex hormone imbalance. Pituitary MRI was a proper choice for imaging work-up: large intrasellar and suprasellar cystic lesion, with rim enhancement and enhancing intracystic nodule, definitely pointed out to a possible RCC with atypical enhancing intracystic nodule. In such case, especially if pituitary hormone level report is not available, the best is to report RCC and CPA as differential diagnosis. Hypopituitarism is typical for symptomatic RCC as well as headache, but hyperprolactinemia is not: pituitary hormone levels have helped us make final, pretreatment, diagnosis. Therefore, if you have a patient with an intrasellar and/or suprasellar expansile cystic pituitary lesion and, according to previously mentioned MRI features, you are not sure if it is a RCC or CPA, look for a pituitary hormone levels to help you decide and report which of those two differential diagnosis is more favoured.

References

1. Park M et al (2015) Differentiation between cystic pituitary adenomas and Rathke cleft cysts: a diagnostic model using MRI. AJNR Am J Neuroradiol 36(10):1866–1873
2. Bonneville JF et al (2005) Magnetic resonance imaging of pituitary adenomas. Eur Radiol 15:543–548
3. Gaddikeri S et al (2013) Rathke cleft cyst: MRI criteria for presumptive diagnosis. Neuroscience 18(3):258–263
4. Wen L et al (2010) Rathke's cleft cyst: clinicopathological and MRI findings in 22 patients. Clin Radiol 65:47–55
5. Bonneville JF (2016) Hemorrhagic pituitary adenoma versus Rathke cleft cyst: a frequent dilemma. http://www.ajnrblog.org. Accessed 01 Apr 2016

Part II

Vascular

Cerebral Proliferative Angiopathy: AVM

7

A 32-year-old female patient, in 8 months of pregnancy, had to perform MRI of the brain as a part of neurological evaluation of ataxia she had suffered from the childhood and never been evaluated before. According to anamnestic data, from a childhood she was motorically clumsy and had problems with coordination, mild degree of hearing loss and a slow rate of speech. During the last 3 years, she described occasional headaches, visual disturbance in the form of oscillopsia while watching television and occasional tremor in right hand. All the symptoms have become pronounced during pregnancy.

In September 2016, MRI of the brain revealed large infratentorial arteriovenous malformation without sign of previous haemorrhage (Figs. 7.1 and 7.2).

I have reported a large arteriovenous malformation of the posterior cerebral fossa, possible cerebral proliferative angiopathy, and recommend consultation of an interventional neuroradiologist regarding digital subtraction angiography after a scheduled caesarean section, to differentiate this vascular malformation as CPA or classical brain AVM. Interventional neuroradiologist appraised this large AVM, according to the Spetzler-Martin scale, as grade V arteriovenous malformation, incurable regarding possible surgery or interventional procedure, but also recommended DSA after delivery.

Caesarean section was scheduled for the beginning of October 2016 and was performed without complications. A patient underwent a recommended DSA at the end of August 2017, which differentiated this large arteriovenous malformation as a classical brain AVM, grade V (Fig. 7.3).

7.1 Cerebral Proliferative Angiopathy or AVM?

When a patient entered MRI machine and examination was commenced, after the first two sequences, sagittal T1WI and axial T2WI were completed, I was a bit astonished by the large infratentorial vascular malformation I saw. It reminded me of "something" I have already seen during lectures on different courses and in the literature but never had a chance to see it in my patients: did I have a patient with cerebral proliferative angiopathy in MRI machine or is it just a large, peculiar classical cerebral arteriovenous malformation?

Cerebral proliferative angiopathy (CPA) is a rare subgroup of AVMs, different from classical brain AVMs, first suggested by Pierre Lasjaunias and his group in 2008. It is congenital condition that differs significantly from classical brain AVMs in terms of epidemiology, clinical presentation, angiographic and histopathological features, natural history and treatment considerations. Classical AVMs consist of a tangle of abnormal arteries and veins without intervening capillary bed [1].

M. Špero, H. Vavro, *Neuroradiology - Expect the Unexpected*,
https://doi.org/10.1007/978-3-319-73482-8_7

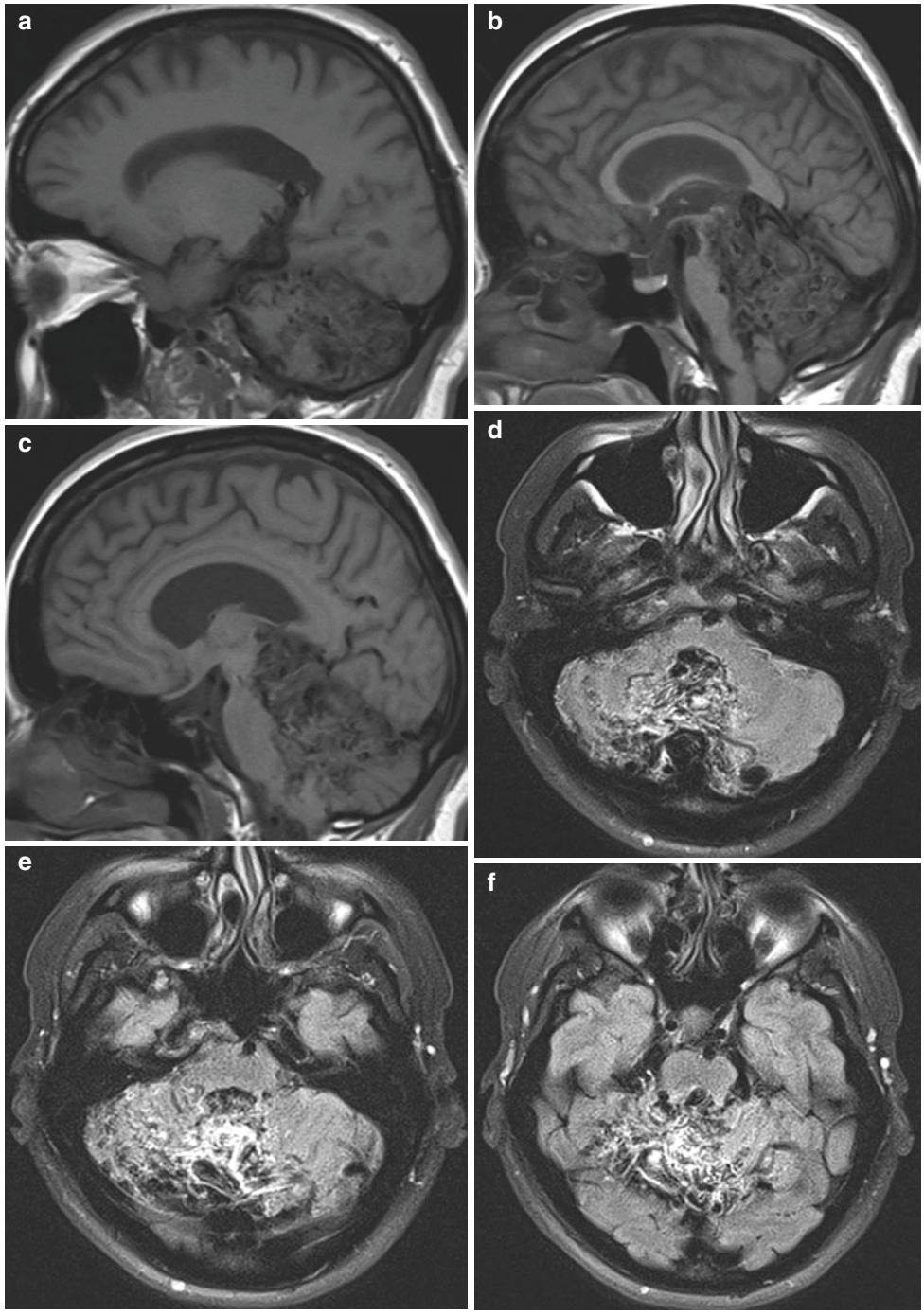

Fig. 7.1 Non-contrast magnetic resonance imaging of the brain, sagittal T1 (**a**–**c**), axial FLAIR (**d**–**f**) and T2WI (**g**–**i**), coronal (**j**–**l**) and sagittal (**m**–**o**) T2WI, axial T2*WI (**p**–**r**), revealed large infratentorial AVM in vermis and predominantly in right cerebellar hemisphere, extending cranially up to mesencephalic tectum and caudally up to foramen magnum. It filled up the fourth ventricle, anteriorly compressed structures of the brainstem, pons and medulla oblongata, while cerebellar tonsils protruded through foramen magnum. AVM consisted of a diffuse network of vascular channels and dilated veins between different vascular territories. Normal brain parenchyma appeared to intermingle between vascular structures of the AVM, with mild reactive marginal gliosis. There were no signs of previous haemorrhage. Cerebral proliferative angiopathy (CPA) or large classical brain arteriovenous malformation

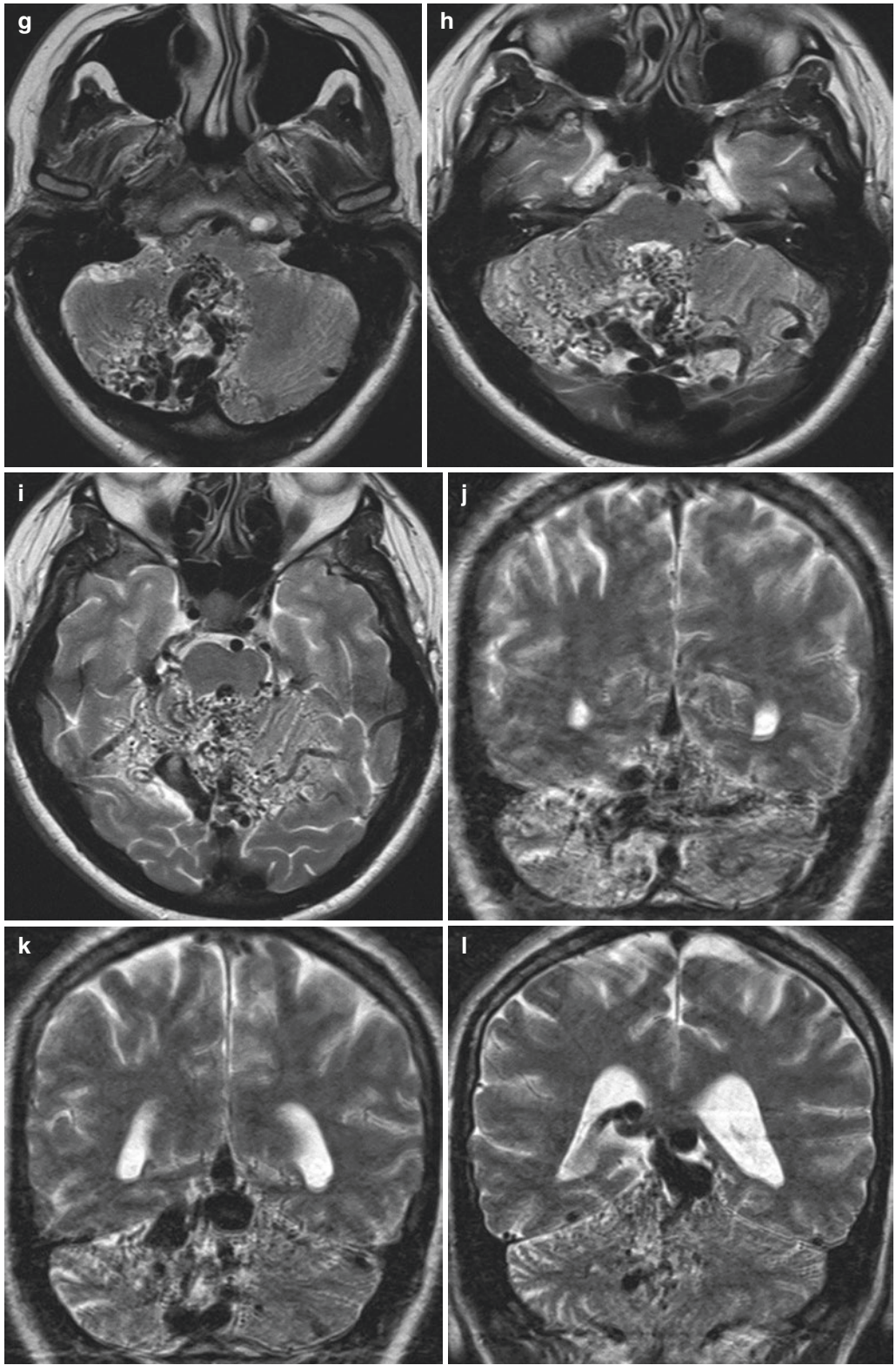

Fig. 7.1 (continued)

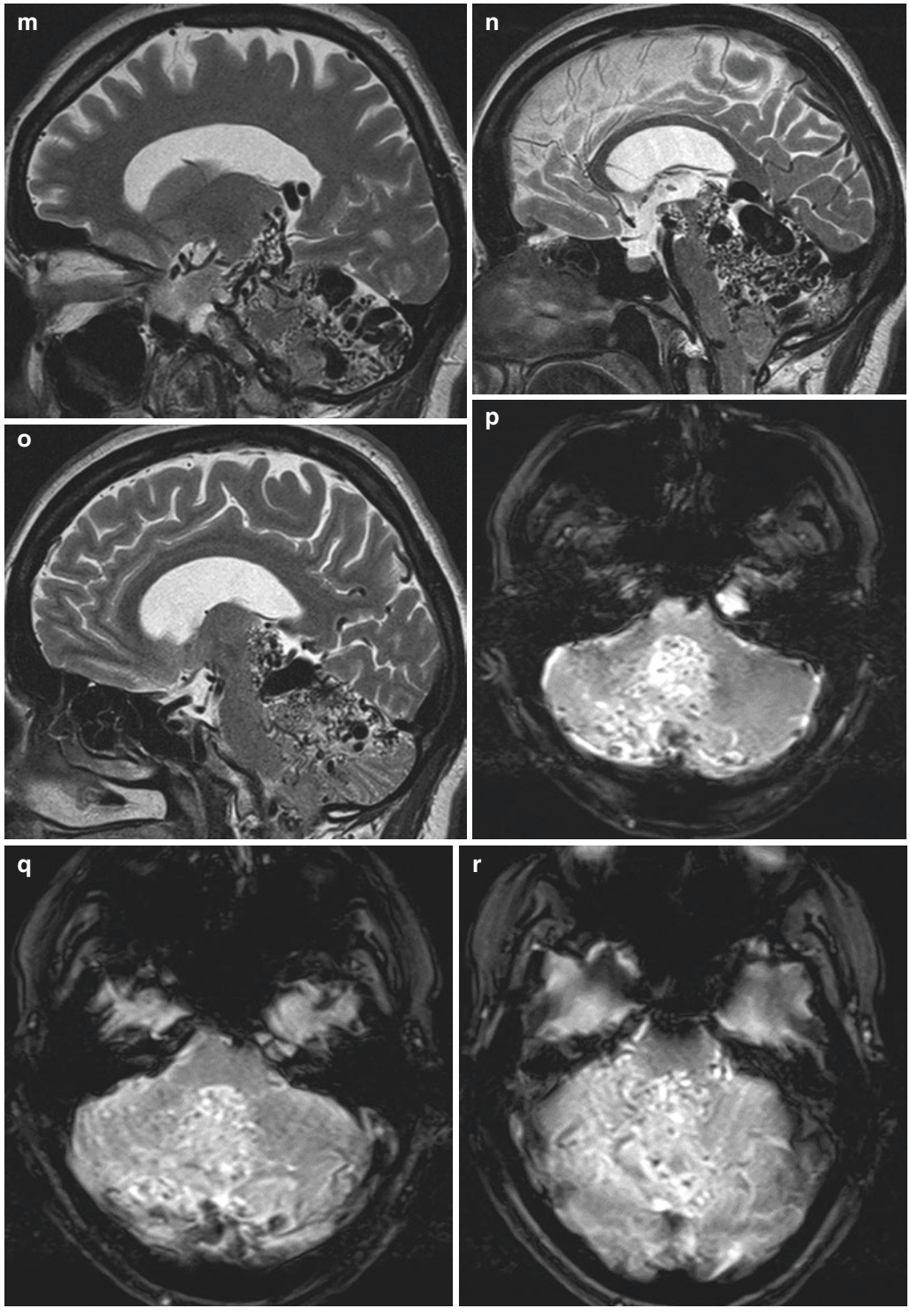

Fig. 7.1 (continued)

Most commonly CPAs present in adolescent and middle-aged females with symptoms depending on the site of CPA, usually headaches, seizures and progressive neurological deficits [1–3]. CPAs are associated with low risk of haemorrhage compared to classical brain AVM, but if presented with haemorrhage, CPAs have a high chance (12%) of recurrent bleeding. CPAs usually have supratentorial location, most commonly in the right hemisphere, while infratentorial location is found in 22% of cases [1, 3].

The pathogenesis of CPA remains unclear; presumably progressive and uncontrolled angiogenesis is induced as a response to cortical ischaemia with the feeding arteries having altered internal elastic lamina and smooth muscle cells and collagenous thickening of the veins. Normal functioning brain is interspersed between anomalous vessels and may present reactive gliosis [1, 2, 4].

Angiographic features of CPA reveal the absence of dominant feeders or flow-related aneurysms: multiple feeding arteries, not or moderately enlarged, contribute equally to a malformation. Nidus is usually large, 3–6 cm, or larger, ill-defined, with scattered "puddling" of contrast persisting into the late arterial and early venous phase within capillary ectasia. Veins are moderately enlarged compared to the size of nidus [1–3]. Perfusion-weighted MRI demonstrates increased blood volume within the nidus with an increased mean transit time which is indicative of capillary and venous ectasias and area of hypoperfusion that could be seen throughout the affected hemisphere [1].

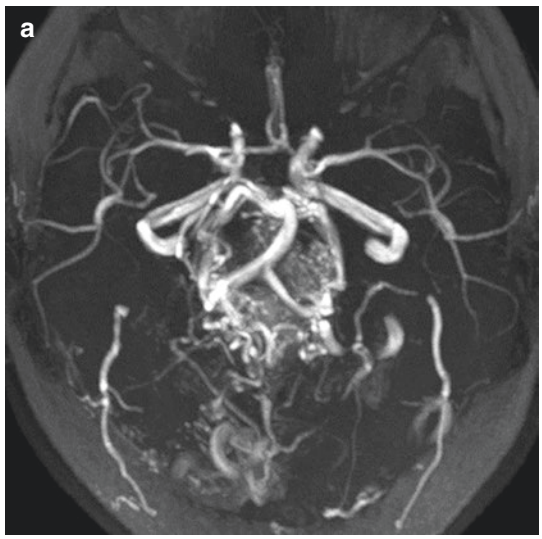

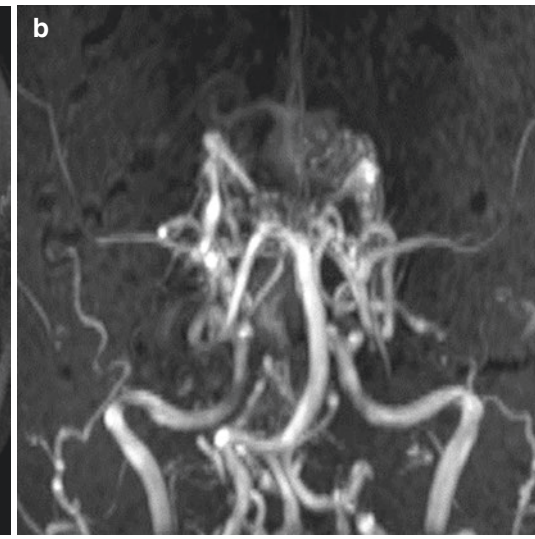

Fig. 7.2 Magnetic resonance angiography, 3D TOF technique (**a**–**c**) and magnetic resonance venography, 3D PC technique (**d**–**f**) revealed dense diffuse network of vascular channels and dilated veins in the midline and predominantly right part of the posterior fossa. There were no dominant arterial feeders and arterial supply came from both posterior cerebral arteries, basilar artery branches and thalamoperforating arteries. Venous drainage was to the straight sinus and to both transverse sinuses, draining veins were enlarged

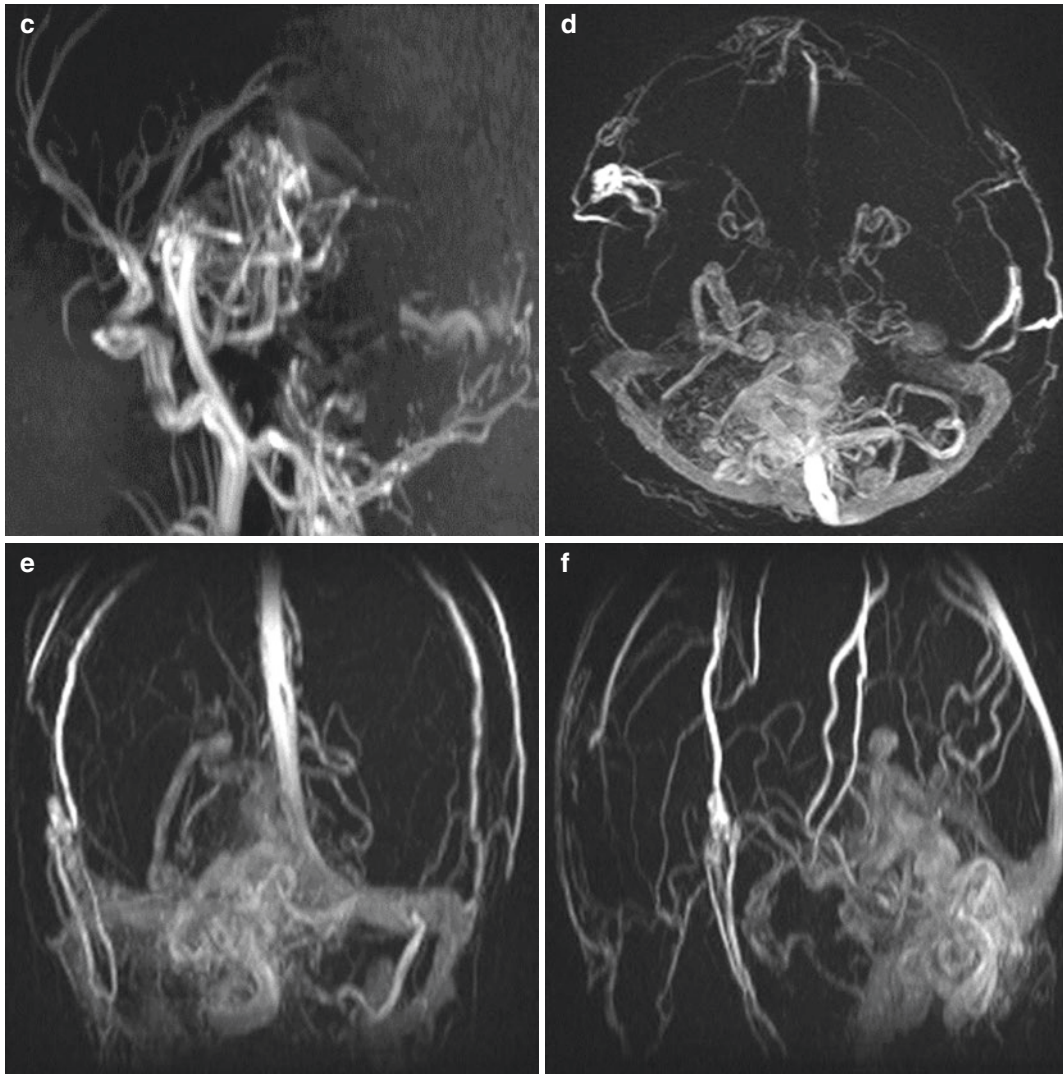

Fig. 7.2 (continued)

MRI features of CPA are described previously. Chronic haemorrhage, gliosis or both may be found in adjacent parenchyma; post-contrast T1W sequences demonstrate enlarged serpiginous vessels.

I have presumed I have a case of CPA in front of me due to patient sex, age and clinical presentation, described MRI features with normal intermingled brain parenchyma in-between vascular structures and absence of large arterial feeders, although veins were remarkably dilated. Case report published by Kumar et al. in 2015, described infratentorial haemorrhagic CPA, led me to suspect that maybe I could be on a right track regarding MRI features [3]. CPA may be diagnosed using MRI and MRA, but DSA remains the "gold standard" to confirm or exclude the diagnosis, because it allows direct vessel visualisation, shunt estimation and possibility of intervention if required. In the case, DSA was performed about 11 months after the brain MRI, confirming angiographic features in terms of classical brain AVM. DSA assessed arterial supply more accurately in comparison to MRA:

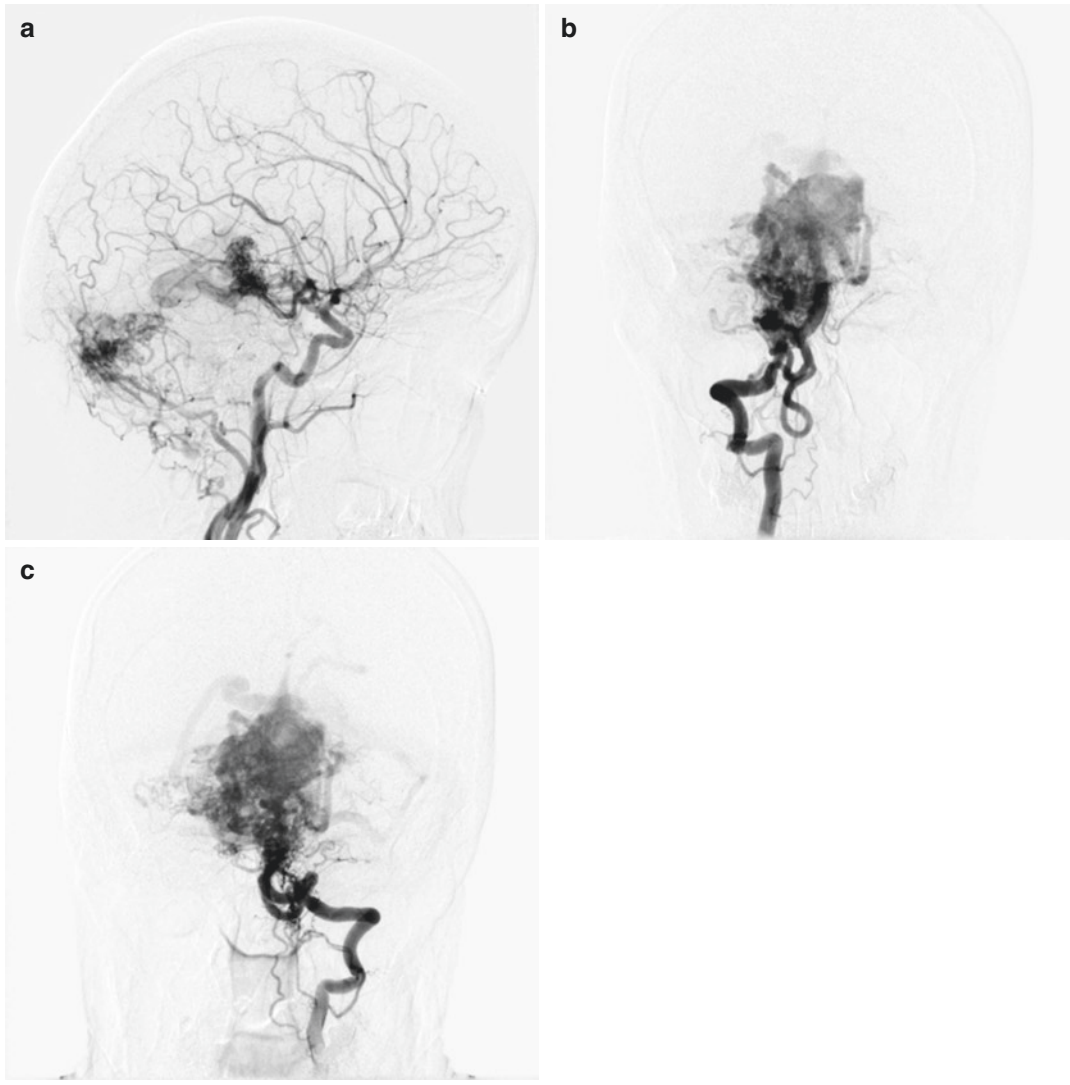

Fig. 7.3 Cerebral digital subtraction angiography (courtesy of assisted professor David Ozretić and professor Marko Radoš), right internal carotid artery lateral view (**a**), right (**b**) and left (**c**) vertebral artery frontal view: confirmed large predominantly infratentorial, plexiform arteriovenous malformation with numerous short feeding arteries that vascularised the greatest part of the nidus in the posterior cerebral fossa. Catheterisation of the right common carotid artery showed vascularisation of the greatest part of the nidus through feeders coming from posterior choroidal arteries over the posterior communicating artery. Catheterisation of the left common carotid artery and vertebral artery showed vascularisation of the nidal segments through the posterior inferior cerebellar artery, superior cerebellar artery and choroidal group of arteries coming from the P1 segment of the posterior cerebral artery. The greatest part of the nidus was drained over deep venous system, dilated draining veins had developed venous ectasias. There were no capillary ectasias and scattered "puddling" of contrast within them, and there were no transdural supply. Therefore, large classical brain arteriovenous malformation, grade V, was reported

there were no dominant arterial feeders but numerous short feeders coming from different arterial territories. The method also confirmed there was no capillary bed and its ectasias with scattered "puddling" of contrast within them, and there were no transdural supply as well. Cerebral DSA was performed by an interventional neuroradiologist and described angiographic features

confirmed vascular malformation not to be a CPA. Therefore large incurable AVM, grade V, was reported at the end.

It is important to differ classical brain AVM and CPA because of different treatment options. Unfortunately, primary treatment in CPA is nor surgery, radiation therapy or embolization because those treatment options carry risk of permanent neurological deficit due to intervening normal brain parenchyma between vascular channels in CPA. Symptomatic medication therapy, including analgesic and antiepileptic drugs, is usually offered to such patients. Limited arterial embolization in non-eloquent areas may be performed for patients presenting with uncontrolled seizures and headaches [1–3, 5].

In case of this patient, MRI features have led me to suspect this large malformation to be CPA, but DSA has confirmed large classical brain AVM. Cerebral DSA did not change treatment options, since this large vascular malformation is considered incurable. Infratentorial CPAs are difficult to manage because critical vessels that originate in the posterior vascular territory ultimately perfuse both the vital structures of posterior fossa and CPA; therefore, any mentioned treatment procedure may be fatal [3].

References

1. Lasjaunias PL et al (2008) Cerebral proliferative angiopathy clinical and angiographic description of and entity different from cerebral AVMs. Stroke 39:878–885
2. Rohit PSG (2015) Diffuse proliferative cerebral angiopathy: a case report and review of the literature. J Radiol Case Rep 9(9):1–10
3. Kumar S et al (2015) Infratentorial haemorrhagic cerebral proliferative angiopathy: a rare presentation of a rare disease. Asian J Neurosurg 10(3):240–242
4. Radalle Biasi P et al (2015) Cerebral proliferative angiopathy – description of a rare clinical entity. Arq Bras Neurocir 34:82–85
5. Liu P et al (2016) Cerebral proliferative angiopathy: clinical, angiographic features and literature review. Interv Neuroradiol 22(1):101–107

Part III

Infections/Metabolic/Toxic

8 Pulmonary Arteriovenous Fistulas and Nocardial Brain Abscess in Close Relatives

This is a story about a 63-year-old female patient, a mother, and a 41-year-old male patient, a son, who were both previously operated because of pulmonary arteriovenous fistulas (PAVFs): mother in 1996 and a son in 1995. In 2013, they were both admitted to our emergency hospital department (EHD) due to neurological symptoms.

On December 19, 2012, mother had a sudden onset of left-sided weakness, but she was admitted to the EHD in 2013 on January 3: during a two-week period, weakness did not progress or improve. At the admission total leukocyte count and C-reactive protein levels were normal; lumbar puncture was not performed.

Patient was hospitalised and diagnostic work-up commenced (Figs. 8.1, 8.2, and 8.3). MRI of the brain (Fig. 8.2) followed the CT performed at the admission (Fig. 8.1) confirming imaging features of brain abscesses.

Seven days after the admission, 63-year-old patient was operated and brain abscesses evacuated.

On September 9, 2013, her son developed tension headache which mildly progressed during the day: he also had difficulties pronouncing some words. Therefore, he looked for a help in the EHD of our hospital. At the admission total leukocyte count was normal, while C-reactive protein level was elevated, measuring 15.5 mg/L (normal level <5 mg/L), lumbar puncture revealed slightly elevated protein level, normal glucose level and 50 white blood cells/μL.

Due to the CT report, patient was hospitalised: MRI of the brain followed the CT examination confirming two brain abscesses in the right temporal lobe (Figs. 8.4 and 8.5).

Neurosurgeon did not trust neuroradiologist report; he has suspected described lesion was a tumour, not an abscess. Three days after the admittance, patient was operated, lesions were evacuated and abscess was confirmed on pathohistology.

Microbiology of abscesses revealed *Nocardia* species as a causative microorganism, both in mother and son. Medicamentous therapy with trimethoprim and sulfamethoxazole followed surgery in both cases.

8.1 Pulmonary Arteriovenous Fistulas and Nocardial Abscess

If you have a patient with a brain abscess and cannot find usual source of infection from the ear, nose, orbits or throat, look further for possible source from the heart, or like in our case, from the lung. Pulmonary arteriovenous fistulas (PAVFs) or malformations are caused by abnormal communications between pulmonary arteries and pulmonary veins, without an intervening

M. Špero, H. Vavro, *Neuroradiology - Expect the Unexpected*,
https://doi.org/10.1007/978-3-319-73482-8_8

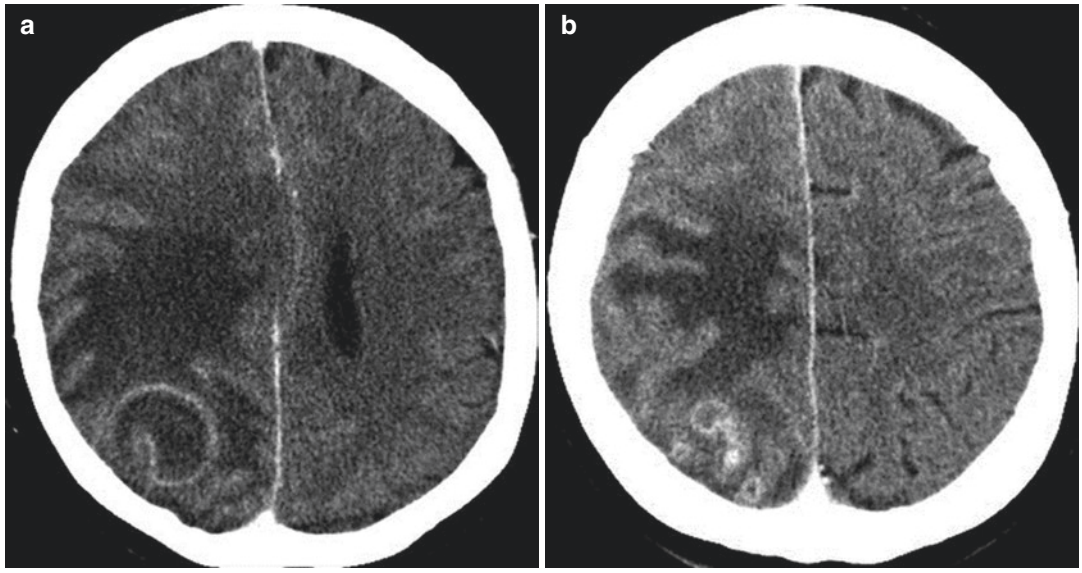

Fig. 8.1 Post-contrast computed tomography of the brain, axial scans (**a**, **b**), performed at the emergency admission revealed subcortical expansile ring-enhancing, hypodense lesion in the right parietal lobe with marked vasogenic oedema. At the upper rim of the lesion, there were several smaller ring-enhancing lesions

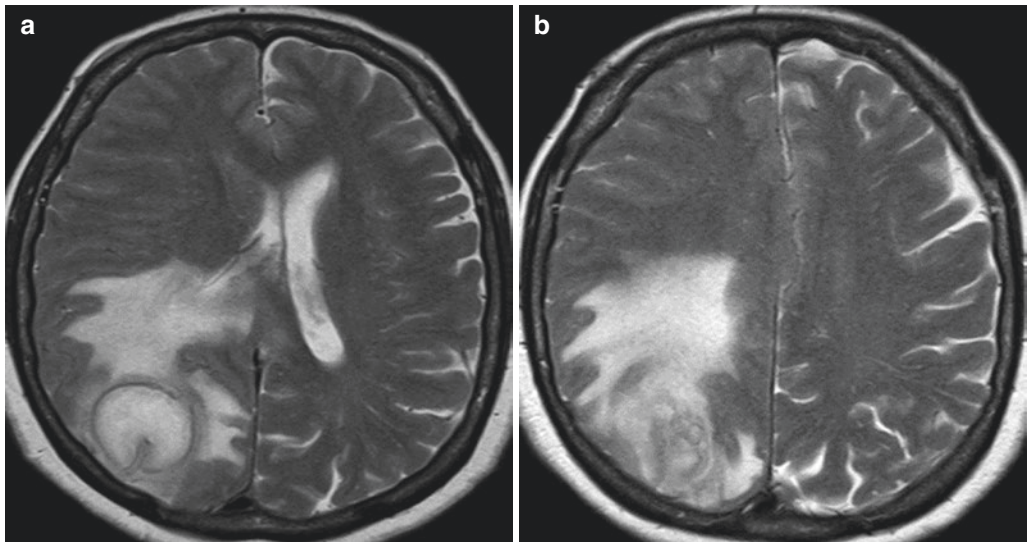

Fig. 8.2 Magnetic resonance imaging of the brain showed brain abscess subcortical in the right parietal lobe parenchyma with several smaller daughter abscesses flourishing from the large parent abscess, surrounded with marked vasogenic oedema: axial (**a**, **b**) and coronal (**g**) T2WI, axial FLAIR (**d**, **e**), axial DWI (**c**), ADC (**f**), sagittal pre-contrast T1WI (**h**), sagittal (**i**), coronal (**j**, **k**) and axial (**l**) post-contrast T1WI. Well-defined oval and round expansile lesions of different size, hyperintense with hypointense collagen capsule on T2WI which were mildly hyperintense on pre-contrast T1WI, showing ring contrast enhancement on post-contrast T1WI. Diffusion was restricted in the abscess wall and cavity

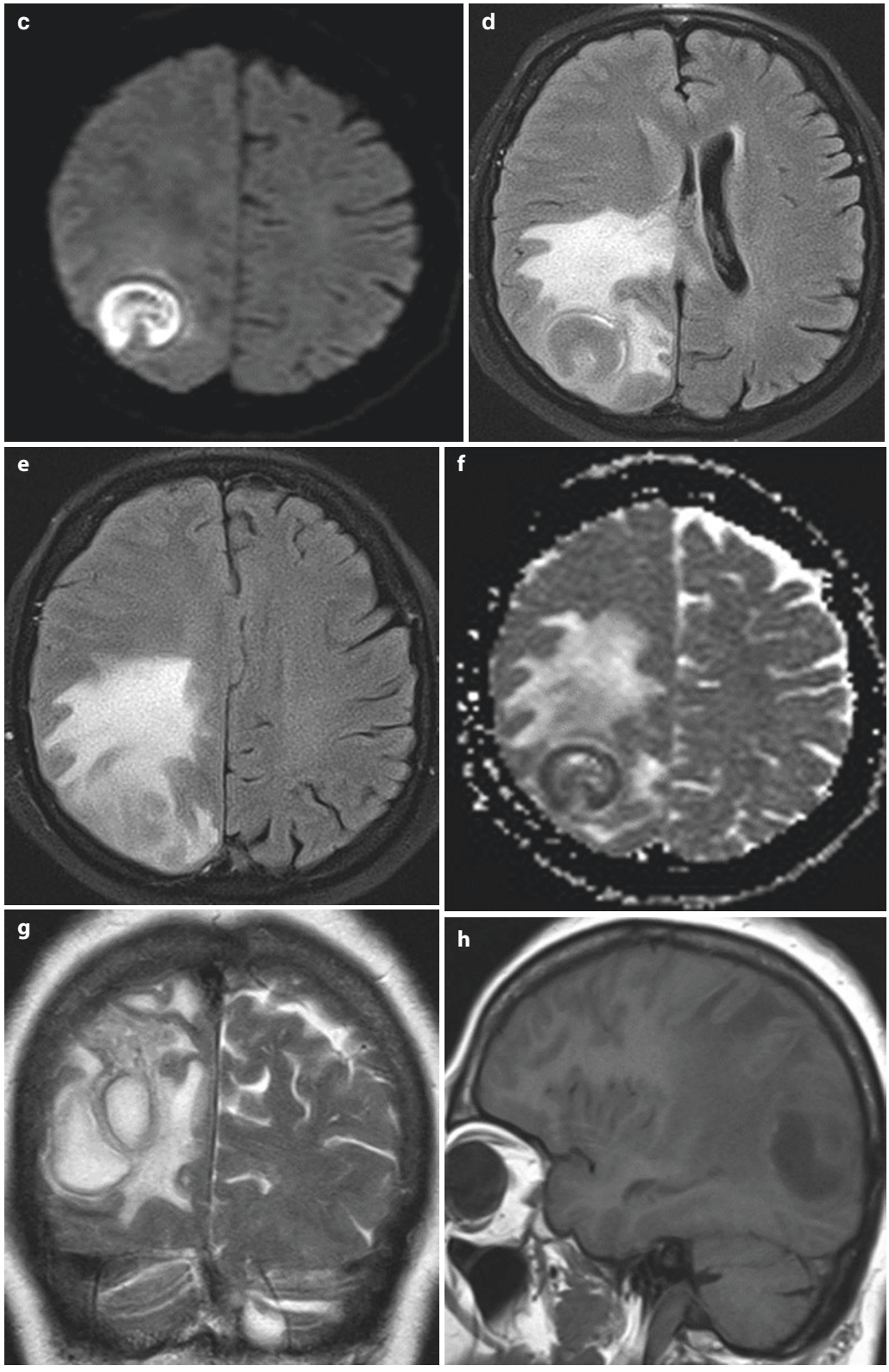

Fig. 8.2 (contineud)

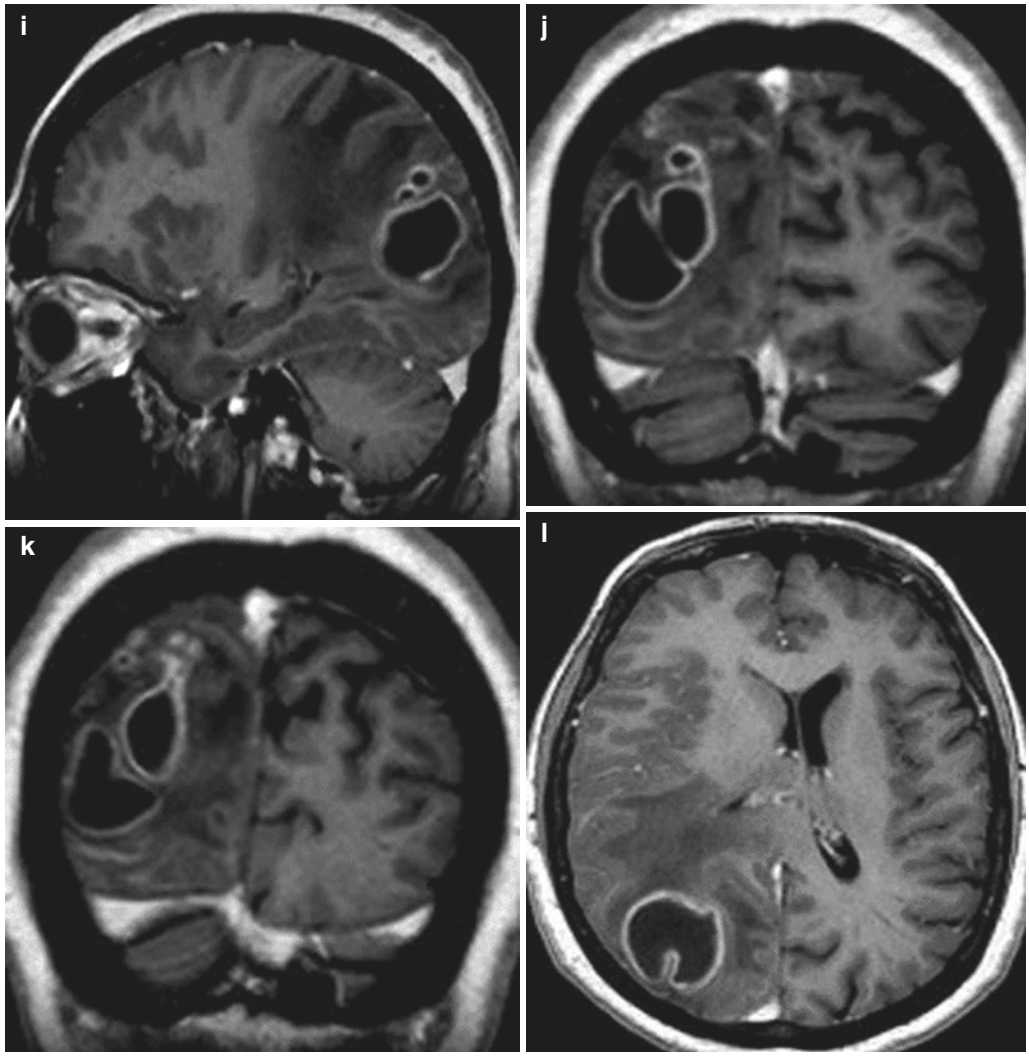

Fig. 8.2 (contineud)

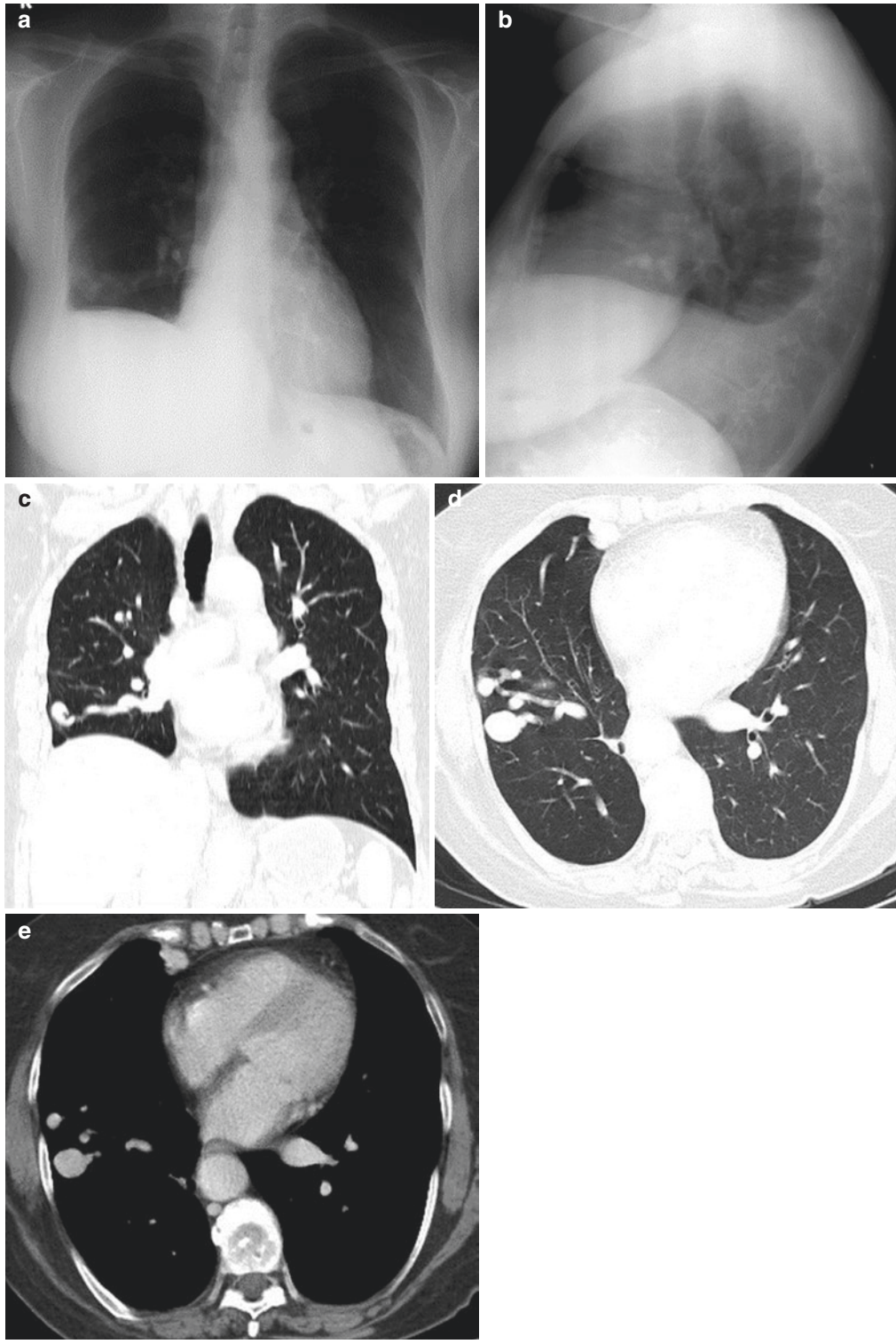

Fig. 8.3 Plain (**a**) and right lateral (**b**) chest radiograph at the admission, coronal (**c**) and axial (**d**, **e**) post-contrast chest computed tomography performed during hospitalisation as a part of diagnostic work-up of a 63-year-old female patient. Chest radiographs and computed tomography revealed postoperative changes after right inferior lobectomy (1996) and fistulous vascular abnormality in the middle pulmonary lobe

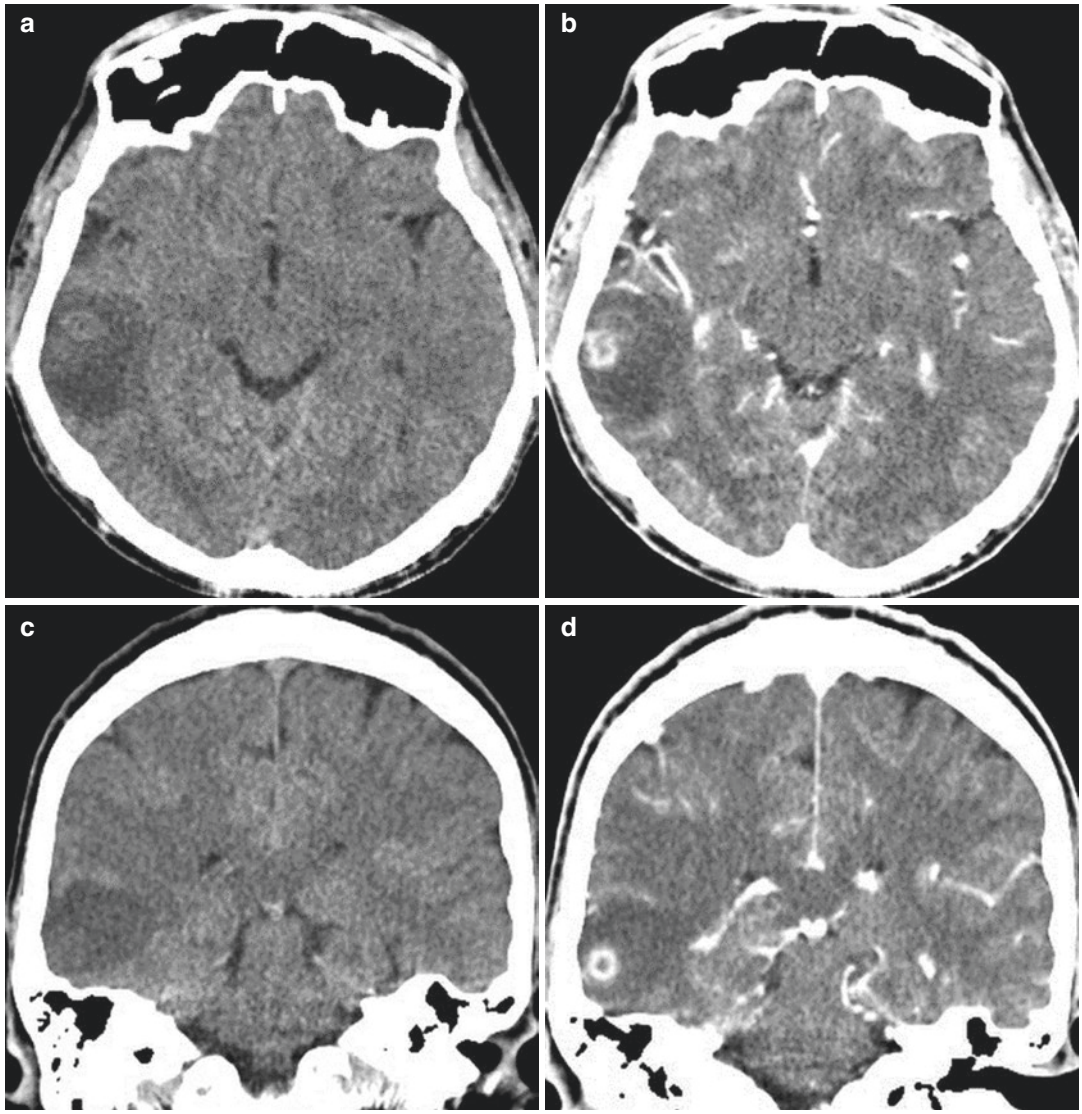

Fig. 8.4 Computed tomography of the brain performed at the emergency admission revealed two subcortical expansile lesions in the right temporal lobe, iso- and hypodense on pre-contrast axial (**a**) and coronal (**c**) scans, showing ring enhancement on post-contrast axial (**b**) and coronal (**d**) scans, surrounded with moderate vasogenic oedema. Radiologist who was on call reported primary or secondary neoplasm

capillary bed, resulting in pulmonary right to left shunt. Most commonly are congenital, but could be acquired in hepatic cirrhosis, mitral stenosis, trauma or chronic infections [1].

Congenital PAVFs are twice as common in female. Up to 70% of PAVFs are unilateral and found in lower lobes. They are classified as simple or complex: simple (about 80%) have a single feeding segmental artery leading to a single draining pulmonary vein, while complex have two or more feeding arteries or draining veins. About 95% PAVFs are supplied by pulmonary arteries, less frequently by systemic arteries, while drainage is usually to left atrium. Individual PAVF measures from 1 to 5 cm in size: usually a single PAVF less than 2 cm in diameter does not cause symptoms [1].

Abnormal vascular connections in PAVFs result in bypassing filtering effect of pulmonary

capillaries and right to left shunting [2, 3]. When feeding arteries are larger than 3 mm in diameter, consequent paradoxical septic or non-septic embolisms result in the most frequently reported central nervous system complications including strokes (18%), transient ischaemic attacks (43%), brain abscesses (9%), migraine headaches (43%) and seizures (8%) [1, 2]. The most serious neurological complication is a brain abscess occurring in about 5 to 10% of patients with PAVFs [3].

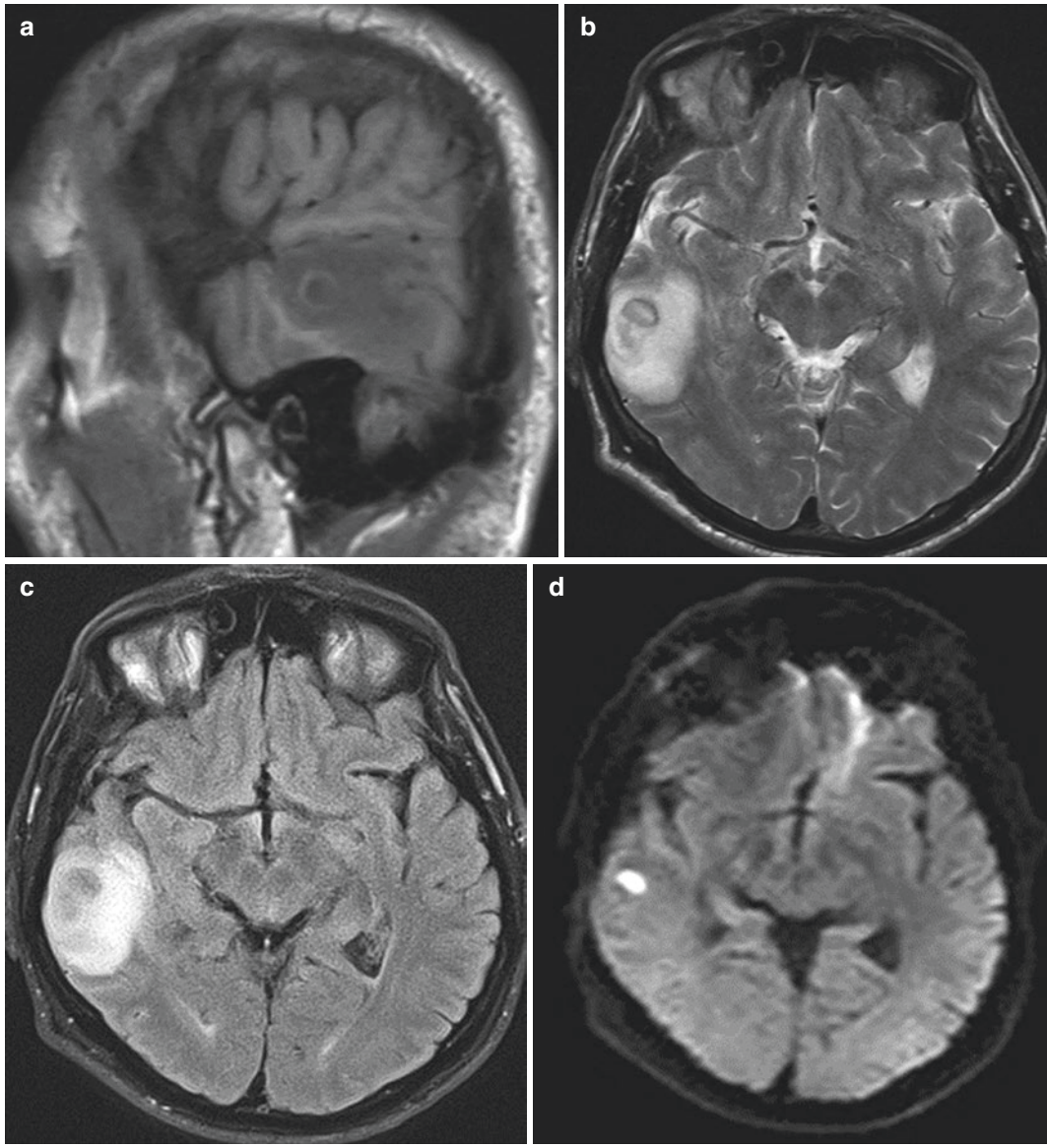

Fig. 8.5 Magnetic resonance imaging of the brain demonstrated two small subcortical brain abscesses in the right temporal lobe surrounded with moderate vasogenic oedema which was not finger-like: pre-contrast sagittal T1WI (**a**), axial T2WI (**b**) and FLAIR (**c**), axial DWI (**d**) and ADC (**e**), axial (**f**), coronal (**g**, **h**) and sagittal (**i**) post-contrast T1WI. Two small, oval, well-circumscribed expansile lesions located one behind the other: anterior lesion had typical imaging features of frank abscess, while posterior lesion did not revealed T2WI hypointense signal of collagen capsule neither restricted diffusion, while on post-contrast T1WI revealed irregular contrast enhancement. On sagittal post-contrast T1WI, it seemed like one lesion was "coming out" from the other

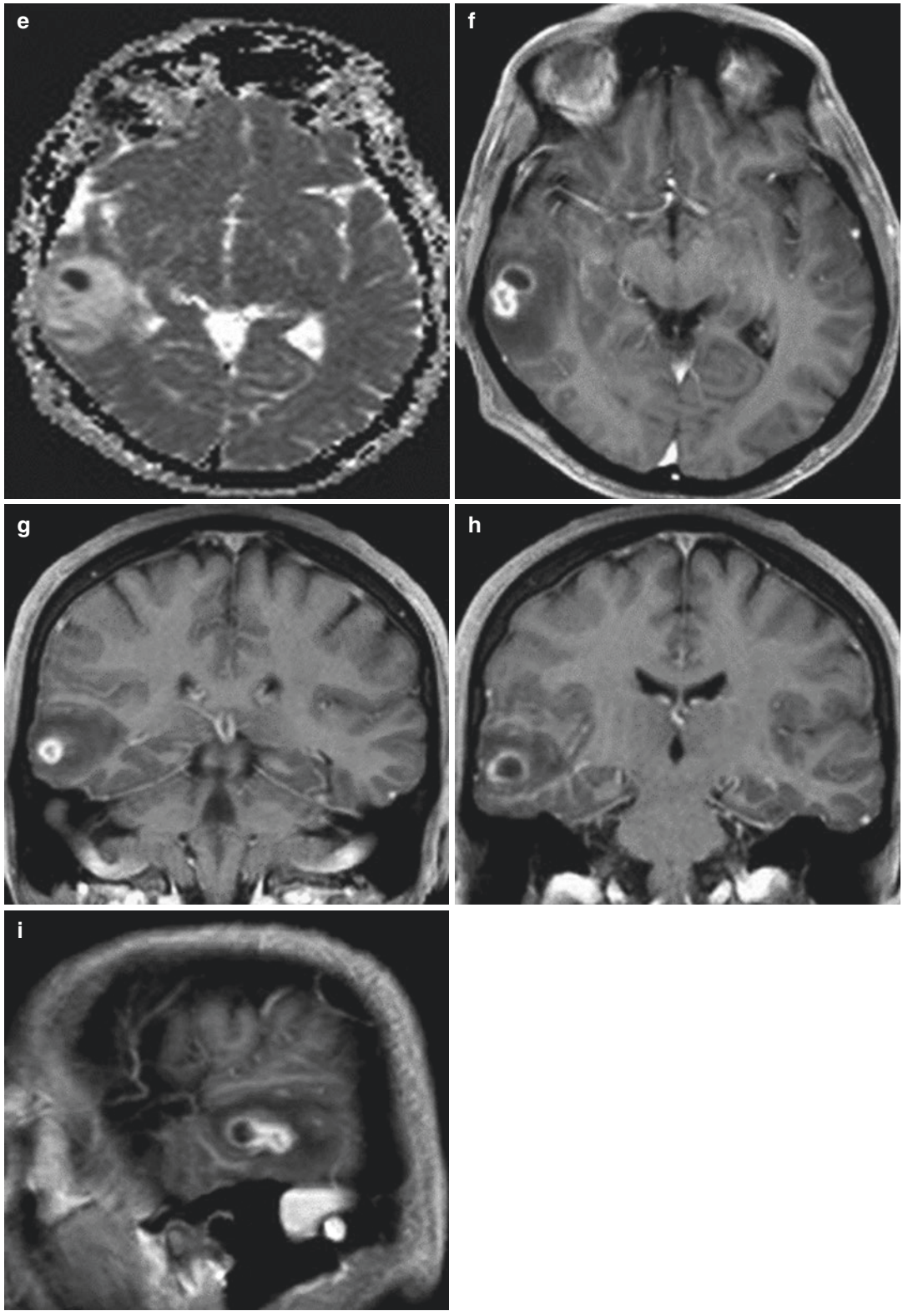

Fig. 8.5 (continud)

Nocardia is a genus of weakly staining Gram-positive, rod-shaped bacteria that forms partially acid-fast beaded branching filaments acting as fungi but being truly bacteria. Those organisms are mostly isolated from plants and soil, while infection usually occurs after inhalation or direct skin inoculation [4]. Nocardial brain abscesses are relatively uncommon (2% of all abscesses) and are usually secondary sequels of haematogenous dissemination from the lungs, as the most common primary site, in immunocompromised patients with predisposing factors such as malignancy, diabetes mellitus, malnutrition and uraemia. But it may also appear in immunocompetent patients [5]. Clinical presentation of this insidious brain infection is not specific and includes headaches, focal neurological deficits and seizures.

It is important not to misdiagnose brain abscess for a metastatic tumour which unfortunately is not uncommon, especially with radiologists who are inexperienced in the field of neuroradiology. On brain CT, it usually presents as round or oval hypodense expansile lesion with thin and ring-enhancing wall, surrounded by vasogenic oedema which may not be present around small abscesses. Surrounding oedema may extend through white matter in finger-like fashion, and in case of a solitary abscess, it may be misdiagnosed for a metastatic tumour, especially if a pulmonary nocardiosis is presented with multifocal nodules or mass. MRI of the brain is the method of choice to distinguish metastasis from brain abscess and possibly refer to it as a pyogenic or fungal abscess.

Pyogenic abscesses of haematogenous origin are usually located at the grey-white matter junction in the distribution of the anterior or middle cerebral arteries [6]. In brain abscess, necrotic debris accumulates centrally, while collagenous capsule is formed around it. Capsule of a brain abscess has isointense to slightly hyperintense rim on T1WI, while on T2WI rim is hypointense due to the presence of paramagnetic free radicals within the activated microglia, collagen and haemorrhage [6–8]. On SWI, pyogenic abscess demonstrates the dual-rim sign as its distinctive feature, and it is not present in fungal abscess. Dual-rim sign consists of two concentric rims surrounding the central cavity at lesion margins: the outer one is hypointense and inner one hyperintense compared with the cavity content on SWI [8]. Pyogenic abscess demonstrates restricted diffusion on DWI with low ADC values in the abscess cavity due to restricted motion of water molecules in the organised purulent setting of microorganisms, macromolecules and intact inflammatory cells. The ring enhancement on post-contrast T1WI is attributed to the disrupted blood-brain barrier and may persist for up to 8 months after medication treatment: reliable signs of good response to medication treatment are shrinkage of the necrotic centre and decrease in capsular hypointensity on T2WI [9]. MR spectroscopy in pyogenic abscess wall reveals amino acids, lipid and lactate and acetate and succinate which are usually seen only in pyogenic abscesses [6].

Nocardial brain abscesses can progress rapidly and have significant morbidity and mortality rates (31%) [5]. Therefore, prompt diagnosis followed by aggressive surgical management and antibiotics treatment according to the drug sensitivity test is necessary. The low specificity of CNS nocardiosis imaging features is a problem, but it is important to recognise abscess as an inflammatory process, not a metastatic tumour or even tuberculosis; therefore, the accurate diagnosis will not be delayed and prompt treatment may commence on time.

References

1. Gossage JR, Kanj G (1998) Pulmonary arteriovenous malformations a state of the art review. Am J Respir Crit Care Med 158:643–661
2. Moradi M, Adeli M (2014) Brain abscess as the first manifestation of pulmonary arteriovenous malformation: a case report. Adv Biomed Res 3:28
3. Nam TK et al (2017) Brain abscesses associated with asymptomatic pulmonary arteriovenous fistulas. J Korean Neurosurg Soc 60(1):118–124
4. Lyu X et al (2017) Radiological findings in patients with nocardiosis: a case series and literature review. Radiol Infect Dis 4:64–69
5. Zhang Y et al (2016) Nocardial brain abscess in an immunocompetent patient and review of the literature. Chin Neurosurg J 2:26

6. Luthra G et al (2007) Comparative evaluation of fungal, tubercular, and pyogenic brain abscesses with conventional and diffusion MR imaging and proton MR spectroscopy. Am J Neuroradiol 28:1332–1338
7. Nandhagopal R et al (2014) Nocardia brain abscess. Q J Med 107:1041–1042
8. Antulov R et al (2014) Differentiation of pyogenic and fungal abscesses with susceptibility-weighted MR sequence. Neuroradiology 56:937–945
9. Sud S et al (2008) Case series: Nocardiosis of the brain and lungs. Indian J Radiol Imaging 18(3):218–221

Cysticercosis: Multiple Metastases

9

Headache and dizziness lasting for 3 weeks made this 55-year-old lady seek medical help at the neurological clinic. Her initial neurological status was normal; personal medical history was unremarkable. The neurologist referred her to a brain CT examination (Fig. 9.1).

A MRI examination of the brain was requested for further differentiation of the lesions (Fig. 9.2).

Further radiologic and serologic work-up was done, and a detailed medical history obtained. The patient remembered consuming uncertified pork meat of dubious quality approximately a year ago.

Immunofluorescent and immunosorbent (ELISA) serology test came positive for cysticercosis.

CT examination of thorax, abdomen and pelvis did not reveal convincing evidence of a possible primary tumour; there were two mediastinal peripherally calcified cystic lesions along the right tracheal wall, of uncertain aetiology. There were also several mildly enlarged paratracheal lymph nodes (Fig. 9.3).

The patient was treated with albendazole for 8 days, but during the course of therapy, her clinical status deteriorated. Meanwhile, the tumour markers serology report came in positive for CA 15.3 and CEA

She was subjected to stereotactic brain biopsy—histopathology reported metastatic brain carcinoma, positive for CK-7 (cytokeratin 7) and TTF-1 (thyroid transcription factor 1).

Ultrasound and CT exams of the neck revealed a nodular lesion in the inferior pole of the left thyroid gland lobe, as well as multiple enlarged lymph nodes. Cytology obtained by FNA of the biggest lymph node revealed a papillary thyroid carcinoma (Fig. 9.4).

Further deterioration of patient's status prompted thoracotomy and removal of the peripherally calcific masses next to the trachea. Histologically, the mass was in keeping with a papillary carcinoma of the thyroid gland.

9.1 Papillary Thyroid Carcinoma

Papillary thyroid carcinoma (PTC) is the most common neoplasm of the thyroid gland, accounting for approximately 70% of thyroid neoplasms and 85% of thyroid malignancies. Approximately 50% of patients have a nodal involvement at presentation, usually of the ipsilateral lymph nodes. The incidence of distant metastasis at the time of diagnosis is generally low. The usual metastatic sites are lung and bone, while brain metastases are extremely rare, with a relatively short time of survival after diagnosis of approximately 12 months [1]. Higher incidence of distant metastasis with a serious impact on survival is found in patients younger than 20 and older than 60 years of age, harbouring higher-grade tumours measuring more than 4 cm and having an extra-thyroid tumour focus at the time of initial examination [2].

M. Špero, H. Vavro, *Neuroradiology - Expect the Unexpected*,
https://doi.org/10.1007/978-3-319-73482-8_9

The presentation of PTC brain metastasis varies from solitary, homogenously enhancing nodular lesions to multiple cystic foci. When multiple cystic, as in this case, the differential diagnoses include multiple microabscesses, fungal infections and cysticercosis.

9.2 Neurocysticercosis

Neurocysticercosis (NC) is a brain infection caused by the pork tapeworm (*Taenia solium*). The time interval between the infection and onset of symptoms is very variable, ranging from 1 to

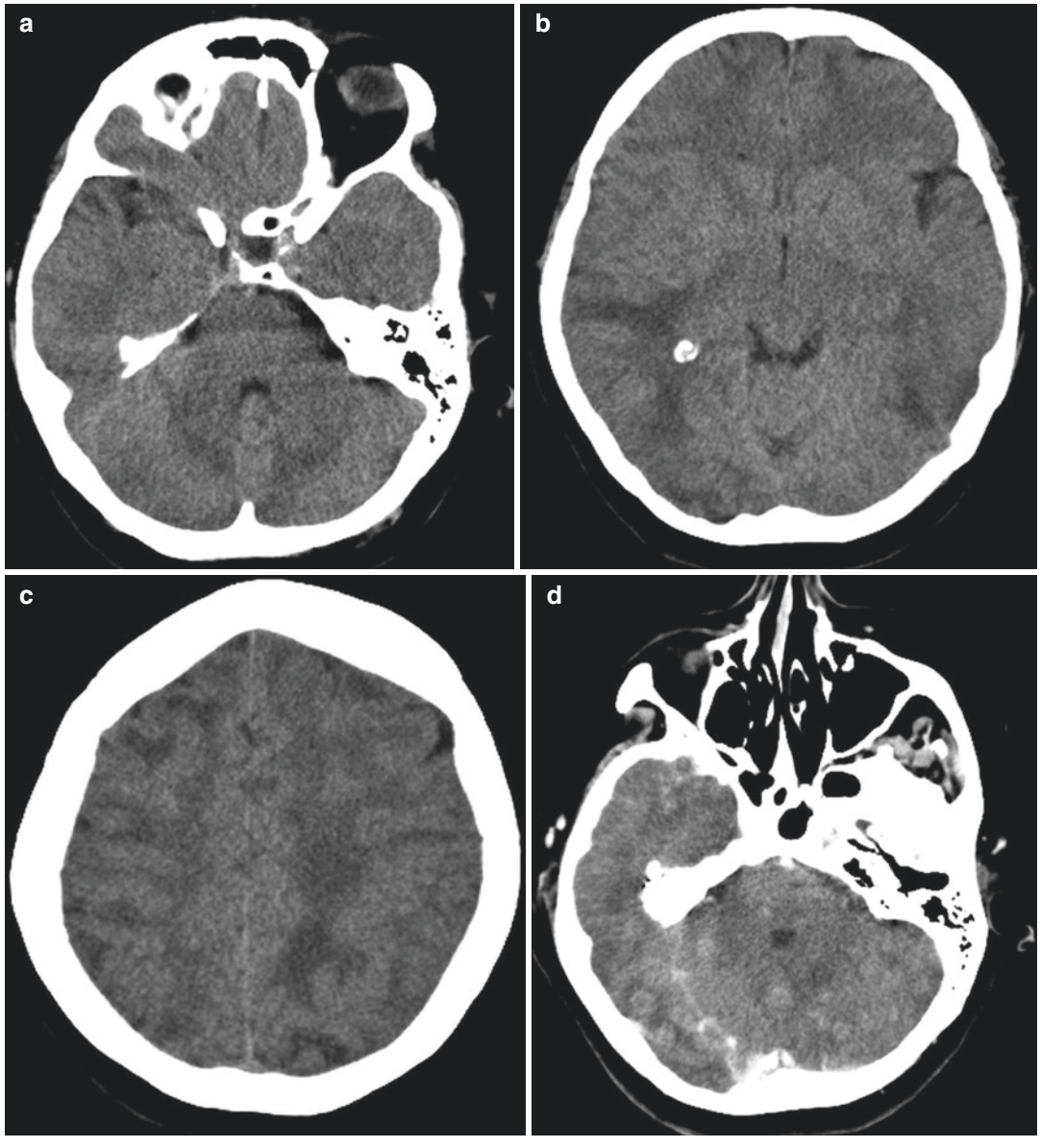

Fig. 9.1 CT examination of the brain. Axial non-enhanced (**a**–**c**) and contrast-enhanced (**d**–**f**) images. The report described numerous infratentorial and supratentorial ring-enhancing lesions up to 10 mm in diameter, some with perifocal oedema, which represent metastases. Differential diagnosis included multiple abscesses

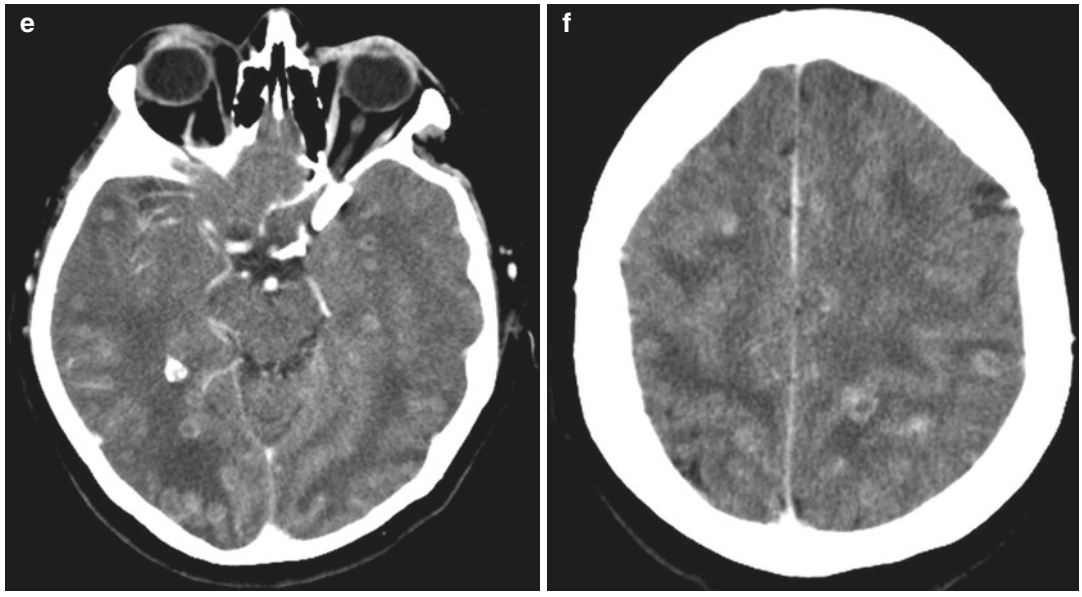

Fig. 9.1 (continued)

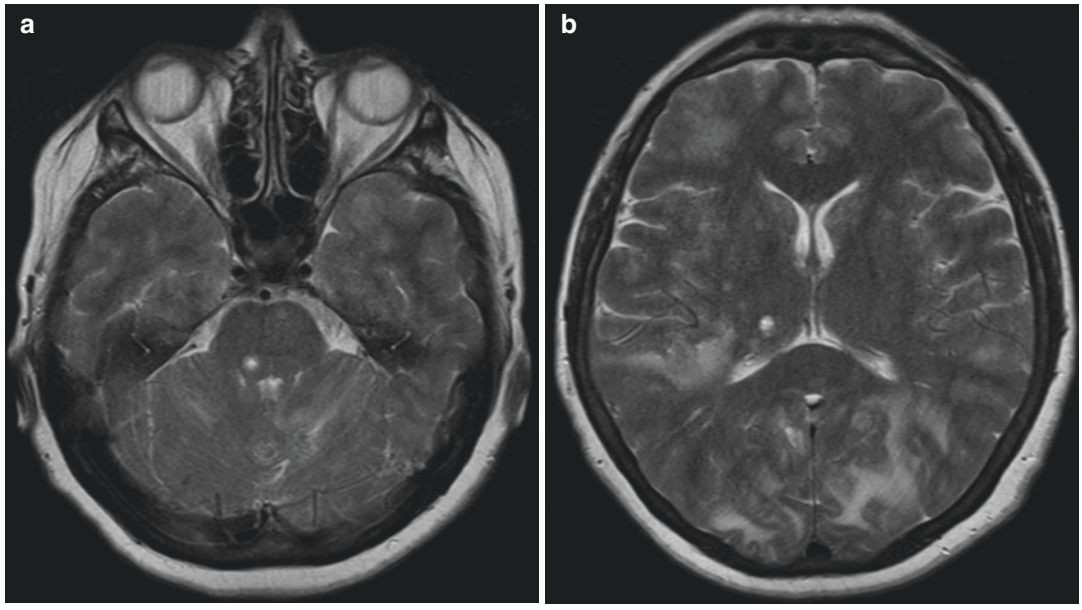

Fig. 9.2 MRI examination of the brain. Axial T2WI (**a**–**c**), DWI (**d**), T2-FLAIR (**e**, **f**), post-contrast axial T1WI (**g**–**i**). Multiple infratentorial and supratentorial parenchymal and subarachnoid cystic lesions, some of them with a tiny solid central nodule, which enhance peripherally and demonstrate perifocal oedema, were thought to represent neurocysticercosis, with most of the lesions in vesicular and colloidal vesicular stage

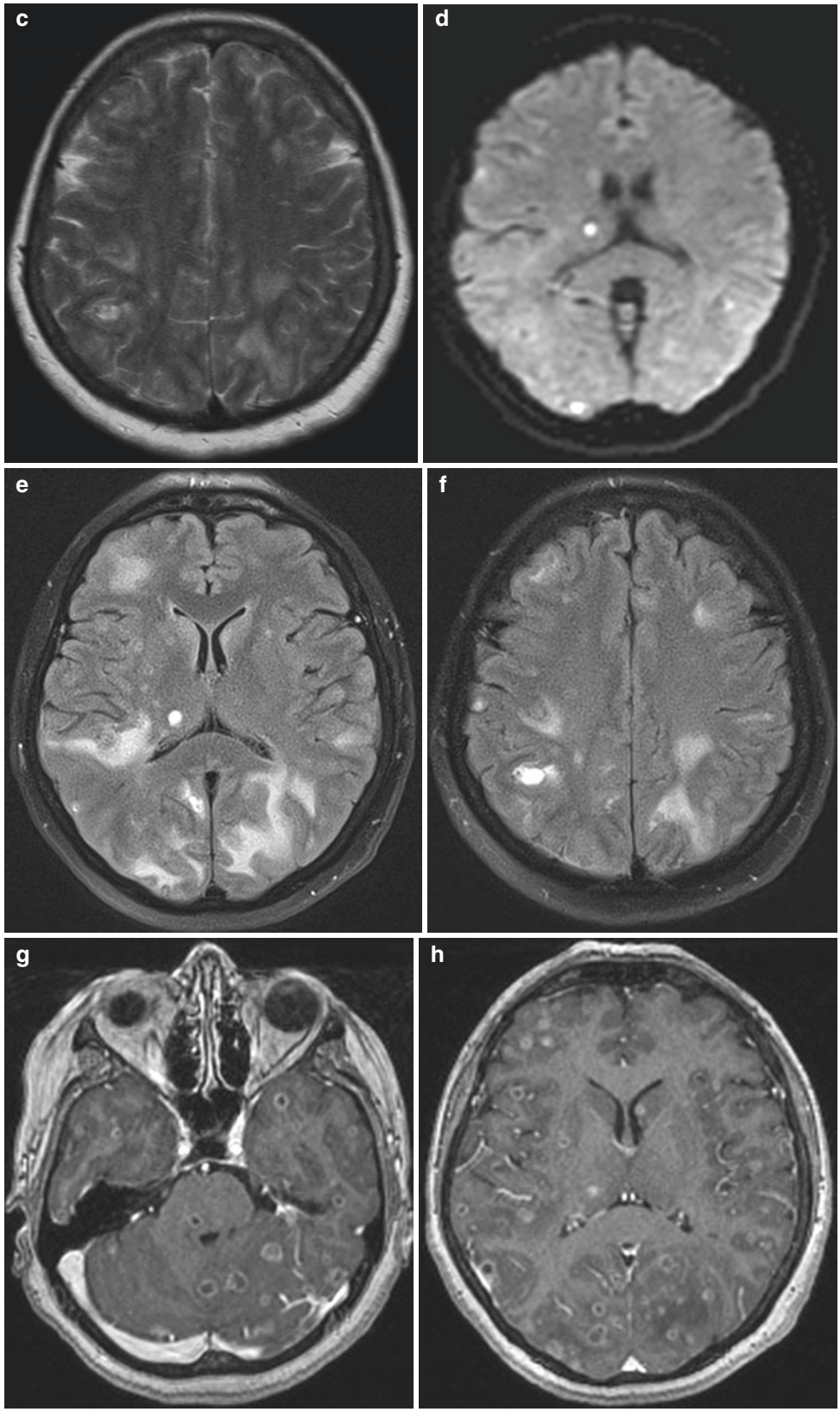

Fig. 9.2 (continued)

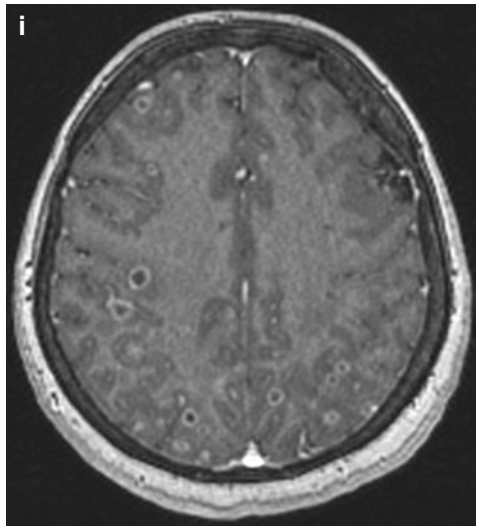

Fig. 9.2 (continued)

30 years. Symptoms may include seizures, headaches, hydrocephalus, neurological deficits and altered mental status. NC represents a leading cause of seizures and epilepsy in the developing world [3]. The radiological appearance of parenchymal NC varies depending on the stage of disease:

1. Vesicular stage is seen as CSF-like cysts with a small eccentric scolex, usually without perifocal oedema and contrast enhancement, although mild peripheral enhancement is possible [4]. The scolex is pathognomonic hallmark of this stage and presents as a bright dot on T2 FLAIR images.
2. Colloidal vesicular stage is represented by a cyst whose wall becomes thicker and enhances with contrast; there is also perifocal oedema.

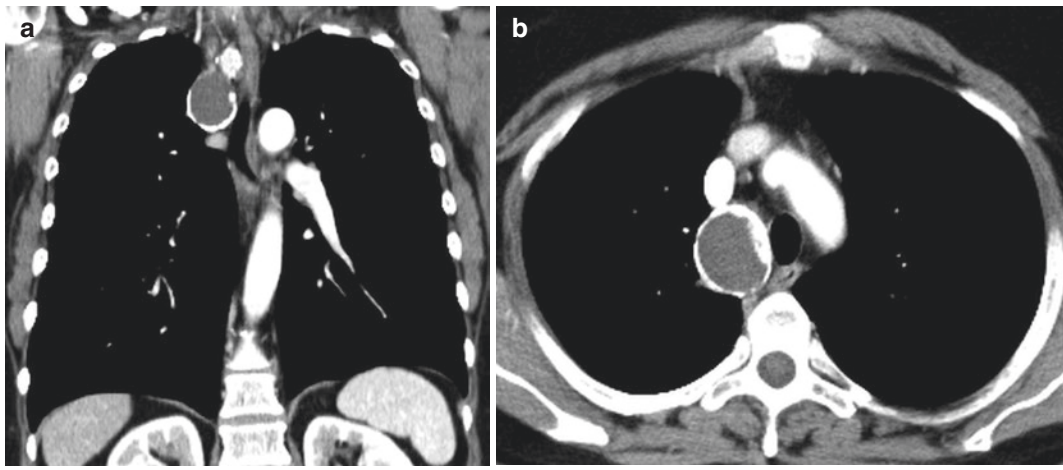

Fig. 9.3 Coronal (**a**) and axial (**b**) contrast-enhanced CT images of the thorax

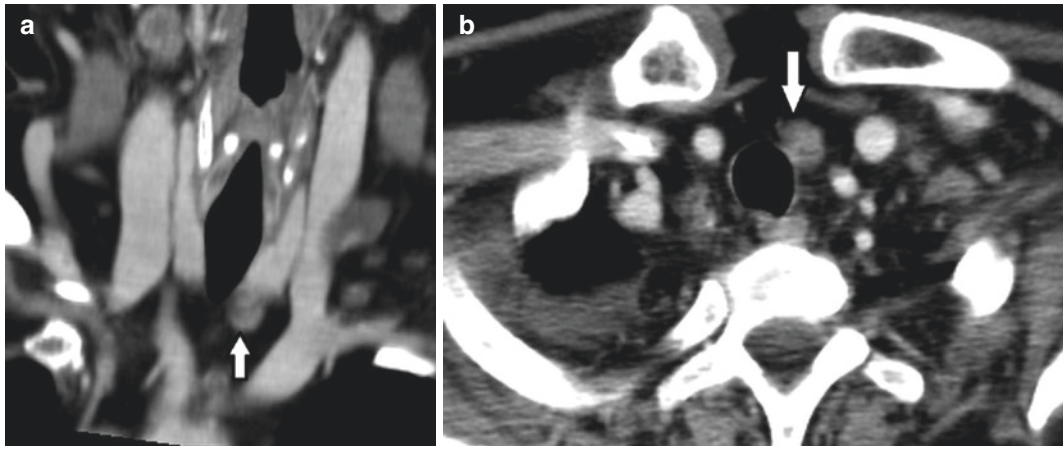

Fig. 9.4 Coronal (**a**) and axial (**b**) contrast-enhanced CT images of the neck showing a 12 mm node protruding caudally from the inferior pole of the left thyroid lobe

The appearance of the intracystic fluid is different from CSF due to an increase in proteinaceous content—hyperdense on CT, slightly hyperintense on T1-weighted images and markedly hyperintense on T2-weighted images and T2-FLAIR images. The scolex decreases in size. In this stage multiple lesions may generate marked immune response of the post, causing diffuse brain oedema and collapse of the ventricular system without midline shift—this is called acute cysticercosis encephalitis and is more often seen in children [5].

3. Granular nodular stage occurs with cyst retraction, while nodular or ring enhancement persists. The surrounding oedema decreases gradually. Pericystic gliosis is a common finding.
4. Nodular calcified stage represents an inactive, final stage—the lesion has shrunk for more than 50% of its original size; it is almost completely mineralised. There is no surrounding oedema. There may be mild peripheral contrast enhancement on MRI, sometimes with minimal oedema [5].

The imaging appearances are heterogenous, as most patients harbour parasites in all four evolution stages.

Neurocysticercosis is the most common parasitic disease of the central nervous system, and it should be considered as a differential diagnosis of multiple brain metastases, especially in endemic areas. In cases with clear peripheral lesion enhancement, metastatic disease must be ruled out in the first place, even though the appearances may suggest neurocysticercosis—several cases of initial misdiagnosis have been reported [6, 7].

References

1. Miranda ER et al (2010) Papillary thyroid carcinoma with brain metastases: an unusual 10-year-survival case. Thyroid 20(6):657–661. https://doi.org/10.1089/thy.2009.0442
2. Hoie J et al (1988) Distant metastases in papillary thyroid cancer: a review of 91 patients. Cancer 61:1–6
3. DeGiorgio CM et al (2004) Neurocysticercosis. Epilepsy Curr 4(3):107–111
4. Rumboldt Z et al (2010) Brain imaging with MRI and CT: an image pattern approach. Cambridge University Press, New York. https://doi.org/10.1017/CBO9781139030854
5. Zhao J-L et al (2015) Imaging spectrum of neurocysticercosis. Radiol Infect Dis 1(2):94–102. https://doi.org/10.1016/j.jrid.2014.12.001
6. Mota PC et al (2011) Lung cancer: atypical brain metastases mimicking neurocysticercosis. Int J Clin Oncol 16:746. https://doi.org/10.1007/s10147-011-0221-7
7. Troiani C et al (2011) Cystic brain metastases radiologically simulating neurocysticercosis. Sao Paulo Med J 129(5):352–356

Ethylene Glycol Poisoning

10

One evening in December 2015, a 34-year-old male came home from a night out with his friend. His mother claimed, at the time he retuned home that evening, her son was sorber, physical and mental status were not altered. Next morning she found him in a living room agitated, restless and disoriented. Ambulance transported him to a hospital: on an emergency admission, he was soporous and had metabolic acidosis with an anion gap, hypercalcemia and slightly increased urea (5.3 mmol/L) and creatinine (126 μmol/L) levels, while CT of the brain was unremarkable (Fig. 10.1).

During next 24-h he became comatose; urea (14 mmol/L) and creatinine (324 μmol/L) levels were rising. Due to the clinical course and status, haemodialysis was performed during following days.

Eight days after the admission, patient restored consciousness and has told doctors he suspected somebody had poured an antifreeze into his drink during a night out. All drug tests, toxins as well as ethylene glycol (EG) derivatives were negative, but those tests were performed after haemodialysis.

Brain MRI was performed 10 days after the admission (Figs. 10.2 and 10.3), without contrast media administration (creatinine 911 μmol/L).

Due to a patient information about possible poisoning, laboratory data and MRI findings that revealed lesions compatible with the acute EG toxicity, kidney biopsy was performed revealing diffuse acute tubular injury with calcium oxalate crystal depositions in tubular lumen and about 30% interstitial inflammation proving acute kidney injury due to the EG toxicity.

Two months after the poisoning, his neurologist reported almost complete neurological recovery, while 4 months after the poisoning, urea (6.3 mmol/L) and creatinine (101 μmol/L) levels were normal.

10.1 Ethylene Glycol Poisoning

Ethylene glycol is a colourless, sweet tasting and nearly odourless fluid, a poisonous form of alcohol. As an organic solvent, it is found in a variety of common household products including antifreeze, de-icing fluids, cleaners, paints, dyes, etc. It may be ingested intentionally in an attempt of suicide, or accidentally by alcoholics, or because of its sweet taste and the ease of access, by children and animals.

Ingestion of small quantity, as little as 100 mL in adult, will result in toxicity [1]. EG poisoning is characterised with development of successive presenting stages including an initial latency phase followed by the onset of severe metabolic acidosis and severe systemic and neurological complications leading to renal insufficiency, cardiorespiratory symptoms and brain oedema with coma within 12–24 h of ingestion. EG poisoning has produced cranial nerve deficits (usually VII nerve dysfunction) after a delay of 5–20 days [2].

M. Špero, H. Vavro, *Neuroradiology - Expect the Unexpected*,
https://doi.org/10.1007/978-3-319-73482-8_10

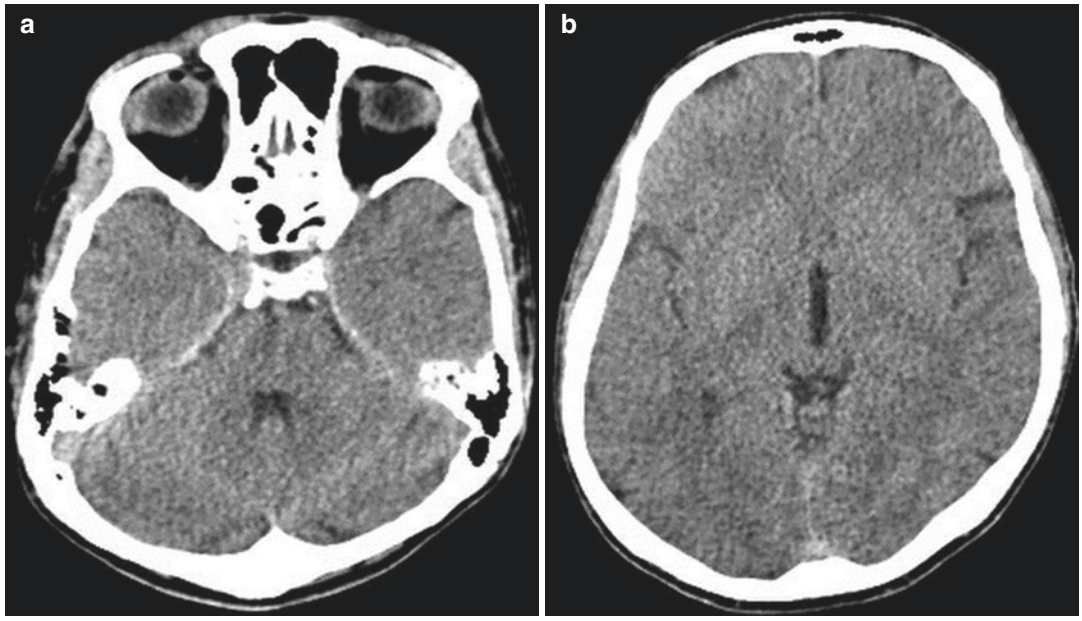

Fig. 10.1 Computed tomography of the brain, axial scan (**a**, **b**), performed on admission: both thalamus and lentiform nuclei were of normal density as well as pons

Except the initial EG-related transient inebriation, central nervous system impairment is usually delayed, evidencing that EG toxicity results from its conversion to toxic metabolites, thus explaining the lack of correlation between symptoms and EG concentrations. It is metabolised in the liver through a series of enzymes into intermediate metabolites: glycolaldehyde, glycolic acid and glyoxylic acid. Those toxic metabolites are cellular poisons. Glycolic acid is mainly responsible for the metabolic acidosis. Glyoxylic acid is converted to oxalic acid which precipitates with calcium into calcium oxalate crystals which are deposited in various tissues. Calcium oxalate crystals deposits in the cerebral vessel walls are responsible for cerebral oedema and ischaemia, as well as in the brain parenchyma having direct toxic effect at the cellular level within the basal ganglia and surrounding white matter [3–5].

In the first 24–48 h after the ingestion, CT and MRI of the brain reveal bilateral basal ganglia oedema or diffuse brain oedema, while 2–3 days after the ingestion, MRI reveals bilateral lesions of basal ganglia, thalami, amygdala, hippocampi, midbrain and upper pons consistent with vasogenic oedema (Figs. 10.2 and 10.3), cytotoxic oedema and ischaemia involving frontal white matter, and haemorrhagic lesions in lentiform nuclei—putamen—could disappear after 5–35 days [5–10]. Lesions with vasogenic oedema are likely reversible [8]. Restricted diffusion within the white matter tracts of the corona radiata was reported with EG toxicity [5]. Putaminal necrosis may be found in subacute and chronic stages. Midbrain, sparing the red nuclei and the corticospinal tracts, as well as medulla oblongata and cerebellum may be involved in case of EG poisoning [8].

The basal ganglia are one of the most metabolically active regions in the brain due to its high energy demand, increased blood flow and richness in neurotransmitters and, therefore, are sensitive to toxic and metabolic disorders, hypoxia and acidosis. Differential diagnosis of EG poisoning therefore includes lesions due to hypoxic ischaemic encephalopathy, carbon monoxide poisoning, toxic encephalopathy, hepatic encephalopathy and hypoglycaemia and possible deep venous cerebral thrombosis (Fig. 10.3).

Making the exact diagnosis may be problematic in the absence of an appropriate history of EG ingestion, but if you are presented a comatose patient with metabolic acidosis with an increased

anion gap, normal chloride level and elevated serum osmolarity, EG poisoning should be strongly suspected [7].

Early treatment with an alcohol dehydrogenase inhibitor fomepizole is very effective: it prevents toxic metabolites formation, metabolic acidosis and injury to the brain and kidneys. Other treatments include alkali to combat acidosis, ethanol as an EG antimetabolite and haemodialysis.

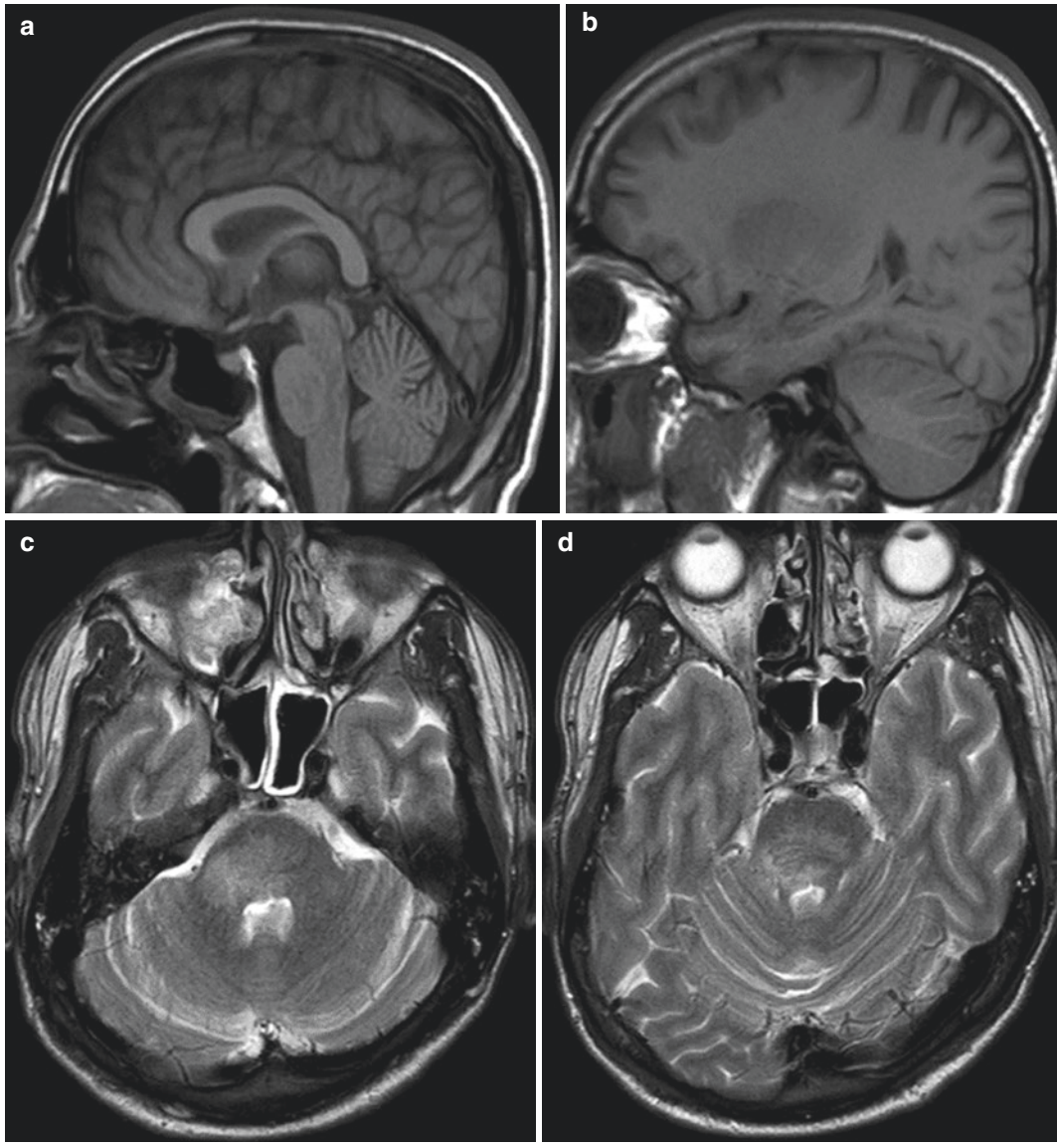

Fig. 10.2 Magnetic resonance imaging, sagittal T1WI (**a**, **b**), axial T2WI (**c**–**e**) and FLAIR (**f**–**h**), revealed symmetrical extensive heterogeneous T2 and FLAIR hyperintensities of slightly voluminous putamen, globus pallidus and external capsule, hyperintensities in both thalami. Asymmetrical T2 and FLAIR hyperintensities in pons, predominantly in the dorsal part which was slightly voluminous with mild compression of the IV ventricle. Involved supratentorial and infratentorial parenchyma was hypointense on T1WI, without sign of haemorrhage

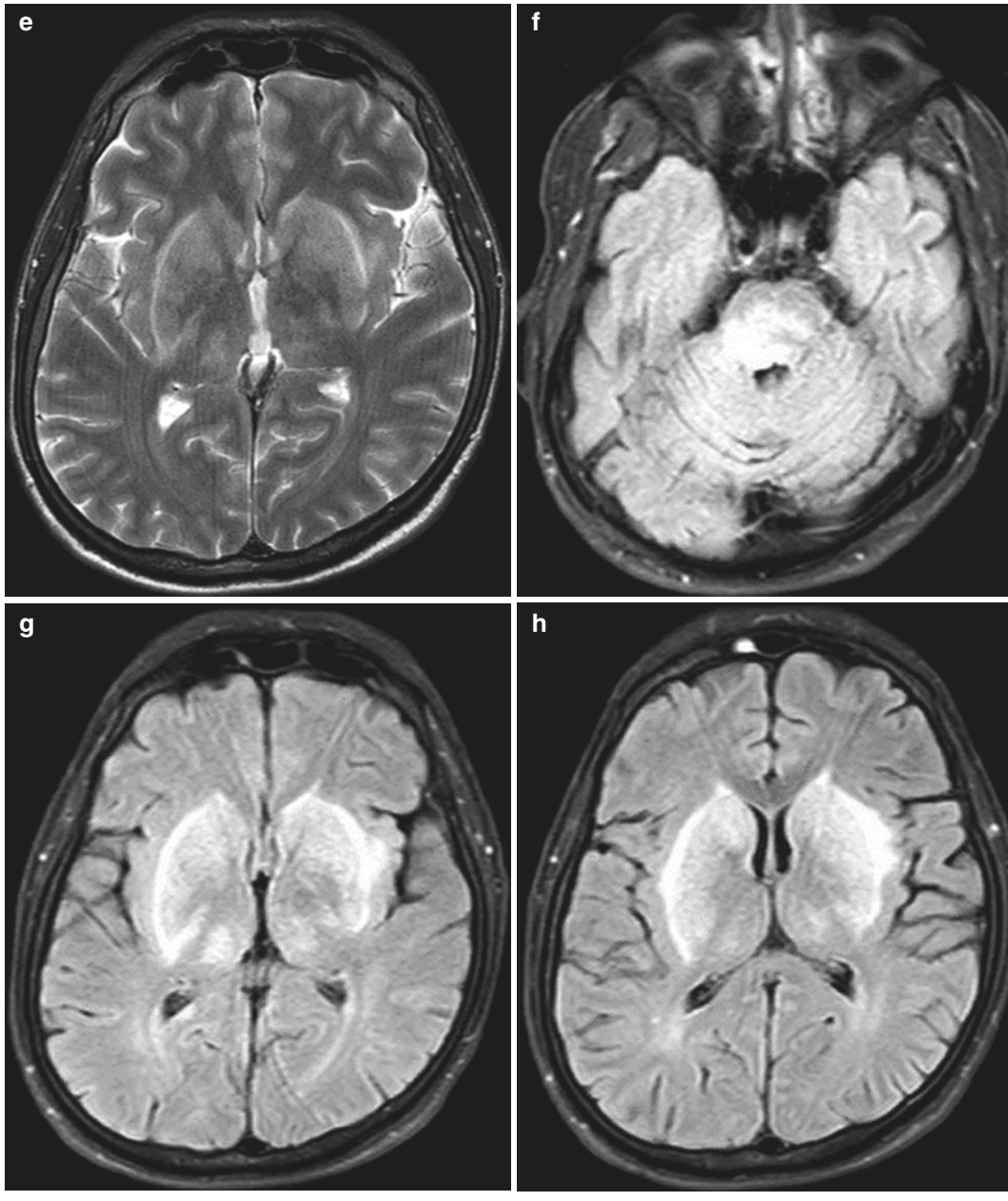

Fig. 10.2 (continued)

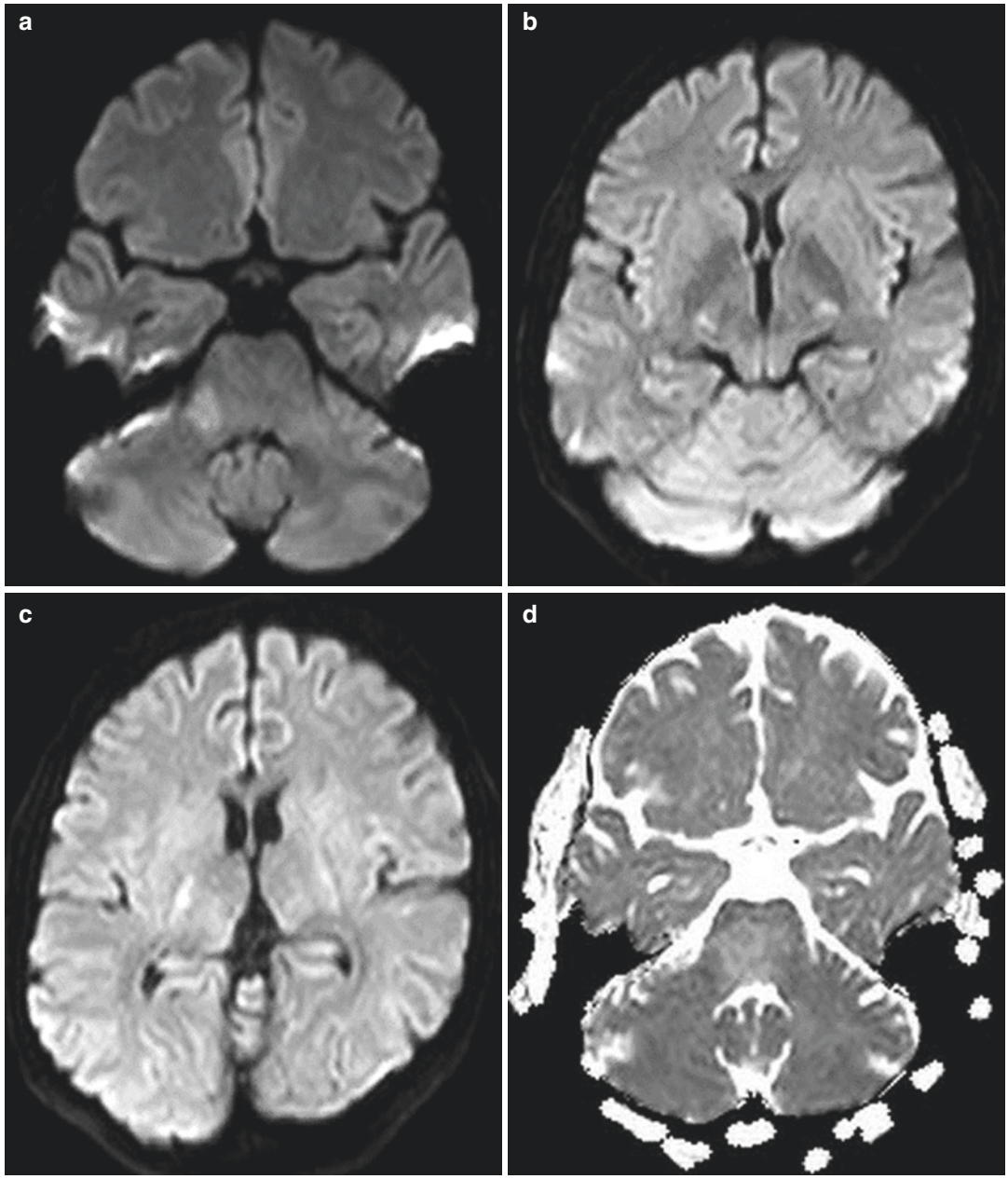

Fig. 10.3 Magnetic resonance imaging, axial DWI (**a**–**c**) and ADC (**d**–**f**): without restricted diffusion of the involved brain parenchyma—lesions were related to vasogenic oedema

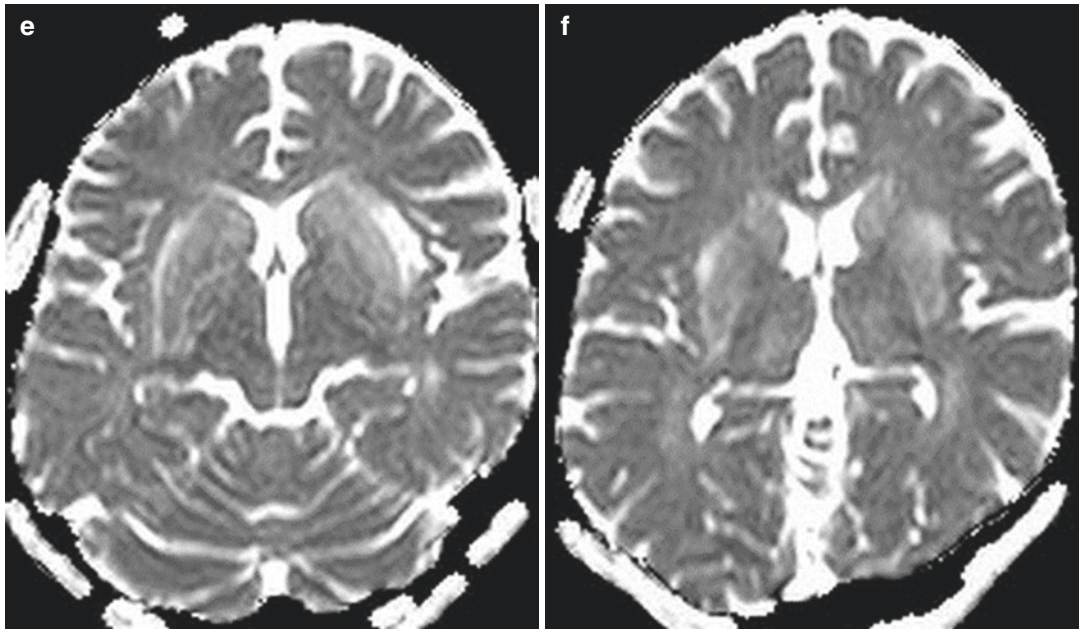

Fig. 10.3 (continued)

References

1. Scally R et al (2002) Treatment of ethylene glycol poisoning. Am Fam Physician 66:807–812
2. Readdy N et al (2010) Delayed neurological sequelae from ethylene glycol, diethylene glycol and methanol poisonings. Clin Toxicol (Phila) 48(10):967–973
3. Davis DP et al (1997) Ethylene glycol poisoning: case report of a record-high level and a review. J Emerg Med 15(5):653–667
4. Gabow PA et al (1986) Organic acids in ethylene glycol intoxication. Ann Intern Med 105(1):16–20
5. Moore MM et al (2008) Ethylene glycol toxicity: chemistry, pathogenesis, and imaging. Radiol Case Rep 3:122. https://doi.org/10.2484/rcr.v3i1.122
6. Zeiss J et al (1989) Cerebral CT of lethal ethylene glycol intoxication with pathologic correlation. AJNR Am J Neuroradiol 10:440–442
7. Corr P, Szolics M (2012) Neuroimaging findings in acute ethylene glycol poisoning. J Med Imaging Radiat Oncol 56:442–444
8. Boukobza M et al (2015) Neuroimaging findings and follow-up in two cases of severe ethylene glycol intoxication with full recovery. J Neurol Sci 359:343–346
9. Maekawa N et al (2015) Brain magnetic resonance image changes following acute ethylene glycol poisoning. Neurol India 63:998–1000
10. Santana-Cabrera L et al (2013) Ethylene glycol toxic encephalopathy. J Neurosci Rural Pract 4(4):477–478

Carbon Monoxide Poisoning Sequelae

11

Two days before being admitted to our university hospital, a young lady (28) was urgently hospitalised at a regional hospital after she had been found unresponsive on the bathroom floor. Carbon monoxide poisoning caused by malfunctioning gas-powered water boiler was suspected. The initial CT exam was reported as normal. Upon waking from coma, she had left-sided hemiparesis. During the next several days, her neurological status became completely normal, but ventricular extrasystolia was noticed, so a suspicion of cardiogenic loss of consciousness arose. A MRI exam of the brain was requested (Fig. 11.1).

The imaging findings were compatible with carbon monoxide poisoning, but not very dramatic since the MRI exam was done 6 days after carbon monoxide inhalation and the patient recovered completely.

An example of CT and MRI findings in the setting of acute carbon monoxide poisoning (in a different patient) is shown in Fig. 11.2:

11.1 Carbon Monoxide Poisoning

Carbon monoxide (CO) is a colourless, odourless, tasteless, non-irritant gas produced by incomplete combustion of carbon-based fuels and substances. It is produced by common household appliances, heating equipment and internal combustion engine motors.

Carbon monoxide poisoning is the most frequent cause of accidental poisoning and can be fatal; it is frequently unrecognised due to its non-specific clinical presentation, unless typical history of CO exposure is provided. The patient is often unresponsive; the clinical findings are highly variable and non-specific. The symptoms may vary from headache, nausea and vomiting to confusion, ataxia, seizures, coma, myocardial infarction and death. Long-term low-level CO exposure may be the cause of chronic fatigue, memory deficits, vertigo, neuropathy, diarrhoea and abdominal pain. There may be a delayed encephalopathy of carbon monoxide intoxication, characterised by a recurrence of neurological or psychiatric symptoms [1]. The lucid interval between acute and recurrent symptoms usually lasts 2–3 weeks. The delayed encephalopathy may end with full recovery but also with progressive deterioration ending in coma or death, which depends on the severity of the initial carbon monoxide intoxication.

The affinity of the CO for heme protein is approximately 250 times that of oxygen—such formation of carboxyhaemoglobin reduces the oxygen-carrying capacity of the blood and the off load of oxygen to tissues is greatly reduced. This causes tissue hypoxia/anoxia. There is also a direct toxic effect of the CO on mitochondria, interfering with oxidative phosphorylation. These lead to anoxic-ischaemic encephalopathy.

M. Špero, H. Vavro, *Neuroradiology - Expect the Unexpected*,
https://doi.org/10.1007/978-3-319-73482-8_11

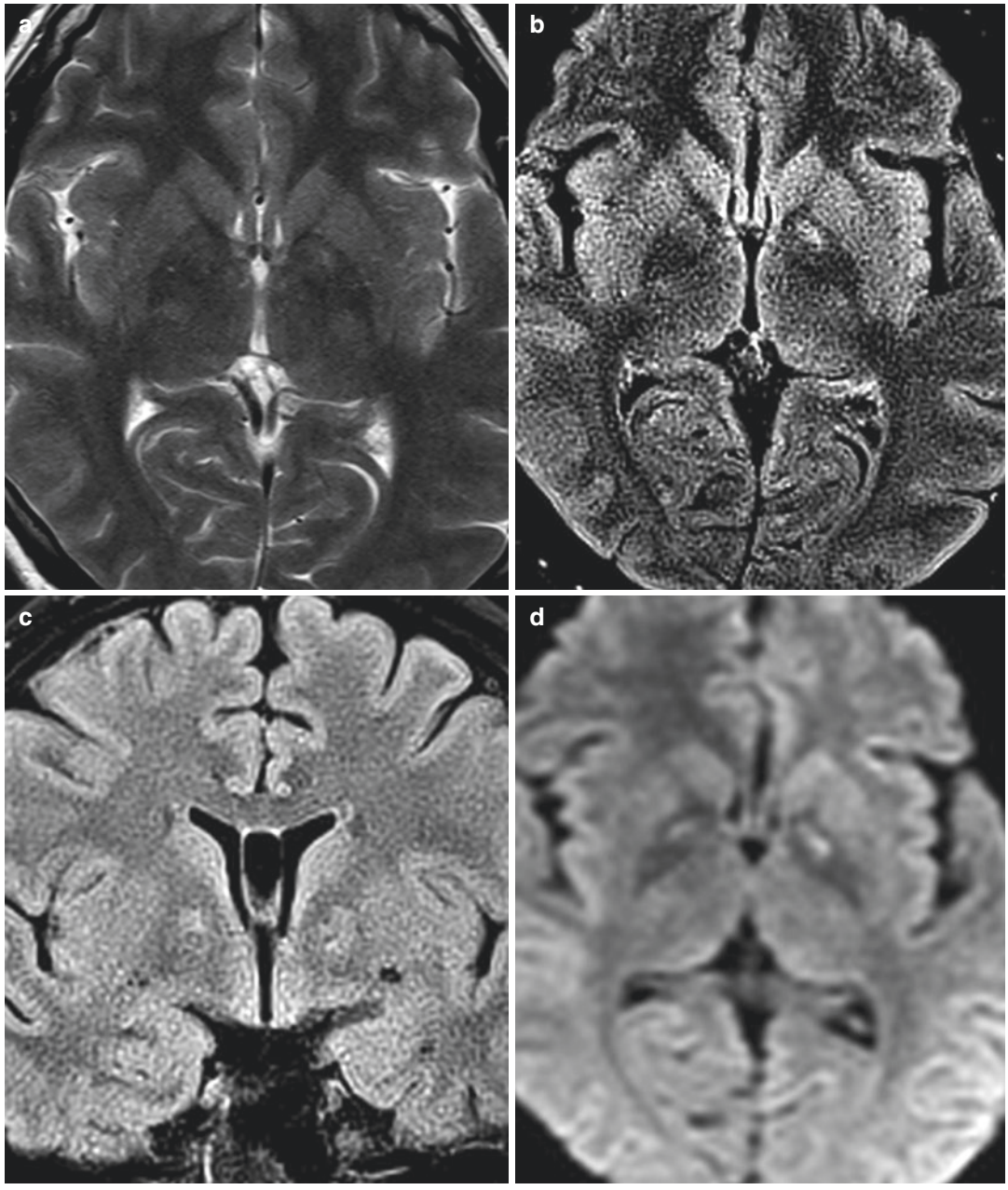

Fig. 11.1 MRI exam of the brain, 6 days after the incident. Axial T2WI (**a**) and axial and coronal T2-FLAIR images (**b**, **c**) show a focal hyperintensity bilaterally in the globus pallidus, best appreciated in the T2-FLAIR images. A mild hyperintensity on the diffusion-weighted image (**d**) in the same areas may be attributed to mild residual cytotoxic oedema or to T2 shine-through—the ADC map (**e**) is normal. There is mild hypointensity in the left globus pallidus shown on the sagittal T1WI (**f**)

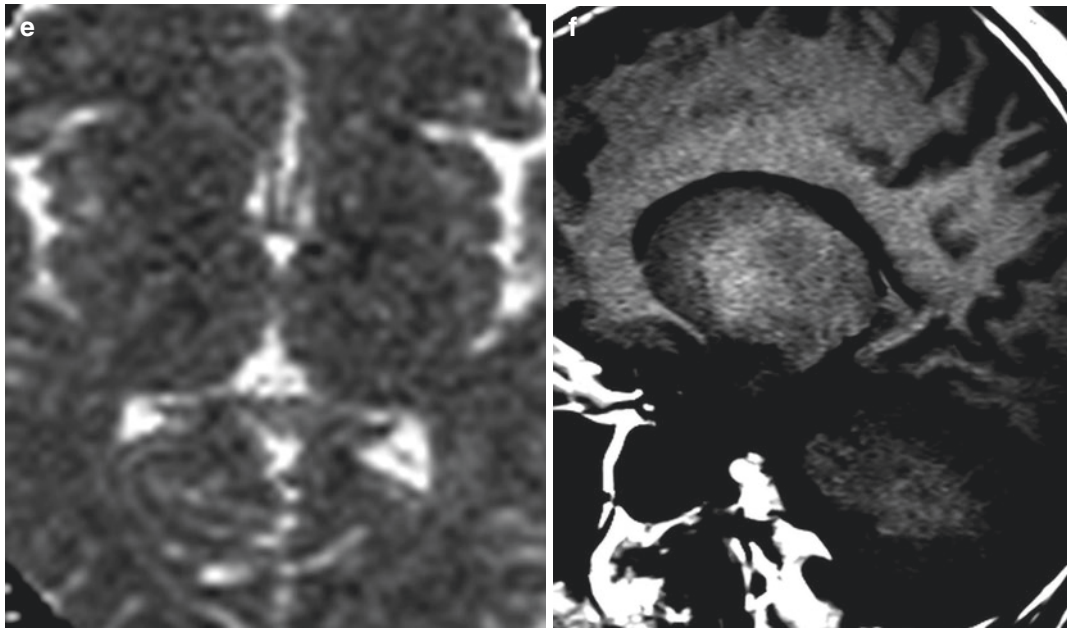

Fig. 11.1 (continued)

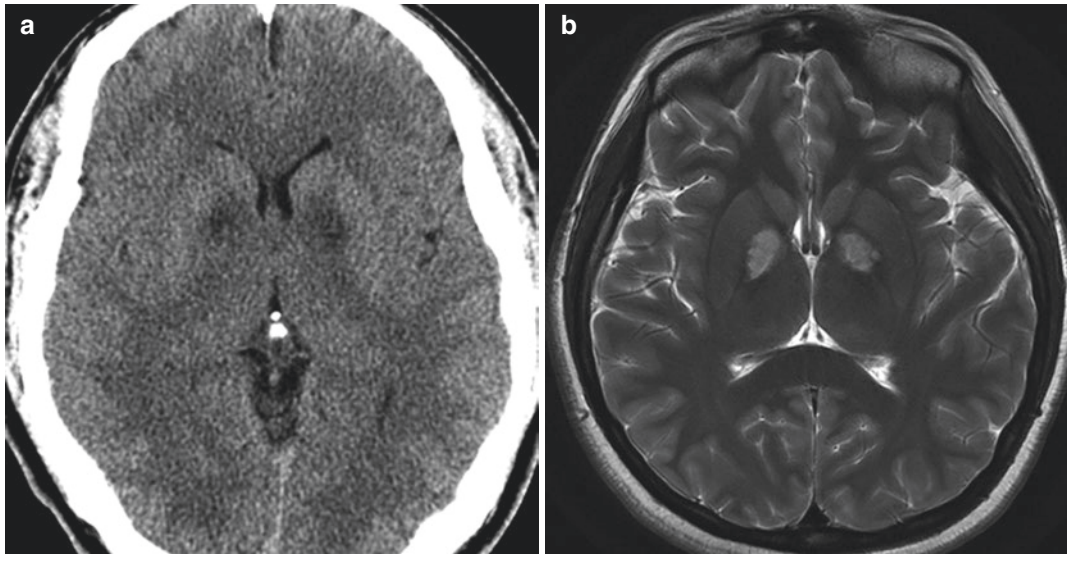

Fig. 11.2 CT and MRI findings in acute carbon monoxide poisoning (images courtesy of Prof. Z. Rumboldt). Non-enhanced CT image (**a**) shows a hypodense area in the globus pallidus bilaterally, compatible with hyperintense areas on MRI T2WI image (**b**). There is also high DWI signal within the lesions (**c**), indicating low diffusivity due to cytotoxic oedema

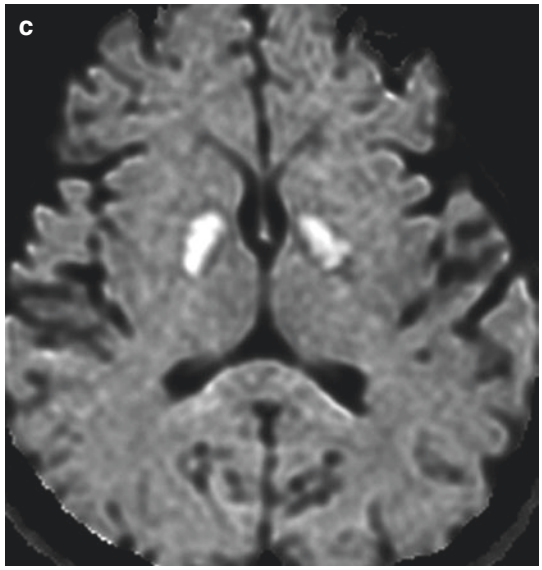

Fig. 11.2 (continued)

Normal blood levels of carboxyhaemoglobin are up to 3% in non-smokers and up to 10% in smokers. A note is made that the standard two-wavelength pulse oximetry cannot differentiate between carboxyhaemoglobin and oxyhaemoglobin [2].

The treatment of CO poisoning consists of administering 100% oxygen, preferably in a hyperbaric setting.

Standard imaging findings in acute CO poisoning include symmetric CT hypodensity in globus pallidus, which is seen as low T1 and high T2 and DWI signal on MRI. There may be a T1 hyperintensity and a rim of low T2 signal, reflecting haemorrhagic necrosis [3]. Patchy peripheral enhancement is possible in the acute phase. There may also be similar abnormalities in the cerebral cortex, hippocampus, and substantia nigra, and cerebellar abnormalities have also been described [2]. In patients who develop a delayed leukoencephalopathy, there are confluent T2 hyperintense areas in the periventricular white matter with mild temporary decrease of diffusivity; the extent and degree of low ADC values are correlated with the clinical course and severity of CO intoxication [1].

Differential diagnoses include other toxic encephalopathies such as cyanide neurotoxicity which may be indistinguishable from carbon monoxide poisoning. Methanol poisoning typically affects the putamina, sparring the globi pallidi. Ethylene glycol (antifreeze) poisoning involves globi pallidi, other basal ganglia and thalami (see Chap. 10). Leigh disease usually presents in infancy or early childhood, with lesions in bilateral basal ganglia, thalami and brainstem. Pantothenate kinase-associated neurodegeneration (PKAN) presents as symmetric T2 hyperintensity within iron-laden hypointense globi pallidi (“eye of the tiger”).

References

1. Ji-hoon K et al (2003) Delayed encephalopathy of acute carbon monoxide intoxication: diffusivity of cerebral white matter lesions. Am J Neuroradiol 24(8):1592–1597
2. Ryan AS et al (2012) Carbon monoxide poisoning: novel magnetic resonance imaging pattern in the acute setting. Int J Emerg Med 5:30
3. Rumboldt Z et al (2010) Brain imaging with MRI and CT: an image pattern approach. Cambridge University Press, New York. https://doi.org/10.1017/CBO9781139030854

CLIPPERS: Infiltrative Brainstem Lymphoma

12

In November 2016, an 80-year-old female patient has fallen while walking: after a fall, she could not move her right leg; therefore she searched for a medical help. The patient described she had mild walking problems due to discrete occasional weakness of a right leg, during a month or two before a fall. According to patient medical data, she was taking antihypertensive medications due to arterial hypertension.

The patient was hospitalised: bone X-rays did not reveal fracture of a right femur or bones of a right lower leg. MRI of the brain was performed and revealed a process in pons and midbrain (Figs. 12.1 and 12.2).

Neuroradiologist who first reviewed the MRI examination has reported possible chronic lymphocytic inflammation with pontine perivascular enhancement responsive to steroids (CLIPPERS) or primary neoplastic process. We have revised the MRI examination and, due to clinical presentation and imaging features (Figs. 12.1 and 12.2), have reported primary neoplastic process infiltrating part of the pons, left cerebral peduncle and part of the thalamus possible lymphoma or glioma. Brain biopsy was performed and revealed primary brain lymphoma. The patient died just before the onset of oncological treatment.

12.1 CLIPPERS or Primary Brain Lymphoma

First described in 2010 by Pittock and his colleagues, CLIPPERS is a relatively new and rare CNS inflammatory disorder, defined as a distinct form of brainstem encephalitis centred on the pons, which is characterized by a predominant T-cell pathology and responsive to immunosuppression with glucocorticosteroids [1]. Histopathology after brain biopsy demonstrated predominantly T-cell infiltration with perivascular predominance in the involved white matter, accompanied by a moderate number of histiocytes and activated microglia [1–3].

There is no definitive sex predilection, and the age of onset ranges between 13 and 86 years: in large series a mean age of onset was in the fifth or sixth decade of life. Clinical course is subacute with progressive gait disorders, ataxia, dysarthria and diplopia as main symptoms [2, 3].

The hallmark of the brain MRI is punctate and curvilinear bilateral symmetrical perivascular enhancement peppering the pons with variable superior extension to the midbrain, inferior extension to the medulla and posterior extension to the middle cerebellar peduncles and cerebellum. Similar type of contrast enhancement may

M. Špero, H. Vavro, *Neuroradiology - Expect the Unexpected*,
https://doi.org/10.1007/978-3-319-73482-8_12

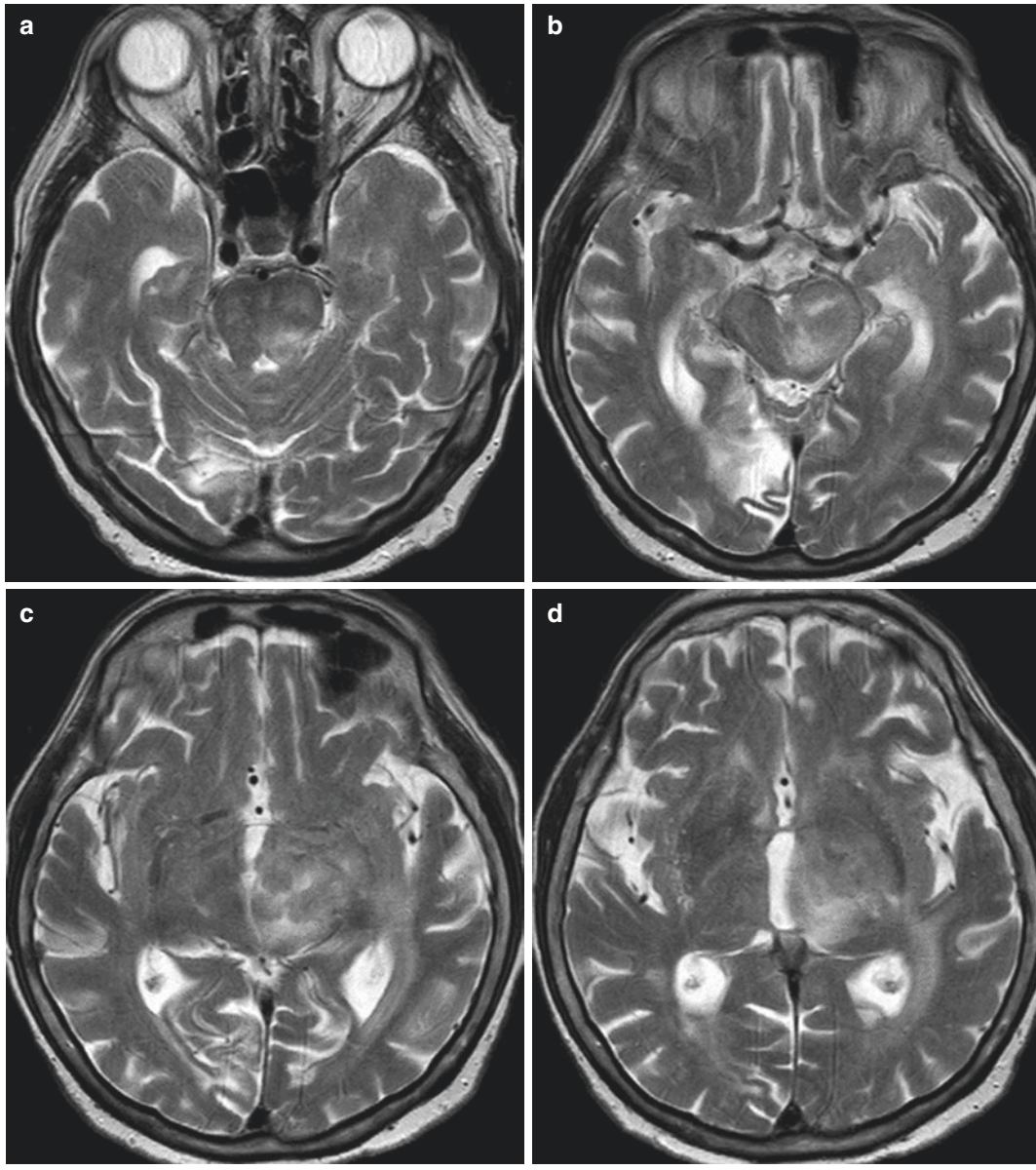

Fig. 12.1 Magnetic resonance of the brain, axial T2WI (**a**–**d**), FLAIR (**e**–**h**) and DWI (**i**) revealed lesion involving posterior and upper part of the left pons, left cerebral peduncle of the midbrain and part of the thalamus. Lesion had an expansive effect and involved parts of the midbrain were more voluminous: it was inhomogeneous, slightly hyperintense on T2WI and FLAIR, diffusion was not resticted

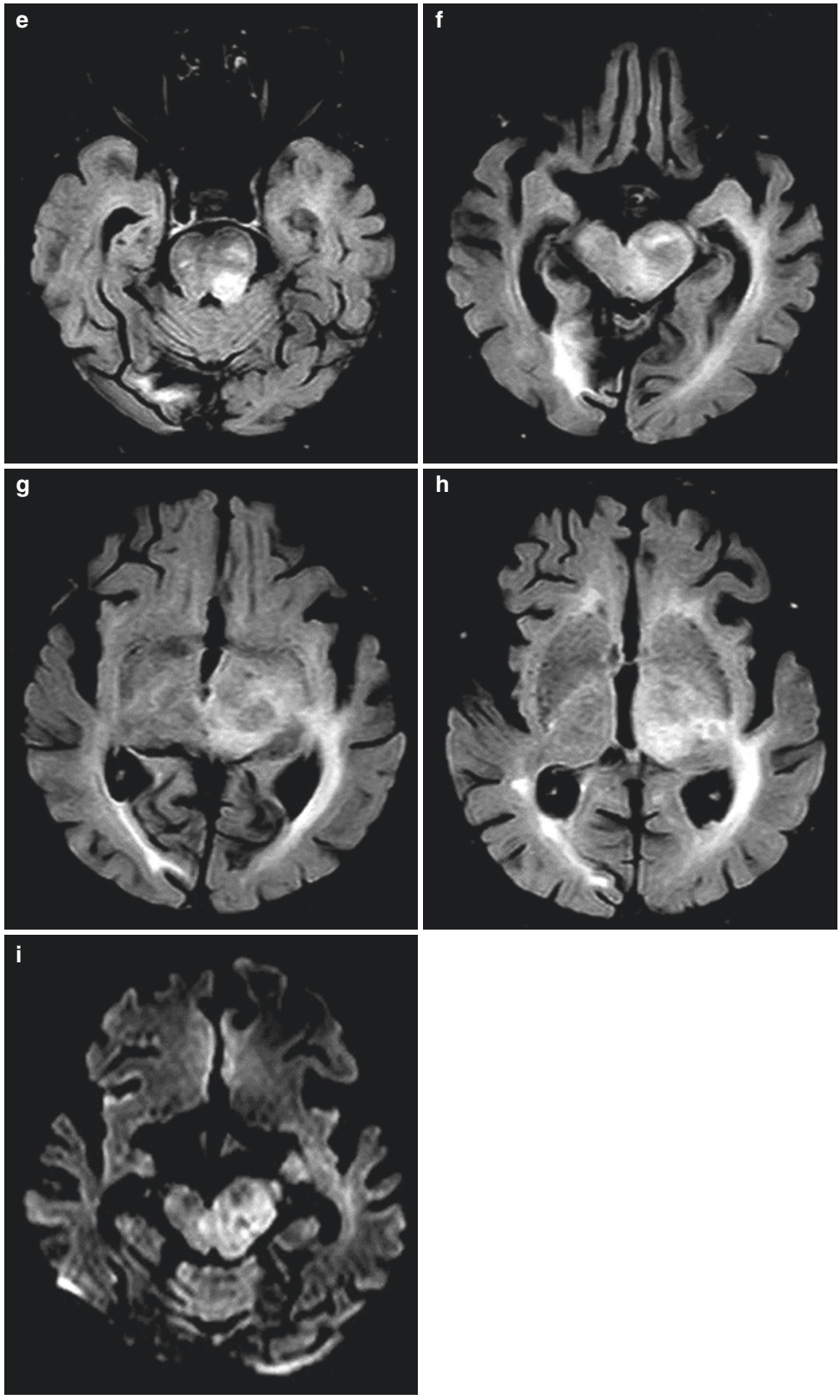

Fig. 12.1 (continued)

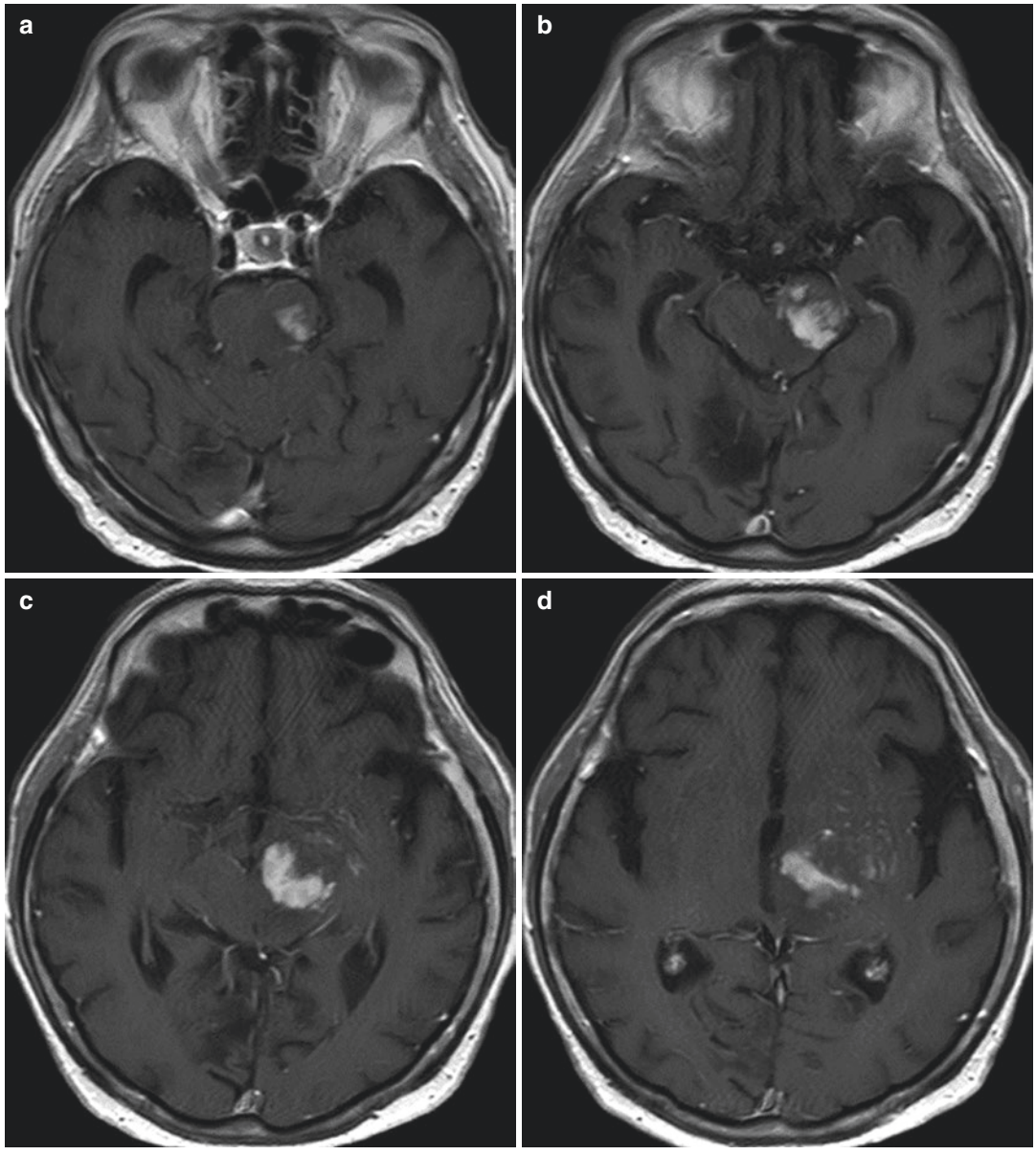

Fig. 12.1 (continued)

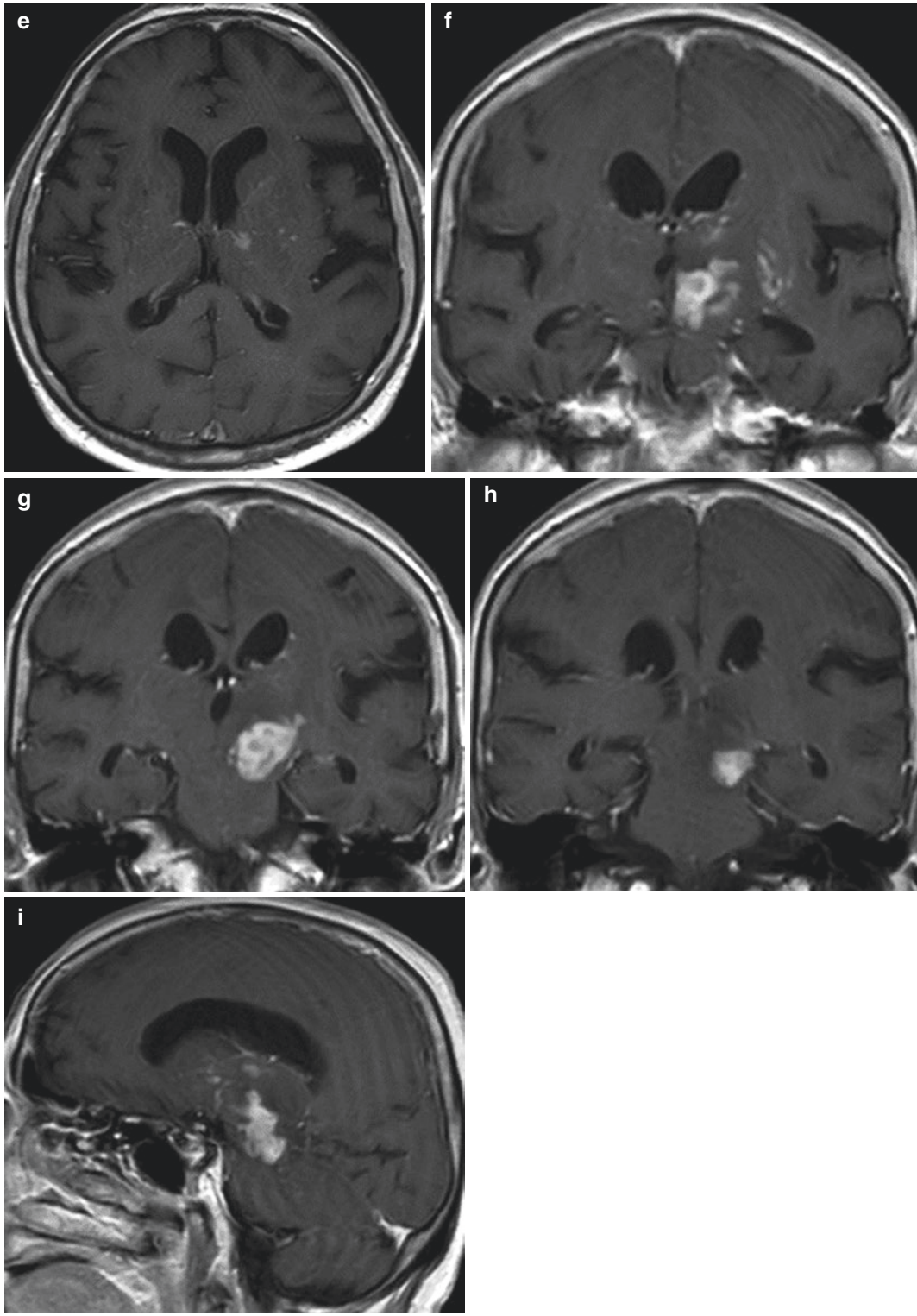

Fig. 12.2 Post-contrast MRI of the brain, axial (**a**–**e**), coronal (**f**–**h**) and sagittal (**i**) T1WI, demonstrated irregular expansile lesion that enhanced inhomogeneously, with punctate and curvilinear contrast enhancement in the left basal ganglia. Gyri around left central sulcus were mildly enlarged, with slightly reduced sulci, probably due to infiltration of the involved tracts (**f**–**h**)

involve the basal ganglia, thalami, internal capsule, corpus callosum and spinal cord, while a cerebral cortex is usually spared. Punctate enhancing foci range in size between 1 and 3 mm, when larger than 3 mm typically have nodular appearance. There are patchy T2WI and FLAIR hyperintensities in areas of contrast enhancement. Usually there is no mass effect or vasogenic oedema which can be minimal as well. Contrast enhancement responds to the lymphocytic perivascular inflammatory pattern and decreases as the patient responds to immunosuppressive therapy [1–3].

Pathogenesis is poorly understood and unknown: according to histopathology after a brain biopsy and clinico-radiological response to immunosuppressive therapies, it suggests an autoimmune or other inflammatory-mediated pathogenesis, while the targeted autoantigen could be located in perivascular regions, probably in pons [1, 3]. Laboratory investigation is usually unrevealing: the most common CSF anomaly is an elevated protein level, while occasional presence of oligoclonal band has been described [1–3].

Although age, subacute onset, involved brain parenchyma and curvilinear contrast enhancement in the basal ganglia may fit into described characteristics of CLIPPERS, clinical symptom of leg weakness; unilateral involvement of the pons, midbrain and thalamus; contrast enhancing irregular process causing mass effect fit into favour of primary brain neoplasms. Differential diagnosis of CLIPPERS includes, among other diagnosis, primary brain lymphoma and glioma as well.

Primary CNS lymphomas nearly are diffuse large B-cell lymphomas. Imaging findings vary with the immune status of a patient. Typical CNS lymphoma neuroimaging features include supratentorial white matter and corpus callosum involvement but may also involve midbrain and cerebellum. CNS lymphomas are hypercellular tumours causing mass effect and marked post-contrast enhancement. Due to its hypercellularity, those are hypointense on T2WI and show restricted diffusion, although, if tumour is atypical, like in immunodeficient and immunocompetent patients, diffusion may not be restricted. On FLAIR sequence those tumours are hyperintense. Primary CNS lymphomas demonstrate marked perivascular or intravascular tumour infiltration that, together with a lack of neoangiogenesis, results in low rCBV but, on post-contrast T1WI, may reveal punctate or curvilinear contrast enhancement as well. Similar type of contrast enhancement may be present in parenchyma around glioma as satellite lesions. In this case it was difficult to decide what kind of tumour process it was, lymphoma or glioma, but due to lack of necrosis in the tumour mass and curvilinear contrast enhancement in the surrounding parenchyma, it made us decide CNS lymphoma as the first differential diagnosis, which was proved by stereotactic brain biopsy [4–6].

References

1. Pittock SJ et al (2010) Chronic lymphocytic inflammation with pontine perivascular enhancement responsive to steroids (CLIPPERS). Brain 133:2626–2634
2. Dudesek A et al (2014) CLIPPERS: chronic lymphocytic inflammation with pontine perivascular enhancement responsive to steroids. Review of an increasingly recognized entity within the spectrum of inflammatory central nervous system disorder. Clin Exp Immunol 175:425–438
3. Bag AK et al (2014) Case 212: chronic lymphocytic inflammation with pontine perivascular enhancement responsive to steroids. Radiology 273:940–947
4. Kickingereder P et al (2014) Primary central nervous system lymphoma and atypical glioblastoma: multiparametric differentiation by using diffusion-, perfusion-, and susceptibility-weighted MR imaging. Radiology 272:843–850
5. Mansour A et al (2014) MR imaging features of intracranial primary CNS lymphoma in immune competent patients. Cancer Imaging 14:22–30
6. Da Rocha AJ et al (2016) Modern techniques of magnetic resonance in the evaluation of primary central nervous system lymphoma: contributions to the diagnosis and differential diagnosis. Rev Bras Hematol Hemoter 38(1):44–54

Part IV

Skull and Orbit Anomalies

Crouzon Syndrome

13

After having several surgeries performed by neurosurgeons and maxillofacial surgeons (at the age of 2, 3 and 8), a 17-year-old girl with an established diagnosis of Crouzon syndrome (craniofacial dysostosis) visited a maxillofacial surgery referral centre for a second opinion on further treatment options (Fig. 13.1).

13.1 Crouzon Syndrome

Crouzon syndrome (CS) is a rare genetic disorder producing characteristic craniofacial features and other associated abnormalities, caused by premature closure of cranial sutures. The premature fusion of skull base causes midface hypoplasia, maxillary hyperplasia, shallow orbits and subsequent vision problems. It may be associated with hydrocephalus, stylohyoid ligament calcification, Chiari I malformation, cervical spine abnormalities and airway obstruction. Other clinical features include hypertelorism, beaked nose, short upper lip and relative mandibular prognathism. The hands and feet are usually normal which is a feature that can be used to distinguish CS from other craniosynostoses [1]. It is caused by a FGFR2 gene mutation on chromosomal locus 10q 25.3-q26 and inherited in the autosomal dominant pattern. The expressivity is variable [2].

CS accounts for approximately 4.8% of all craniosynostosis cases [2]. The prevalence rate is 1 in 25,000 live births. There is no race or sex predilection, but frequency of sagittal or metopic craniosynostosis is higher in boys, whereas coronal craniosynostosis is more frequent in girls.

Differential diagnosis includes other syndromes which feature similar craniofacial abnormalities, such as Pfeiffer syndrome, apert syndrome, Saethre-Chotzen syndrome, Carpenter syndrome and Jackson-Weiss syndrome.

Early diagnosis is crucial, as CS should be managed as early as possible by a multidisciplinary approach. Treatment usually begins during the first year of life with cranial decompression and correction of midfacial hypoplasia. Early craniectomy treats increased intracranial pressure. A technique of craniofacial disjunction followed by gradual bone distraction may correct exophthalmos and improve aesthetics of the middle face [3].

Crouzon syndrome was named after L.E. Octave Crouzon, a French physician who first described the condition in 1912.

M. Špero, H. Vavro, *Neuroradiology - Expect the Unexpected*,
https://doi.org/10.1007/978-3-319-73482-8_13

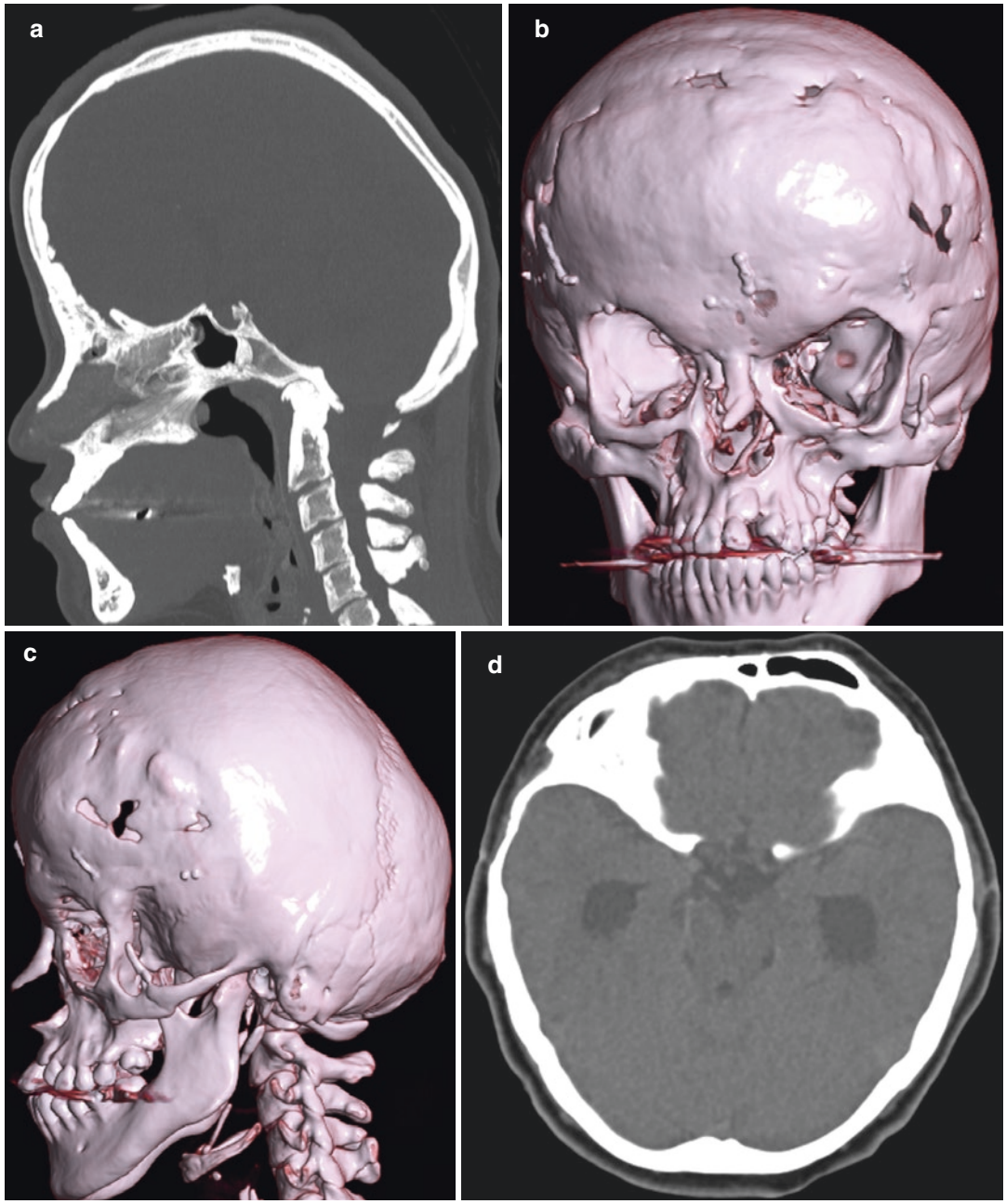

Fig. 13.1 Low-dose CT exam of the head revealed abnormal calvarial shape (**a**–**c**) with small anterior cranial fossa (**d**), shallow orbits with exophthalmos (**e**), mild midfacial hypoplasia, beak-shaped nose (**f**) deviated to the right with a right nasal bone defect (**g**), significant left convexity nasal septum deviation and several calvarial bone defects (**b**, **c**, **i**) in keeping with previous surgical procedures. No significant mandibular prognathia was detected. Additionally, there was a left-sided stylohyoid ligament calcification (**f**, **h**—marked by an *arrow*). Intracranially, corpus callosum agenesis with subsequent specifically shaped lateral ventricles was seen (**i**). Chiari malformation was not evident. No evidence of upper cervical spine fusion was seen

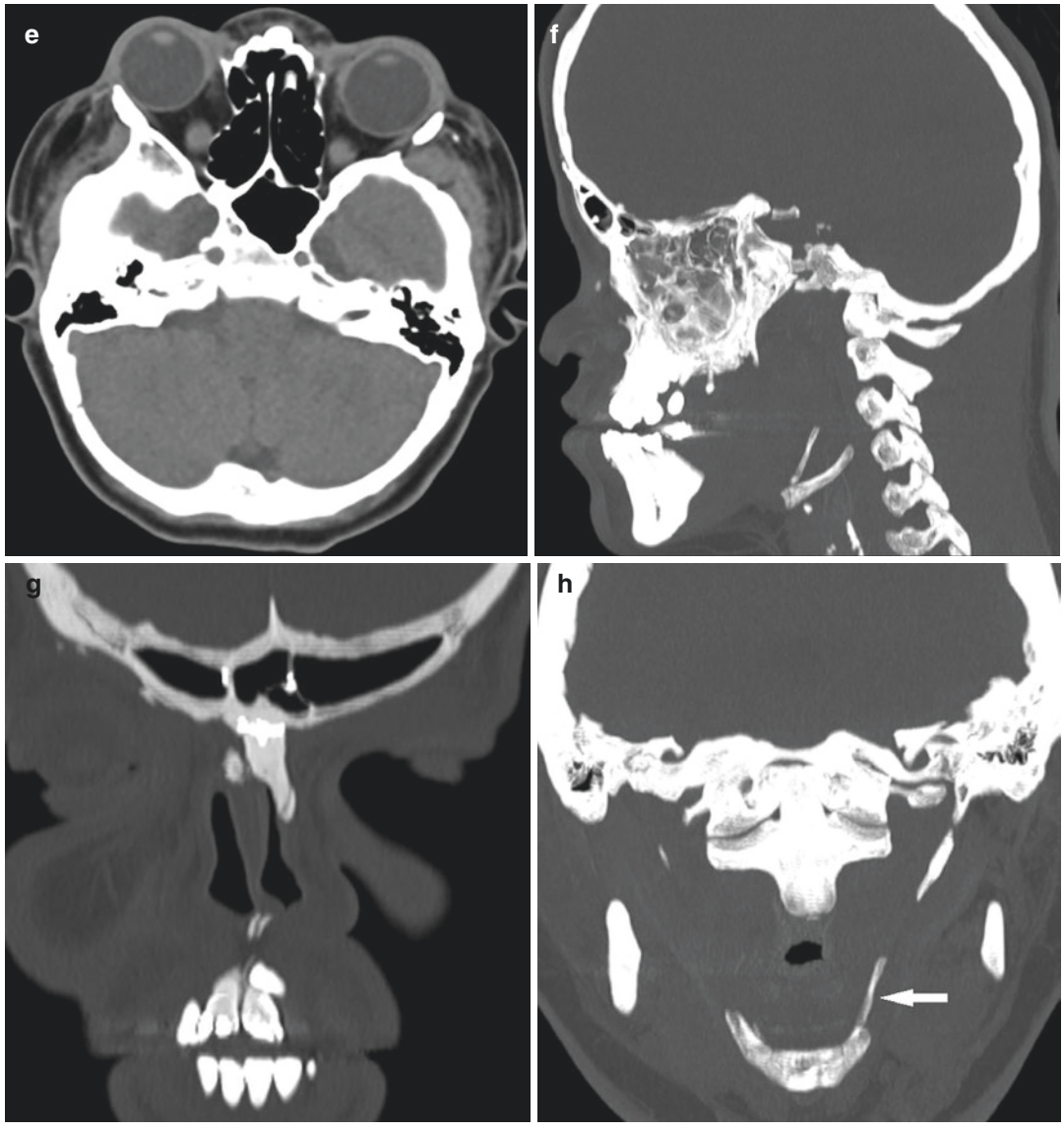

Fig. 13.1 (continued)

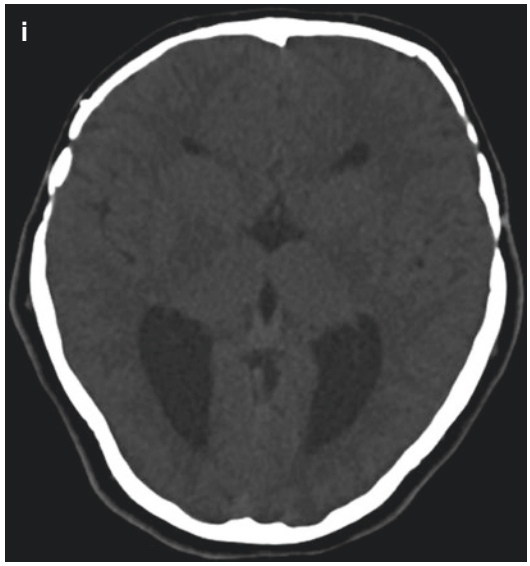

Fig. 13.1 (continued)

References

1. Pournima G et al (2011) Crouzon syndrome: a case report. Eur J Dent Med 10:1–5
2. Padmanabhan V et al (2011) Crouzon's syndrome: a review of literature and case report. Contemp Clin Dent 2(3):211–214. https://doi.org/10.4103/0976-237X.86464
3. Mohan RS et al (2012) Crouzon syndrome: clinico-radiological illustration of a case. J Clin Imaging Sci 2:70. https://doi.org/10.4103/2156-7514.104303

Primary Intraosseous Haemangioma of the Skull Base

14

An ophthalmologist had noticed a mild right eye exophthalmos on a 42-year-old female patient during a regular vision check-up. The patient was referred to a CT exam of orbits in her hometown (Fig. 14.1).

The CT report stated a bony tumour involving the right-sided greater wing of sphenoid bone, orbital wall and temporal bone. Differentially, the findings were felt to be in keeping with fibrous dysplasia or spongious osteoma.

The patient was further referred to a maxillofacial surgery referral centre where consultants were worried about a potentially missed malignant diagnosis—osteosarcoma, in particular.

They had performed tumour biopsy and requested a subsequent MRI exam in order to obtain more imaging data on the lesion and exact locations of the tissue sampling (Fig. 14.2).

The MRI findings were compatible with an intraosseous haemangioma of the skull base.

Please note a small occipital meningioma (arrow in image e) on the right and a choroid plexus xanthogranuloma (arrowhead in image e) in the posterior horn of the left lateral ventricle—both represent incidental findings.

The biopsy results were available after MRI exam had been done; histopathological analysis did not reveal any malignant tumour tissue, just bony material with some myxoid stroma and endothelium—the findings were in keeping with an intraosseous haemangioma and compatible with the MRI report findings.

Two months later, the patient started complaining of right-sided facial and cervical pain. The local clinical status was unchanged. The repeat MRI findings were stable. A decision was made that a joint maxillofacial and neurosurgical team would perform surgery (Fig. 14.3).

Histopathology report: torn bone pieces, normal in structure, fatty bone marrow and vascular spaces with variable wall thickness, most of them capillary in appearance. Impression: intraosseous haemangioma.

The patient recovered normally, and there was resolution of exophthalmos.

14.1 Primary Intraosseous Haemangioma

Primary intraosseous haemangioma is a benign vascular tumour, often found in the vertebral column but less frequently within the skull vault, the most common sites being frontal and parietal bone. Its occurrence in the skull base, such as in this case, is extremely rare [1]. When multiple bones of the orbit are involved, it is called primary intraosseous orbital haemangioma. It accounts for 0.7–1% of all bone tumours. It is slow-growing and predominantly asymptomatic, except in cases of compression of the adjacent soft tissue structures or producing a lump by expanding the outer bony table. Neurological symptoms are uncommon as the tumour tends to

M. Špero, H. Vavro, *Neuroradiology - Expect the Unexpected*,
https://doi.org/10.1007/978-3-319-73482-8_14

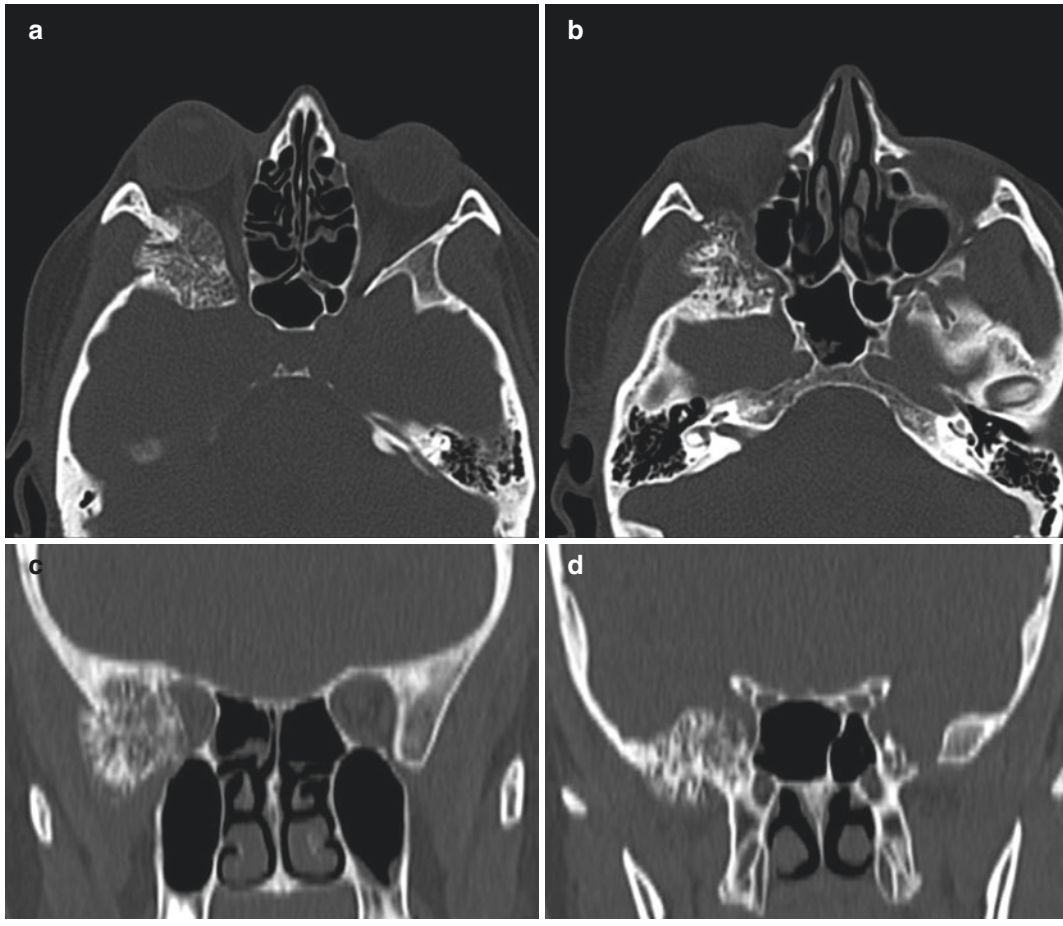

Fig. 14.1 CT exam of the orbits—axial scans (**a**, **b**) and coronal reformats (**c**, **d**)—shows a well-delineated bony expansile lesion within the right greater sphenoid wing which demonstrates spongy, trabecular, "honeycomb" structure. There is compression of the right-sided lateral rectus muscle and right eye proptosis

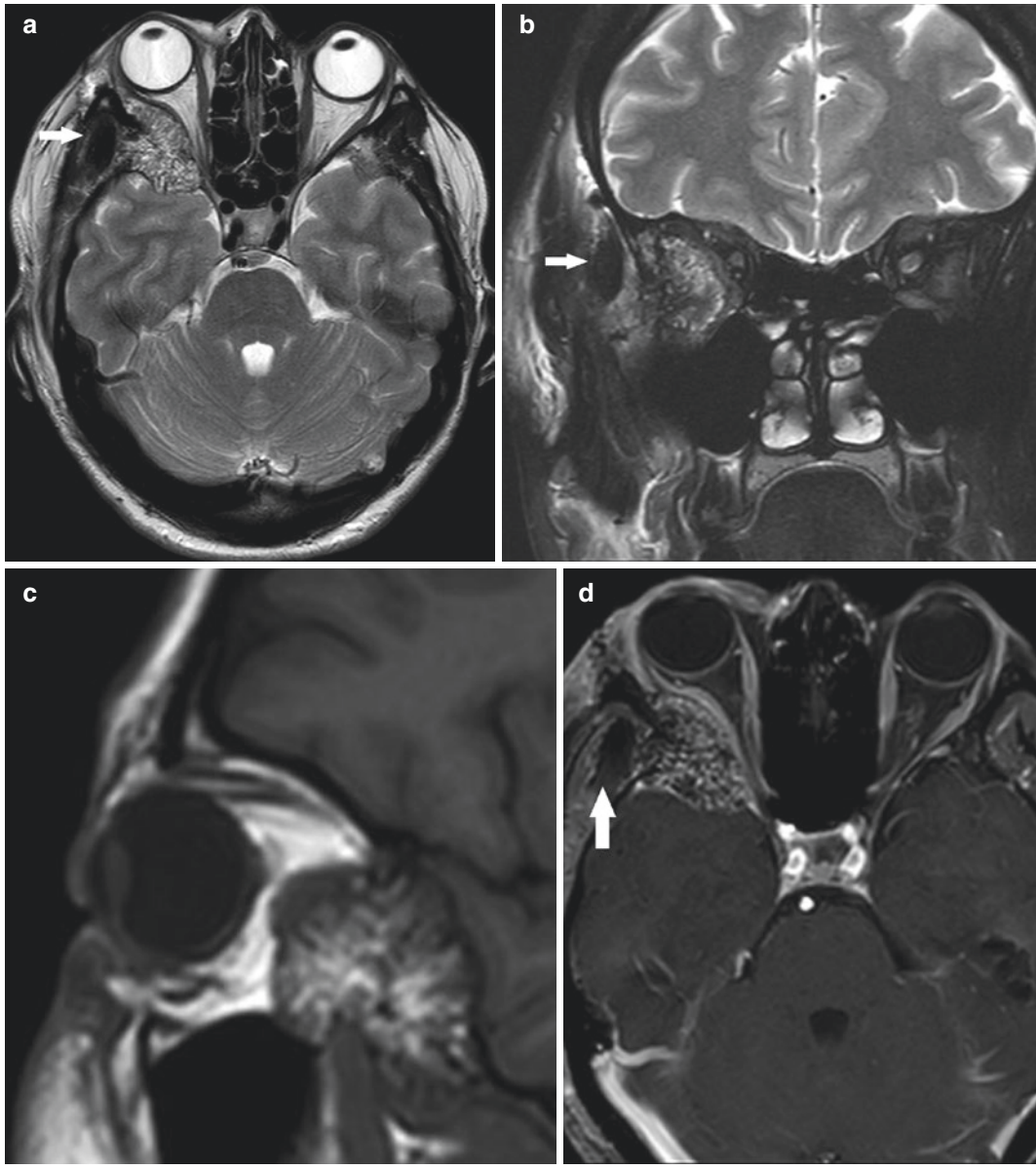

Fig. 14.2 MRI exam of the brain and orbits—axial T2WI (**a**), coronal T2 FS (**b**), sagittal T1WI (**c**), post gadolinium axial T1WI (**d**, **e**). There is a right-sided, large, trabecular expansile lesion of the greater sphenoid wing, peripherally also involving the lesser sphenoid wing, protruding into the right orbit and anterior aspect of the middle cranial fossa, causing proptosis of the right eye. There is moderate contrast enhancement. A small post biopsy defect is evident in the lateral half of the tumour (*arrow* in images **a**, **b** and **d**). There is no evidence of dural infiltration

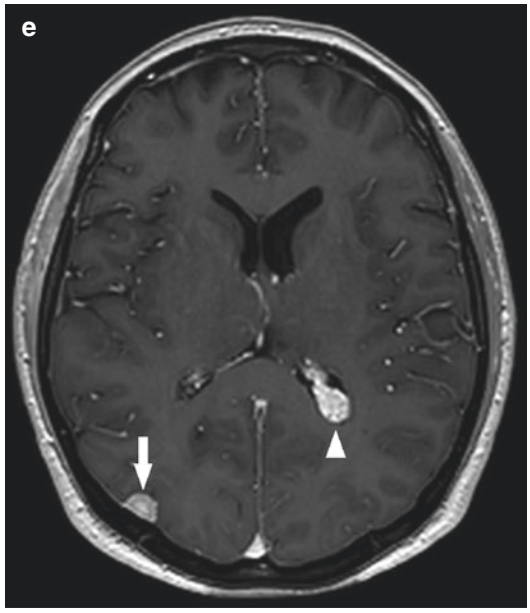

Fig. 14.2 (continued)

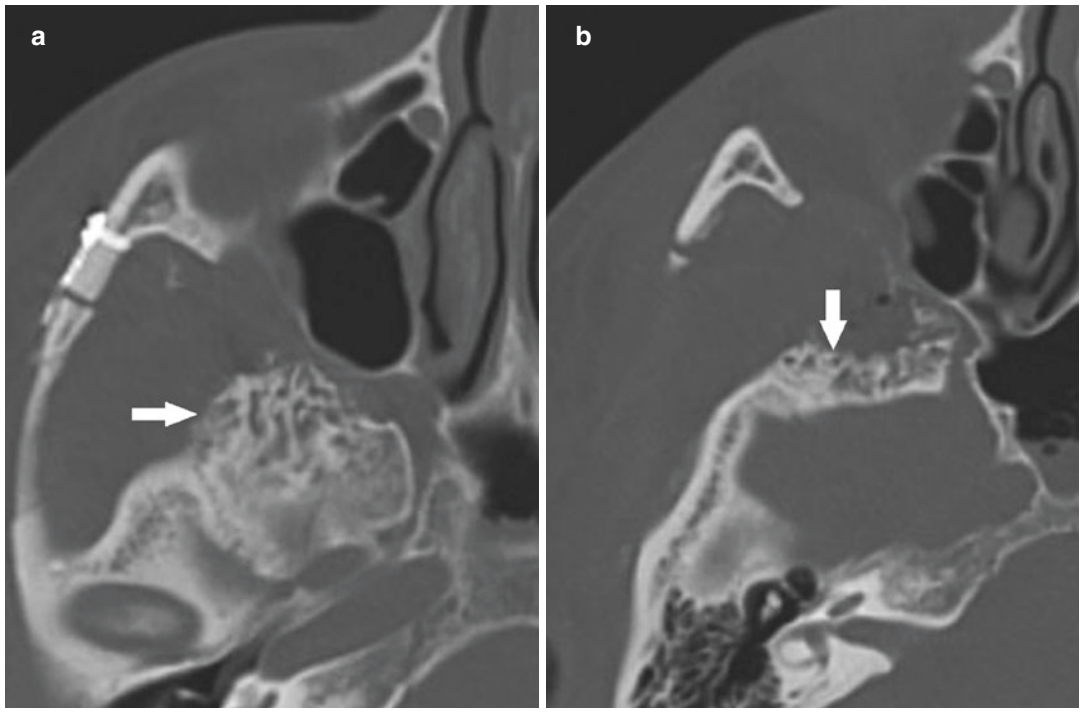

Fig. 14.3 Postoperative CT exam—axial images (**a**, **b**) and coronal reformatted image (**c**) demonstrates osteotomy, with a small residual basal portion of the haemangioma (*arrows*)

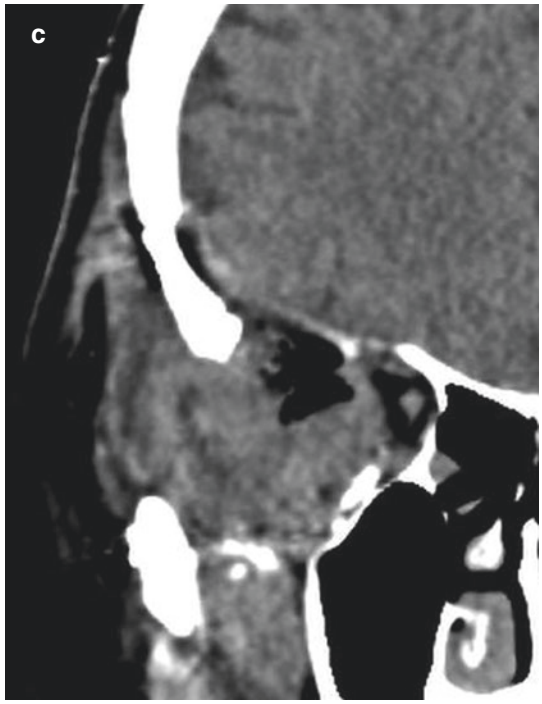

Fig. 14.3 (continued)

expand externally rather than internally. The prevalence is highest among women in the fourth and fifth decade of life. Trauma is considered to be a predisposing factor. If orbit is involved, proptosis and loss of vision are possible; temporal bone involvement may result in hearing loss and facial nerve paralysis, whereas maxillary and mandibular locations are prone to bleeding after tooth extraction and in surgery.

Skull haemangiomas may be venous, cavernous or capillary, according to the predominant vascular network [2]. The cavernous type is composed of large thin-walled vessels and sinusoids lined with a single layer of endothelium; the capillary haemangioma is composed of fine vascular network filled with blood—these two types are frequently seen together, as a mixed-type haemangioma. They may also contain fat, muscle and fibrous tissue and thrombi.

On imaging, intraosseous haemangioma may be misdiagnosed as intraosseous meningioma, as the latter is far more frequent [3]. Confusion with fibrous dysplasia is not uncommon, the main difference being "ground-glass" appearance of the fibrous dysplasia as opposed to "honeycomb" appearance of the haemangioma.

The treatment of choice is en bloc resection with normal bony margin and bone reconstruction. Other treatments include radiation therapy, embolization and curettage. Radiotherapy is generally avoided due to the risk of radiation-induced malignancy; it is the last resort for the unresectable or residual tumours. The drawbacks of curettage are excessive bleeding and high recurrence rate [4].

References

1. Liu JK et al (2003) Primary intraosseous skull base cavernous hemangioma: case report. Skull Base 13(4): 219–228. https://doi.org/10.1055/s-2004-817698
2. Yang Y et al (2016) Primary intraosseous cavernous hemangioma in the skull. Medicine (Baltimore) 95(11):e3069
3. Politti M et al (2005) Intraosseous hemangioma of the skull with dural tail sign: radiologic features with pathologic correlation. Am J Neuroradiol 26(8):2049–2052
4. Park BH et al (2013) Primary intraosseous hemangioma in the frontal bone. Arch Plast Surg 40(3):283–285. https://doi.org/10.5999/aps.2013.40.3.283

Intraosseous Meningioma (of the Greater Wing of the Sphenoid Bone)

15

As an out-hospital patient, a 45-year-old female patient was referred to a head CT due to proptosis of the left eye accompanied with facial asymmetry lasting for several months. Occasionally, she felt sharp pain in the medial angle of the left eye.

Brain CT has revealed a hyperostotic mass of the left greater sphenoid wing with feathered or speculated margins, consistent with intraosseous meningioma (Fig. 15.1).

Due to described CT features, lesion was reported as intraosseous meningioma: MRI of the brain and orbit was recommended and performed several days after the CT examination. MRI confirmed CT finding of intraosseous meningioma causing eye bulb protrusion, while on post-contrast T1WI, it demonstrated adjacent dural thickening and enhancement (Figs. 15.2 and 15.3).

A patient was operated, and part of the hyperostotic intraorbital bone was removed. Pathohistology confirmed intraosseous meningioma. After the operation, left lateral orbital muscle was not compressed, and left bulb did not protrude anymore. Her face did not have asymmetric appearance anymore. Follow-up MRI and CT examinations do not demonstrate enlargement of the rest of the tumour by now.

15.1 Intraosseous Meningioma

Meningiomas are the most frequent benign brain tumours. They arise from meningothelial cells found in the arachnoid membrane and line arachnoid villi associated with intradural venous sinuses and their tributaries. The vast majority are intradural lesions located intracranial in the subdural space, arising along the dural venous sinuses, over the cerebral convexities and in the region of the falx cerebri, although they can develop anywhere in the brain and spine [1]. Extradural meningiomas develop in extracranial sites in the head and neck, but most common are intraosseous meningiomas accounting for about two thirds of all extradural meningiomas [2].

Intraosseous meningiomas (IOMs) are rare, slow-growing tumours, usually involving frontotemporal region of the calvarium and orbits. They are generally benign tumours, but published studies indicate that IOMs are more likely to be malignant than their intradural counterparts. IOMs do not show gender predominance and occur predominantly later in life, with a median patient age at diagnosis in the fifth decade. These tumours have a bimodal incidence peak, one in the second decade, and second peak during the fifth to seventh decades of life [3]. IOM of the greater sphenoid wing clinically presents with pain, proptosis, vision problems, possible swelling and consequently aesthetic problems.

The aetiology is still not clarified: there are several proposed explanations suggesting the origin of intraosseous meningioma. Azar-Kia et al. suggested that IOM arises from ectopic arachnoid cap cells trapped in the cranial sutures during

M. Špero, H. Vavro, *Neuroradiology - Expect the Unexpected*,
https://doi.org/10.1007/978-3-319-73482-8_15

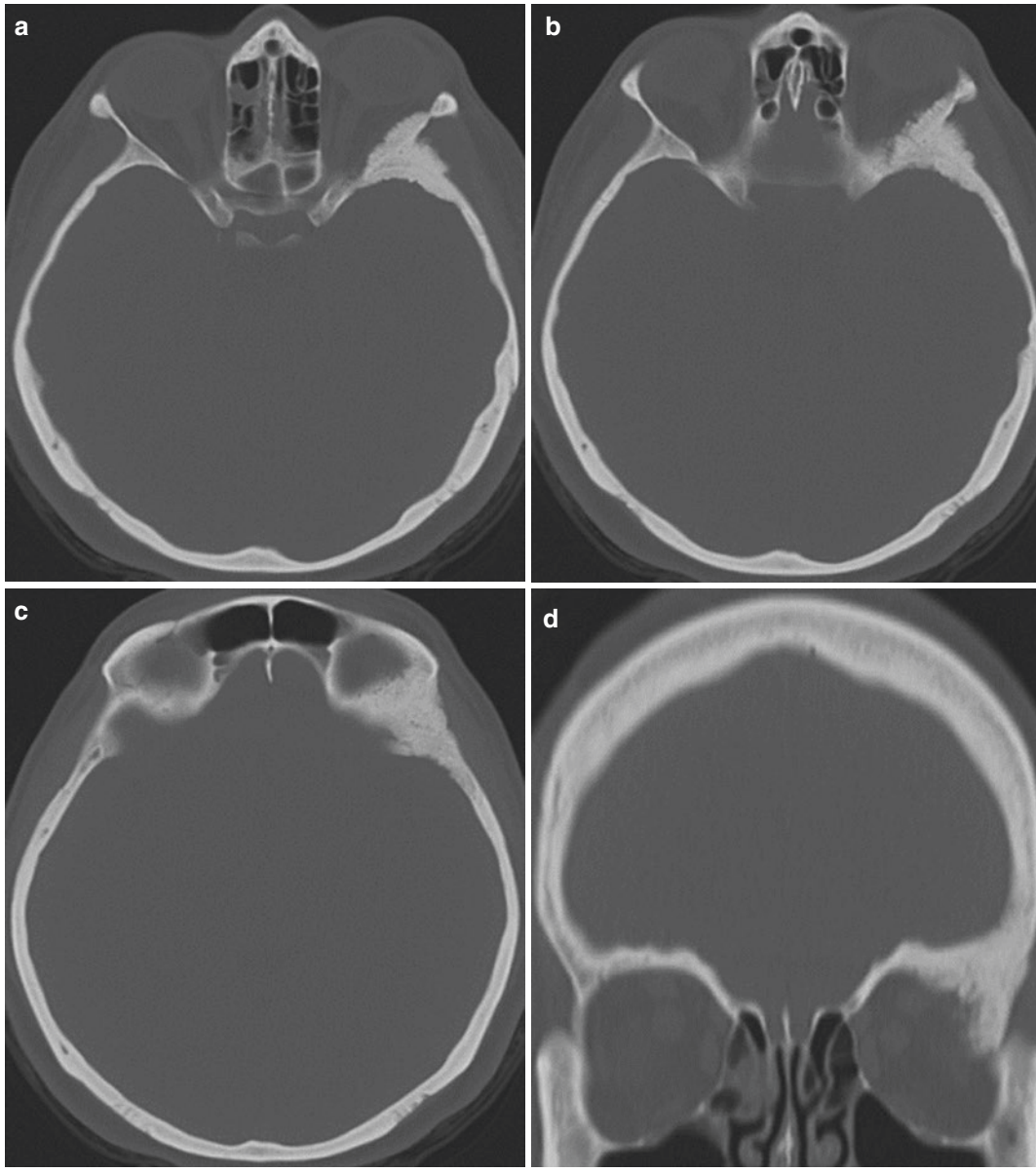

Fig. 15.1 Computed tomography of the brain, axial (**a**–**c**, **h**), coronal (**d**–**f**, **i**) sagittal (**g**) planes revealed hyperostotic lesion within the left greater sphenoid wing with extension into the frontal bone and thickening of the lateral orbital wall. The inner and outer tables showed a feathered or speculated appearance, while inner table bowed toward the brain. Left lateral rectus muscle was mildly enlarged and compressed (**e**, **i**), while the left eye bulb protruded (**a**, **b**, **h**)

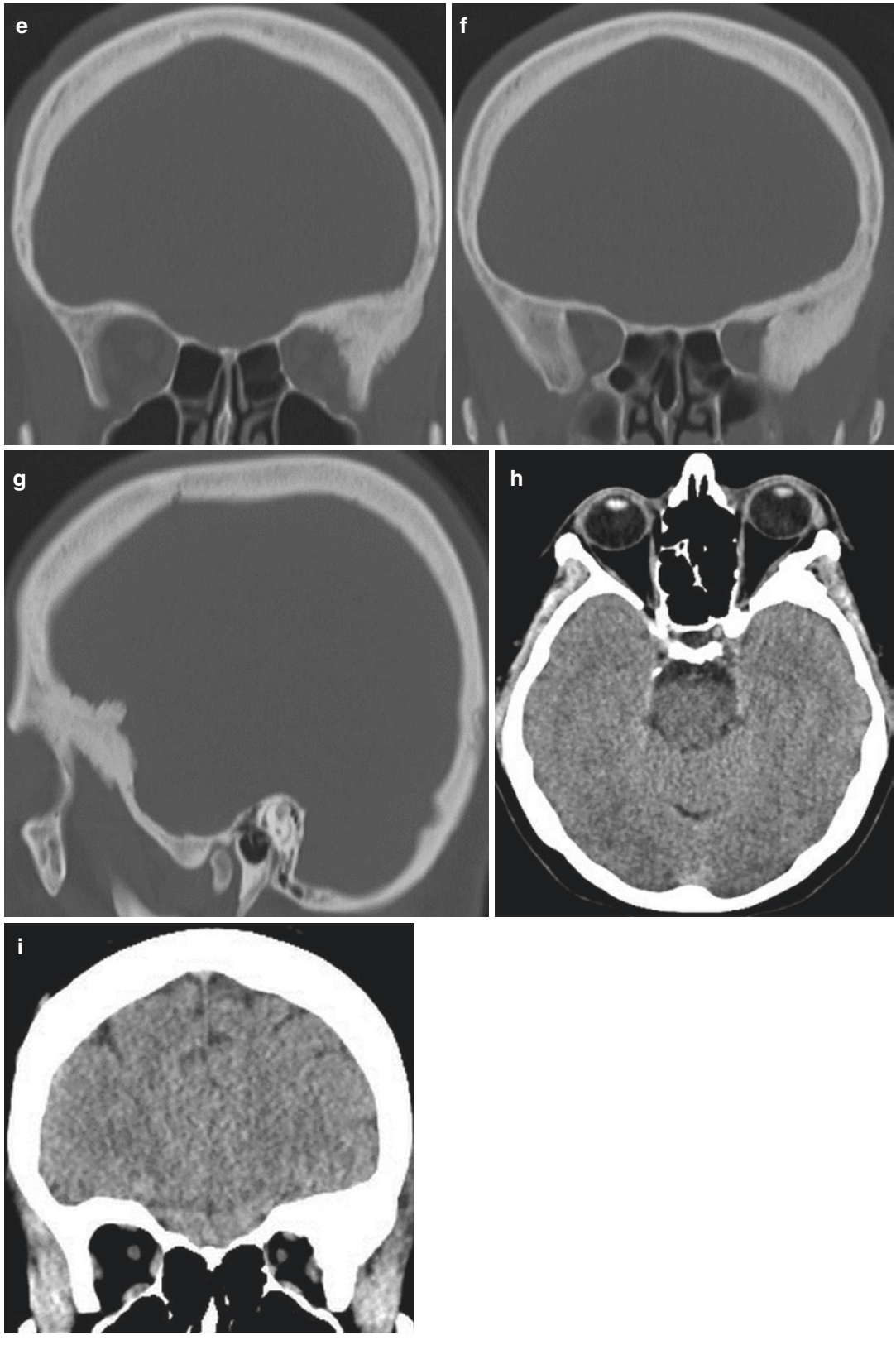

Fig. 15.1 (continued)

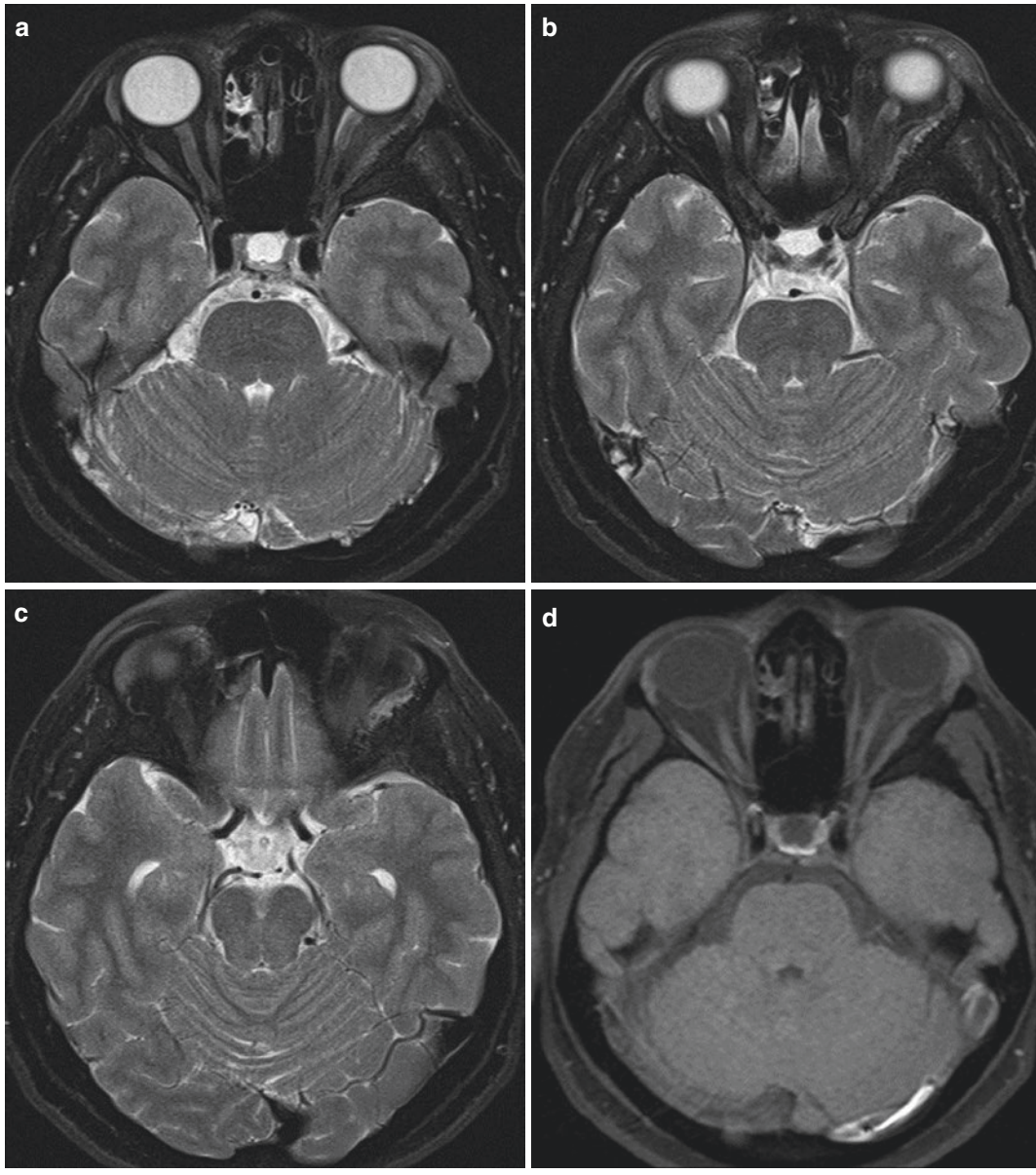

Fig. 15.2 MRI of the orbit, pre-contrast axial T2FSWI (**a**–**c**) and T1FSWI (**d**–**f**), post-contrast axial T1FSWI (**g**–**i**) demonstrated calvarial thickening of the left greater sphenoid wing and left lateral orbital wall, hypointense on pre-contrast T1FSWI and T2FSWI, without contrast enhancement on post-contrast T1FSWI suggesting osteoblastic form of the intraosseous meningioma. Contrast enhancement of the mildly thickened adjacent dura overlying adjacent anterior part of the left temporal lobe, without soft tissue mass. Left eye bulb protruded

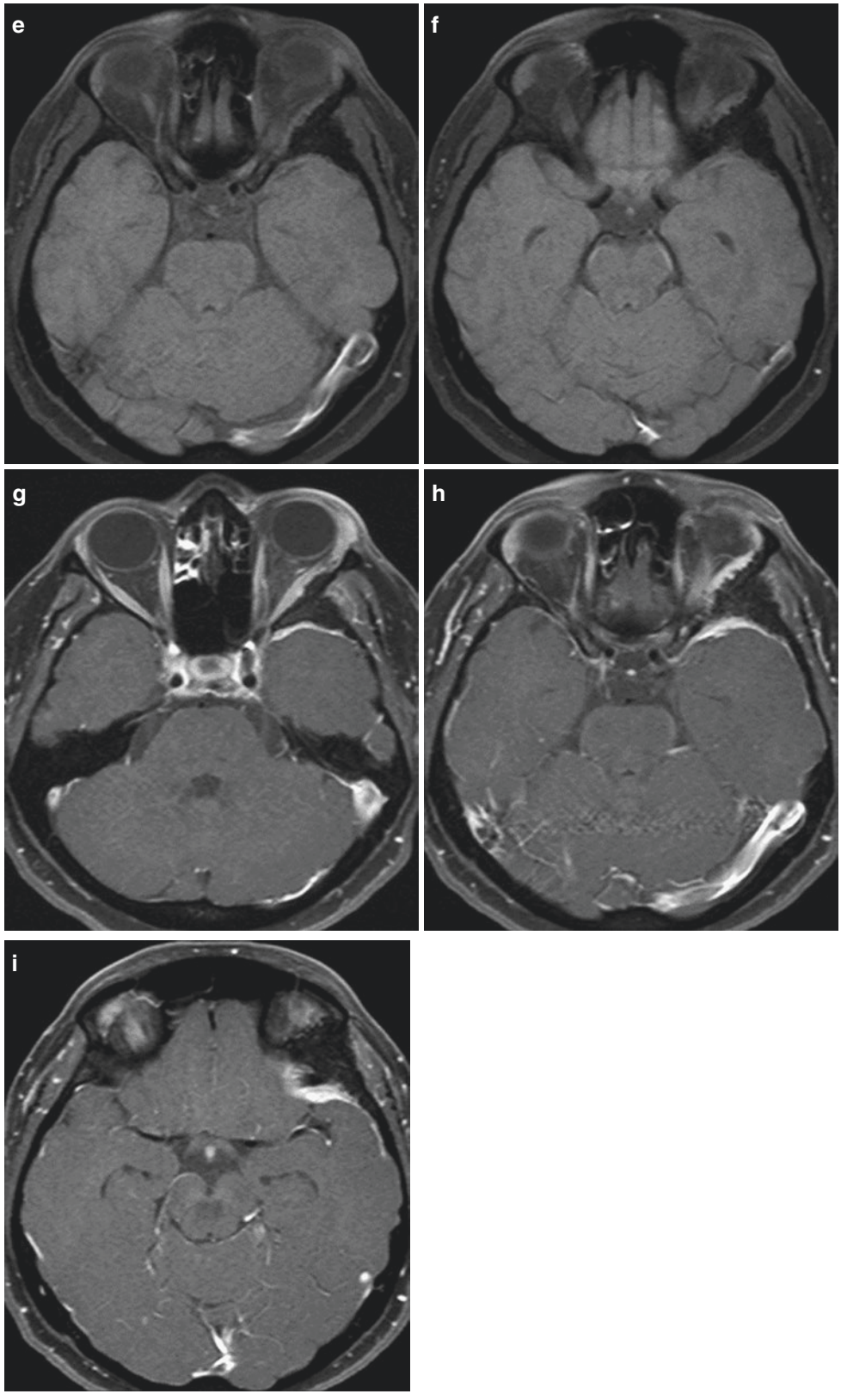

Fig. 15.2 (continued)

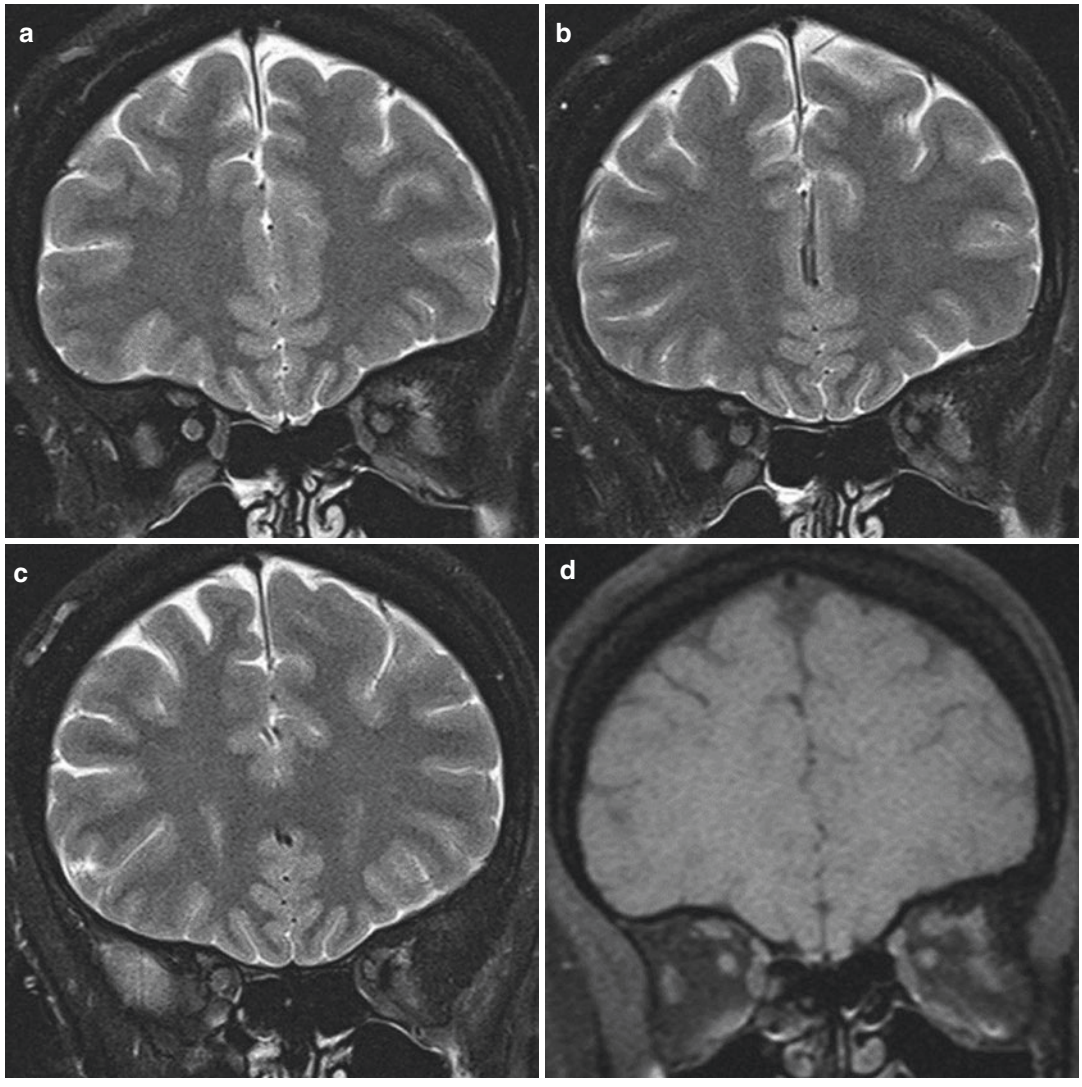

Fig. 15.3 MRI of the orbit, coronal pre-contrast T2FSWI (**a**–**c**) and T1FSWI (**d**–**f**), post-contrast T1FSWI (**g**–**i**). Lateral wall and part of the orbital roof was involved with sclerotic mass. Enhanced dura has encroached planum sphenoidale (**h**, **i**). There were mild mass effect on the left lateral rectus muscle and mild intraorbital contrast enhancement of reactive tissue adjacent to the sclerotic bone, between left superior and lateral rectus muscle (**g**, **h**)

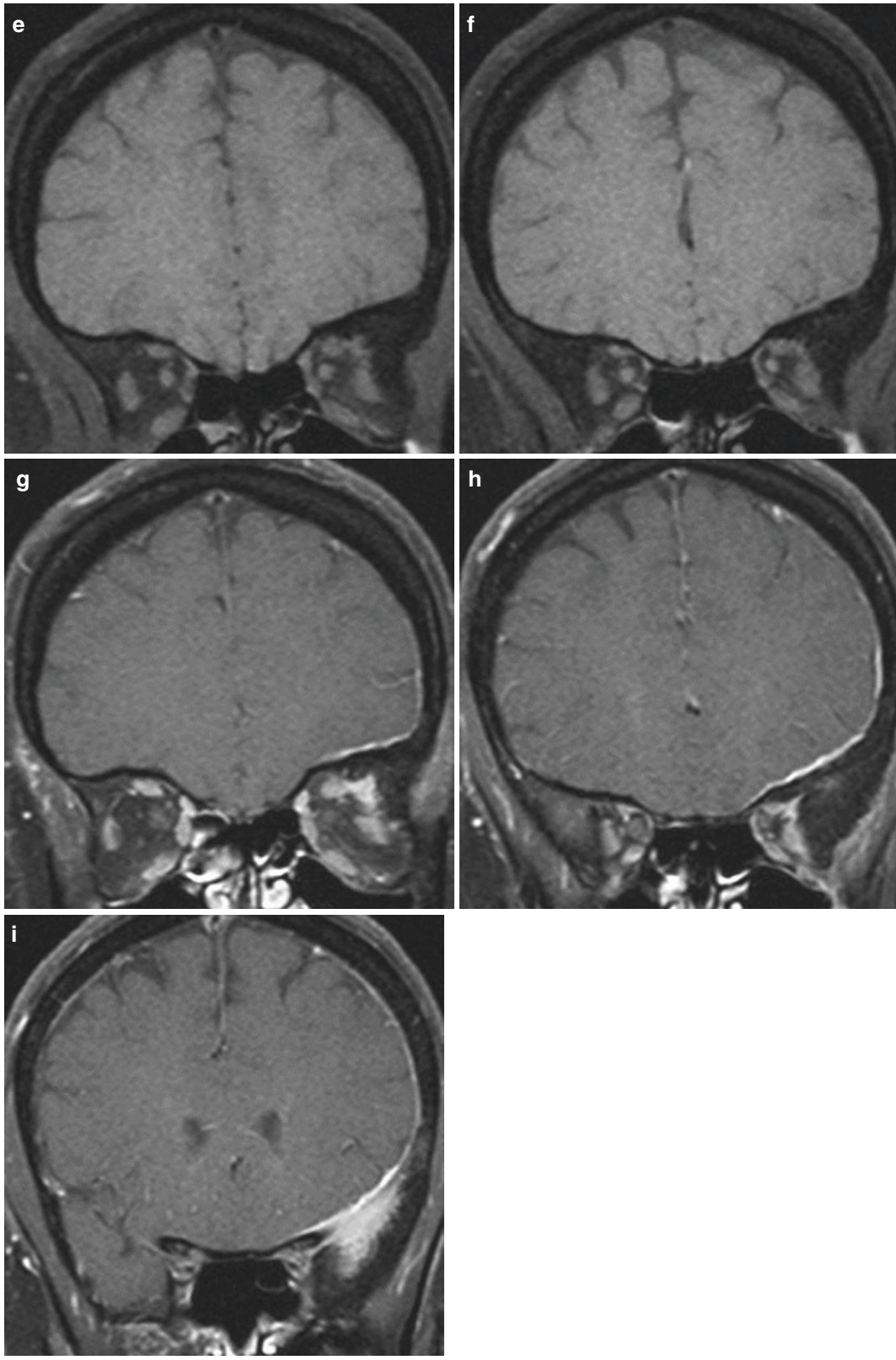

Fig. 15.3 (continued)

moulding of the head at birth: according to the literature, most of IOMs are suture-related masses [4]. Second explanation is that they arise from dura and arachnoid entrapped by previous trauma, while the third suggestion is that extradural meningioma arises from the multipotent mesenchymal cells, explaining mass located far from the head and neck [1, 5].

Lang et al. have suggested to classify primary extradural meningiomas into type I (purely extracalvarial), type II (purely calvarial) and type III (calvarial lesions extending beyond the calvaria). Each type is further divided into subgroup B (skull base) and C (convexity) [6].

Radiologically, intraosseous meningioma is classified as osteoblastic, osteolytic or mixed osteoblastic-osteolytic type. IOMs are mostly osteoblastic type characterised by intraosseous mass growth leading to significant hyperostosis of an involved bone with, usually, soft tissue growth of a surrounding dura. CT with bone window shows focal hyperostotic bone lesion with feathered appearance of the inner table, which is hypointense on T1WI and T2WI on MRI, while both imaging techniques show contrast enhancement of the adjacent thickened dura and dural soft tissue mass if present [1–3, 5, 7]. MRI allows better delineation in the evaluation of soft tissue component and extradural extension. Thickened and enhanced dura adjacent to the bony tumour is a result of reactive inflammation or tumoural invasion. Pial enhancement, focal dural nodules or dural thickening of more than 5 mm is highly accurate in predicting neoplastic dural invasion [2]. Osteolytic lesions typically cause thinning, expansion and interruption of the inner and outer cortical layers of the skull [3].

In this case, tumour was sphenoid bone lesion extending beyond calvaria, therefore classified as type III B tumour. According to clinical presentation, patient age, typical location of the hyperostotic lesion with lateral orbital wall involvement and other described CT and MRI features (Figs. 15.1, 15.2, and 15.3), diagnosis of the IOM of the greater sphenoid wing was obvious to us and later histologically confirmed. Histological findings pathognomonic of IOM include uniform spindle-shaped cells arranged in whorls and interconnecting fascicles.

Differential diagnosis includes fibrous dysplasia (FD), meningioma en plaque, osteoma, osteosarcoma and Paget disease. It is important to differentiate IOM from fibrous dysplasia due to different treatment options. FD is a developmental disease that commonly occurs at young age and stops to grow after bone maturation. IOM appears after puberty and continues to grow slowly. IOM and FD expand the bone. In FD the inner table of the skull is typically smooth, while in IOM there is irregularity of the inner table, particularly at the site of origin, almost always with associated dural reaction. Therefore, this irregularity is the key to distinguish IOM and FD on imaging, as well as a soft tissue involvement and contrast enhancement [1, 2, 7].

Total tumour removal with wide surgical resection followed by cranial reconstruction is the treatment of choice. Adjuvant therapy, including gamma knife, chemotherapy and bisphosphonate therapy, is indicated in patients with malignancy and for non-resectable tumours [2, 3].

References

1. Vlychou M et al (2016) Primary intraosseous meningioma: an osteosclerotic bone tumour mimicking malignancy. Clin Sarcoma Res 6:14–19
2. Lee SJ et al (2015) Primary intraosseous meningioma in the orbital bony wall: a case report and review of the literature review. J Korean Soc Radiol 72(1):68–72
3. Elder JB et al (2007) Primary intraosseous meningioma. Neurosurg Focus 23(4):1–9
4. Azar-Kia B et al (1974) Intraosseous meningioma. Neuroradiology 6:246–253
5. Hussaini SM et al (2010) Intraosseous meningioma of the sphenoid bone. Radiol Case Rep 5(1):357–360
6. Lang FF et al (2000) Primary extradural meningiomas: a report on nine cased and review of the literature from the era of computerized tomography scanning. J Neurosurg 93:940–950
7. Shaftel SS et al (2017) Intraosseous meningioma mimicking fibrous dysplasia. Sci Pages Ophthalmol 1(1):25–27

Fibrous Dysplasia: Osteosarcoma

16

Skull deformity, predominantly frontal, has been something this 62-year-old lady has lived with since childhood. A diagnosis of craniofacial fibrous dysplasia was established by the previous X-ray, CT and MRI exams, as well as by bone biopsy, and the appearances were stable for years. The patient's personal medical history also included surgery and chemotherapy for breast cancer 12 years ago (Fig. 16.1).

Six months before admission to the hospital, the patient noticed a moderate enlargement of the deformity in the left frontal region: at that time, FNA confirmed fibrous dysplasia. Further growth warranted a follow-up CT exam (Fig. 16.2).

A localised resection of the expanded bone in the left frontal region was done. Intraoperative biopsy confirmed fibrous dysplasia. However, postoperative extended histopathology analysis revealed osteosarcoma on grounds of previous fibrous dysplasia. The resection borders could not be determined in the available tissue specimen. Another surgery was done, this time larger in extension (Fig. 16.3).

16.1 Craniofacial Fibrous Dysplasia

Fibrous dysplasia (FD) is a tumour-like, non-neoplastic congenital disease, probably caused by a somatic mutation early in embryonic life, featuring defective osteoblastic differentiation and maturation. Immature bone is intermixed with excessively proliferated fibrous tissue.

It may affect a single bone (monostotic, 70% of cases, most common in ribs) or multiple bones (polyostotic, usually unilateral limb lesions). Any bone may be affected. Craniofacial fibrous dysplasia (CFD) occurring in multiple adjacent craniofacial bones is regarded as monostotic, and it accounts for up to 25% of monostotic form. It may be one of the features in McCune-Albright syndrome [1]. CFD behaves as a chronic, slowly progressive mass lesion, usually self-limiting, rarely progressing after the third decade of life. Complications are usually caused by compression of skull foramina, nerves and vessels—such as visual loss, proptosis, hearing loss and headache.

M. Špero, H. Vavro, *Neuroradiology - Expect the Unexpected*,
https://doi.org/10.1007/978-3-319-73482-8_16

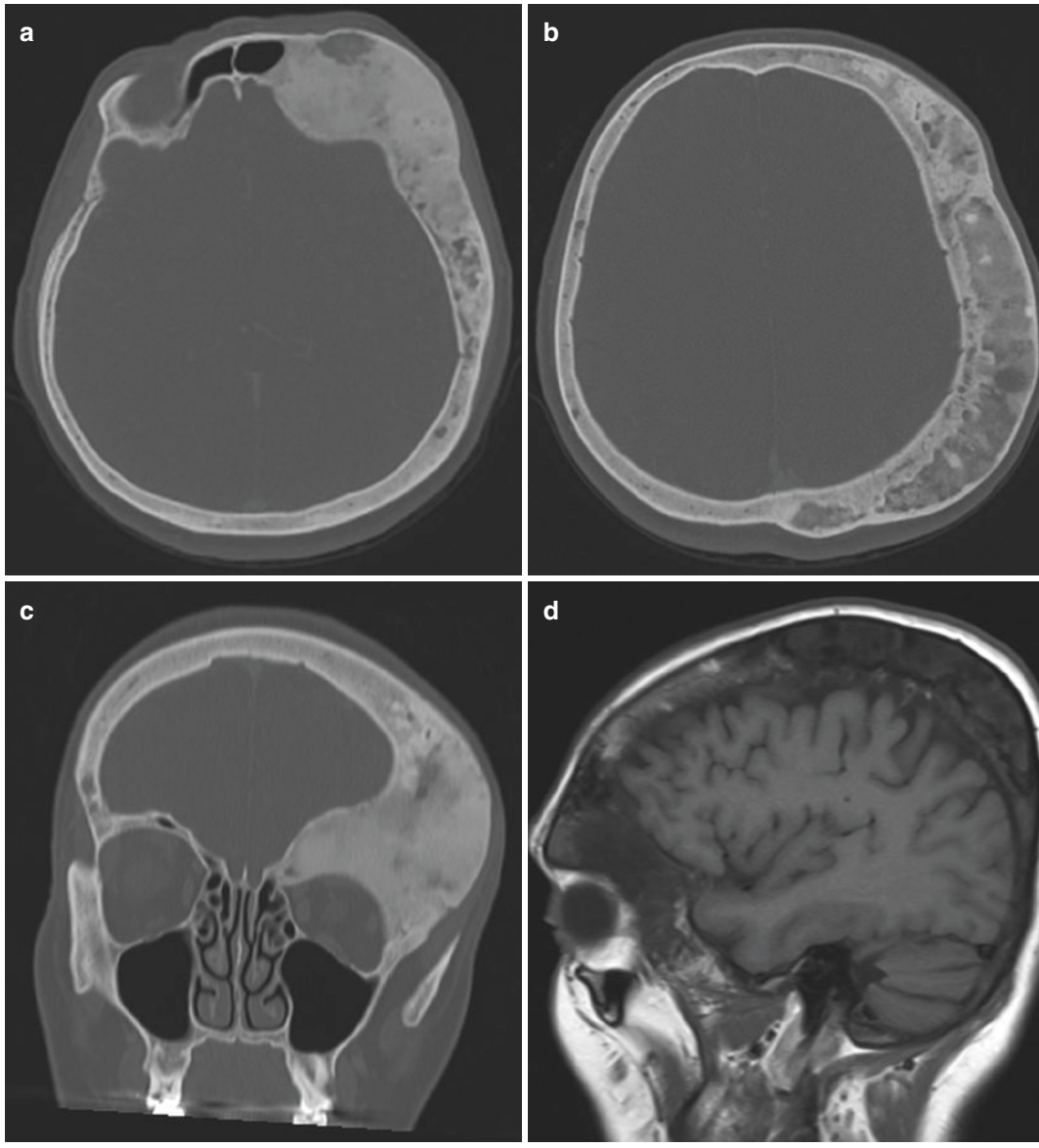

Fig. 16.1 Non-contrast-enhanced axial (**a**, **b**) and coronal (**c**) CT and sagittal T1WI (**d**), axial T2WI (**e**) and coronal T2WI (**f**) MRI images of the (monostotic; see text) fibrous dysplasia involving the left frontal, parietal, sphenoid and temporal bone. Note the facial asymmetry with left orbital deformity (**c**, **f**). CT images demonstrate loss of normal corticomedullary differentiation in the expanded bones, replaced by a ground-glass pattern with focal lucencies and scleroses. MRI images show heterogenous bone signal

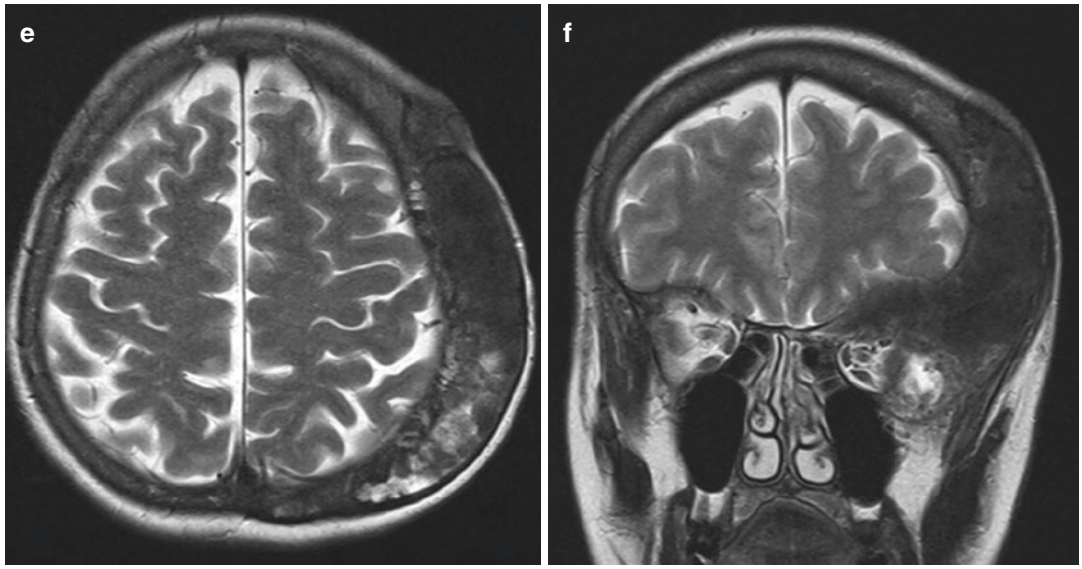

Fig. 16.1 (continued)

CT imaging features ground-glass expansile lesion centred in the medullary bone layer, with inner cortical scalloping and heterogenous sclerosis. There is no periosteal reaction.

MR imaging features consist of heterogenous signal, mostly intermediate in T1WI and low in T2WI and heterogenous contrast enhancement.

The transition to normal bone is often indistinct.

Differential diagnosis includes Paget disease which usually spares facial bones and is more sclerotic; intraosseous meningioma which tends to be sclerotic, does not spare the cortical bone and often abuts the intracranial compartment; sclerotic metastases which are usually smaller in size and focal in distribution; and cemento-ossifying fibroma which is usually distinct from the adjacent normal bone.

The risk for malignant transformation in FD is approximately less than 1% in the monostotic form and up to 4% in the polyostotic form, being the most frequent in McCune-Albright syndrome patients [2]. Prior radiation exposure is also recognized as a risk factor for malignant transformation. The most common sites of malignant transformation in monostotic form of fibrous dysplasia are facial and skull bones. Osteosarcoma accounts for approximately 70% of malignant transformation cases, followed by fibrosarcoma (20%) and chondrosarcoma (10%). The appearance of the benign fibrous dysplasia makes malignant transformation difficult to identify. Sarcomatous transformation may appear in form of cystic osteolytic areas, cortical destruction and heterogeneously enhancing soft tissue mass, such as in this case. The patient should be instructed to bring any change in symptoms to physician's attention. Rapid growth, especially in adults, pain without history of trauma and significant change in radiologic appearance are some of the signs of possible malignant transformation. Yearly X-rays are advocated for screening [3]. The cure for FD or ways to prevent malignant transformation still do not exist.

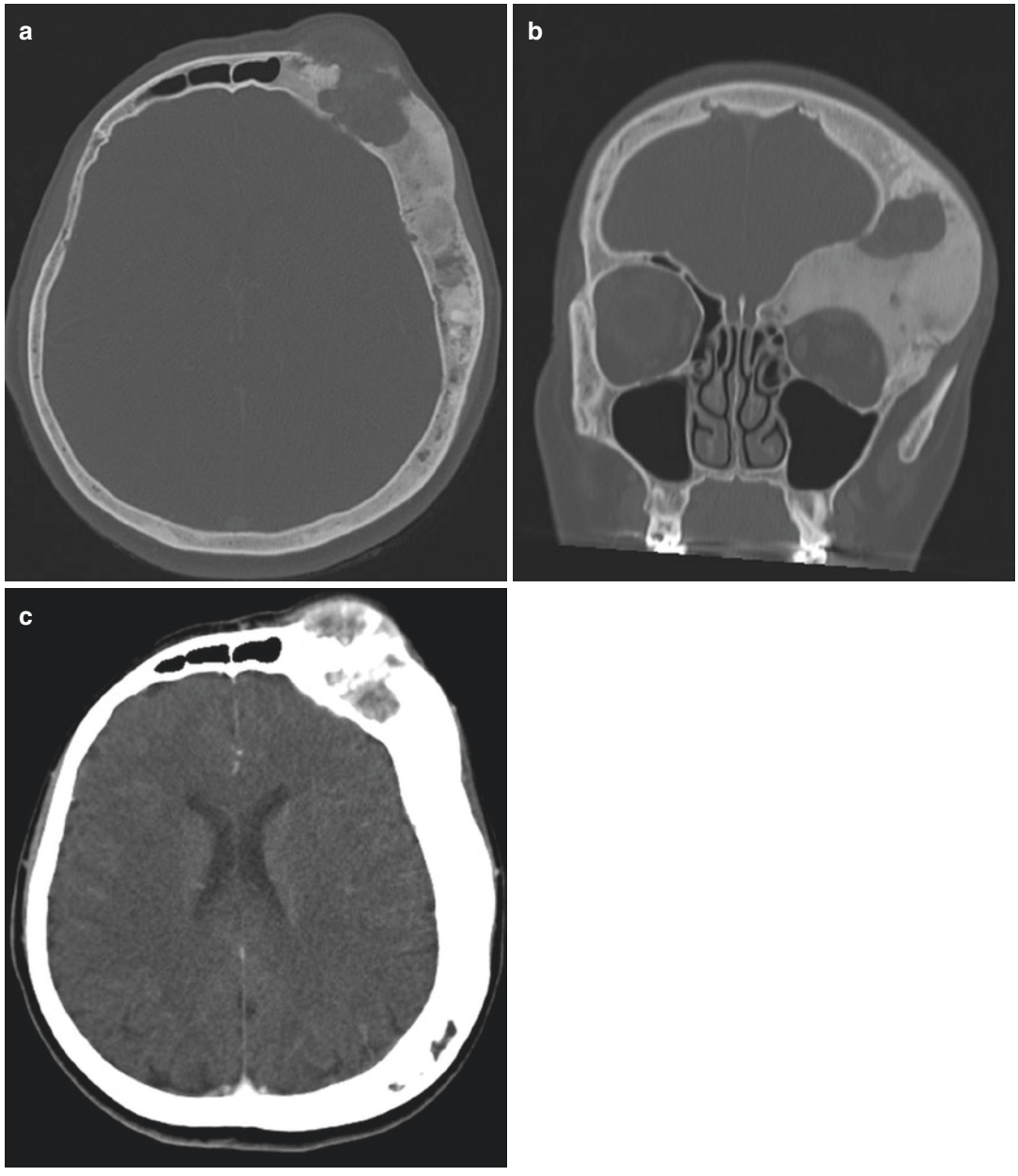

Fig. 16.2 Contrast-enhanced follow-up CT images of the head—note the left frontal bone defect (**a**, **b**) caused by an irregularly enhancing (**c**) osteolytic expansile lesion, not evident in Fig. 16.1

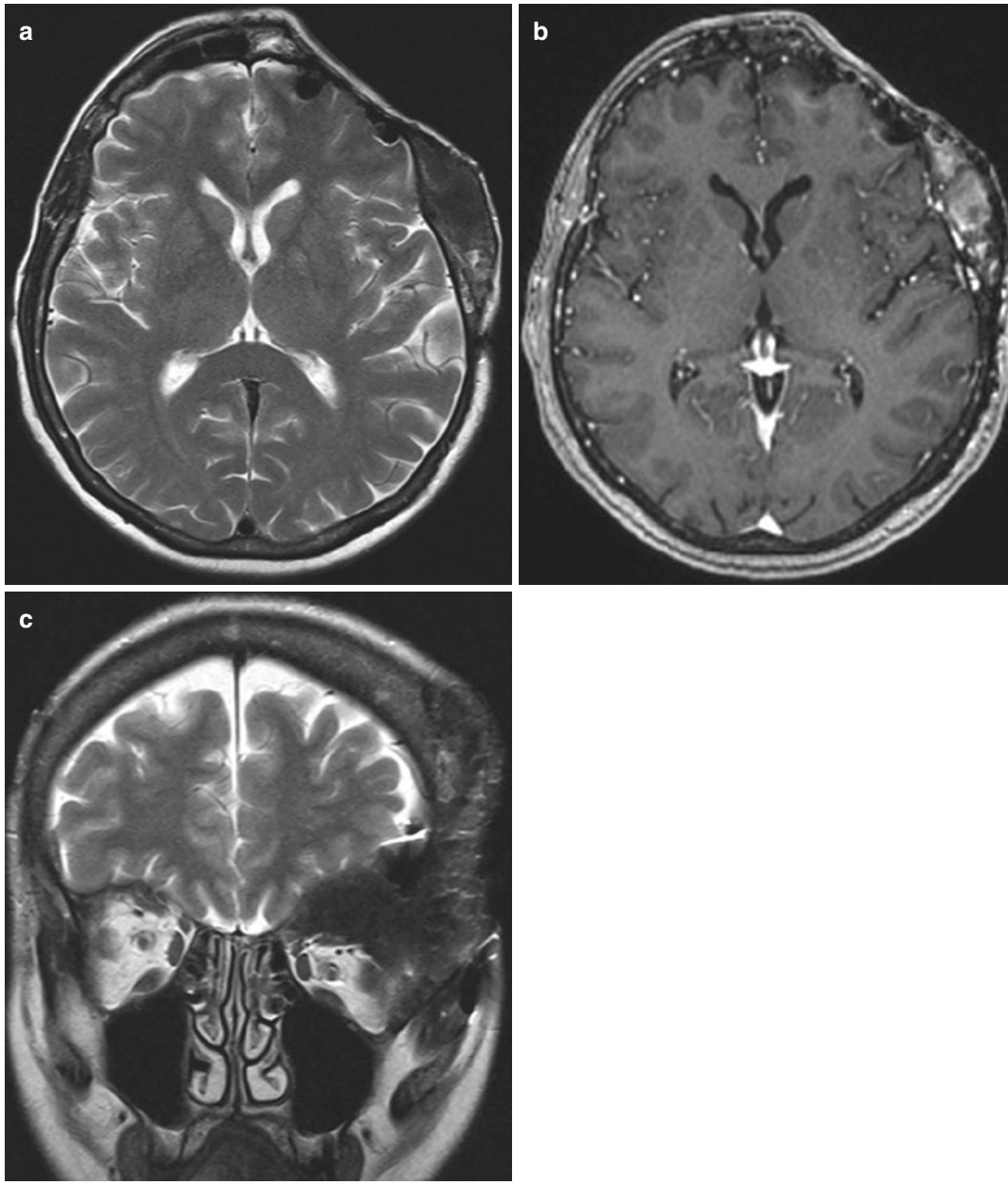

Fig. 16.3 Postoperative MRI of the head—axial T2WI (**a**), axial post-contrast T1WI (**b**), coronal T2WI (**c**). There are postoperative bony defects and characteristic post gadolinium enhancement of the remaining dysplastic bones (**b**)

References

1. Larheim TA, Westesson P-LA (2006) Maxillofacial imaging, vol 81. Springer, Berlin
2. Riddle ND, Bui MM (2013) Fibrous dysplasia. Arch Pathol Lab Med 137(1):134–138
3. Mardekian SK, Tuluc M (2015) Malignant sarcomatous transformation of fibrous dysplasia. Head Neck Pathol 9(1):100–103

Sphenoid Wing Meningocele

17

At the end of April 2016, a 29-year-old female patient came to our MRI unit, as an out-hospital patient, for a brain MRI (Figs. 17.1 and 17.2). Her only symptom was headache: non-specific diffuse headache during several years, sometimes on daily basis.

About a year ago, she has performed MRI of the brain in a private clinic where radiologist has reported a right temporal arachnoid cyst.

According to the described imaging features (Figs. 17.1 and 17.2), the meningocele of the greater wing of the sphenoid bone was reported spontaneous, because there were no information about other possible aetiologies. Arachnoid cysts represent intra-arachnoid CSF-containing cysts that do not communicate with the ventricular system or adjacent subarachnoid spaces, which are most commonly located supratentorial in the middle cranial fossa. Large anterior temporal arachnoid cyst may thin adjacent greater sphenoid wing but will not cause expansile defect in the bone.

A patient was not a middle-aged obese female; there were no clear information about visual problems, but according to MRI features, there were three imaging characteristics attributable to an idiopathic intracranial hypertension: prominent arachnoid pits, slitlike ventricles and prominent subarachnoid space around the optic nerves showing vertical tortuosity (Fig. 17.2). The lesion was previously misdiagnosed as temporal arachnoid cyst: in a control interval, it did not change in size. For the time being, follow-up MRI of the brain is recommended, and surgical treatment is a next step in a patient management.

17.1 Sphenoid Wing Meningocele

The term meningocele describes a herniation of meninges and CSF through a bony defect in a skull: CSF egresses from the intracranial cavity through an abnormal communication between the subarachnoid space and a bone. Unless otherwise specified, these lesions are referred as CSF fistulas [1]. Meningocele may be congenital due to a failure of normal skull development with a bone defect, acquired non-traumatic (surgery, tumour, dysplasia, osteoradionecrosis) or posttraumatic, and spontaneous without clear cause [1, 2].

Currently it is widely accepted that spontaneous meningocele in the skull base is a result of a multifactorial process that involves both elevated intracranial pressure and anatomic predisposition involving thinning of the cranial base [1]. Those may occur anywhere in the skull base: in occipital bone, at cribriform plate or temporal bone. Subset of spontaneous meningoceles occur off the midline in the lateral sphenoid bone, known as sphenoid lateral spontaneous cephaloceles (SLSCs).

M. Špero, H. Vavro, *Neuroradiology - Expect the Unexpected*,
https://doi.org/10.1007/978-3-319-73482-8_17

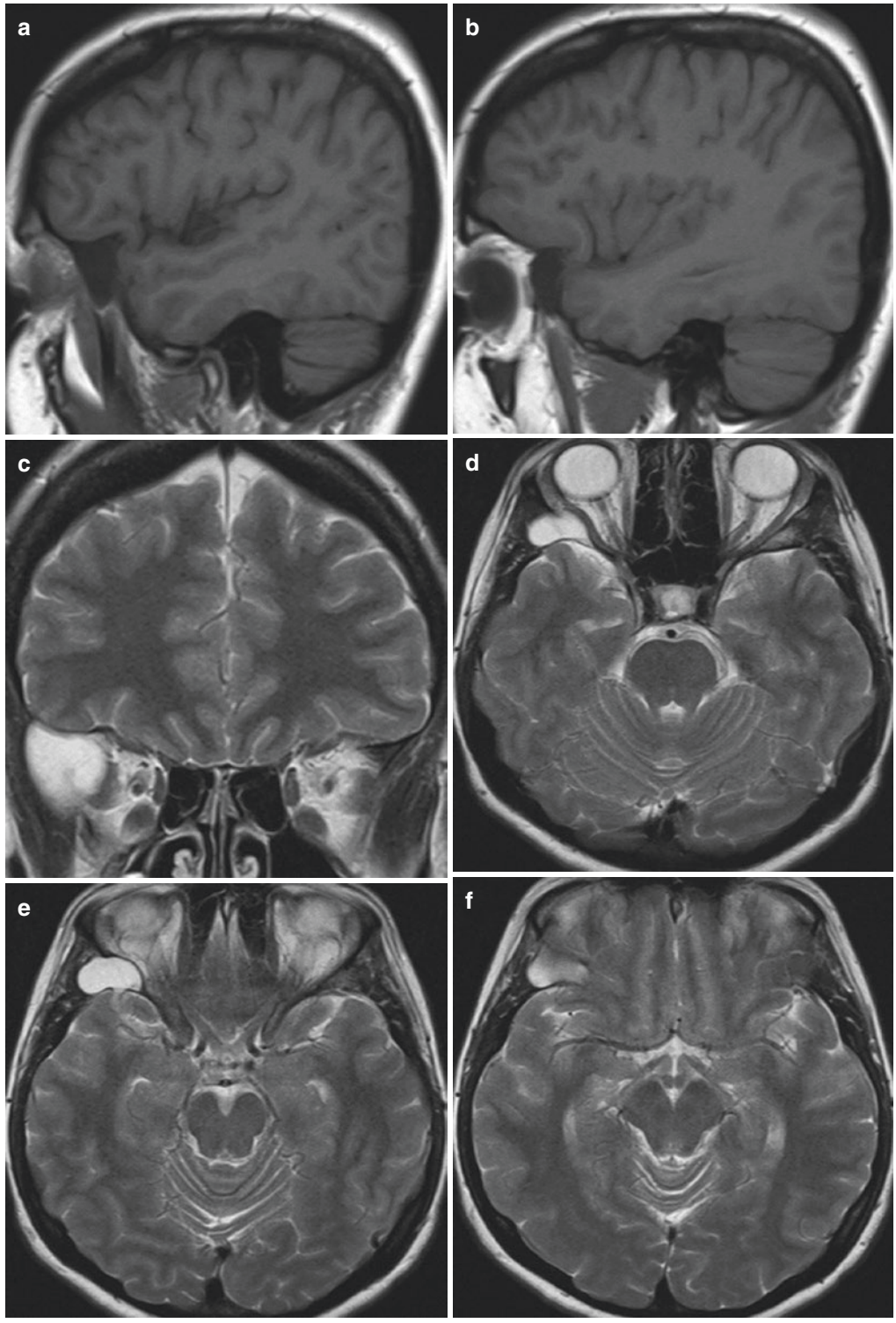

Fig. 17.1 Magnetic resonance imaging of the brain, non-contrast, sagittal T1WI (**a**, **b**), coronal (**c**) and axial (**d**–**f**) T2WI, axial FLAIR (**g**–**i**), axial DWI (**j**), ADC (**k**), SWI (**l**), axial (**m**, **n**) and sagittal (**o**) CISS revealed expansile cystic lesion in the greater wing of the sphenoid bone containing only fluid, causing a defect in the bone. Signal intensity of the cyst fluid was similar to CSF on all sequences, while the lesion communicated with adjacent subarachnoid space through a narrow defect

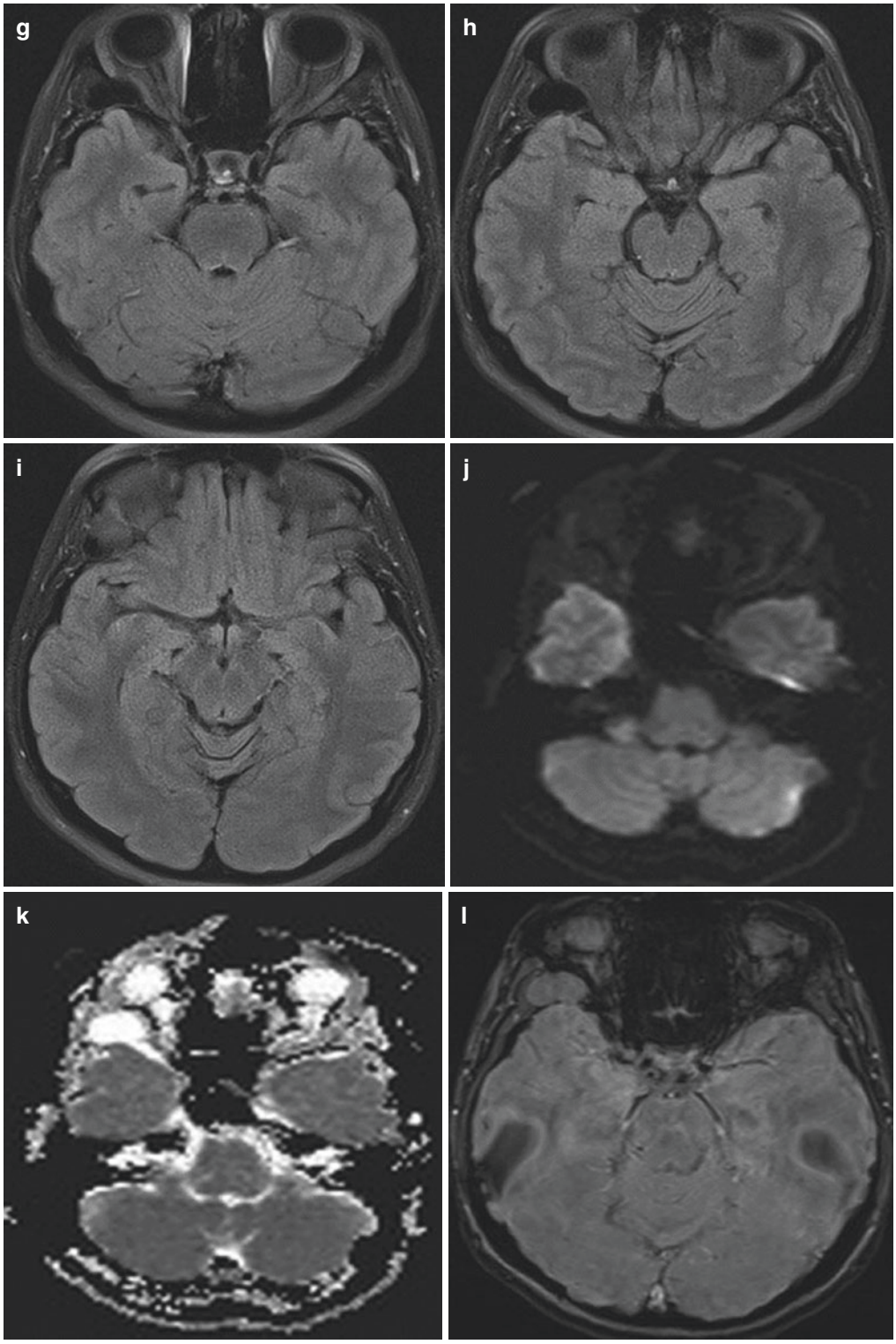

Fig. 17.1 (continued)

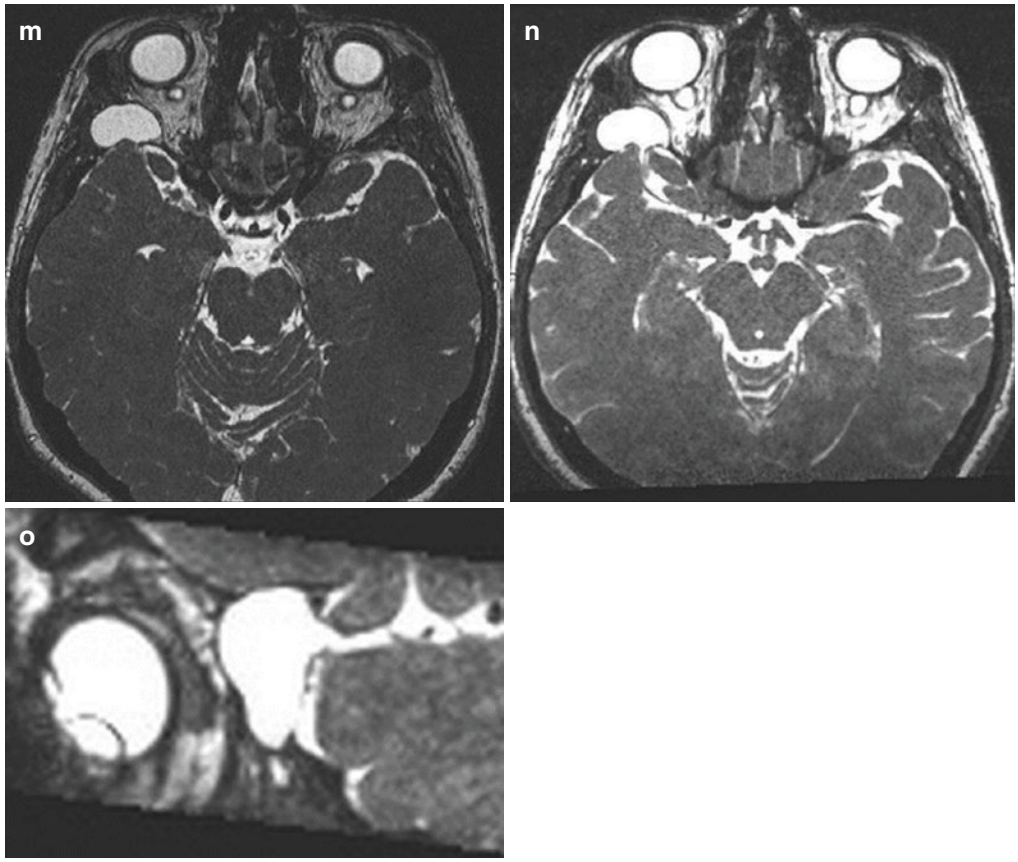

Fig. 17.1 (continued)

There are two types of SLSCs described in the literature: type I herniates into a pneumatised lateral recess of the sphenoid sinus usually presenting with headache and/or CSF leak. Type II herniates into the greater sphenoid wing with scalloping bone defect, may be an incidental finding or may present with headache and/or seizures [2].

The most important mechanism underlying the development of SLSC is likely related to altered CSF dynamics in aberrant arachnoid granulations: those are arachnoid granulations found outside, instead of the inside, dural venous sinuses, resulting in small concave pits in the inner table of the calvaria or the skull base [2–4]. Usually are incidental and asymptomatic, but in the setting of persistently elevated CSF pressure, egress of CSF from the aberrant arachnoid granulations may be impaired leading to granulations' progressive enlargement and scalloping of the underlying bone [5].

Spontaneous meningoceles most commonly occur in middle-aged obese women with clinical symptoms and imaging features of elevated intracranial pressure.

In the evaluation of SLSC, CT and MRI are complementary imaging techniques: CT demonstrates bone defect and adjacent anatomical structures, and post-contrast CT scans show relation between bone defect and dural sinus, while MRI reveals content of herniated tissue. Three-dimensional CISS sequence provides superior topographic information: therefore I personally use it to investigate a wide range of pathologies when routine MRI sequence does not provide desired anatomic information. In the particular case, I used it to demonstrate more clearly meningocele and

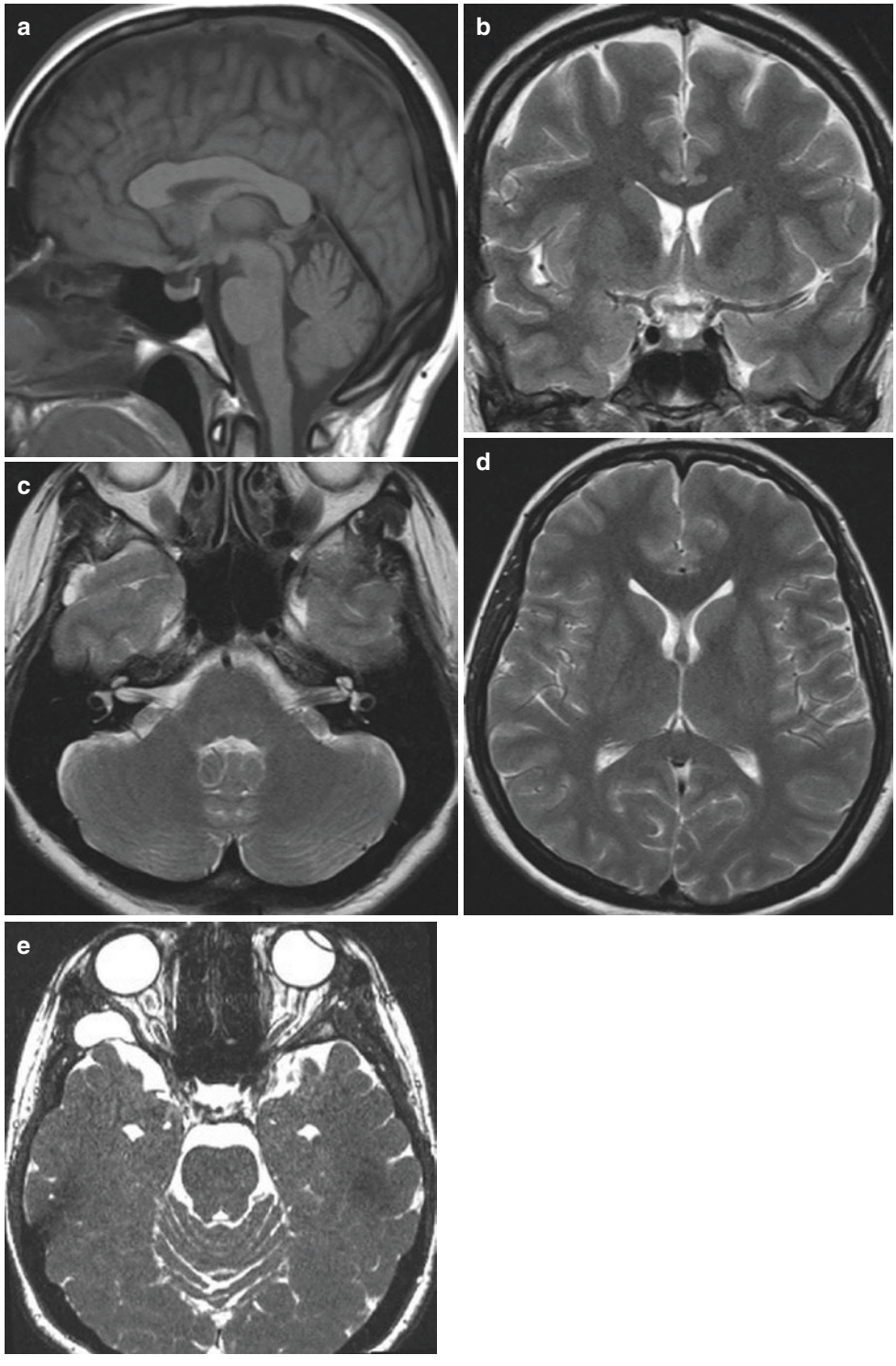

Fig. 17.2 Magnetic resonance imaging of the brain, sagittal T1WI (**a**), coronal (**b**), and axial (**c**, **d**) T2WI, axial CISS (**e**). Sella and hypophysis were of normal size and shape (**a**, **b**), there were no tonsillar ectopia (**b**), lateral and third ventricles were narrow and slitlike (**b**, **d**), and there were prominent arachnoid pits of the sphenoid wing (**c**). CISS sequence more clearly revealed prominent subarachnoid space around the optic nerves and vertical tortuosity of the nerves (**e**)

arachnoid pits, to reveal the exact communication between meningocele and adjacent subarachnoid space and to better visualise optic nerve changes.

Some SLSCs may resolve spontaneously, if are incidental imaging finding and asymptomatic, no treatment is needed. Otherwise, surgical repair is recommended to prevent meningitis or intracranial abscess.

If you see an expansile cystic lesion in the sphenoid bone, do not mistake it for a temporal arachnoid cyst; always ask yourself where the lesion is located, intracranial or extracranial in a bone. If you use 3D CISS sequence, you will be able to report more details regarding anatomical relations and depict communication between a lesion and subarachnoid space at the same time.

References

1. Alonso RC et al (2013) Spontaneous skull base meningoencephaloceles and cerebrospinal fluid fistulas. Radiographics 33:553–570
2. Settecase F et al (2014) Spontaneous lateral sphenoid cephaloceles: anatomic factors contributing to pathogenesis and proposed classification. AJNR Am J Neuroradiol 35(4):784–789
3. Schlosser RJ et al (2006) Spontaneous cerebrospinal fluid leaks: a variant of benign intracranial hypertension. Ann Otol Rhinol Laryngol 115:495–500
4. Almontasheri A et al (2012) Arachnoid pit and extensive sinus pneumatisation as the cause of spontaneous lateral intrasphenoidal encephalocele. J Clin Imaging Sci 2:1–6
5. Connor SEJ (2010) Imaging of skull-base cephaloceles and cerebrospinal fluid leaks. Clin Radiol 65:832–841

Occipital Bone Intradiploic Encephalocele

18

A 77-year-old lady was referred for a routine MRI examination of the brain because of recent intermittent dizziness and unsteadiness. No other neurological abnormalities were noted, and there were no developmental abnormalities nor history of trauma.

MRI did not show any focal cerebellar lesions, but our attention was drawn to an internal table and diploic defect on the right side of the occipital bone, adjacent to the right occipitotemporal suture (Fig. 18.1).

The findings were in keeping with an intradiploic occipital meningoencephalocele.

Additional CT exam was performed (Fig. 18.2).

18.1 Intradiploic Encephalocele

Encephalocele (also, encephalocoele) or meningoencephalocele consists of brain tissue and meninges herniated through a skull defect. They are very rare in adults, and more commonly they are encountered in infants as saclike protrusions of the brain and meninges through openings in the skull, representing incomplete closure of the neural tube during foetal development. Approximately 75% of cases are occipital.

Intradiploic encephalocele (IE) is an extremely uncommon entity and usually an incidental finding. In adults it can simulate a lytic lesion, consequently raising suspicion of a number of differential diagnoses, such as eosinophilic granuloma, plasmacytoma, metastasis, osteosarcoma, cavernous haemangioma and epidermoid or dermoid cyst. The presence of CSF within the lytic lesion, lack of outer table bone defect and absence of other malignant features may suggest benign cystic lesions, such as posttraumatic or intradiploic arachnoid cyst and intraosseous leptomeningeal cyst. However, none of them contain herniated brain parenchyma which is a hallmark of an intradiploic encephalocele [1].

So far, there are less than a dozen articles documenting IE [2]. IE aetiology remains unclear, and several possibilities have been considered. The theory proposed by Patil and Etemadrezaie [3] is accepted by most authors—it proposes a blunt trauma as the cause of the internal table rupture, with associated dural tear. The brain tissue subsequently herniates through the dural tear into the diploic defect generated by trauma. Unfortunately, it is difficult to document the trauma which may have caused the defect as minimal trauma is easily forgotten, especially if it

M. Špero, H. Vavro, *Neuroradiology - Expect the Unexpected*,
https://doi.org/10.1007/978-3-319-73482-8_18

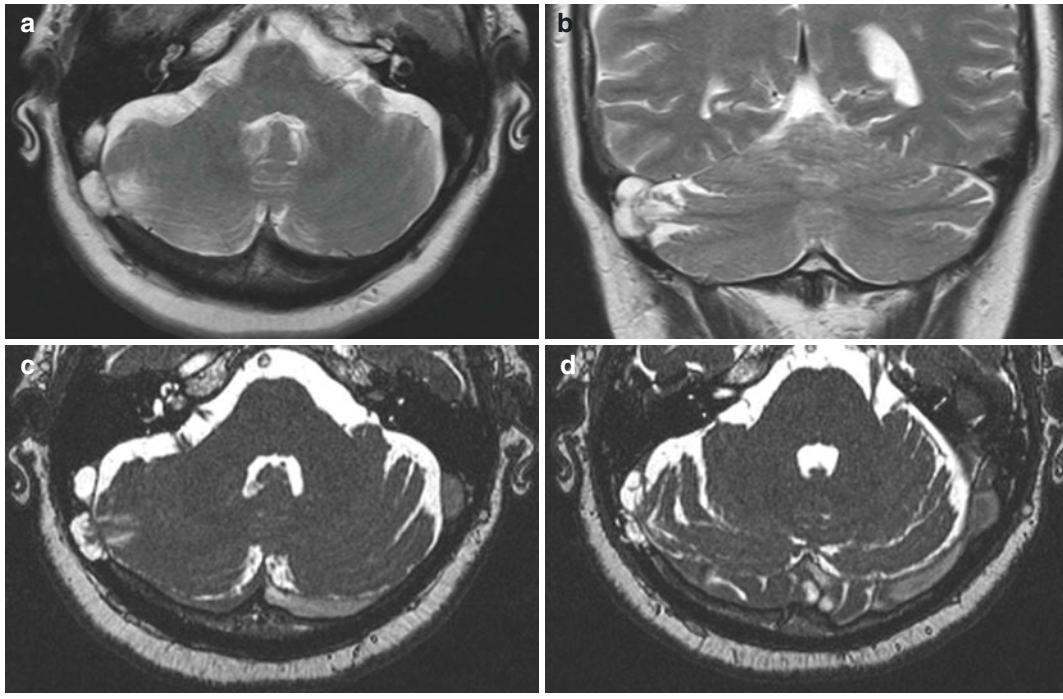

Fig. 18.1 MRI exam of the brain—axial and coronal T2WI (**a**, **b**), axial 3D CISS images (**c**, **d**). There is a 12 mm bony defect in the right side of the occipital bone, adjacent to the occipitotemporal suture and just posterior to the right sigmoid dural venous sinus, involving the inner table and the diploë, reaching the thinned outer table of the bone. The defect is filled with CSF and retracted right cerebellar folia, causing enlargement of the intervening CSF spaces. There is no evidence of gliosis or haemorrhage. The right sigmoid dural venous sinus appears hypoplastic or slightly compressed, with normal flow void. The rest of the appearances is unremarkable

took place many years ago. A congenital anomaly is a less plausible aetiology, given that congenital encephaloceles involve both inner and outer table discontinuity in the midline and are generally accompanied by other malformations, which is not the case with any of the reported IEs. Intracranial hypertension may play a role in IE development, either as idiopathic intracranial hypertension or a short-term increase in intracranial pressure such as in violent cough [4]. Most of the reported IEs were parietal, with exception of a single iatrogenic frontal intradiploic encephalocele. The case reported here seems to be the first case of an occipital IE in an adult reported in literature.

Clinical manifestations are often absent; if there are some symptoms, they affect the functional brain area of the herniated portion of the brain or adjacent parenchyma. While the herniated tissue itself may not be injured, the tension on the adjacent parenchyma may cause symptoms. Another proposed mechanism is vascular constriction with subsequent ischaemic events.

Before deciding on IE treatment, it is necessary to establish a convincing relationship of the parenchymal hernia and the symptoms—functional imaging may be of help. The treatment usually consists of aggressive surgery involving parenchymal amputation, which may be unnecessary in the absence of neurological deficit.

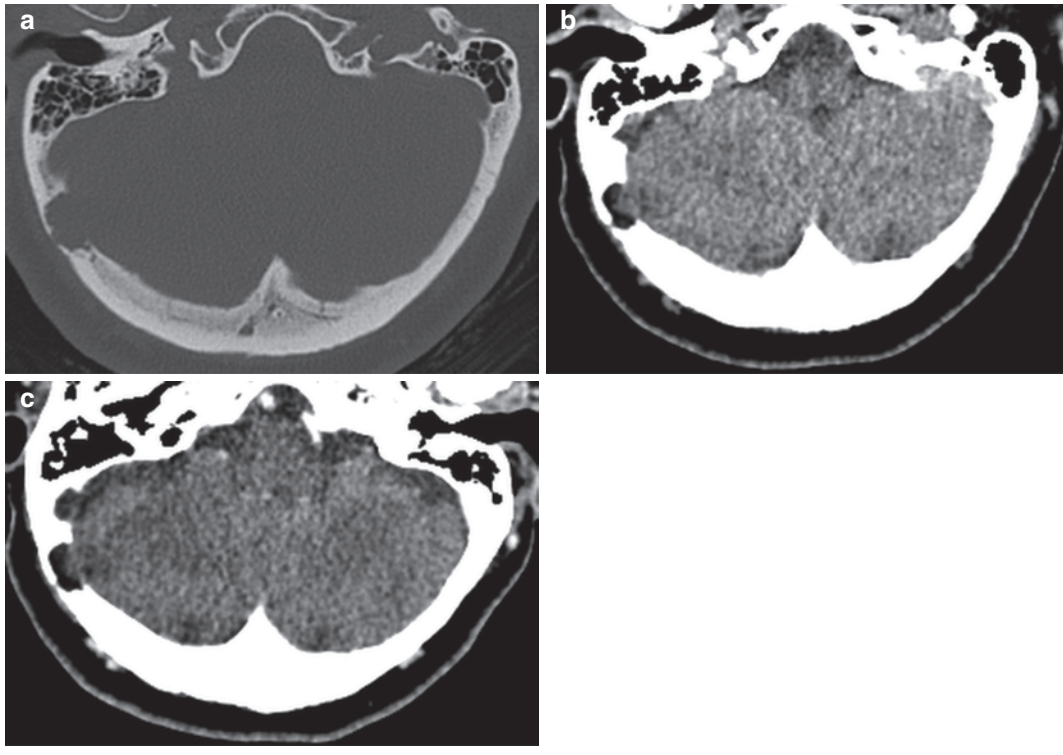

Fig. 18.2 CT exam of the brain, axial images. In the bone window setting (**a**), there is a lytic lesion in the intradiploic space of the right occipital bone, adjacent to the occipitotemporal suture, with a defect of the inner table and marked thinning of the outer table of the bone. In the brain window setting (**b**, **c**), there is evidence of cerebellar parenchyma protrusion into the bony defect

References

1. Shi C et al (2017) Symptomatic parietal intradiploic encephalocele—a case report and literature review. J Neurol Surg Rep 78(1):e43–e48
2. Arevalo-Perez J, Millán-Juncos JM (2015) Parietal intradiploic encephalocele: report of a case and review of the literature. Neuroradiol J 28(3):264–267
3. Patil AA, Etemadrezaie H (1996) Posttraumatic intradiploic meningoencephalocele. Case report. J Neurosurg 84:284–287
4. Loumiotis I et al (2010) Symptomatic left intradiploic encephalocele. Neurology 75(11):1027

Intraorbital Aspergilloma

19

Several months after he had undergone heart transplantation and was started on immunosuppressive therapy, this 60-year-old gentleman started feeling retrobulbar pain, redness and swelling of his right eye, with double vision on lateral gaze. On examination, the lateral and downward right eye movement was limited, and there was oedema of the superior and inferior eyelid and proptosis. The left eye was unremarkable.

A CT exam of the orbits was done (Fig. 19.1).

The right-sided intraorbital space occupying lesion was described as inflamed mucocoele. Fine needle aspiration was recommended as the

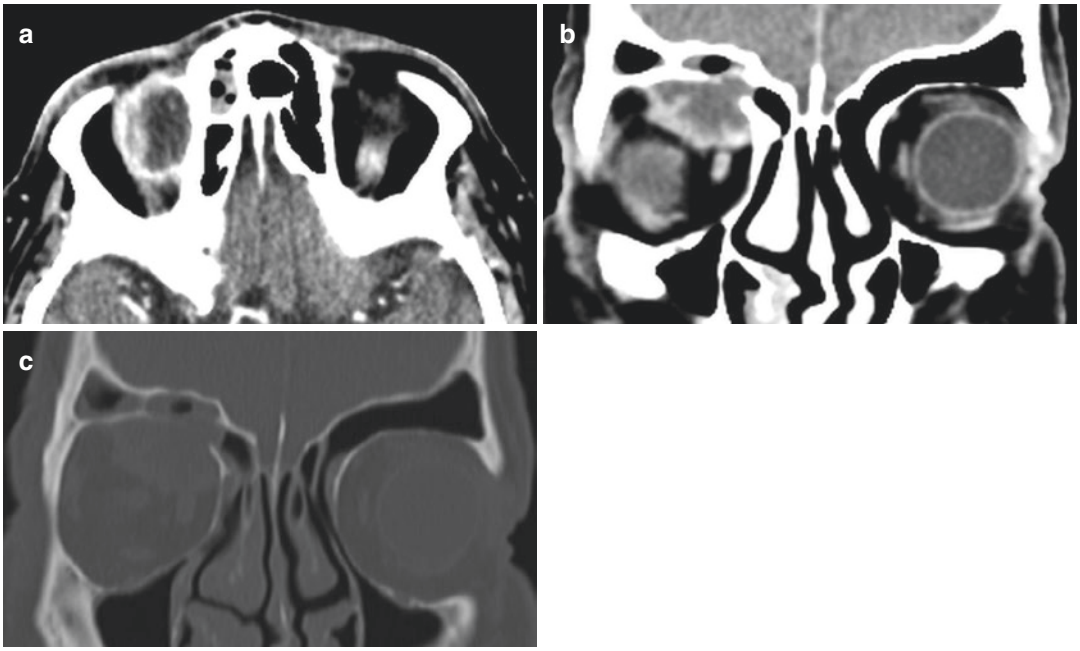

Fig. 19.1 Contrast-enhanced CT exam of both orbits—axial (**a**) and coronal (**b**) soft-tissue imaging and coronal (**c**) bone imaging algorithms show a cystic space occupying lesion with enhancing, irregular, thick margins in the medial superior aspect of the right orbit. Adjacent to it, there is a 7 mm bony defect of the orbital roof/frontal sinus inferior wall (probably due to a previous surgery). The lesion displaces the globe caudally, laterally and anteriorly

M. Špero, H. Vavro, *Neuroradiology - Expect the Unexpected*,
https://doi.org/10.1007/978-3-319-73482-8_19

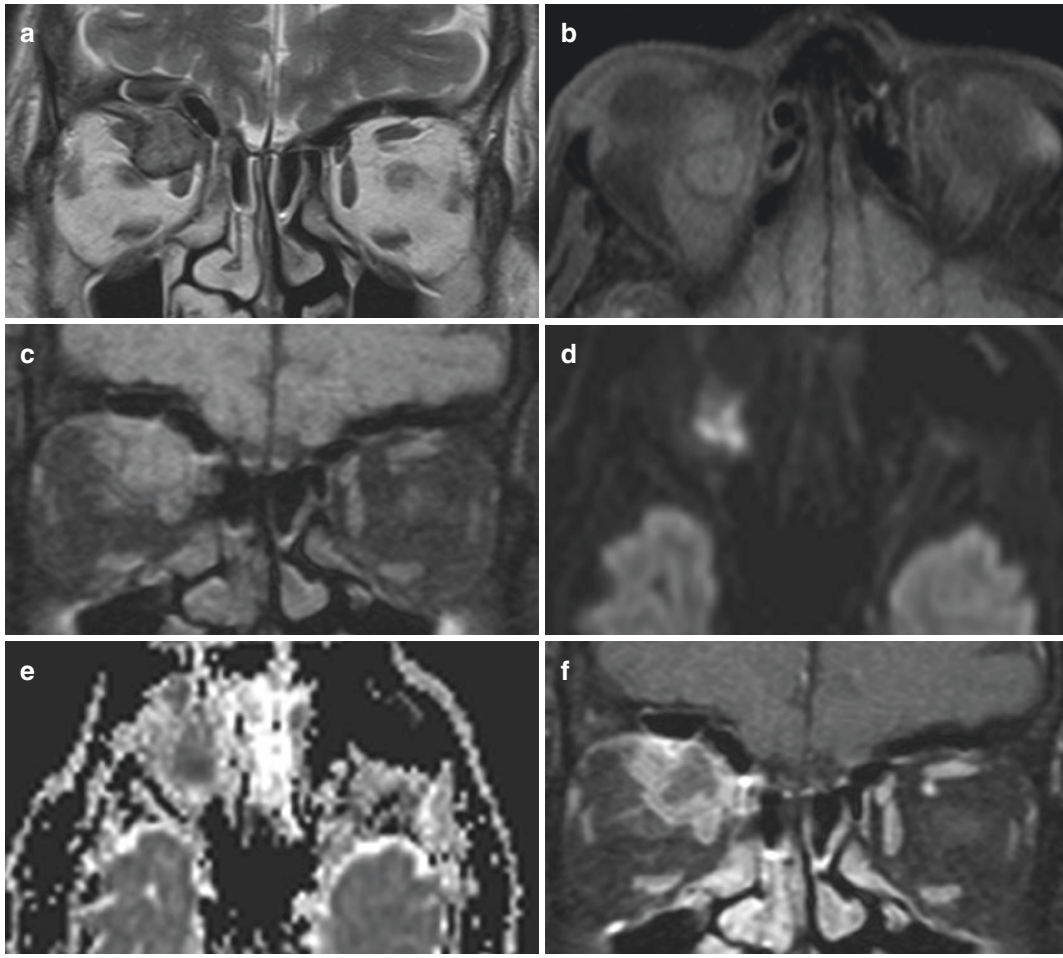

Fig. 19.2 MRI exam of the orbits—coronal T2WI (**a**), axial T2FSWI (**b**), coronal T2FSWI (**c**), axial DWI (**d**), axial ADC map (**e**), post-contrast coronal T1FSWI—shows a space-occupying lesion in the cranial medial aspect of the right orbit, originating in the extraconal compartment, protruding into the intraconal compartment between the upper and medial rectus muscle. There is thick, irregular peripheral enhancement of the lesion. Note the high DWI (**d**) signal coupled with low ADC (**e**) signal in the lesion, indicating thick cyst contents suggestive of an abscess. The right superior oblique muscle is compressed, and it enhances with contrast (**f**) which is probably of reactive inflammatory aetiology

next step, but the cytology report was inconclusive and unremarkable.

Later on, lesion biopsy was performed in a regional hospital, and a diagnosis of intraorbital aspergilloma was established.

A MRI exam of the orbits was recommended (Fig. 19.2).

Three weeks after the MRI exam, the aspergilloma was surgically resected through the upper eyelid (Fig. 19.3).

Four months later, the patient experienced aggravation of the symptoms, and another MRI exam of the orbits was done (Fig. 19.4).

The maxillofacial surgeons performed surgical exploration of the right orbit, with complete resection of the aspergilloma (Fig. 19.5).

The patient has constantly been on immunosuppressive therapy after heart transplantation; regular myocardial biopsies showed no signs of transplant rejection.

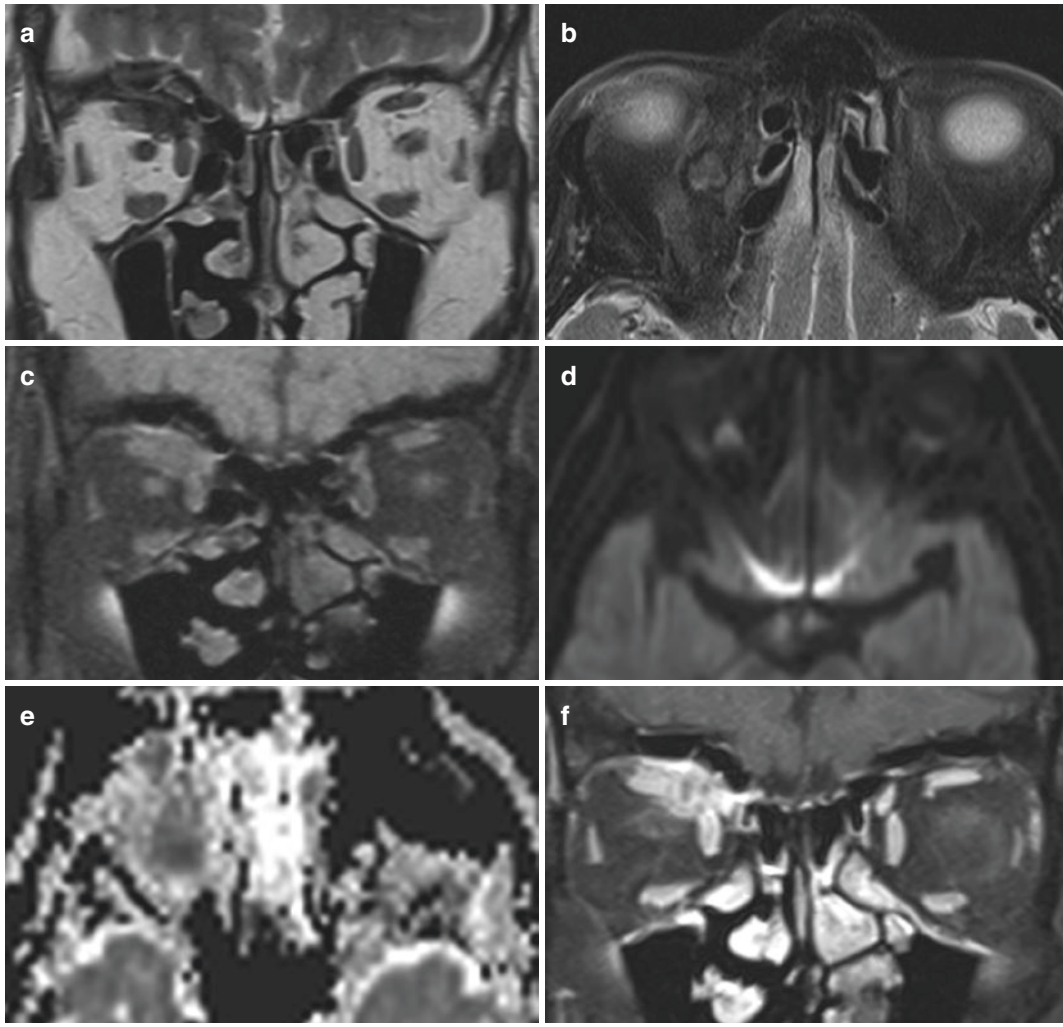

Fig. 19.3 MRI exam of the orbits 2.5 months after evacuation of right orbital aspergilloma. Coronal T2WI (**a**), axial T2FSWI (**b**), coronal T1FSWI (**c**), axial DWI (**d**), axial ADC map (**e**), post-contrast coronal T1FSWI (**f**). There is a residual aspergilloma in the cranial medial aspect of the right orbit, and the mass effect has been partially resolved

19.1 Intraorbital Aspergilloma

Intraorbital aspergilloma is a rare lesion, although aspergillus is a ubiquitous fungus. The spores are found in the soil and decaying organic matter, get airborne and daily get inhaled by most of the people. In the immunocompetent patients, they are usually eliminated by the immune system but can be the cause of a chronic sinusitis, with possible expansion of the sinuses and structural changes of the facial skeleton [1]. An aspergilloma may occur in incompletely aerated sinuses. Generally, no invasion, necrosis or reactive changes of the adjacent tissues are seen in the immunocompetent persons. However, in immunocompromised patients, such as in this case, aspergillus may cause invasive granulomatous inflammation with fibrosis or a fulminant necrotising form with vascular invasion.

Aspergillosis usually spreads to the orbit directly from adjacent paranasal sinuses, rarely haematogenously from the lung. The most

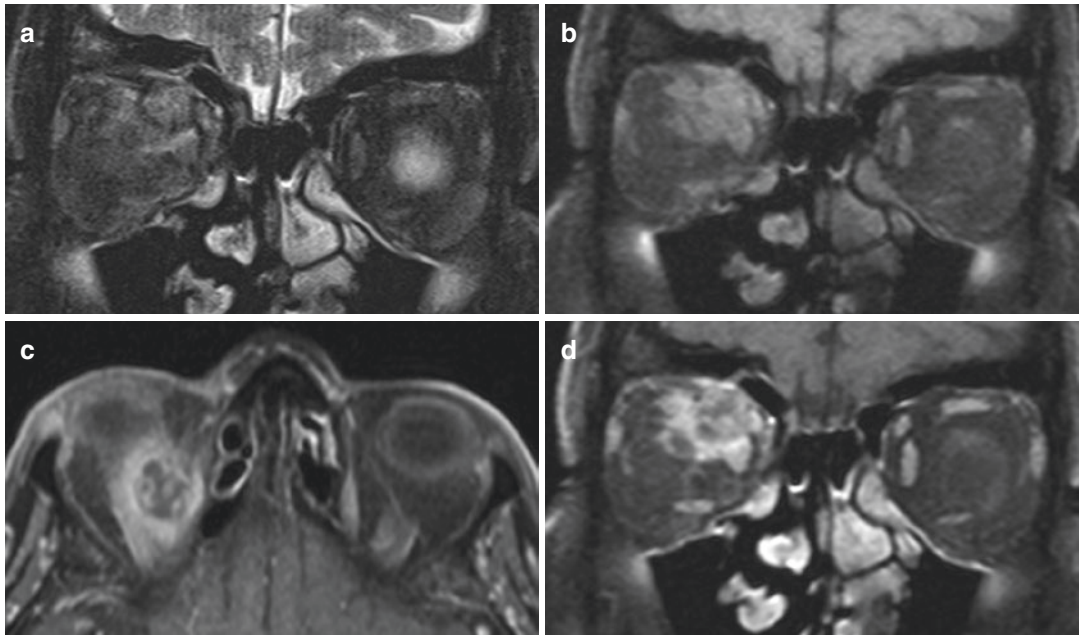

Fig. 19.4 Follow-up MRI exam of the orbits—coronal T2FSWI (**a**), coronal T1FSWI (**b**), post-contrast axial (**c**) and coronal (**d**) T1FSWI—demonstrates progression in size of the irregular aspergilloma residue, with inhomogeneous peripheral enhancement and mild inflammatory reaction of the adjacent soft tissues

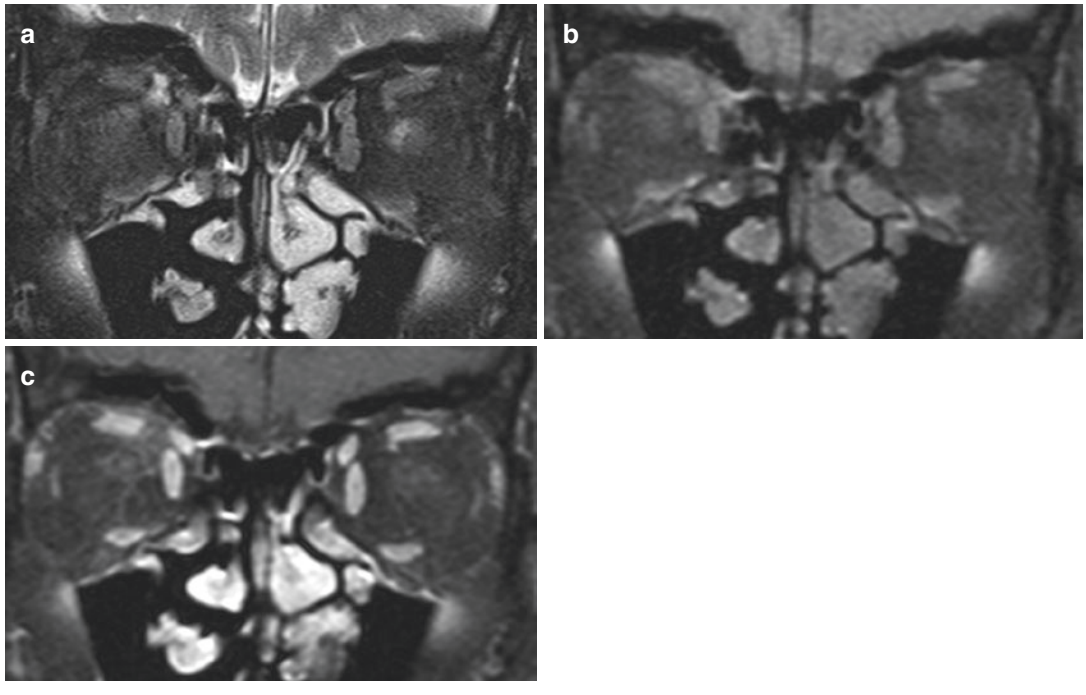

Fig. 19.5 Follow-up MRI exam of the orbits 18 months post surgery—coronal T2FSWI (**a**), coronal T1FSWI (**b**), post-contrast T1FSWI (**c**)—does not show any signs of active inflammation; there are some scarring and a small inactive residual nodal lesion seen in the superior medial aspect of the right orbit. The patient's symptoms have resolved

common site of infection is posterior orbit, presenting as orbital apex syndrome involving ophthalmoplegia, pain, loss of vision, loss of sensation in the infraorbital nerve and proptosis. The cavernous sinus is usually also affected. Invasive form with penetration of bone and blood vessel walls and intracranial spread is not uncommon, presenting a treatment challenge.

CT imaging shows a peripherally or inhomogeneously enhancing intraorbital mass and, usually, opacification of the adjacent paranasal sinuses. In this case the frontal sinus opacification has mostly resolved previously. The characteristic calcification within the mass is only seen in less than 50% of cases. MRI will help differentiate the mass further, showing possible involvement of the optic nerve or adjacent muscles, as well as possible signs of abscess formation with central increased DWI signal and peripheral low T2 signal.

As intraorbital aspergillosis mostly stems from adjacent paranasal sinuses, differential diagnosis includes most of the extraorbital lesions extending into the extraconal space, such as other infections, mucocoele, metastatic tumours and sinonasal tumours (squamous cell carcinoma, adenocarcinoma, adenoid cystic carcinoma, lymphoma). Differential diagnosis may be narrowed if there are MRI features of abscess, such as in this case.

For definitive diagnosis of invasive aspergillosis, a tissue sample is needed, obtained either by FNA or biopsy.

Systemic and local antifungal therapy remains the mainstay of treatment, but surgical debridement is often performed [2]. Reversal of immunosuppression is important, if at all possible.

References

1. Karcioglu ZA (ed) (2015) Orbital tumors diagnosis and treatment. Springer, New York
2. Sivak-Callcott JA et al (2004) Localised invasive sino-orbital aspergillosis: characteristic features. Br J Ophthalmol 88:681–687

Van Buchem Disease, Sclerosteosis or Something Else?

20

Due to dull headaches and enlarged hands, feet and mandible, endocrinologist referred a 39-year-old female patient to MRI of the brain (Fig. 20.1).

In 2009, during preoperative preparation due to collateral ligament injury, knee X-rays have been performed and have demonstrated bone thickening: bone biopsy and histomorphometry have been proposed, but never performed, because a patient has been avoiding diagnostic workup until the autumn 2016.

According to anamnestic data, she had "drumstick"-shaped fingers since birth, during childhood she has been a little bit higher compared to other children, childhood photos have showed mildly pronounced mandible. Family photos have showed her father and grandfather had mild mandibular prognathism. Menstrual cycle has always been normal.

In the age of 30, she has noticed hand, feet and mandible enlargement—now without further enlargement. Diffuse dull headaches occur periodically once a month and resolve completely on analgesic drugs. During the last 6 years, she noticed mild hearing loss in the left ear and vague mild balance disorder. For several years, she has suffered from sleep apnea symptoms.

In late autumn 2016, an extensive diagnostic workup was commenced and revealed normal hormone levels, no abnormalities in routine blood tests (alkaline phosphatase level was normal), bilateral mixed hearing loss and small hard palate exostosis. Officially, serum sclerostin levels are not possible to measure in any of biochemical laboratories in our country, only abroad.

MRI Imaging features suggested sclerosteosis (Fig. 20.1). Due to generalised thickening of the skull, cranial CT was recommended to assess degree of the bone thickening as well as the possible narrowing of the neural exit foramina and canals (Fig. 20.2).

Differential diagnosis included sclerosteosis and Van Buchem disease. Regarding patient phenotype, as an adult, she is not much taller than female coevals and does not have finger abnormality characteristic for patients with sclerosteosis like radial deviation, syndactyly or both; Van Buchem disease was a more obvious diagnosis. To confirm or exclude possible differential diagnosis, a genetic testing has been conducted at Department of Medical Genetics, University of Antwerp in Belgium. By the time we concluded this manuscript, we have got the information that mutation in the SOST gene seemed to be excluded, and testing of a few other candidate genes was in progress. Such information was expected because a patient does not have a Duch ancestry, and "de novo" mutation was presumed.

M. Špero, H. Vavro, *Neuroradiology - Expect the Unexpected*,
https://doi.org/10.1007/978-3-319-73482-8_20

Fig. 20.1 Magnetic resonance of the brain, sagittal T1WI (**a**) and T2WI (**b**, **c**), coronal T2WI (**d**–**f**) and axial T2WI (**g**–**i**), revealed generalised thickening of the skull with irregularities of the brain surface due to bony elevations of the inner table: occipital bone was thick as 3.5 cm, sphenoid bone as 10 mm, rest of the skull bones up to 2.5 cm. Sella turcica was shallow, but widened, pituitary gland had concave cranial surface, and stalk was narrow as well as the infundibular recess of the third ventricle. Cerebellar tonsils were elongated, beak-like in shape, and descended below the level of foramen magnum. Subarachnoid space over the convexity was reduced; sulci over the convexity were narrow. Hypoglossal canals were not compressed (**g**), and cisternal space surrounding the brainstem was reduced and narrow as well as pontocerebellar angles (**g**, **h**). Lateral ventricles appeared normal (**i**)

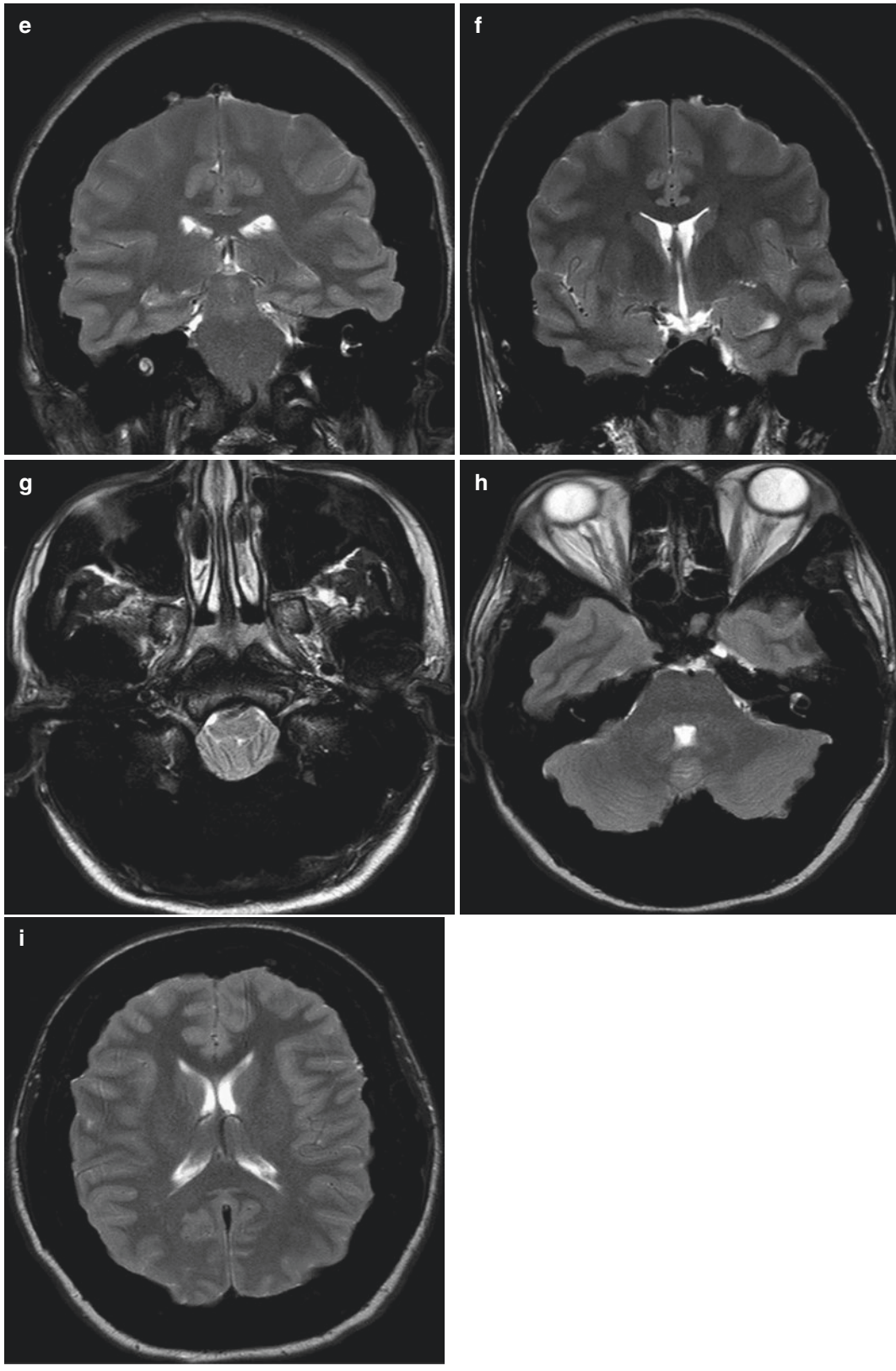

Fig. 20.1 (continued)

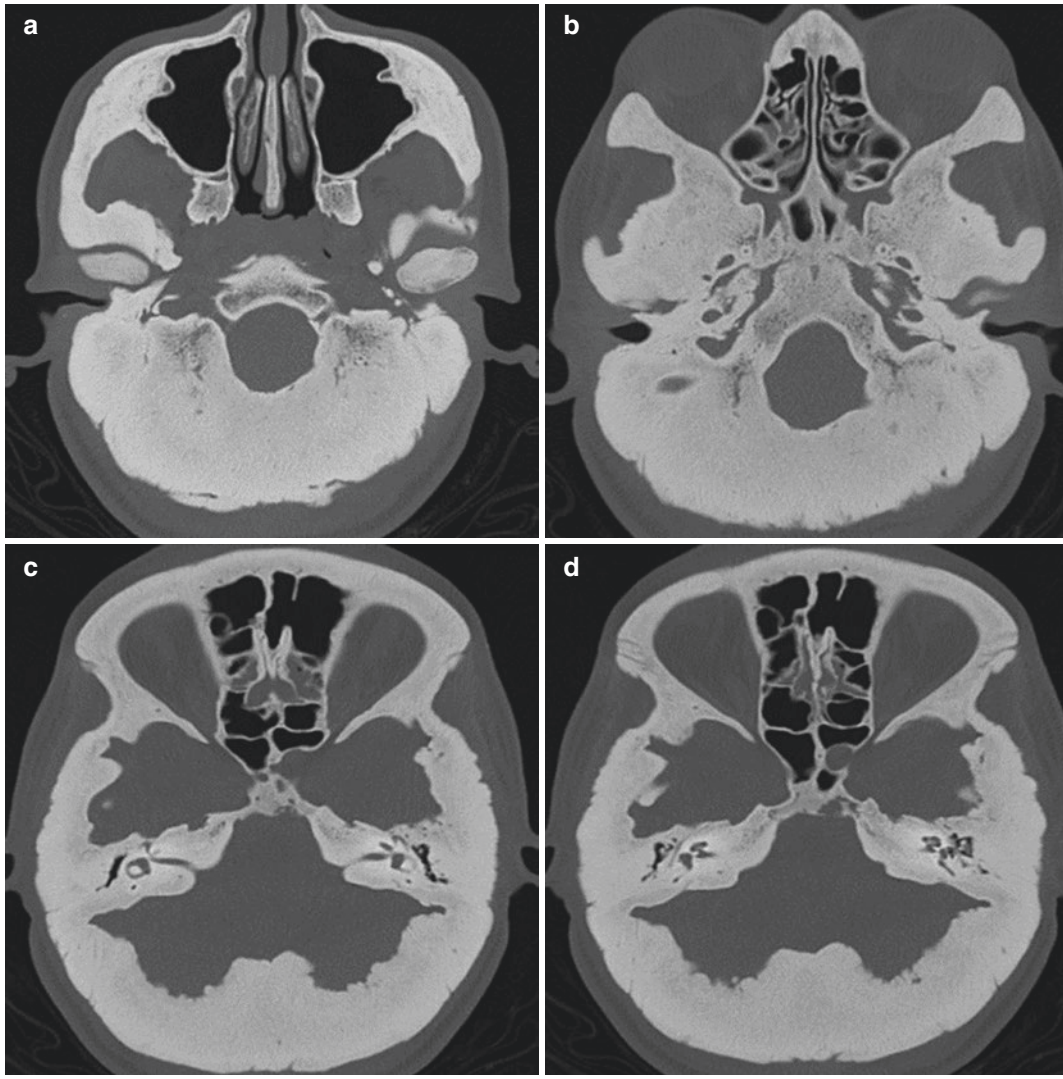

Fig. 20.2 Computed tomography of skull bones (high-spatial-resolution bone algorithm), axial scans (**a**–**f**) and sagittal scan (**g**) of the skull base and the rest of the cranium (**a**–**f**) and coronal (**h**) and oblique (**i**) VRT. Massive hyperostosis of the skull base and vault, as well as the mandible (**h**, **i**) and petrous bones: bones were dense and thick with loss of diploe due to cortical thickening. Mandible was particularly enlarged, assuming a square form, prognathic. Hypoglossal canals (**a**) and foramen ovale (**b**) were not compressed, while foramen rotundum (**b**) was narrowed. Internal auditory canals were extremely narrow, while external auditory canals were not occludes. Mastoid cells were not developed; dense abnormal bone was encroaching upon otherwise normal inner ear structures in the narrow tympanic cavities (**c**, **d**). Facial canals were compressed (**d**). Upper orbital fissures and optic canals were mildly narrow due to involvement of lateral orbital walls (**e**, **f**). Small exostosis in the posterior part of hard palate (**g**)

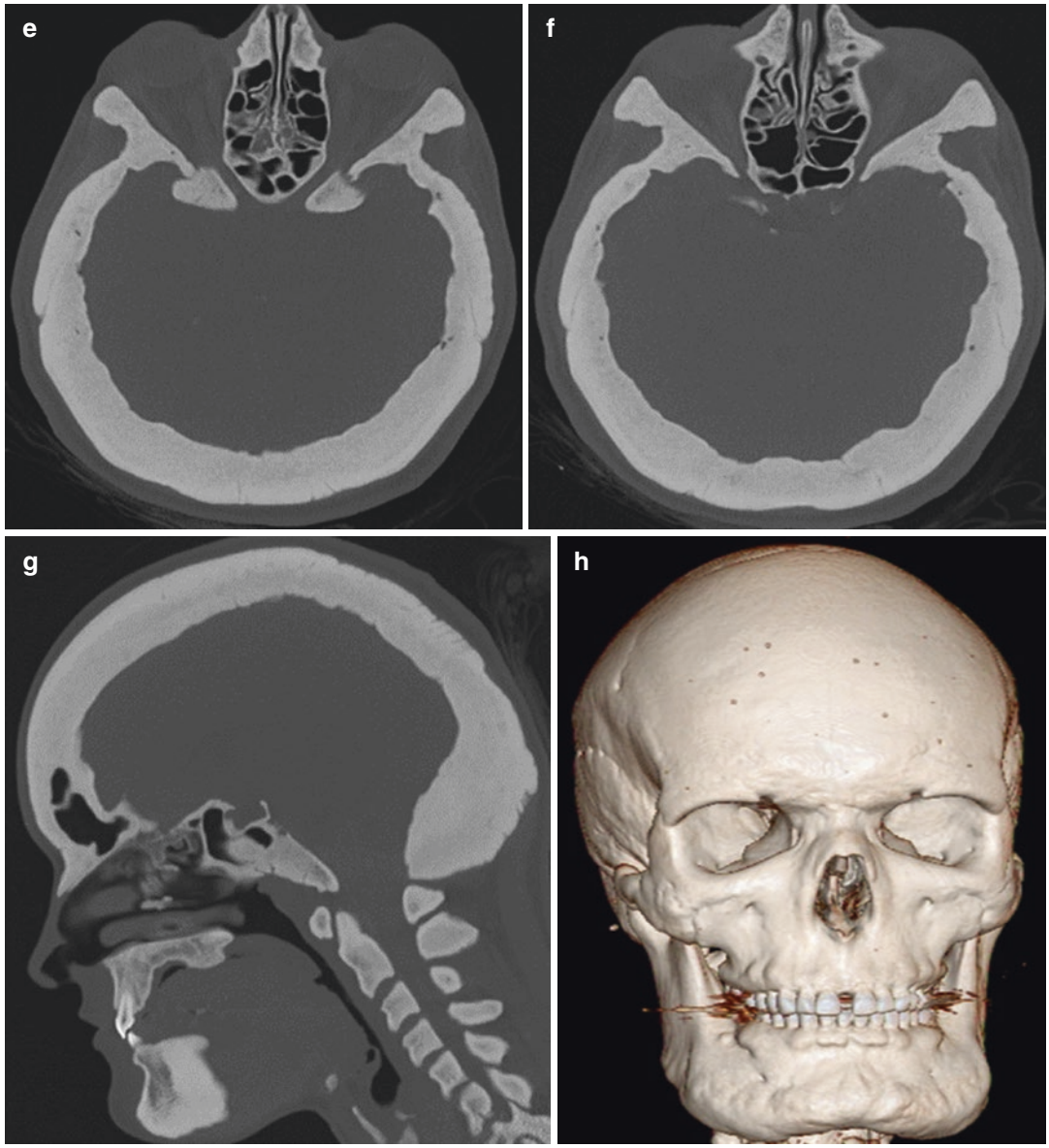

Fig. 20.2 (continued)

Fig. 20.2 (continued)

20.1 Van Buchem Disease or Sclerosteosis

Van Buchem disease (VBD) and sclerosteosis are very rare diseases that belong to the group of craniotubular hyperostoses or osteopetroses that involve bony overgrowths that alter contour and increase skeletal density, mainly involving the skull and long, tubular bones. Sclerosteosis was first described in 1958 and is most common among Afrikaners, mainly white, of Dutch origin in South Africa, although small number of individuals and families have been reported in other parts of the world, including Brazil, United States, Germany, Senegal and Turkey. Van Buchem disease was first described in 1955 by Van Buchem as "hyperostosis corticalis generalisata familiaris", in a fishing village in the Netherlands among descendants from 151 inhabitants who survived the plague in 1637 and appears more frequently in persons of Dutch ancestry [1–3].

Both are autosomal recessive disorders: sclerosteosis is caused by mutation in the SOST gene encoding sclerostin on chromosome 17q12-q21 which leads to osteoblast hyperactivity, while VBD is caused by a 52 kb deletion downstream of the SOST gene on chromosome 17q12-q21, which results in lack of a SOST-specific regulatory element in osteoblasts leading to impaired inhibition of osteoblastic bone formation [3, 4]. Sclerostin is a protein produced almost exclusively from osteocytes that inhibits bone formation by both osteoblasts and osteocytes. It acts as a negative regulator of bone formation inhibiting the Wnt signalling pathway on molecular level, which plays a critical role in osteoblast development and function [4, 5]. Undetectable levels in sclerosteosis and very low levels of sclerostin in VBD result in excessive bone growth and increased bone strength: mainly affected are cranial bones and diaphysis of long, tubular bones.

Described neuroimaging features are similar in sclerosteosis and VBD: you will not be able to distinguish it only on cranial CT and MRI. Associated clinical features, age of onset, molecular genetic test results and disease progression must be taken into account when establishing a differential diagnosis.

Sclerosteosis is characterised by a progressive bone thickening, tall stature, finger abnormalities—syndactyly and/or radial deviation—and enlargement of the skull. Patients usually appear normal at birth, with possible exception of syndactyly, while other manifestations appear early in life during the first decade of life [4, 6].

Patients with VBD have phenotype similar to patients with sclerosteosis but less severe including increased bone mass with enlargement of the mandible and macrocephaly, normal stature and no finger abnormalities [4, 6].

In both conditions, in the third decade of life, clinical features and complications usually stabilise, with no new clinical findings or progression, but are less severe in VBD because of slower progression of the bone overgrowth after the first years, in comparison to sclerosteosis [4].

Hyperostotic skull and facial bones distort the shape of a patient's face who usually has massive square prognathic chin, in sclerosteosis also frontal bossing, and cause foraminal stenosis resulting in cranial nerve compression with facial palsy, hearing loss and increased intracranial pressure that may result in sudden death from impaction of the brainstem into the foramen magnum in sclerosteosis, while in VBD is not so frequent and usually craniotomy is not necessary.

Mixed hearing loss, in those patients, could be explained by marked narrowing of the external and internal auditory canals and impediment of the bony middle and inner ear structures. Neuroradiologist should look for signs of increased intracranial pressure like herniation of cerebellar tonsils, depletion of subarachnoid space and distension of the subarachnoid space along the optic nerves which can alternatively be caused by narrowing of the optic nerve canals preventing fluid drainage. Low position of cerebellar tonsils could also be a result of occipital bone hypertrophy. On imaging methods, ventricles appear normal in size and shape because elevated intracranial pressure is not a result of obstructed CSF flow and/or absorption [6].

Van Buchem disease is clinically similar to sclerosteosis; however, the main clinical differences between two diseases are gigantism and hand abnormalities present in sclerosteosis but never in VBD. Therefore if you have a patient with imaging features described above, look for clinical signs which can help you in reporting more obvious diagnosis, and always recommend genetic test to confirm or exclude possible diagnosis.

References

1. Fayez A et al (2015) A novel loss-of-sclerostin function mutation in a first Egyptian family with sclerosteosis. Biomed Res Int 2015:517815, 8 pages. https://doi.org/10.1155/2015/517815
2. Bhadada SK et al (2013) Novel SOST gene mutation in a sclerosteosis patient and her parents. Bone 52(2):707–710
3. Van Hul W et al (1998) Van Buchem disease (hyperostosis corticalis generalisata) maps to chromosome 17q12-q21. Am J Hum Genet 62:391–399
4. Yavropoulou MP et al (2014) The sclerostin story: from human genetics to the development of novel anabolic treatment for osteoporosis. Hormones 13(4):476–487
5. Lewiecki EM (2014) Role of sclerostin in bone and cartilage and its potential as therapeutic target in bone disease. Ther Adv Musculoskelet Dis 6(2):48–57
6. Wengenroth M et al (2009) Case 150: Van Buchem disease (hyperostosis corticalis generalisata). Radiology 253:272–276

Part V

Unusual Spine

Neurinoma: Chondrosarcoma of the Thoracic Spine

21

A 29-year-old female patient suffered from sideropenic anaemia due to a menorrhagia: in October 2013, during preoperative workup of uterine myoma, chest X-ray was performed and revealed large left-sided paravertebral expansile mass at a level of left upper lobe of a lung. Anamnestic data disclosed that in 2007 she occasionally felt thoracic back pain but recommended chest X-ray was not performed. Due to anaemia, she was feeling fatigue in physical activity: she did not have other symptoms.

In November 2013, she was admitted to a hospital, and diagnostic workup has been commenced. CT of the thorax (Fig. 21.1) and MRI of the thoracic spine (FIg. 21.2) were performed and revealed large, oval expansile left paravertebral lesion at the level of T4–T5 segment involving and widening left neural foramina.

According to described CT and MRI features (Figs. 21.1 and 21.2), paraspinal thoracic tumour of possible neural origin was reported, although calcifications in extradural schwannoma are rare. Chondrosarcoma, due to "benign" imaging features, was not our first choice. A patient was operated in November 2013: total resection was performed, while pathohistology revealed chondrosarcoma grade II. There was no tumour recurrence on regular MRI follow-ups (previous MRI examination was in January 2017).

21.1 Spinal Chondrosarcoma

Chondrosarcoma is a malignant tumour of connective tissue, characterised by formation of cartilage matrix by tumour cells. It is the second most common primary malignant tumour of the spine in adults. Males are affected two to four times more frequently than female, with a peak prevalence between 30 and 70 years. Most spinal chondrosarcomas are low-grade tumour; hence clinical course is usually long. Clinically they are presented with pain, palpable mass and neurological deficit [1–3].

Thoracic and lumbar spine are more frequently affected, while sacrum is affected rarely. Primary chondrosarcoma originates "de novo" in the vertebral body, posterior element or both, while secondary chondrosarcoma occurs mostly as a result of malignant transformation within the cartilage cap of a pre-existing benign tumour such as osteochondroma.

Primary and secondary chondrosarcoma are histologically similar: three different grades are recognized for both, representing the most reliable predictors of clinical behaviour. Grade I chondrosarcoma grows relatively slow; histological appearance is similar to cells of normal cartilage, and is less aggressive, and rarely metastasize. Grade III chondrosarcoma is faster-growing

M. Špero, H. Vavro, *Neuroradiology - Expect the Unexpected*,
https://doi.org/10.1007/978-3-319-73482-8_21

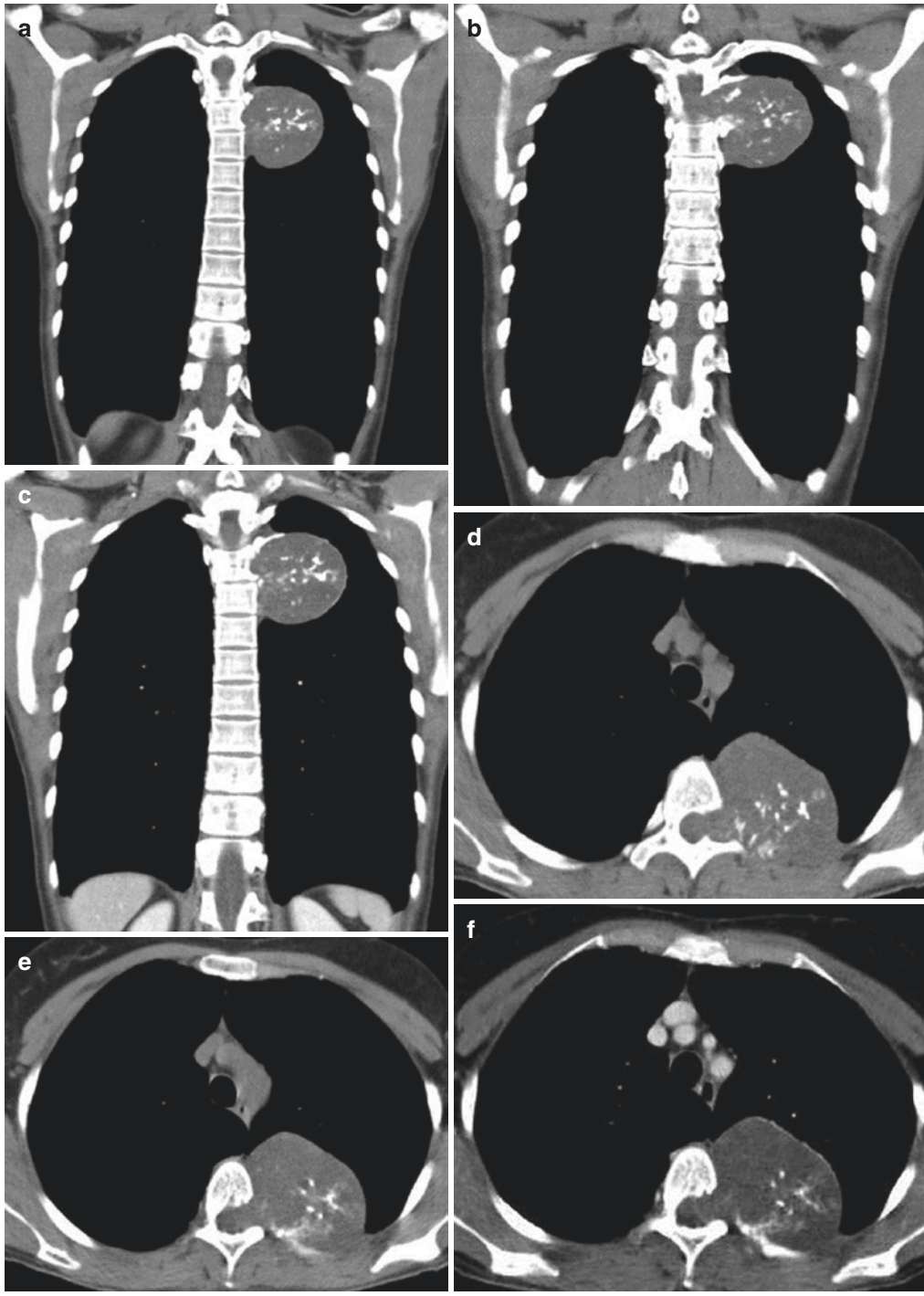

Fig. 21.1 CT of the thorax, pre-contrast coronal (**a**, **b**) and axial (**d**, **e**) plane and post-contrast coronal (**c**) and axial (**f**) scans demonstrated large (44 × 72 × 64 mm) soft tissue left paravertebral mass at the level of T4–T5 segment. Tumour was oval and well-circumscribed, hypodense with amorphous calcifications and did not reveal contrast enhancement on post-contrast scans. Tumour has widened left neural foramina of the T4–T5 segment and did not destruct adjacent third, fourth and fifth left rib or left transverse process of the fourth and fifth thoracic vertebra. Left transverse process of the T4 vertebra and left fourth rib were scalloped, while left lamina of the fourth vertebra was thinned and scalloped. There was no pulmonary metastases or mediastinal lymphadenopathy

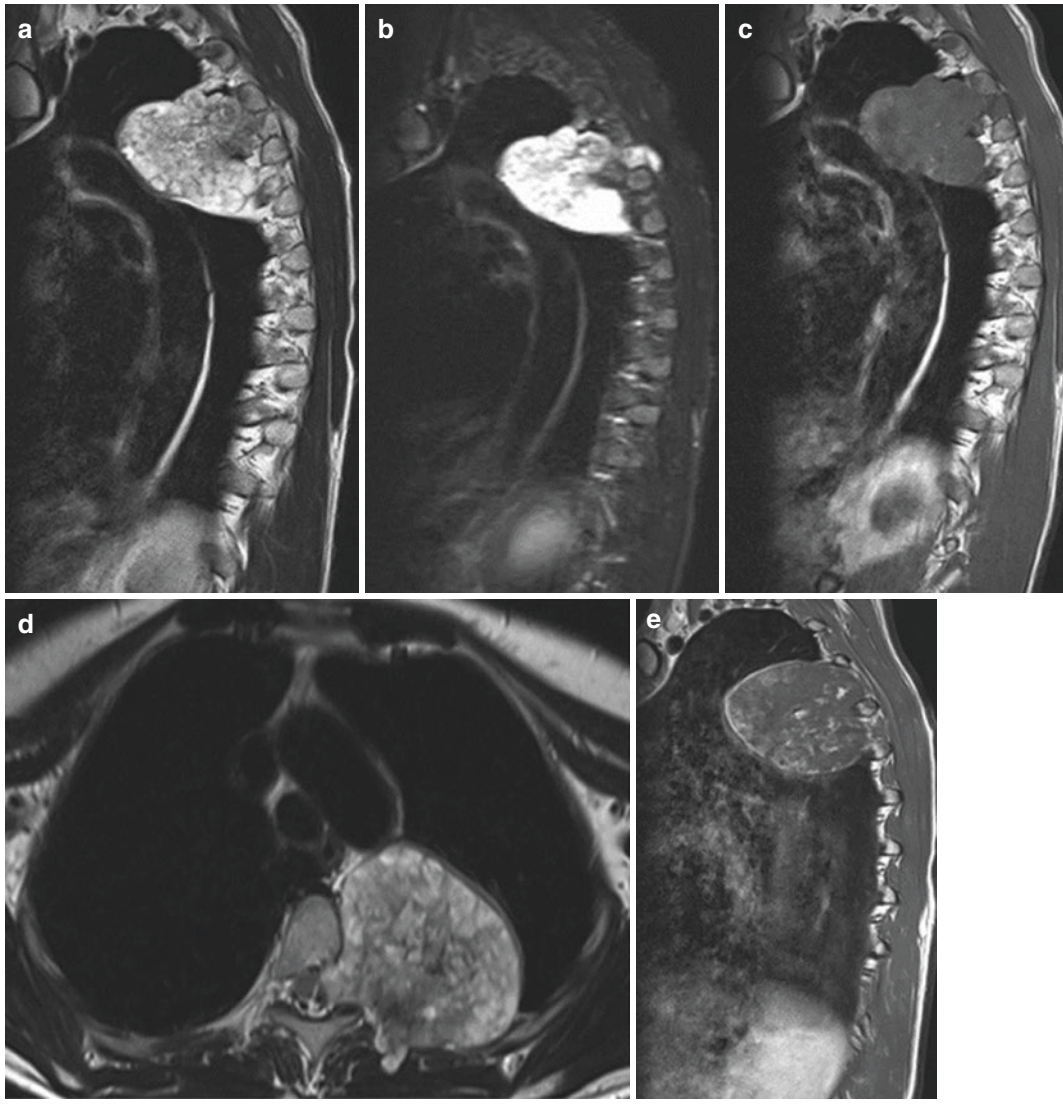

Fig. 21.2 Magnetic resonance of the thoracic spine, pre-contrast sagittal T2WI (**a**), TIRM (**b**) and T1WI (**c**), axial T2WI (**d**) and T1WI (**g**), post-contrast sagittal (**e**), coronal (**f**) and axial (**h**) T1WI showed oval, well-circumscribed tumour, heterogenous, but predominantly hyperintense on T2WI and hypointense on T1WI, which on post-contrast T1WI demonstrates peripheral and heterogeneous contrast enhancement. Tumour widened left neural foramina of the T4–T5 segment, entered left lateral epidural space and mildly compressed thoracic medulla, without signal intensity changes in terms of compressive myelopathy. There was no bone oedema of the adjacent part of the fourth and fifth vertebral body, left lamina and transverse process

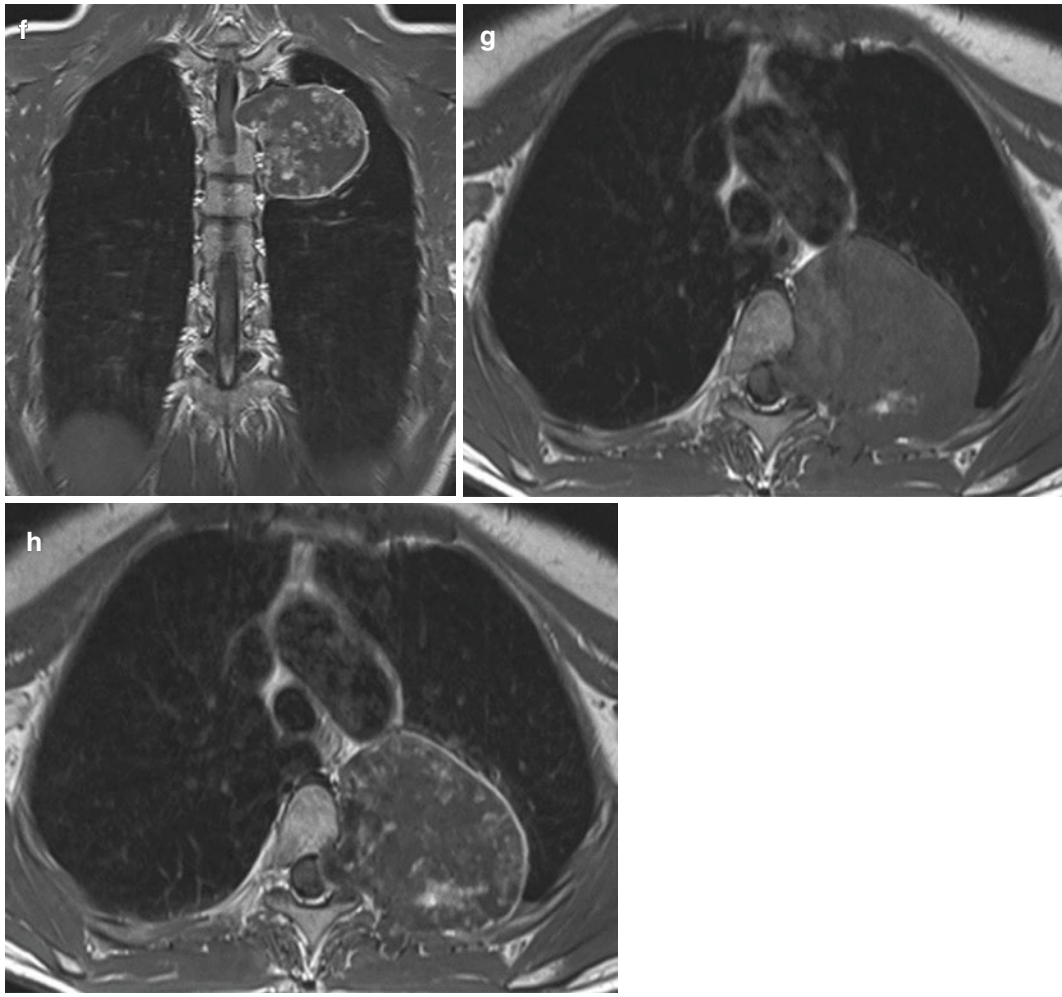

Fig. 21.2 (continued)

tumour, more anaplastic and invasive to surrounding tissues, lymph nodes and organs: metastases occurs in 70% of patients. Grade II chondrosarcoma holds some of the characteristics of grade I and grade II [3].

Imaging features of chondrosarcoma include large mass with bone destruction and mineralised chondroid matrix in the form of amorphous calcification seen as rings and arcs on CT, while non-mineralised part of a tumour is hypodense. On MRI, non-mineralised part of chondrosarcoma has low to intermediate signal intensity on T1WI and is heterogeneously hyperintense on T2WI due to a high water content of hyaline cartilage, while calcifications are seen as signal void. Contrast enhancement may be lobular, septal, nodular or diffuse. Surrounding bone oedema, soft tissue and spinal canal involvement is best evaluated by MRI [1–4].

Spinal chondrosarcoma may present diagnostic difficulties [5]. Differential diagnosis includes chondroblastic osteosarcoma, chondromatosis, chordoma, ganglioneuroblastoma and schwannoma. Neuroblastic tumours are rare after the age

of 10, while schwannomas rarely have calcifications. Location, no evidence of surrounding bone destruction, widening of neural foramina, propagation into spinal canal and signal intensities lead us to think maybe it could be an atypical or degenerated tumour originating from a nerve sheath. Malignant tumour was not our top differential diagnosis. But if you have a patient with a paraspinal mass which imaging features refer to "benign" type of tumour, think about possible malignant diagnosis, especially if one imaging feature of a lesion does not fit into differential diagnosis you consider.

Chondrosarcomas are not considered sensitive to radiotherapy or chemotherapy. The most successful treatment for spinal chondrosarcoma is complete en bloc resection: it provides the best chance of survival and the lowest rate of local recurrence. When en bloc resection is not possible, partial removal followed by radiotherapy is an optional treatment [2, 3, 5].

References

1. Razek A, Castillo M (2010) Imaging appearance of primary bony tumors and pseudo-tumors of the spine. J Neuroradiol 37:37–50
2. Lloret I et al (2006) Primary spinal chondrosarcoma: radiologic findings with pathological correlation. Acta Radiol 47(1):77–84
3. Katonis P et al (2011) Spinal chondrosarcoma: a review. Sarcoma 2011:378957, 10 pages
4. Rodallec MH et al (2008) Diagnostic imaging of solitary tumors of the spine: what to do and say. Radiographics 28:1019–1041
5. Strike SA, McCarthy EF (2011) Chondrosarcoma of the spine: a series of 16 cases and a review of the literature. Iowa Orthop J 31:154–159

Sacral Aneurysmal Bone Cyst

22

An 18-year-old female was referred to the MRI unit due to the pain in the left coxofemoral region with slightly increased urge to urinate which she developed after falling from a train stairs on iced ground about 2 years before the symptom onset. After the fall, bone X-ray was not performed, and, for a short period of time after the fall, she was treated with non-steroidal anti-inflammatory drugs.

Magnetic resonance imaging of the lumbosacral spine was performed using gadolinium contrast media (Fig. 22.1).

Computed tomography of the sacrum was performed after the MRI to demonstrate bone changes, cortical changes and possible periosteal reaction (Fig. 22.2).

Due to the anamnesis of previous trauma, patient age, location as well as lesion imaging features, main differential diagnosis was sacral aneurysmal bone cyst (ABS). Due to patient age and imaging features of the lesion, differential diagnosis also included a GCT of the bone (GCTOB) without solid component and a telangiectatic osteosarcoma. Bone biopsy is the only method to confirm the exact pathological process. In this case, bone biopsy confirmed ABC without elements of possible underlying process.

Due to the size and location of the sacral ABC, denosumab treatment was conducted during 12 months: 120 mg subcutaneous per week during the first month of treatment and 120 mg subcutaneous per month during the following 11 months, with vitamin D2 and calcium carbonate supplementation to prevent hypocalcaemia, a rare but serious toxicity of denosumab.

After 1-year denosumab treatment (April 2017), pain in the left coxofemoral region regressed and by now is rarely present, but during the second 6 months of the treatment, she still had increased urge to urinate, especially during at night. After completing 1-year denosumab treatment, physical examination is unremarkable, while CT and MRI revealed evidence of bone formation without further tumour progression in size (Figs. 22.3 and 22.4).

22.1 Sacral Aneurysmal Bone Cyst

Going through the literature, you can find resembling definitions of ABC, defining it as rare benign expansile and osteolytic bone lesion consisting of blood-filled spaces, separated by fibrous septa containing osteoclast giant cells and trabeculae of the bone or osteoid, not lined by endothelium. It may affect all age groups; most common are in the first two decades of life with slightly higher prevalence in females [1, 2]. ABCs most commonly occur in the metaphyseal region of long bones, especially distal femur of proximal tibia; pelvis and posterior elements of the spine are also commonly involved, while sacrum is rarely involved (3%) [2, 3].

M. Špero, H. Vavro, *Neuroradiology - Expect the Unexpected*,
https://doi.org/10.1007/978-3-319-73482-8_22

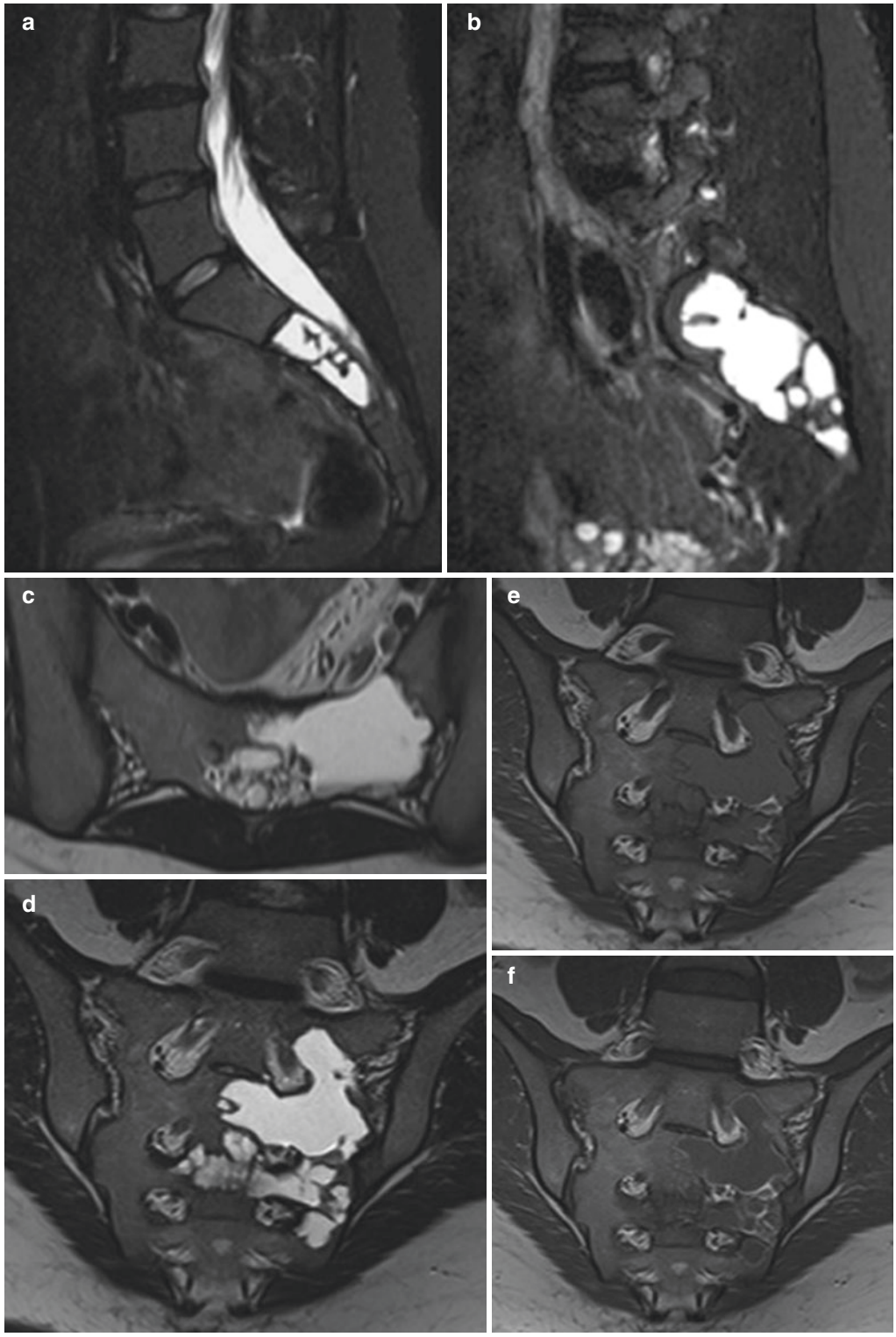

Fig. 22.1 Pretreatment magnetic resonance imaging, sagittal STIR (**a**, **b**), axial T2WI (**c**), coronal T2WI (**d**) and pre-contrast (**e**) and post-contrast (**f**) T1WI revealed expansile, lobulated, multiseptated lytic, cystic lesion in the left sacrum: hypointense on T1WI and hyperintense T2WI with several discreet dark fluid-fluid levels. Septa and cyst walls were enhanced. After intravenous administration of gadolinium contrast media, the septa and the cyst walls enhanced

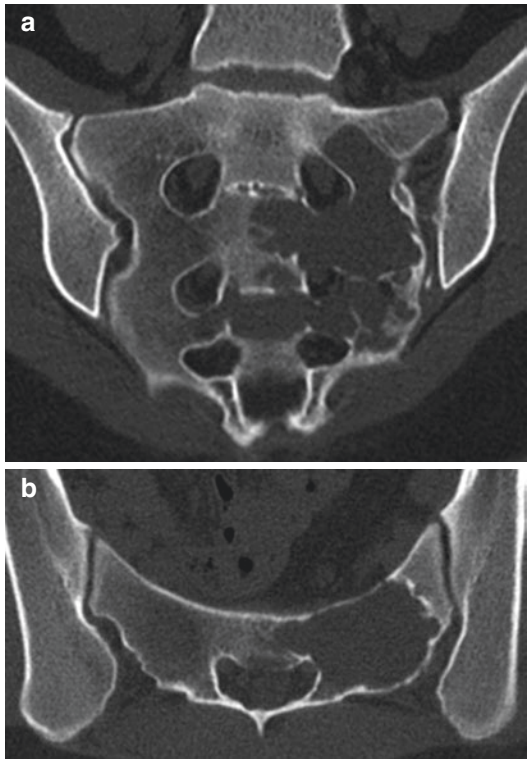

Fig. 22.2 Pre-treatment computed tomography of the sacrum, coronal (**a**) and axial (**b**) scan, demonstrated expansile, lobulated lytic lesion in the left sacrum: S1 to S4 vertebra, mainly involving S2 and S3 vertebra at which level lesion crossed the midline and reached right neural foramina – there was no clear solid component or periosteal reaction, cortical bone was slightly to moderately thinned, while lateral margin of the lesion was slightly sclerotic

Although the condition was first described in 1942 by Jaffe and Lichtenstein [4], its etiopathogenesis is still uncertain: lesions may be primary (70%) or secondary (30%). For primary ABC it is now proven that those can be real benign primary tumour associated with a specific pattern of genetic alterations that result in the activation of the gene USP6 located on chromosome 17p13 [5, 6]. Vascular factors and trauma are considered an initiating factor in their pathogenesis as well. Secondary ABC can arise within pre-existing bone tumours such as GCT of the bone, chondroblastoma, chondromyxoid fibroma, osteoblastoma and fibrous dysplasia or malignant tumours such as osteosarcoma, chondrosarcoma and hemangioendothelioma [7].

Clinical presentation in sacral ABC includes pain, bowel or urinary bladder symptoms and possible neurological symptoms.

CT and MRI are imaging methods of choice in assessment of the ABCs revealing expansive and lytic, well-circumscribed lesions. Overlying cortex is thinned and generally intact, lacking any periosteal reaction [8]. CT allows the exact three-dimensional location and measuring of an ABC, which usually has density of about 20 Hounsfield units, and may show the cavitary septa structure and fluid-fluid (serum/blood) levels as well [7, 8]. MRI shows fluid content in multilobulated cystic lesion with intracavitary fluid-fluid levels detected on T2WI, which are not specific but are highly suggestive for ABC. High-to-low T1- and T2-weighted signal intensity in the fluid-fluid levels is due to blood product of baring age. Oedema of a surrounding bone may be present on MRI [8–10]. After gadolinium injection, post-contrast T1WI shows enhancement of the cyst walls and internal septa. Solid tissue component in an ABC may suggest osteosarcoma or secondary ABC [1]. CT and MRI should be carefully studied in order to identify any concomitant tumour.

Biopsy is essential for diagnosing ABC and differentiating it from GCT of bone and telangiectatic osteosarcoma, as well as from other tumours in spinal location [1, 8]. The fluid-fluid levels on MRI and CT are not sufficient to elucidate the differential diagnose of primary ABC because telangiectatic osteosarcoma as well as GCT of the bone may contain those levels. Osteoblastoma, eosinophilic granuloma or malignant tumour can be mistaken for ABC in spinal locations, and only biopsy enables diagnosis. Histopathologically, there are two varieties of ABC: classic cavitary (95%) and solid (5%) form [8].

It is recommended to wait 4–6 weeks after the biopsy, if possible, before initiating treatment, to allow the trepanation orifice to fill and, in some cases, the cyst to begin involution, which is rare, but not surprising in case of ABC [1, 11].

Treatment of pelvic and sacral ABC is difficult due to the relative inaccessibility of the lesions, associated intraoperative bleeding, proximity of a lesion to neurovascular structures

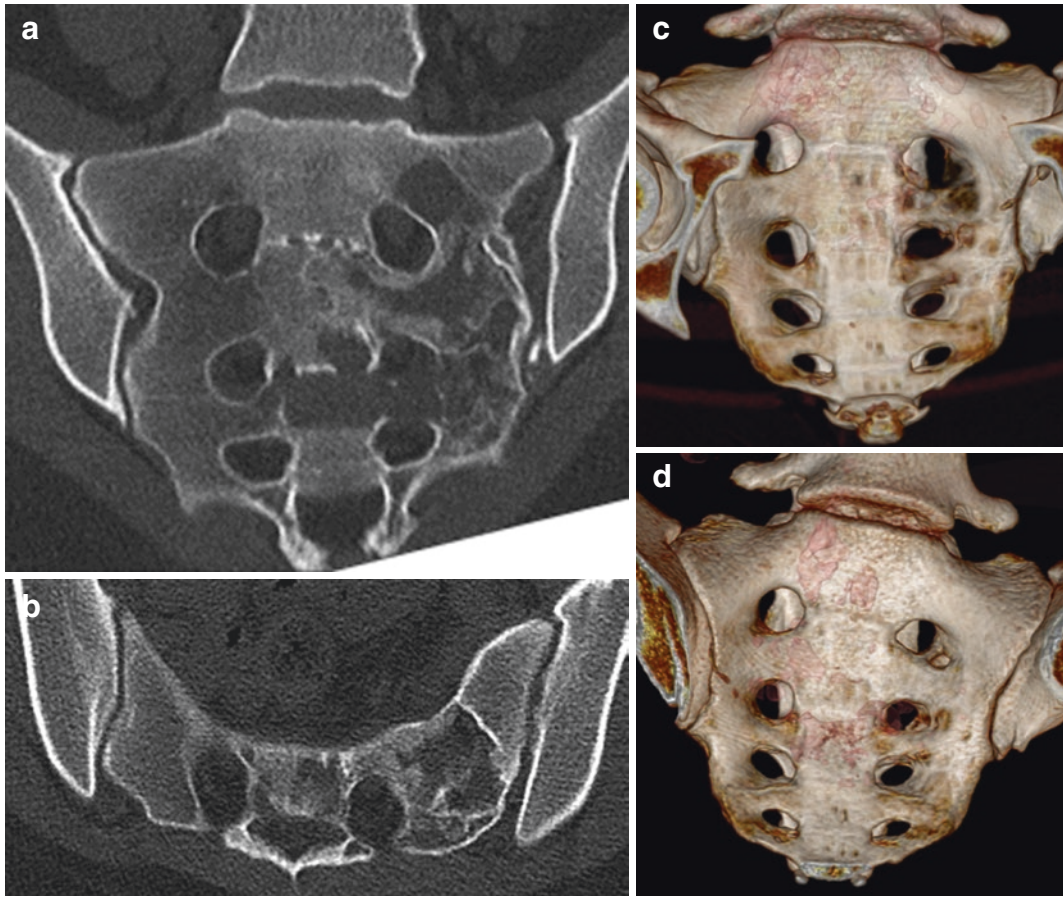

Fig. 22.3 Computed tomography of the sacrum, coronal (**a**) and axial (**b**) scan, 12 months after denosumab treatment, coronal pretreatment (**c**) and post-treatment (**d**) volume rendering technique (VRT). CT revealed regression of the cystic formation in the lesion and partial replacement of the cystic formation with solid, bone marrow-like tissue in peripheral parts of the lesion in S1, S2 and S4 vertebra, while the cystic lesion persisted in the S3 vertebra

and vulnerability of the acetabulum or sacroiliac joint. Therefore, the method of treatment (wide resection, intralesional curettage and filling by graft, cement or bone substitute, selective embolisation, radiotherapy) of sacral and pelvic ABCs must be individualized based on location, extent and aggressiveness of the lesion [12].

In a GCT of the bone, tumour cells secrete the cytokine receptor activator of nuclear factor κ-B ligand (RANKL), which initiates bone turnover upon binding to its cognate receptor, receptor-activator of nuclear κ-B (RANK). Therefore, RANKL is an essential factor in the development and progression of the bone GCT [13]. Denosumab is a human monoclonal antibody that binds RANKL, thus preventing its binding to RANK, reducing osteoclasts and decreasing bone destruction [13, 14]. By altering tumour environment, it may lead to bone formation as well. Therefore, denosumab has been used with excellent results in the treatment of osteoporosis, skeletal metastases and GCTs of the bone [14, 15]. Recent studies have suggested clear immunohistochemical similarity and relationship between GCTs of the bone and ABCs justifying the hypothesis that denosumab may also have positive effects on ABCs. From 2013 to 2016, seven cases of ABCs (one forearm, three spinal, three sacral) treated with denosumab were published in the literature: all revealed resolution or recovery from initial symptoms, no progression in size of the lesion and evidence of bone formation on CT or MRI, while one

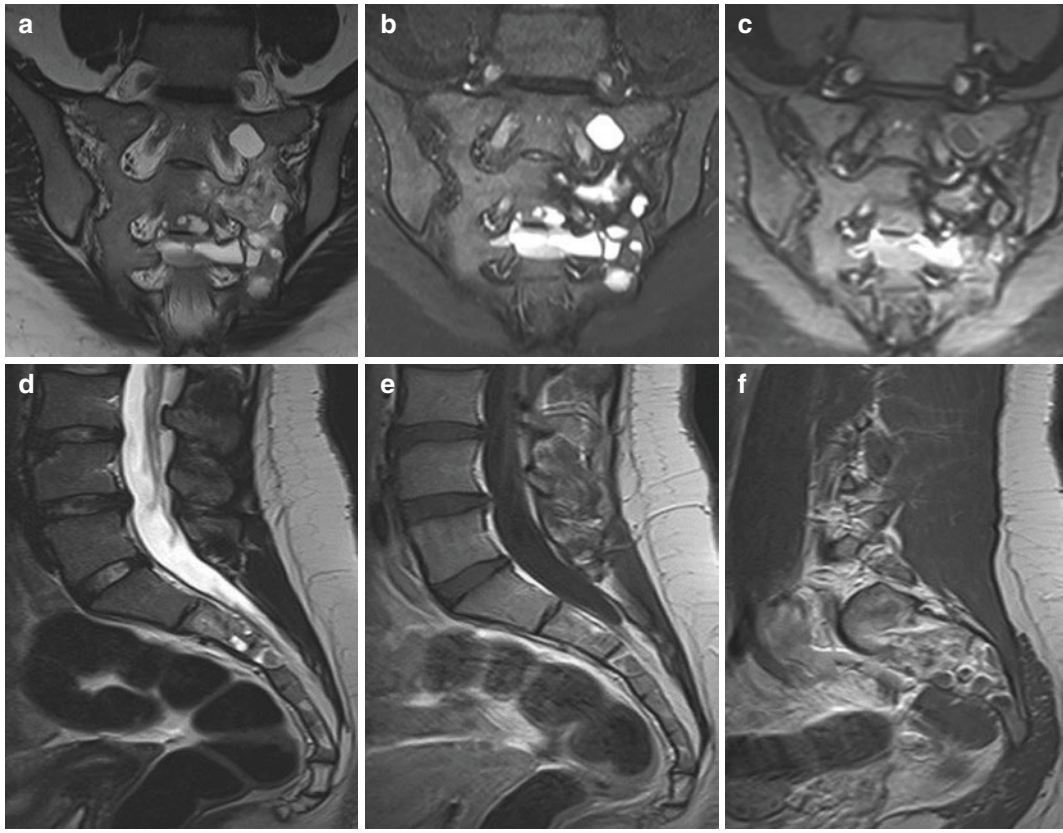

Fig. 22.4 Magnetic resonance imaging coronal T2WI (**a**), coronal T2FS (**b**), post-contrast coronal T1FSWI (**c**), sagittal T2WI (**d**) and sagittal post-contrast T1WI (**e**, **f**), after 12 months of denosumab treatment: there was no further progression in ABC size, with clear signal alterations; fluid-fluid levels in S3 vertebra and peripheral contrast enhancement were more pronounced

revealed almost complete ossification of the lesion [5, 14–16]. These data support the idea of a prospective study to confirm the effectiveness of denosumab as a treatment option in ABCs.

References

1. Mascard E et al (2015) Bone cysts: unicameral and aneurysmal bone cyst. Orthop Traumatol Surg Res 101:S119–S127
2. Yalcinkaya M et al (2016) Surface aneurysmal bone cyst: clinical and imaging features in 10 new cases. Orthopedics 39(5):897–903
3. Brastianos P et al (2009) Aneurysmal bone cysts of the sacrum: a report of ten cases and review of the literature. Iowa Orthop J 29:74–78
4. Jaffe HL, Lichtenstein L (1942) Solitary unicameral bone cyst with emphasis on roentgen picture, the pathologic appearance and the pathogenesis. Arch Surg 44(6):1004–1025
5. Pauli C et al (2014) Response of an aggressive periosteal aneurysmal bone cyst (ABC) of the radius to denosumab therapy. World J Surgl Oncol 12:17
6. Oliveira AM et al (2004) USP6 and CDH11 oncogenes identify the neoplastic cell in primary aneurysmal bone cysts and are absent in so-called secondary aneurysmal bone cysts. Am J Pathol 165(5):1773–1780
7. Bajracharya G et al (2007) Aneurysmal bone cyst of the pelvis: a challenge in treatment: review of the literature. Int J Orthop Surg 8(1):1–6
8. Radulescu R et al (2014) Aneurysmal bone cyst–clinical and morphological aspects. Romanian J Morphol Embryol 55(3):977–981
9. Girish G et al (2012) Imaging review of skeletal tumours of the pelvis – part i: benign tumours of the pelvis. Sci World J 2012:290930. https://doi.org/10.1100/2012/290930
10. Diel J et al (2001) The sacrum: pathologic spectrum, multi-modality imaging, and subspecialty approach. Radiographics 21:83–104

11. Cottalorda J, Bourelles S (2007) Aneurysmal bone cyst in 2006. Rev Chir Orthop Reparatrice Appar Mot 93(1):5–16
12. Yildirim E et al (2007) Treatment of pelvic aneurysmal bone cysts in two children: selective arterial embolization as an adjunct to curettage and bone grafting. Diagn Interv Radiol 13:49–52
13. Pelle DW et al (2014) Targeting RANKL in aneurysmal bone cysts: verification of target and therapeutic response. Transl Res 164(2):139–148
14. Lange T et al (2013) Denosumab: a potential new and innovative treatment option for aneurysmal bone cysts. Eur Spine J 22:1417–1422
15. Skubitz KM et al (2015) Response of aneurysmal bone cyst to denosumab. Spine (Phila Pa 1976) 40(22):E1201–E1204
16. Ghermandi R et al (2016) Denosumab: non-surgical treatment option for selective arterial embolization resistant aneurysmal bone cyst of the spine and sacrum. Case report. Eur Rev Med Pharmacol Sci 20:3692–3695

Postductal Coarctation of the Aorta with Neurovascular Conflict

23

A 54-year-old lady working as a kindergarten teacher has been complaining of several years' history of left-sided cervical brachial syndrome recently in progression, not reacting to medication or physical therapy. She had bilateral tinnitus and occasional dizziness, not dependent on head movements. There was no history of headache, no hand weakness and no trunk or leg neurological abnormalities.

Duplex Doppler ultrasound demonstrated normal carotid and vertebral artery haemodynamics within the neck but slower blood flow within the intracranial segments of both vertebral arteries. A physiatrist recommended MRI exam of the cervical spine (Fig. 23.1).

The multiple aberrant arteries raised suspicion of a structural arterial abnormality, so a CT angiography of the aortic arch and supra-aortic arteries was recommended for further analysis (Fig. 23.2).

The patient was not prone to any surgical or interventional treatment.

23.1 Coarctation of the Aorta

Coarctation of the aorta is a congenital malformation which may only be presented by subtle and non-specific clinical signs and thus overlooked until older age. It ranges from discrete narrowing at the insertion of the ductus arteriosus (which may be patent) to severe tubular hypoplasia. The common feature to all grades of coarctation is flow disturbance in the thoracic aorta, increased afterload on the left ventricle, hypertension in the upper body and hypoperfusion of the lower body. The incidence is approximately 4 in 10,000 live births and accounts for 5–8% of all congenital heart defect. If untreated, mean life expectancy of patients is 35 years, with 90% of patients not reaching the age of 50 [1] due to complications such as congestive heart failure, aortic dissection, systemic hypertension, coronary heart disease and stroke.

Native coarctation is caused by either a ridge-like protrusion of the thickened aortic wall media into the aortic lumen or, less frequently, by tubular hypoplasia. Recoarctation refers to restenosis after initially successful surgical or endovascular treatment (up to 10% of treated cases, mostly in children) [2].

Chronic aortic lumen stenosis in coarctation of the aorta provokes enlargement of collateral vessels, including spinal cord arteries which may dilate enough to produce compressive myelopathy [3]. Compression by enlarged arteries may affect not only the spinal cord but the spinal nerves as well, such as in this case. The spinal and intracranial arteries in patients with aortic coarctation are prone to developing aneurysms—in case of rupture, subarachnoid haemorrhage will develop.

Treatment of aortic coarctation in adults consists of surgical approach or percutaneous balloon angioplasty, usually with subsequent stent placement and medical therapy.

M. Špero, H. Vavro, *Neuroradiology - Expect the Unexpected*,
https://doi.org/10.1007/978-3-319-73482-8_23

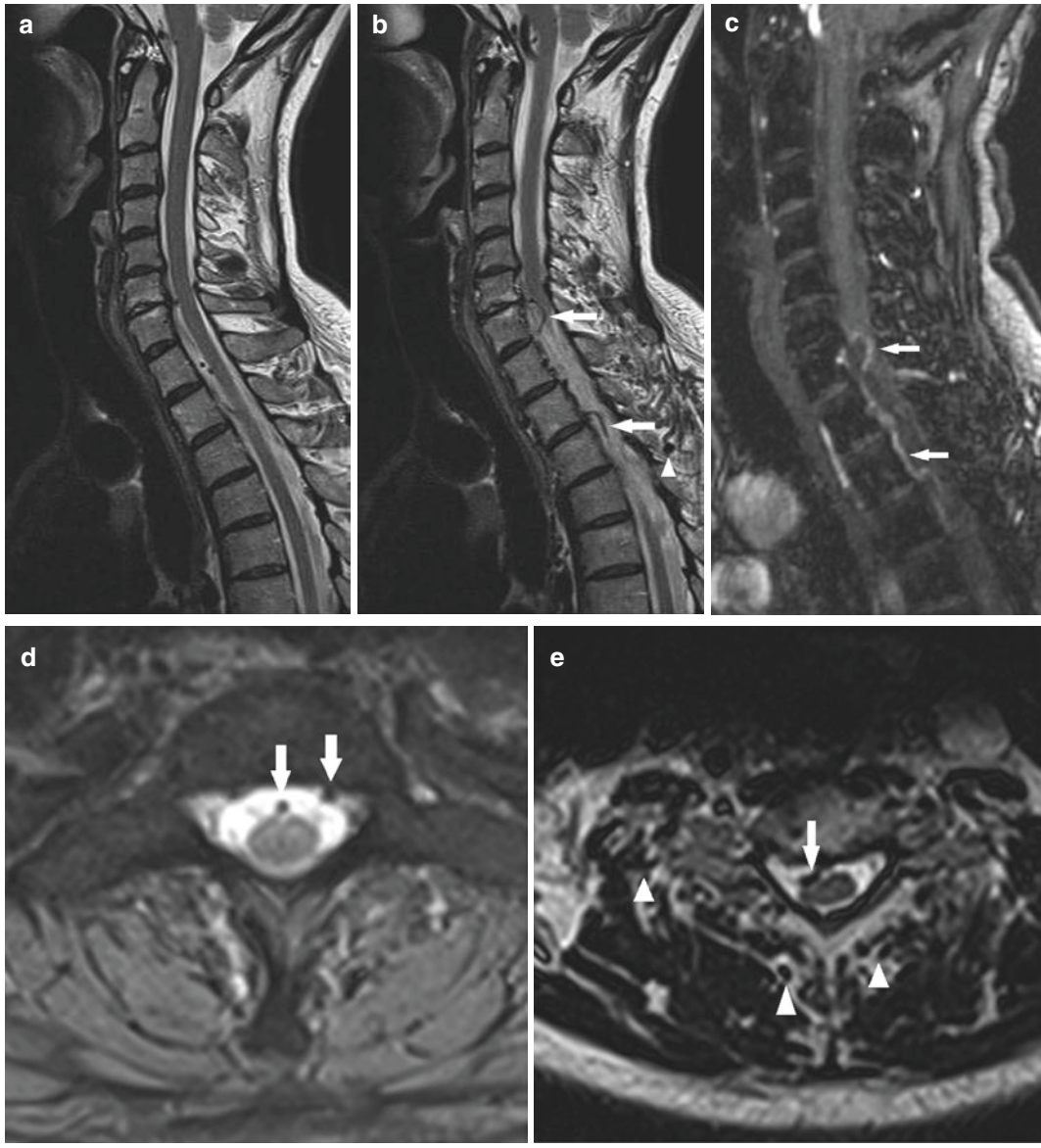

Fig. 23.1 MRI exam of the cervical and proximal thoracic spine. Sagittal T2WI (**a**, **b**), sagittal MIP 3D-TOF MRA reformatted image (**c**), axial T2WI (**d**, **e**), axial 3D-TOF MRA reformatted image (**e**). There is multilevel mild to moderate intervertebral disc degeneration (**a**, **b**) but without evidence of spinal nerve or spinal cord compression by the discs. However, in the lower cervical and upper thoracic spinal canal, several abnormal flow voids are visible, both intradural and extradural (arrows in (**b**, **d**, **e**)). There are also numerous serpiginous flow voids (arrowheads in (**b**, **e**)) in the paravertebral soft tissues of the cervical-thoracic junction. 3D-TOF MRA (**c**, **f**) sequence shows high-flow vessels consistent with hypertrophic arteries in the paravertebral space; there are also enlarged arteries in the extradural space and subdural space within the spinal canal (arrows in (**c**, **f**)). Bilateral intradural and extradural arteries cross the spinal neural foramina at the C7–T1 level bilaterally, especially on the left (**f**) with compression of the left-sided C8 spinal nerve

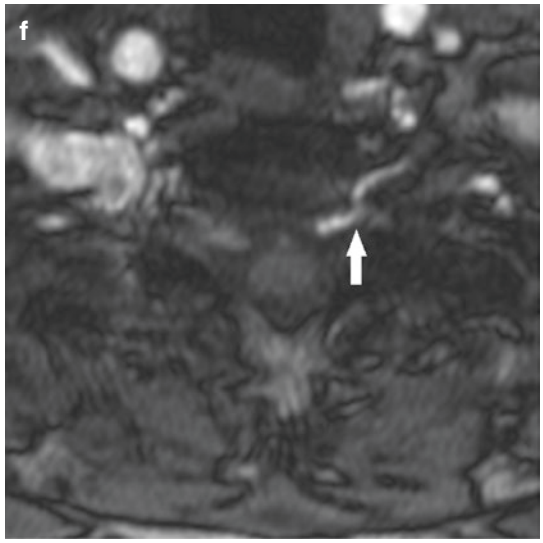

Fig. 23.1 (continued)

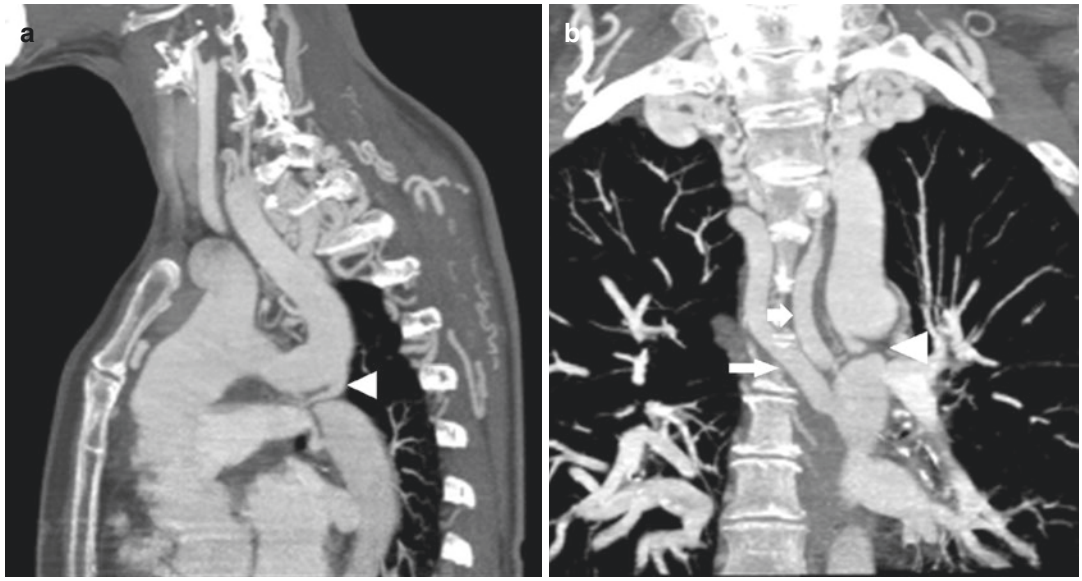

Fig. 23.2 CTA of the aortic arch and supra-aortic arteries demonstrates a high-grade aortic coarctation distal to the origin of the left subclavian artery (arrowhead in (**a**, **b**)), with extensive collateral arterial network consisting of enlarged internal thoracic, intercostal (**c**), thoracoacromial and subscapular arteries, thyrocervical trunks and vertebral arteries with their respective branches. VRT image (**d**) shows hypertrophic posterior rami of the posterior intercostal arteries. Hypertrophic radicular arteries are clearly visible in neural foramina at C7–Th1 level (**e**). Collateral arteries (**f**) are supplied from the moderately hypertrophic brachiocephalic trunk, left common carotid and left subclavian artery. Note the two hypertrophic paravertebral arteries supplying the aorta immediately distal to the coarctation (arrows in (**b**)). The pulmonary arteries are normal. The descending thoracic aorta distal to the coarctation is mildly hypoplastic

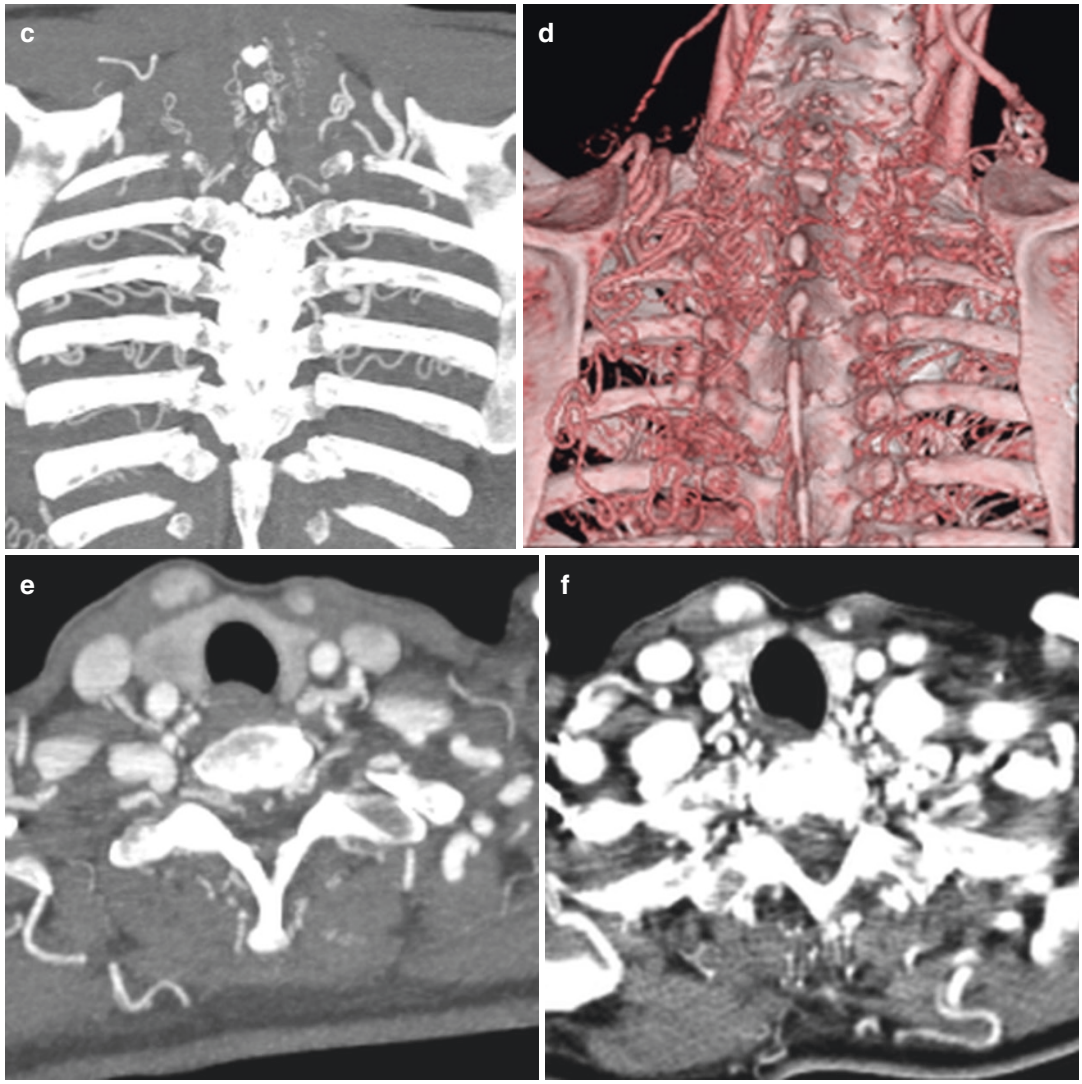

Fig. 23.2 (continued)

References

1. Jurcut R et al (2011) Coarctation of the aorta in adults: what is the best treatment? Case report and literature review. J Med Life 4(2):189–195
2. Suradi H, Hijazi ZM (2015) Current management of coarctation of the aorta. Glob Cardiol Sci Pract 2015:44. https://doi.org/10.5339/gcsp.2015.44
3. Mourya C et al (2016) Myelopathy in adult aortic coarctation: causes and caveats of an atypical presentation. Indian J Radiol Imaging 26(4):451–454. https://doi.org/10.4103/0971-3026.195775

Acute Transverse Myelitis: Primary Spinal Cord Lymphoma

24

Three weeks prior to admission, this 66-year-old lady complained of paraesthesiae in her feet, with cranial progression to the umbilical level and bilateral leg weakness. She also lost the urge to urinate and defecate. In the following 2 weeks, she developed paraplegia and incontinence. Personal medical history was unremarkable, with no evidence of trauma, fever or tick bite and no pain at all.

EMG study results of both upper and lower extremities were unremarkable. Brain CT was normal.

A MRI exam of the spine was done (Fig. 24.1).

Methylprednisolone therapy had been started, and the patient was transferred to a larger clinical hospital for further workup where samples of serum and CSF were taken for analysis and a follow-up MRI exam was performed (Fig. 24.2).

The serum and CSF were negative for oligoclonal bands (for demyelination) and AQP4 antibodies (for NMO). However, there was a large number of cells within the CSF, predominantly blasts. The immunophenotype analysis revealed a B-cell non-Hodgkin lymphoma. The peripheral blood analysis and bone marrow analysis did not show evidence of lymphoma infiltration.

It was concluded that this was a case of a primary spinal cord lymphoma.

24.1 Primary Spinal Cord Lymphoma

Primary spinal cord lymphoma is extremely rare, accounting for approximately 3.3% of all primary CNS lymphomas (PCNSL), and only 1% of or lymphoma is in the body. Eighty-five percent are non-Hodgkin lymphomas [1]. Most of them are B-cell type tumours. The classification as "primary" implicates there is no evidence of systemic lymphoma at the time of diagnosis. Somewhat more commonly lymphoma involves the vertebral bodies or epidural compartment. Secondary intramedullary invasion of the spinal cord by leptomeningeal disease is also possible [2].

Common presentation is focal neurologic deficit, including pain, paraesthesias and paresis. On MRI imaging, there is typically an intramedullary T2 hyperintense lesion, as opposed to the brain lymphoma where T2 signal tends to be hypointense. The gadolinium enhancement is often avid. There may be some surrounding oedema. They usually do not feature cysts, and secondary syringomyelia is rare. CSF analysis is often non-specific, requiring additional histopathological evaluation [3].

M. Špero, H. Vavro, *Neuroradiology - Expect the Unexpected*,
https://doi.org/10.1007/978-3-319-73482-8_24

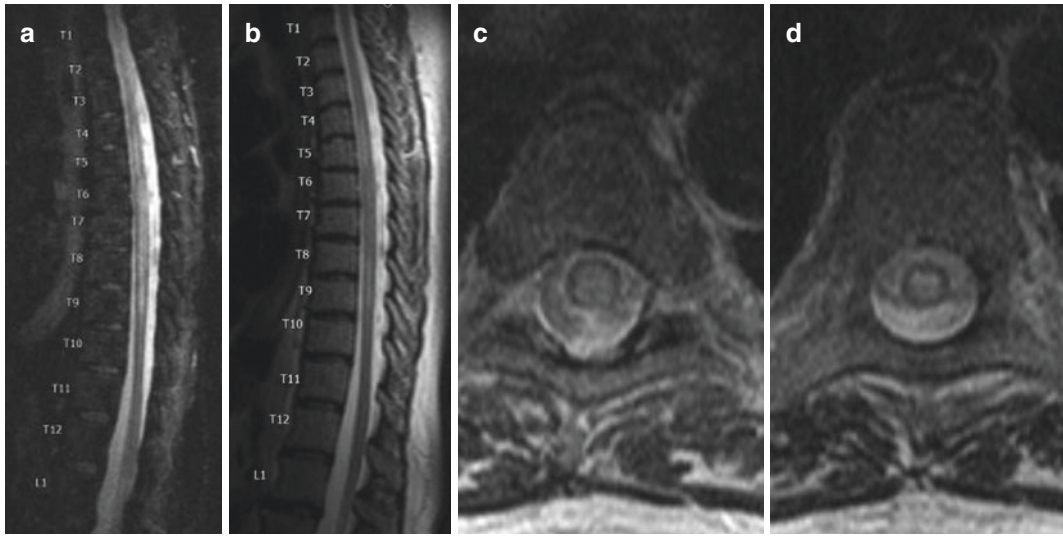

Fig. 24.1 Initial MRI of the thoracic spine—sagittal STIR sequence (**a**), sagittal T2WI (**b**), axial T2WI at the T6 level (**c**), axial T2WI at the T8 level (**d**)—reported as "prominent central cord canal in segments T4–T10 in keeping with hydromyelia"

The differential imaging considerations include glioma, metastasis and inflammatory processes such as multiple sclerosis or acute transverse myelitis. In series of cases analysed by Guzey et al. [4], out of 46 cases diagnosed with MRI, there was an initial misdiagnosis in 24 cases—10 of them were diagnosed as transverse myelitis or multiple sclerosis.

Transverse myelitis features extension through at least 3–4 spinal segments and involvement of more than two thirds of the cross-sectional area of the cord. It does not involve diffusion abnormalities. The enhancement pattern varies from no enhancement to homogenous enhancement (Fig. 24.3). Symptoms and signs are bilateral, evolve over hours or days and include paraparesis, tetraparesis, sphincter dysfunction and a clearly defined level of sensory impairment.

Fig. 24.2 MRI exam of the cervical and thoracic spinal cord. Sagittal T1WI (**a**), T2WI (**b**,**c**), post-contrast T1WI (**d**), axial T2WI (**e**–**g**). There is a structural spinal cord lesion at levels T5–T8, enhancing with contrast. At the proximal and distal end of the lesion, there are T2 hyperintense areas which do not enhance, consistent with oedema rather than syrinx or hydromyelia. There is minimal cord expansion. The features were thought to be compatible with transverse myelitis; the differential diagnosis included neuromyelitis optica (NMO)

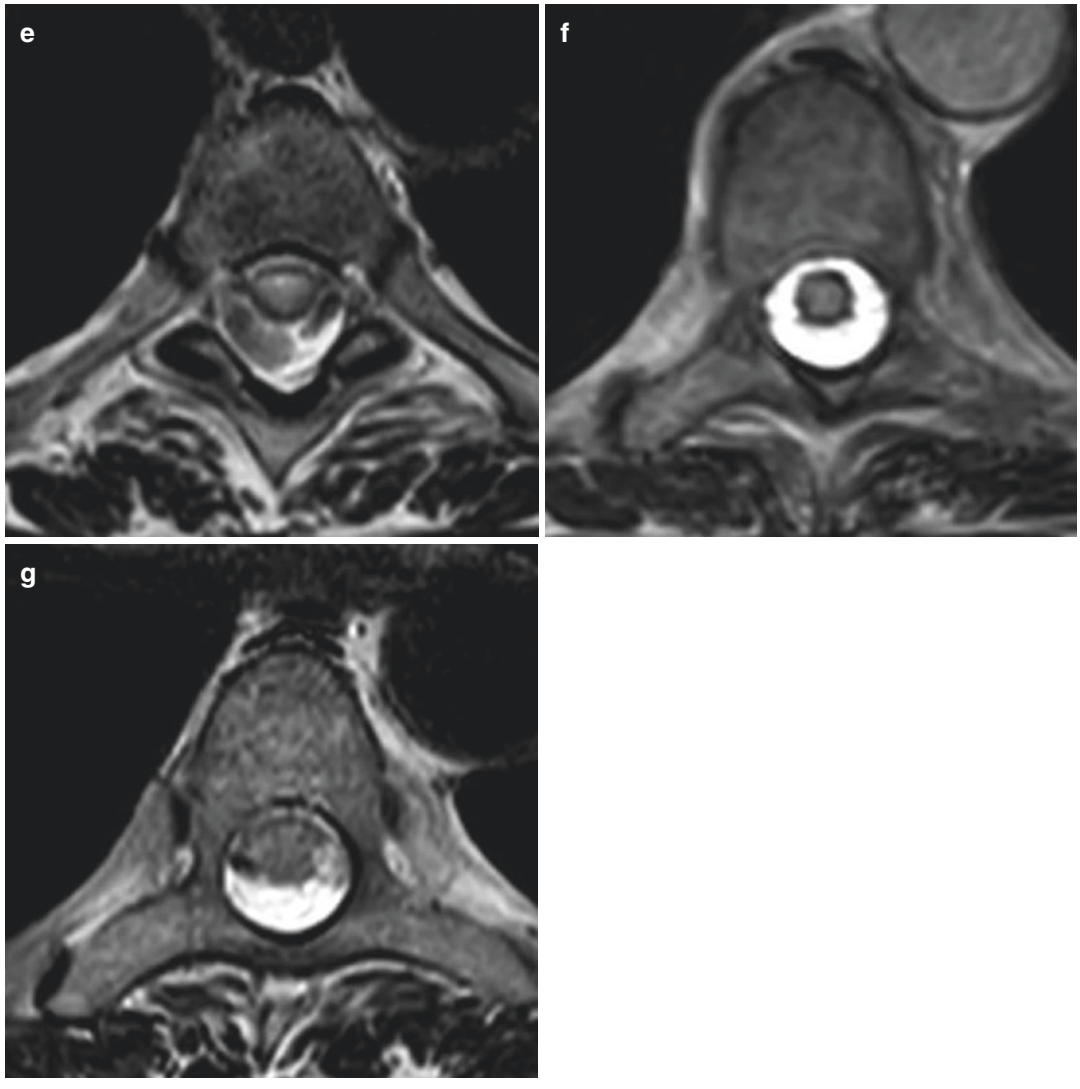

Fig. 24.2 (continued)

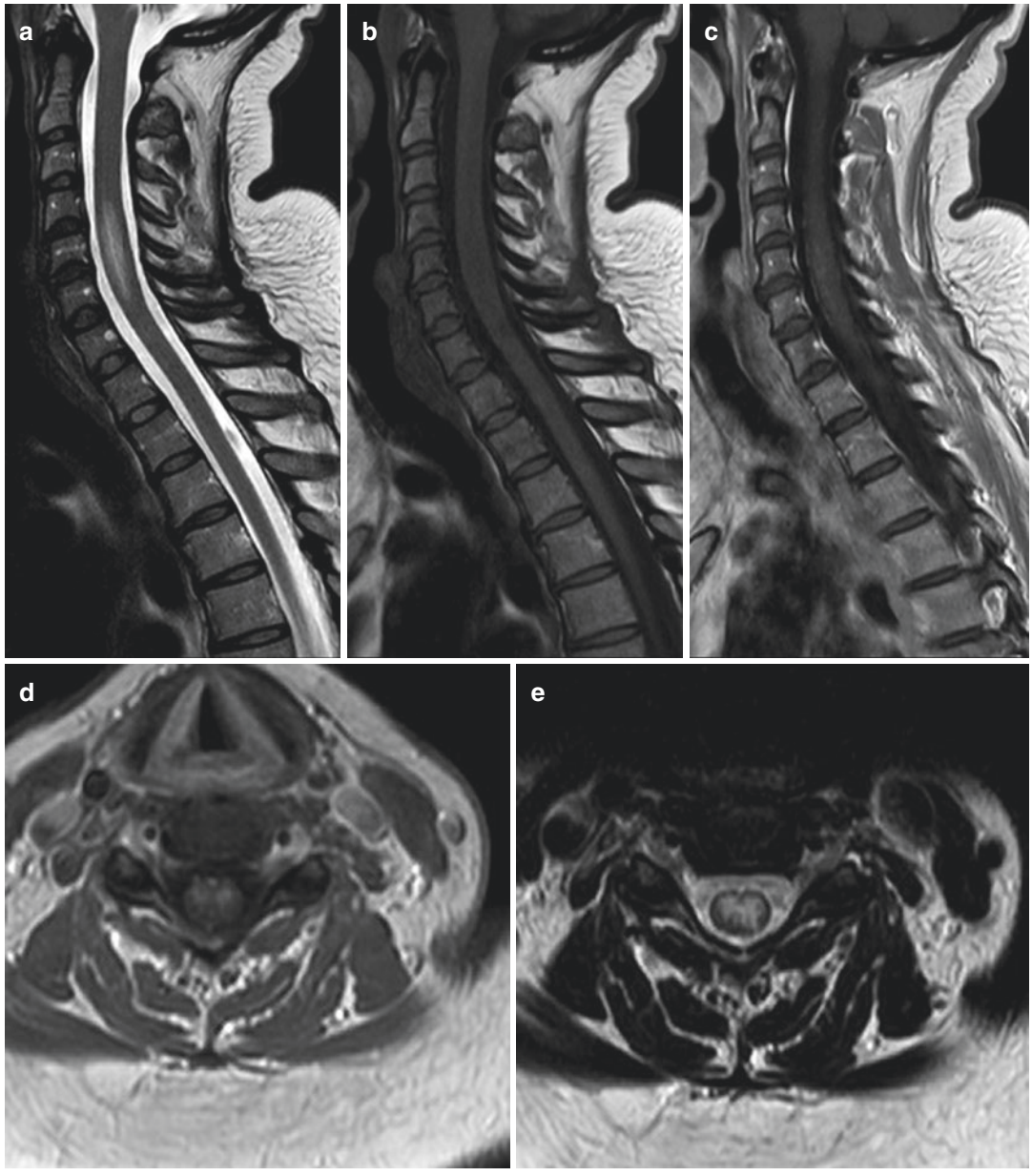

Fig. 24.3 MR images of transverse myelitis. Compare with Fig. 24.1. Sagittal T2WI (**a**) and T1WI (**b**), post-contrast sagittal (**c**) and axial (**d**) T1WI, axial T2WI (**e**). There is a faintly and inhomogeneously enhancing central spinal cord lesion in segments C4–C6, mildly expanding the cord

References

1. Abul-kasim K et al (2008) Intradural spinal tumors: current classification and MRI features. Neuroradiology 50(4):301–314. https://doi.org/10.1007/s00234-007-0345-7
2. Haque S et al (2008) Imaging of lymphoma of the central nervous system, spine, and orbit. Radiol Clin North Am 46(2):339–361. https://doi.org/10.1016/j.rcl.2008.04.003
3. Newton HB, Jolesz FA (2008) Handbook of neuro-oncology neuroimaging. Academic Press, Amsterdam, p 479
4. Guzey FK et al (2015) Primary spinal intramedullary lymphoma: a case report and review of the literature. JSM Neurosurg Spine 3(1):1049

Part VI

Something Different

Garfish Sting

25

This is a bit bizarre case about a 36-year-old woman who was spending summer vacation on an island on the Adriatic Coast. One morning at the beginning of August 2016, she was swimming in shallow waters along a beach when, quite bizarre, a garfish or sea needle jumped out from the sea and plunged its sharp beak into patient's right eye. Garfish has elongated jaws presenting as a long, narrow beak.

Patient was transported to a hospital on a mainland from where she was transported to one of the several hospitals in the capital city where ophthalmologists tried to remove the beak. When she arrived at a university hospital, computed tomography of the orbit was performed (Fig. 25.1).

Due to a near vicinity of the inferior rectus muscle and the optic nerve, precise procedure of the beak removal was required. Therefore, a patient was transferred to our hospital where maxillofacial surgeon was able to remove the rest of the beak without any damage to the adjacent orbital structures, especially the optic nerve and inferior rectus muscle; thus the vision and eye movements were preserved. There was no eye infection afterwards (Fig. 25.2).

25.1 Garfish Sting

The garfish or needlefish (family Belonidae) is a pelagic fish primarily inhabiting close to a water surface, in very shallow marine waters, or at the surface of the open sea of the Atlantic, the Mediterranean Sea, the Caribbean Sea and the Baltic Sea. The needlefish is a long and slender fish with a laterally compressed body and elongated jaws with sharp teeth forming a beak, which can grow to about 50–75 cm in length [1–3].

All needlefish feed primarily on smaller fishes, which they catch with an upward sweep of the head. When undisturbed, needlefishes move along with an undulating motion of the body. Needlefish is capable of making short jumps out of the water: this jumping activity is greatly excited by artificial light from fishing boats at night. In a case of "human-needlefish" encounter, a fish is usually excited or chased by larger fishes and on rare occasion inflicts injuries and deep puncture wounds to the chest, abdomen, arms, legs or neck, often breaking off inside the victim in the process [4].

This is a really bizarre case because a needlefish inflicted an injury by plunging a beak into a patient's eye. At the time, most of the daily newspapers reported about the case and medical procedures resulting in successful removal of the beak from the eye. In this particular case, ichthyologist has explained that, while swimming in the sea, our patient probably found herself in a way of a moving needlefish flock; this particular garfish was probably catching a prey when jumped out of the sea and "stumbled upon" our patient's eye. Probably a fish body broke off in the process

M. Špero, H. Vavro, *Neuroradiology - Expect the Unexpected*,
https://doi.org/10.1007/978-3-319-73482-8_25

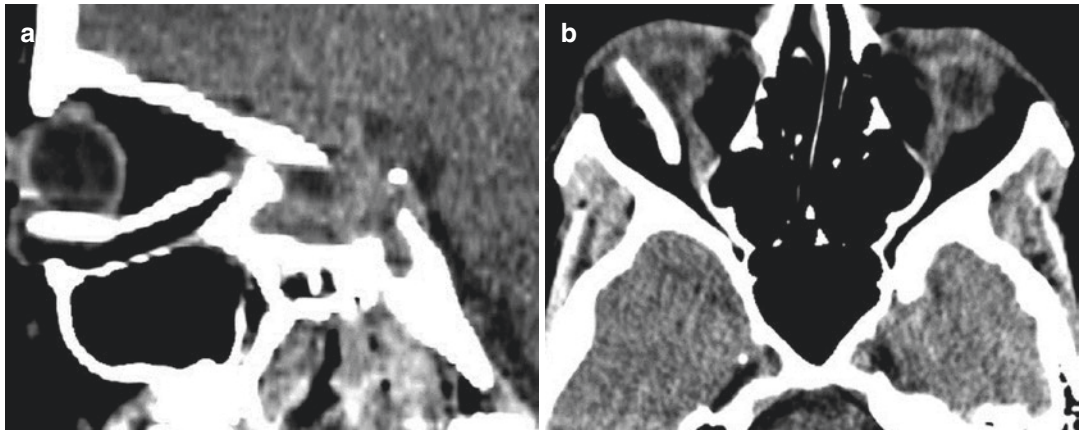

Fig. 25.1 Computed tomography of the orbit, sagittal (**a**) and coronal (**b**) scan, demonstrated the beak extending just below the inferior part of the eye bulb, right next to the inferior rectus muscle, few millimetres away from the optic nerve, through the orbital fat tissue, ending in the posterior part of the inferior rectus muscle. Tissue around the beak, just below the eye bulb, was oedematous; orbital fat tissue did not reveal density changes. Ophthalmologists tried to remove the beak but were able to remove the small part of the beak placed just below the eye bulb; they were not able to remove the rest of the beak

while the beak remained deep in a patient eye. Our patient was lucky because the beak did not damaged the inferior rectus muscle and because it did not hit the optic nerve. At the end, joint forces and knowledge of ophthalmologist and maxillofacial surgeon resulted in a successful removal of the beak from the eye, while vision and eye movements remained intact. This is one of the many injuries inflicted by a garfish and published in daily newspapers or even published in scientific literature. Those injuries could have a serious sequel, like a case of a traumatic carotid-cavernous sinus fistula in a boy due to a penetrating injury caused by a needlefish while he was fishing with his father on Hawaii [4], or even a death outcome [5]. This is a really bizarre case of a garfish sting with a positive outcome for a patient with a preserved eyesight after medical intervention.

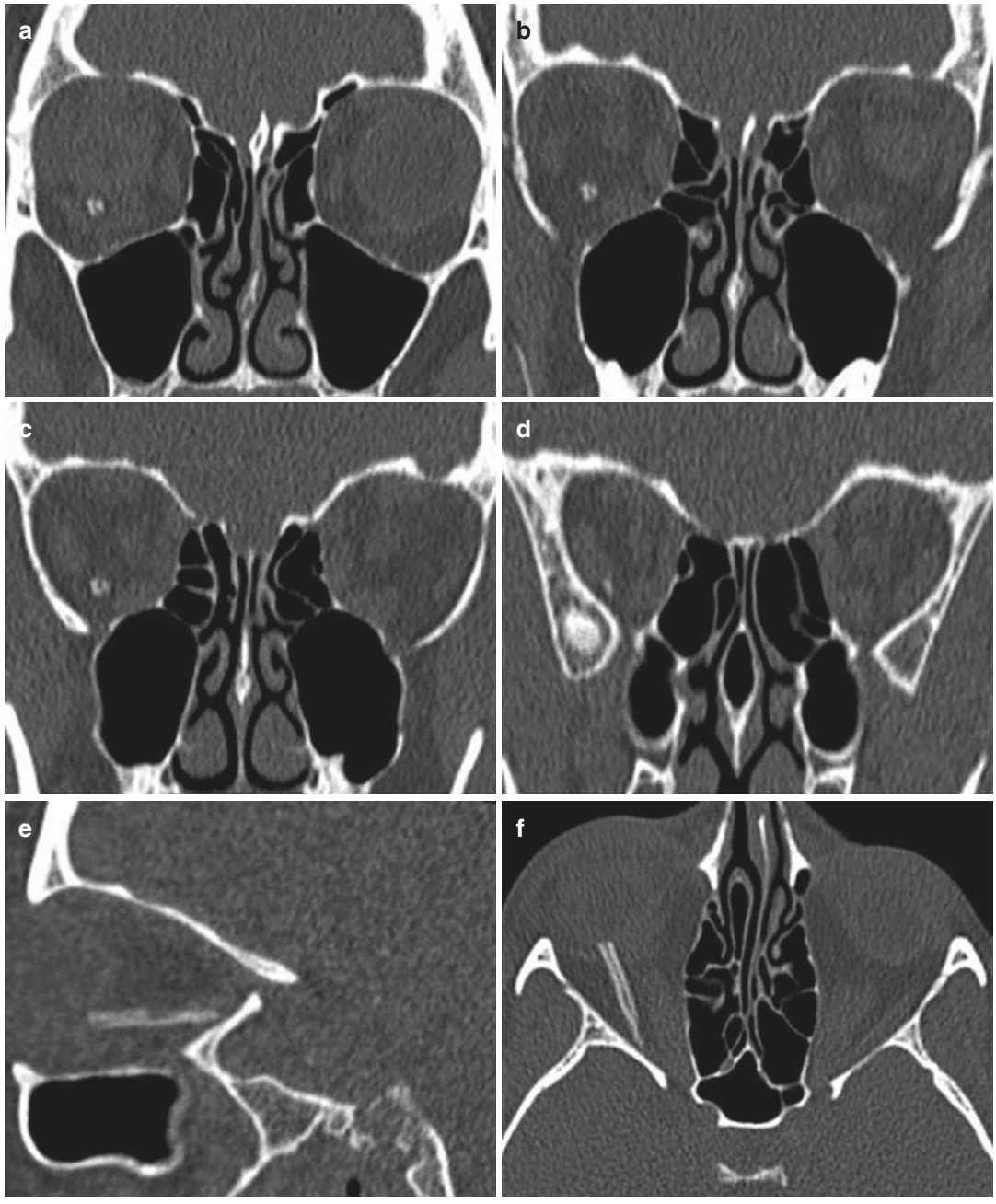

Fig. 25.2 Computed tomography of the orbit, coronal (**a**–**d**, **g**–**j**), sagittal (**e**, **k**) and axial (**f**, **l**) scans, performed just before maxillofacial surgeon removed the rest of the beak. Ophthalmologist managed to remove a part of the beak just below the eye bulb. The rest of the beak remained in the orbit, extending through the orbital fat tissue, just next to the inferior rectus muscle, few millimetres away from the optic nerve, and ended in the posterior part of the inferior rectus muscle

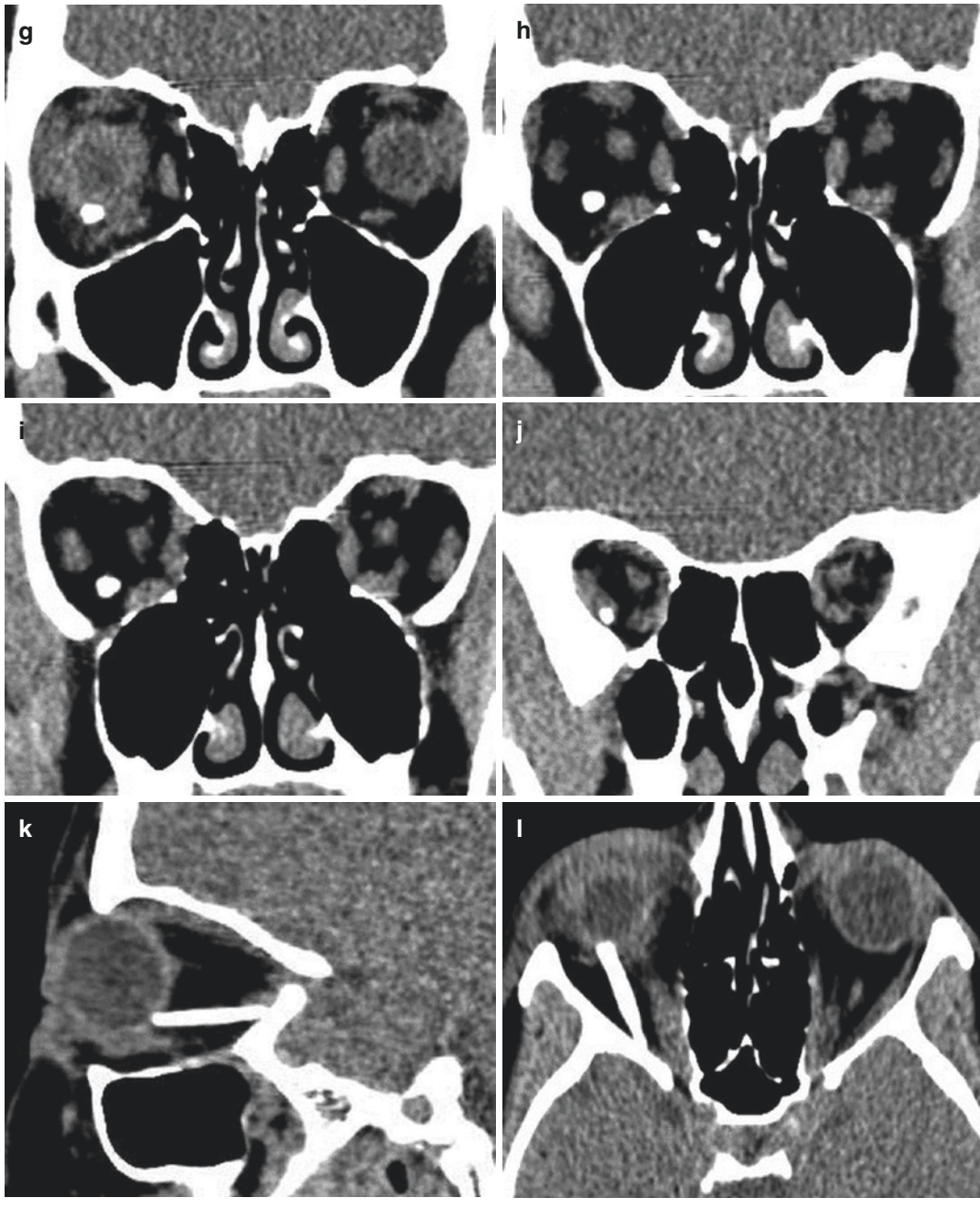

Fig. 25.2 (continued)

References

1. Collette BB et al (1998) Encyclopedia of fishes. Academic Press, San Diego. pp 144–145. isbn: 0-12-547665-5
2. Colette BB, Parin NV (1986) Belonidae. In: Whitehead PJP (ed) Fishes of the north-eastern Atlantic and the Mediterranean. UNESCO, Paris, pp 604–609
3. Zorica B, Čikeš Keč V (2013) Age, growth and mortality of the garfish, belone belone (L. 1761) in the Adriatic Sea. J Mar Biol Assoc U K 93(2):365–372
4. McCabe MJ et al (1978) A fatal brain injury caused by a needlefish. J Neuroradiol 5(3):137–139
5. Needlefish stabs diver to death in Vietnam (2007) Deutsche Press Agenteur. http://www.digitaljournal.com/article/226080/Needlefish_stabs_diver_to_death_in_Vietnam. Accessed 02 Sept 2017

A Dural Surprise

26

In April 2017 this previously healthy young gentleman (34) started suffering from occasional headaches in the right frontal region. MRI imaging he was referred to in May showed somewhat unexpected pathology (Fig. 26.1).

The patient was scheduled for surgery; a contrast-enhanced CT scan of the head was performed as part of preoperative neuronavigation workup(Fig. 26.2).

The surgery was uneventful, the involved dura and bone were resected, and intraoperative histopathology report was compatible with a meningioma.

However, after detailed histopathology analysis of all resected tissue samples, the histopathological diagnosis was changed to non-Hodgkin lymphoma—diffuse large B-cell lymphoma (DLBCL).

Subsequently, CT screening of the thorax, abdomen and pelvis was requested, as well as follow-up MRI of the whole neural axis. The body CT was negative, as well as whole neural axis MRI. The bone marrow biopsy was unremarkable.

There were no other foci of lymphoma (Fig. 26.3).

It was concluded that the lesion was a primary dural aggressive non-Hodgkin lymphoma-diffuse large B-cell lymphoma. Immunochemotherapy (R-CHOP protocol) was started.

26.1 Intracranial Primary Dural Diffuse Large B-Cell Lymphoma

Primary dural lymphoma (PDL), without leptomeningeal, parenchymal or systemic involvement, is very rare, making less than 1% of all brain lymphomas. Most of the cases are low-grade B-cell lymphomas [1]. High-grade primary diffuse large B-cell lymphoma (DLBCL) of the dura, such as in this case, is an extremely rare entity.

PDL differs from the primary central nervous system lymphoma (PCNSL; see Chap. 2) by the clinical presentation, prognosis and tumour biology. It originates outside of the central nervous system, in immunocompetent patients. The dura normally does not contain any lymphoid tissue; it is presumed that a chronic inflammatory meningeal process may precede the occurrence of PDL [2].

The rarity of the PDL and the imaging characteristics which include en plaque dural infiltration, enhancement (with dural tail signs), increased DWI signal and intraosseous propagation are the reasons why this lesion is commonly mistaken for an aggressive meningioma. If there is vasogenic oedema of the underlying brain parenchyma and/or osteolysis rather than hyperostosis of the adjacent bone, it is more likely that the lesion represents a lymphoma than a meningioma [1, 2]. The clinical appearances are also similar to meningioma. Symptoms depend on the

M. Špero, H. Vavro, *Neuroradiology - Expect the Unexpected*,
https://doi.org/10.1007/978-3-319-73482-8_26

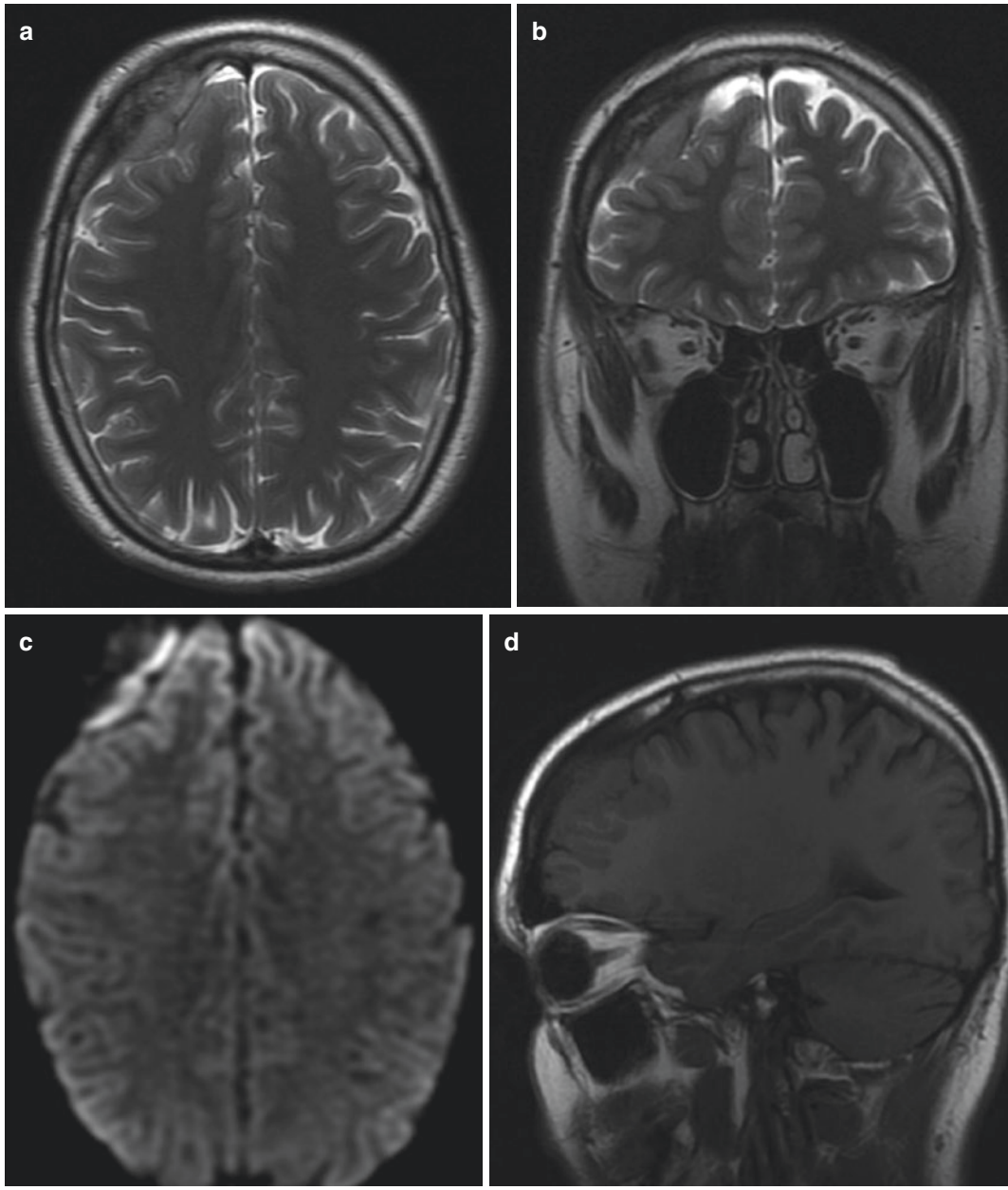

Fig. 26.1 Initial MRI exam of the head. Axial (**a**) and coronal (**b**) T2WI, axial DWI (**c**), sagittal non-contrast (**d**) and contrast-enhanced (**e**) T1WI, axial contrast-enhanced T1WI (**f**). There is a right-sided frontal extra-axial space-occupying lesion, isointense in T1WI (**d**), hypointense in T2WI (**a**–**c**), avidly enhancing with gadolinium contrast (**e**, **f**), with evidence of intradiploic propagation. Note the increased DWI signal of the lesion (**c**) which indicates compact cellularity. The lesion abuts the brain parenchyma, without evidence of brain infiltration. Most probable diagnosis stated in the report was meningioma with intraosseous invasion

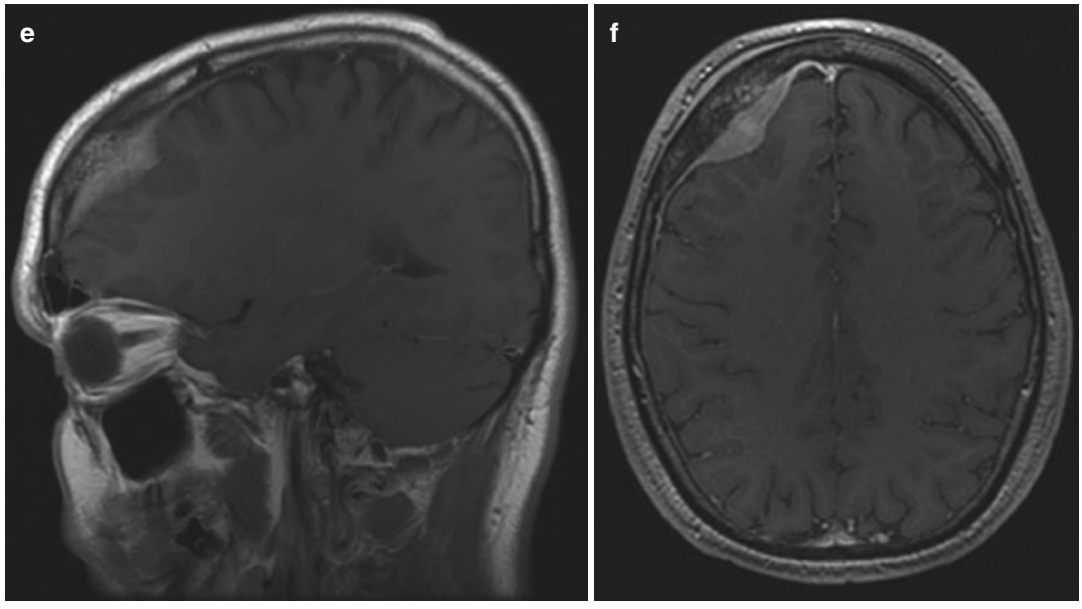

Fig. 26.1 (continued)

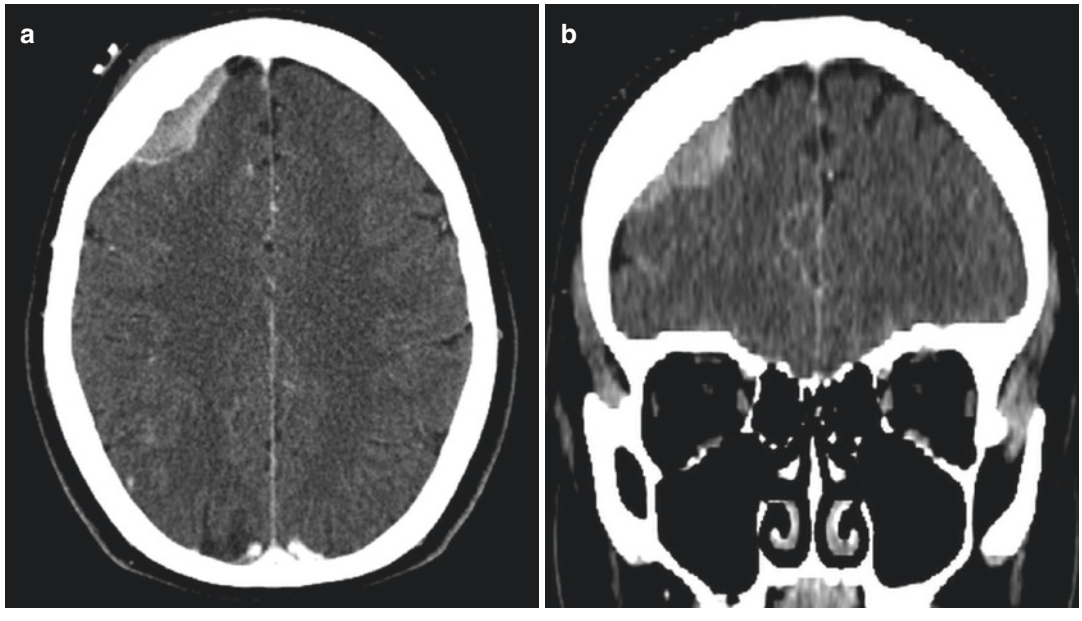

Fig. 26.2 Initial CT exam of the head (for neuronavigation purposes). As on previous MRI exam, there is a right frontal extra-axial enhancing space-occupying lesion (**a**, **b**) with evidence of bone infiltration (**c**)

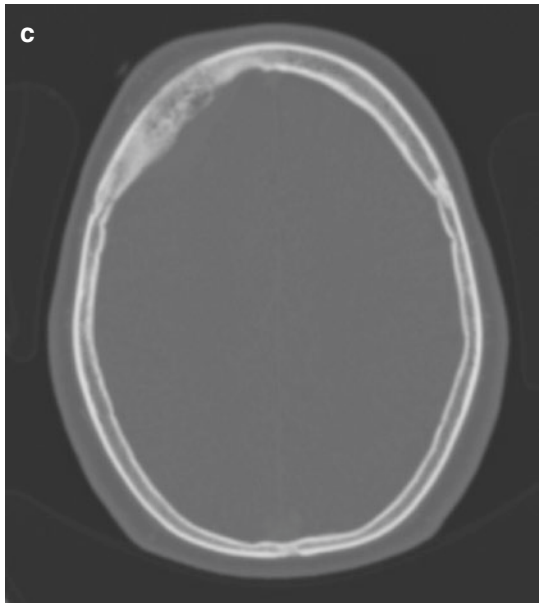

Fig. 26.2 (continued)

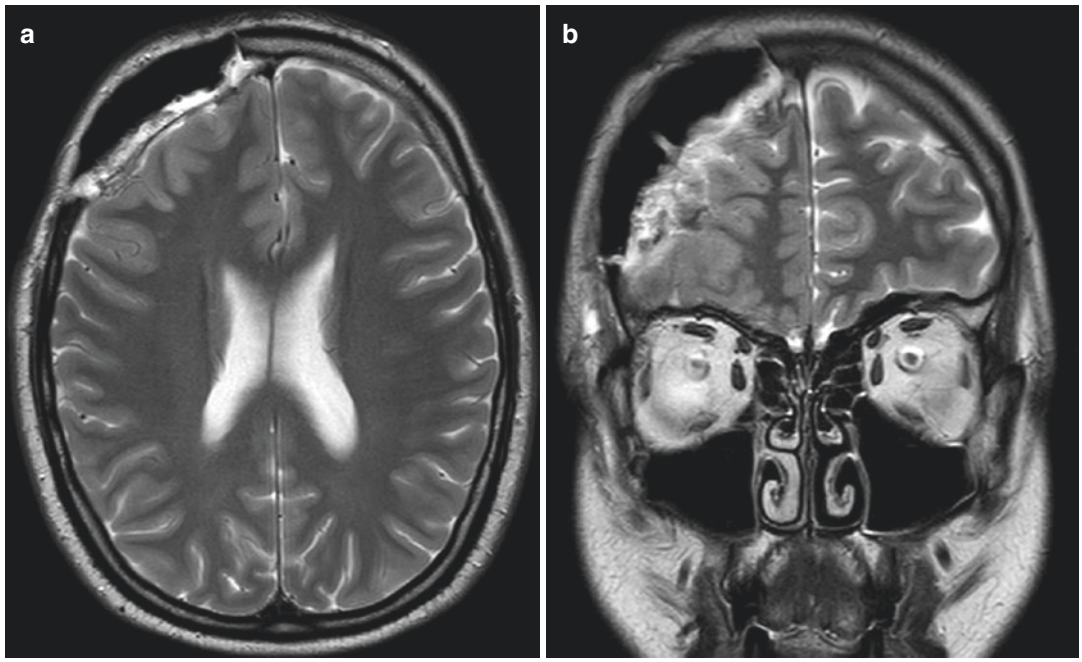

Fig. 26.3 Follow-up MRI of the brain with MRI of the whole spine. Axial (**a**) and coronal (**b**) T2WI and post-contrast axial T1WI (**c**) show evidence of right-sided frontal craniectomy with a small extradural postsurgical collection, without significant compression of the brain parenchyma. There is no evidence of residual tumour. In sagittal T2WI (**d**–**f**) and post-contrast T1WI (**g**, **h**), there is no evidence of space-occupying lesions or abnormal enhancement in the spinal canal. The spinal cord is unremarkable

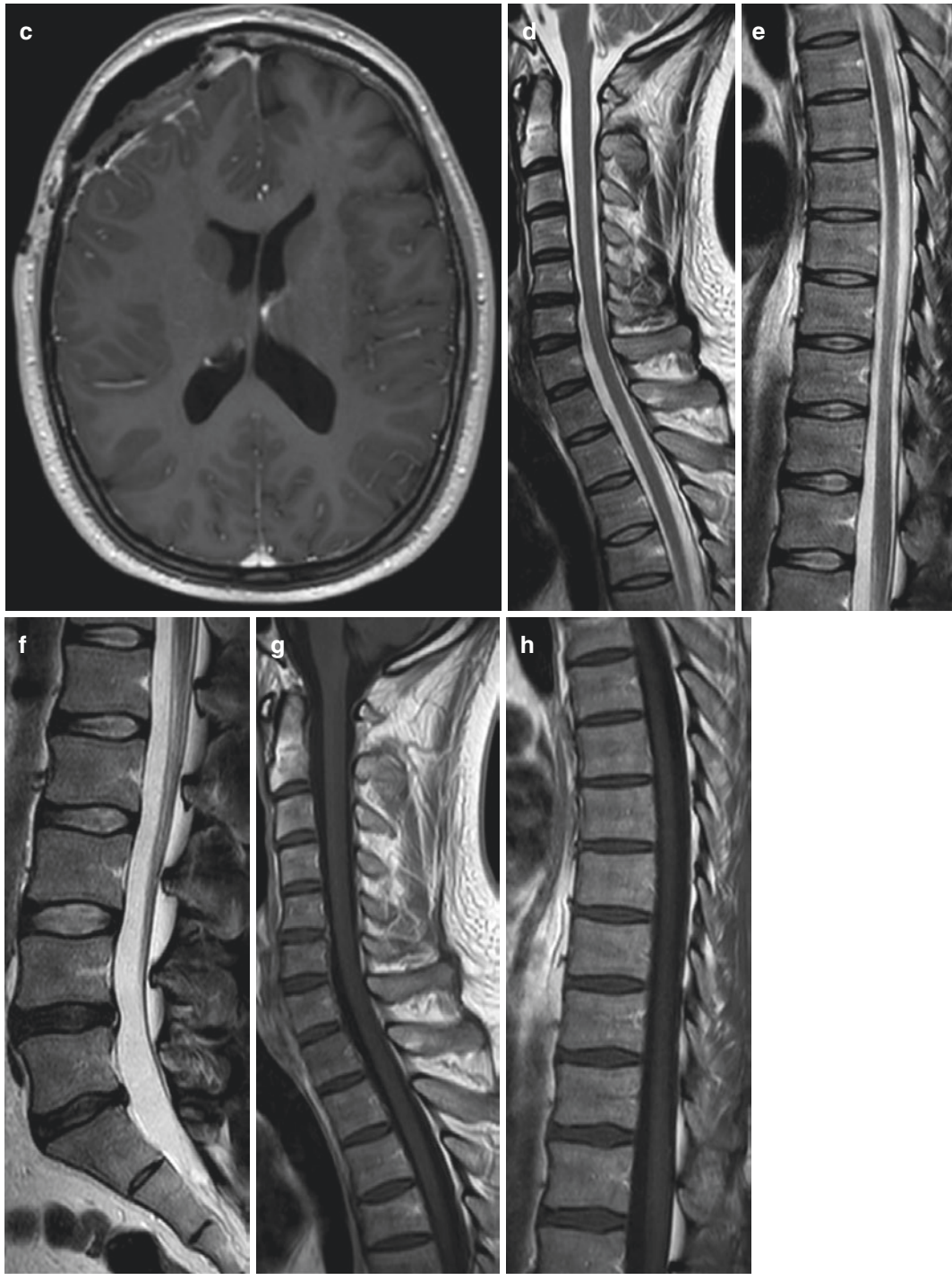

Fig. 26.3 (continued)

tumour location and may include headaches, nausea, ataxia, seizures, focal sensory or motor deficits and loss of hearing and vision in case of progressive dural involvement. Spinal PDL often presents with radicular pain and paraparesis [3].

Apart for meningioma, differential diagnoses include dural metastasis, gliosarcomas, leiomyosarcomas, haemangiopericytomas, plasmacytomas, solitary fibrous tumours, neurosarcoidosis and tuberculomas.

References

1. Brito ABC et al (2014) Intracranial primary dural diffuse large B-cell lymphoma successfully treated with chemotherapy. Int J Clin Exp Med 7(2):456–460
2. Iwamoto FM, Abrey LE (2006) Primary dural lymphomas: a review. Neurosurg Focus 21(5):E5
3. Said R et al (2011) Clinical challenges of primary diffuse large B-cell lymphoma of the dura: case report and literature review. ISRN Hematol:945212. https://doi.org/10.5402/2011/945212

Leptomeningeal Surprise

27

At the beginning of February 2017, a 59-year-old male patient was admitted to the EHD of our hospital due to ataxia, headache with nausea and vomiting, lasting for 7 days. He was not febrile; he did not have any other symptoms like abdominal pain, loss of weight or problems with swallowing. According to anamnestic data, he was taking medications for arterial hypertension. CT of the brain was performed at the admittance: radiologist who was on call reported small oval, mildly hyperdense lesion in the roof of the fourth ventricle surrounded with mild vasogenic oedema, possible expansile, neoplastic process (Fig. 27.1).

MRI of the brain was the next diagnostic procedure that was performed (Figs. 27.2 and 27.3).

MRI of the brain demonstrated T2 and FLAIR slightly hyperintense content diffusely distributed along the folia of both cerebellar hemispheres and vermis, showing nodular and linear contrast enhancement due to leptomeningeal spread of malignant cells or leptomeningeal carcinomatosis. Both vestibulocochlear and left trigeminal cranial nerves demonstrated contrast enhancement consisted with perineural spread of malignant cells.

Lumbar puncture and CSF analysis were recommended: CSF analysis confirmed malignant cells of epithelial origin. Laboratory data revealed slightly enlarged serum levels of urea, bilirubin and gamma-glutamyltransferase, as well as high levels of tumour markers, carcinoembryonic antigen, alpha-fetoprotein and cancer antigens 19-9 and 125.

CT of the chest and abdomen was performed revealing only several celiac lymph nodes measuring up to 10 mm: there were no metastasis in the lung parenchyma or liver and no enlarged mediastinal or hilar lymph nodes. There were no signs of oesophageal process on CT scans as well. Finally, esophagogastroduodenoscopy revealed small (10 mm) polypoid lesion above the oesophageal Z line involving one third of the oesophageal circumference: biopsy was performed, and oesophageal adenocarcinoma was confirmed.

Patient died 14 days after the admittance, before there was a chance to start with oncological treatment.

27.1 Leptomeningeal Carcinomatosis

Leptomeningeal carcinomatosis (LMC) is one of the most serious complications that can occur in cancer patients representing metastatic tumour cells involving leptomeninges and circulating CSF. It usually occurs in case of a breast or lung cancer and melanoma or in case of lymphoma and leukaemia [1]. It is very rare in case of gastrointestinal malignancy. Gastrointestinal solid tumours usually give metastasis in liver, lung, peritoneal cavity or abdominal lymph nodes.

M. Špero, H. Vavro, *Neuroradiology - Expect the Unexpected*,
https://doi.org/10.1007/978-3-319-73482-8_27

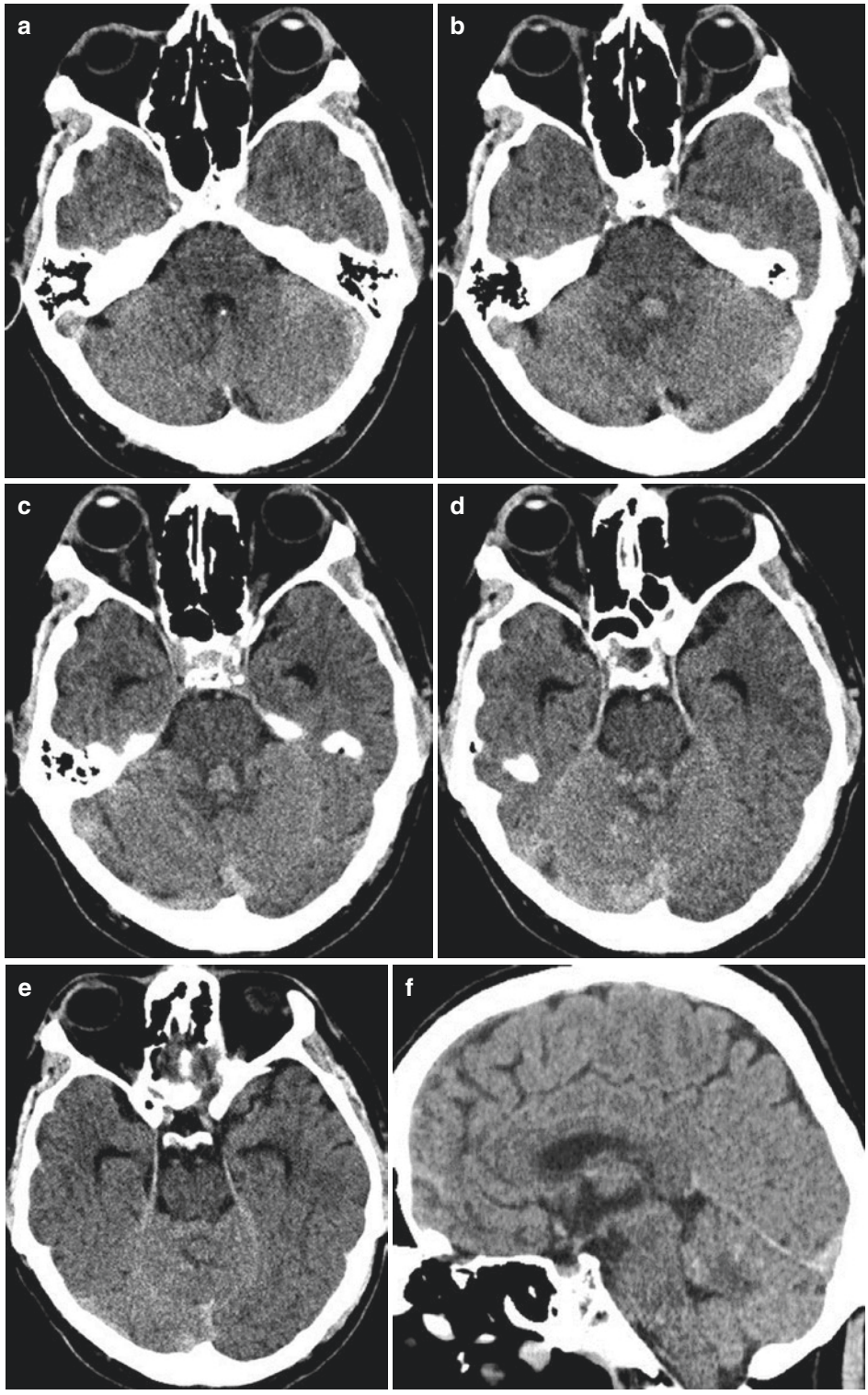

Fig. 27.1 Pre-contrast CT of the brain revealed oval, expansile slightly hyperdense lesion in the vermis, surrounded with mild vasogenic oedema (**a**–**c**). If you look closely, there was also slightly hyperdense content in the folia of the right cerebellar hemisphere (**d**–**f**)

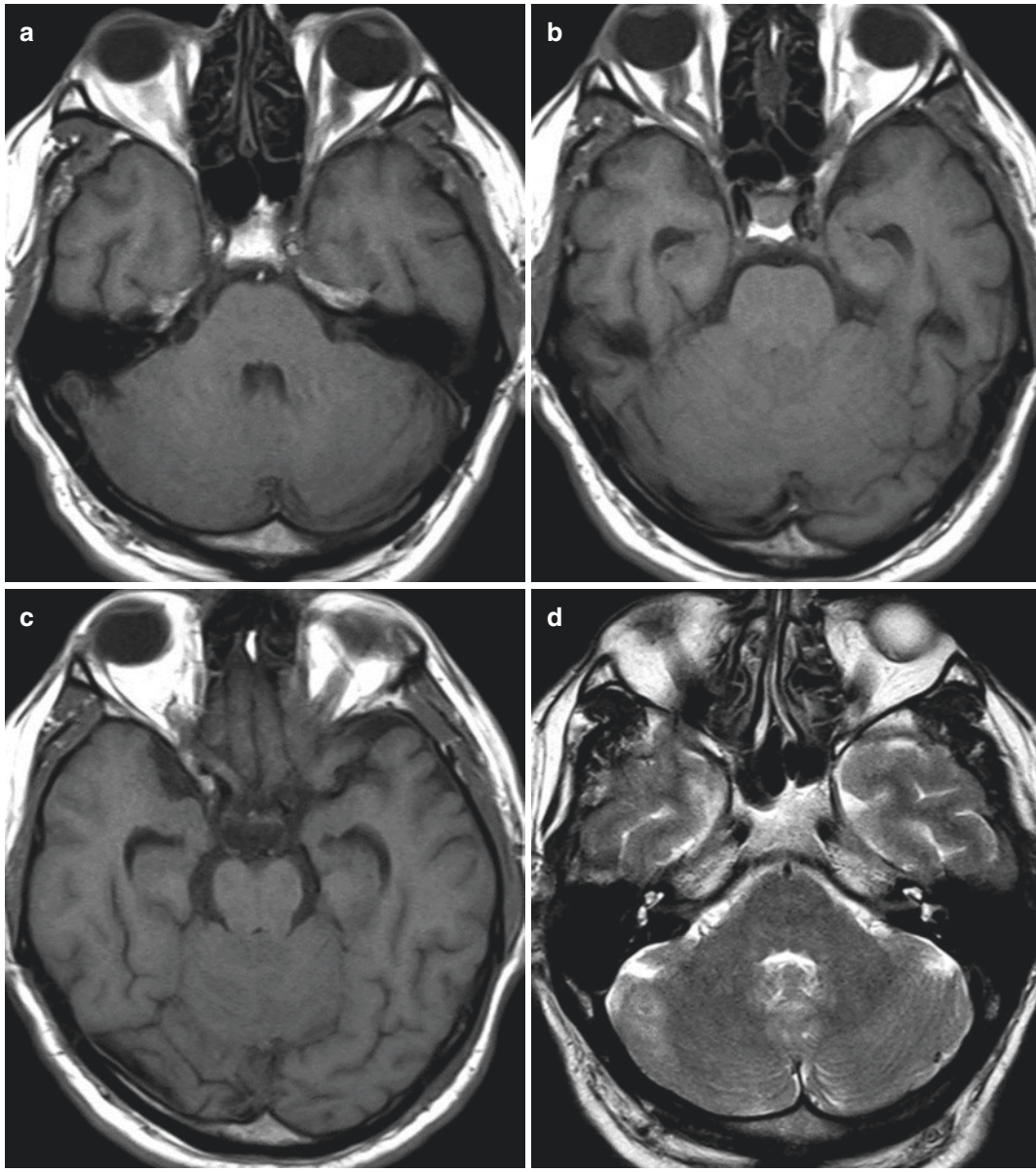

Fig. 27.2 Non-contrast MRI of the brain, axial T1WI (**a**–**c**), axial T2WI (**d**–**f**) and axial FLAIR (**g**–**i**), revealed slightly hyperintense content on T2WI and FLAIR in the folia of both cerebellar hemispheres and vermis that was hypointense on T1WI. Both vestibulocochlear nerves were hypointense on T2 and FLAIR sequences, slightly enlarged. CSF flow was not obstructed

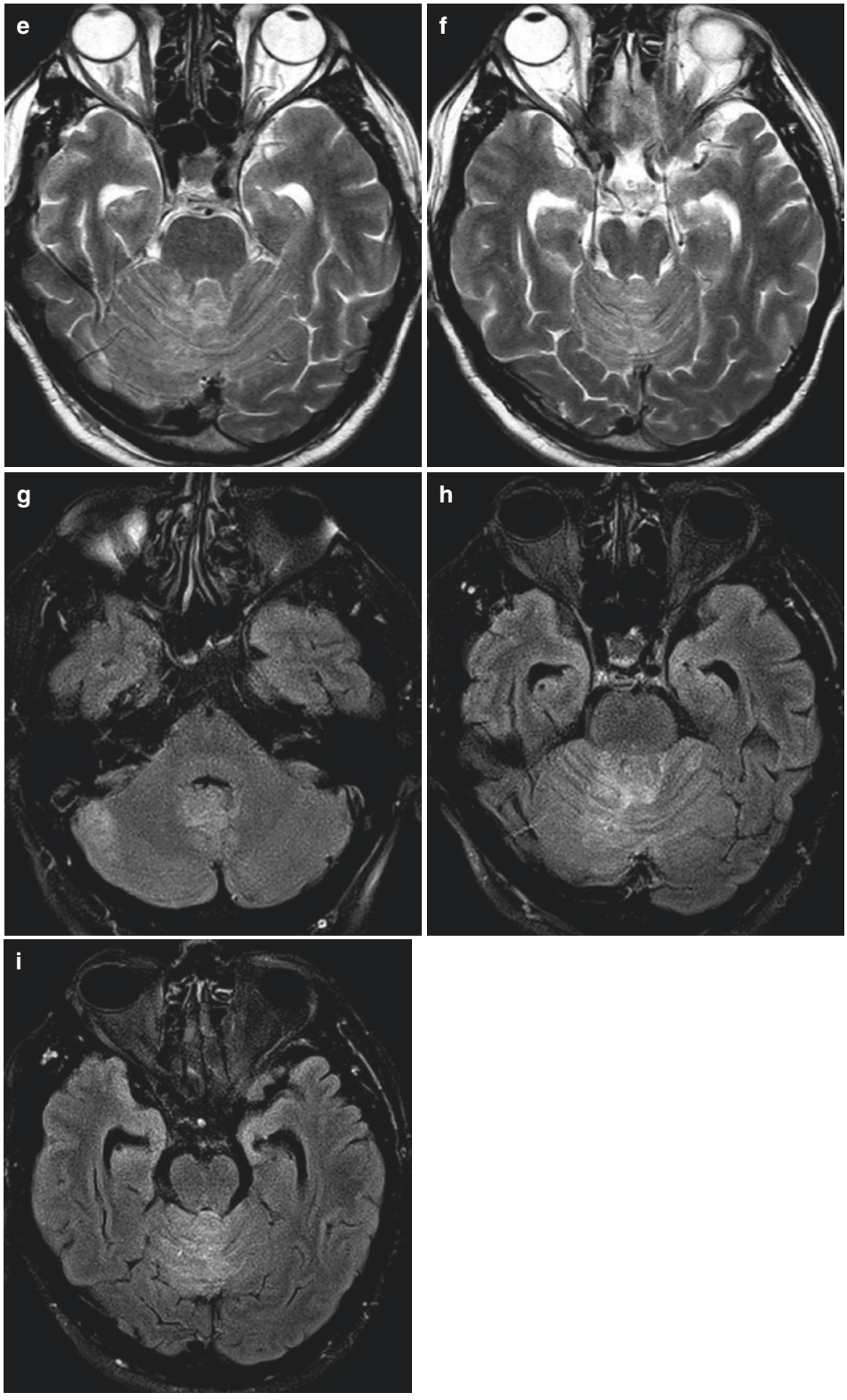

Fig. 27.2 (continued)

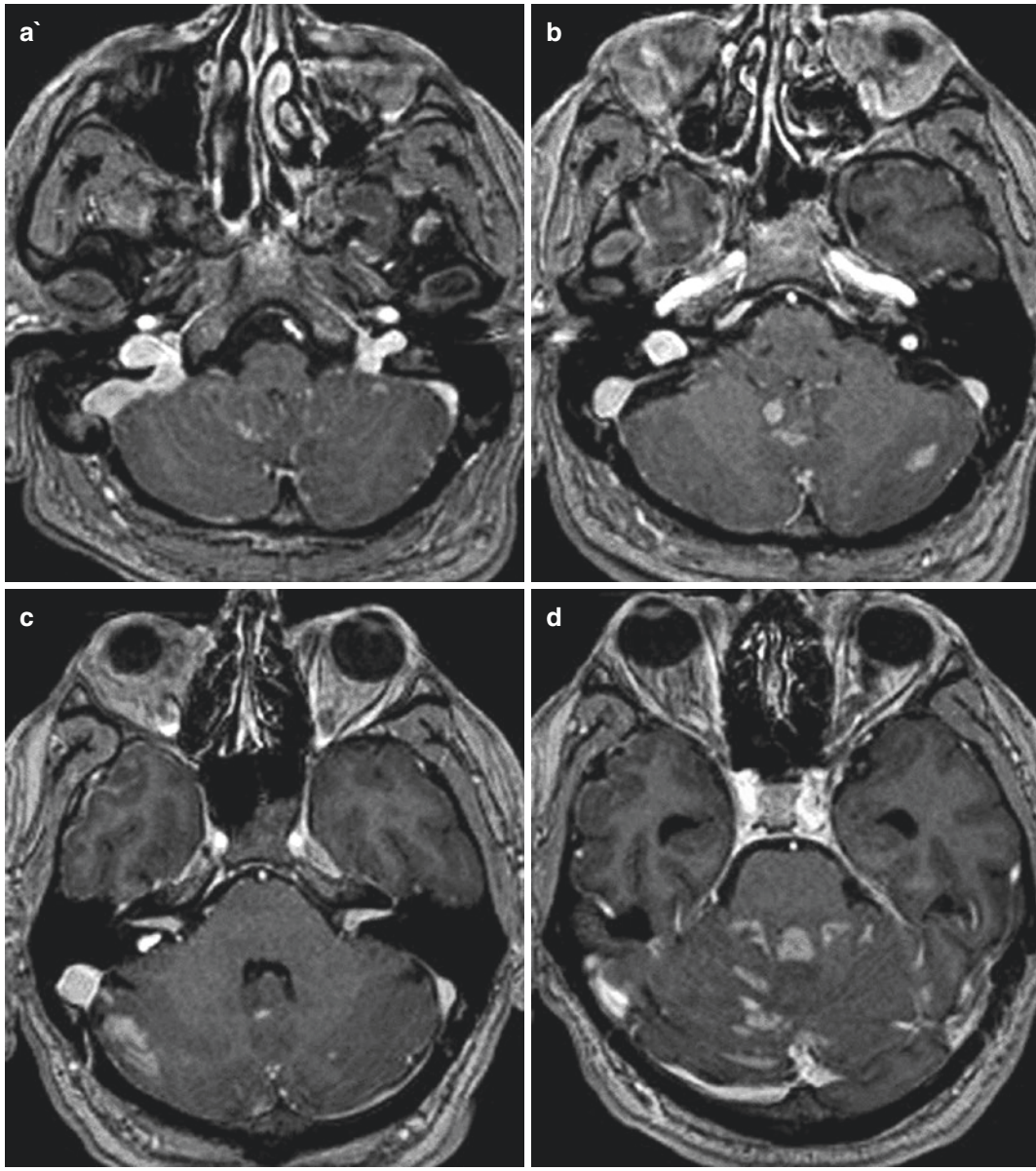

Fig. 27.3 Post-contrast MRI of the brain, axial (**a**–**f**), sagittal (**g**–**i**) and coronal (**j**–**l**) T1WI, demonstrated linear and nodular contrast enhancement of the content distributed diffusely along the folia of both cerebellar hemispheres and vermis, protruding towards the roof of the forth ventricle. Both vestibulocochlear nerves were enhanced; left fifth cranial nerve was not enlarged but mildly enhanced

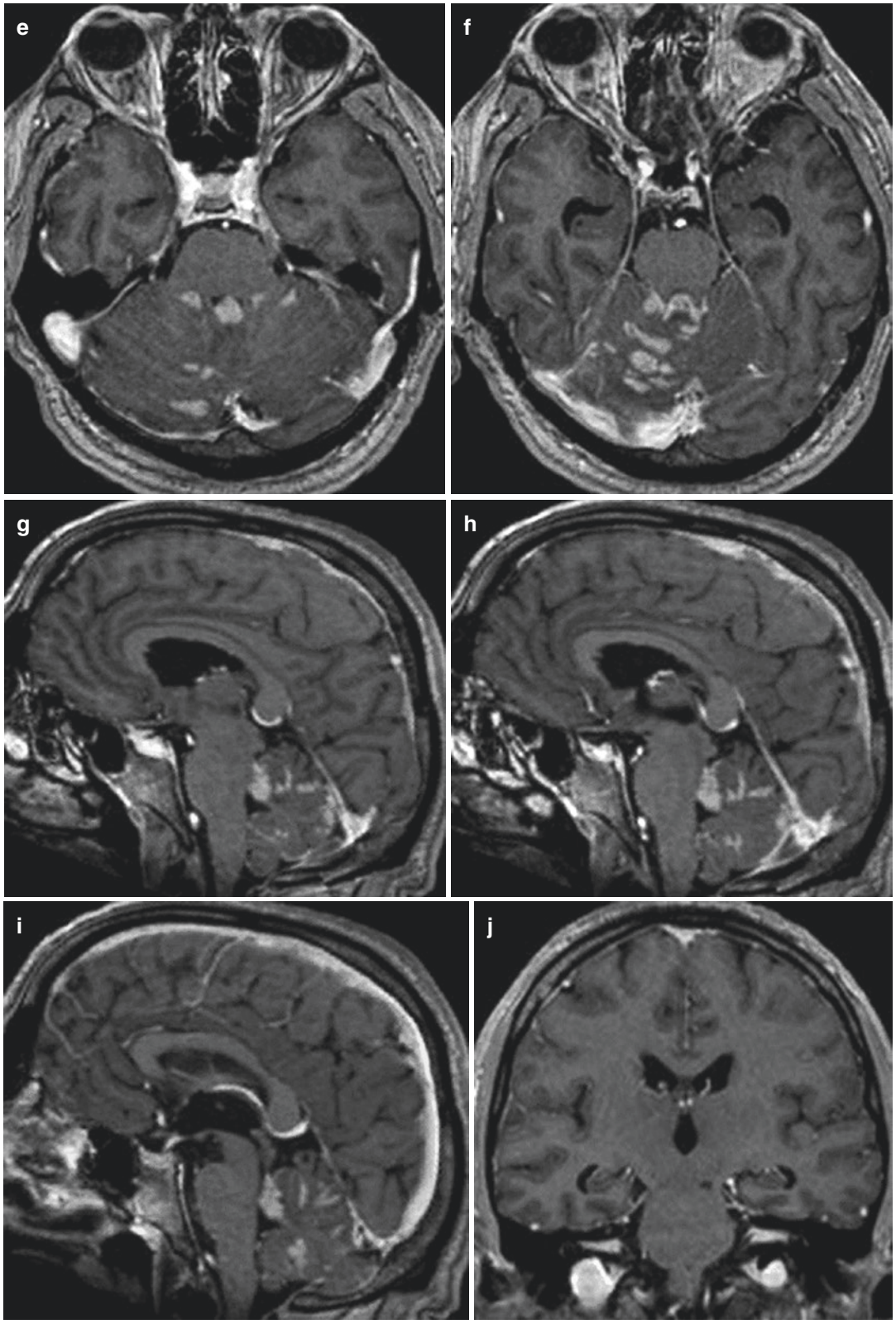

Fig. 27.3 (continued)

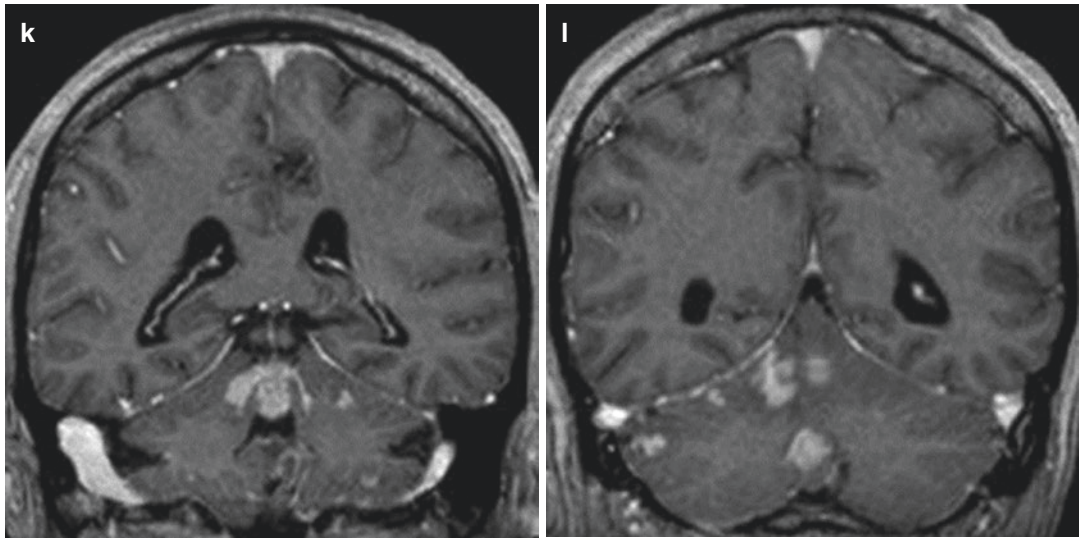

Fig. 27.3 (continued)

CNS metastasis of solid gastrointestinal tumours is usually in a form of parenchymal metastasis, sometimes dural metastasis, but leptomeningeal involvement is extremely rare.

Leptomeningeal carcinomatosis is very rare in oesophageal cancer. Cancer cells may invade the meninges through different pathways including haematogenous spread and endoneural or perineural spread and through perivascular lymphatic routes, or it may be a case of a direct spread from the CNS. The most common presenting features of leptomeningeal metastasis are headache, changes in mental status, cranial nerve palsies and neck stiffness [2].

The diagnosis of LMC is a combination of cytological examination and neuroimaging methods, CT and MRI [3].

It is not easy to detect LMC on non-contrast brain CT: if it is not suspected and contrast media applied, it could be misdiagnosed.

FLAIR imaging has been known to be sensitive for parenchymal lesions but also have shown sensitivity for leptomeningeal processes [4]. Hyperintense signal in sulci, folia or cisternal spaces on FLAIR images should warn radiologist of possible pathological content, like blood, pus in infectious inflammation, granulomatous inflammation due to a systemic disease or malignant cells in case of a malignant process. In case of a haemorrhage, signal intensity of blood on other standard sequences depends on the age of haemoglobin degradation products, but CT is usually helpful, as well as clinical presentation. In case of granulomatous or infectious inflammation, patient data, clinical presentation, laboratory data and CSF analysis help us in decision-making. When primary malignant process is known, it is not a problem to make a diagnosis. When it is unknown, neuroradiologist should recommend further workup, possibly in right direction regarding expected malignancies as well as unexpected one like oesophageal or gastric tumour.

LMC gives linear and/or nodular pattern of leptomeningeal contrast enhancement. Contrast-enhanced T1W imaging is the most sensitive single sequence for depicting leptomeningeal metastases. Therefore, FLAIR imaging gives us information of a leptomeningeal content, while contrast-enhanced T1W imaging confirms LMC.

If you have a patient without signs of haemorrhage or infectious inflammatory disease, systemic disease is unknown, as well as primary malignant process, think about a possible metastatic leptomeningeal involvement from an unknown oesophageal or gastric malignancy. Therefore, recommend further diagnostic workup of gastrointestinal tract. In recent times, there

are more and more reports of LMC due to oesophageal carcinoma spread, maybe because now those patients live longer than before and have a time to develop LMC.

Despite oncological treatment like intrathecal chemotherapy or radiation therapy, survival of patients with LMC due to oesophageal carcinoma is poor: median survival is 3–6 months [3, 5].

References

1. Oh SY et al (2009) Gastric leptomeningeal carcinomatosis: multi-center retrospective analysis of 54 cases. World J Gastroenterol 15(40):5086–5090
2. Akhavan A, Navabii H (2012) Leptomeningeal metastasis from squamous cell carcinoma of oesophagus with unusual presentation. BMJ Case Rep 2012:bcr0220125846
3. Aulakh AS et al (2012) Leptomeningeal carcinomatosis in esophageal cancer: case report and review of literature. J Gastrointest Cancer 43(Suppl 1):S84–S88
4. Singh SK et al (2002) MR imaging of leptomeningeal metastases: comparison of three sequences. AJNR Am J Neuroradiol 23:817–821
5. Dam T et al (2013) Meningeal carcinomatosis: a metastasis from gastroesophageal junction adenocarcinoma. Case Rep Med 2013:245654, 4 pages. https://doi.org/10.1155/2013/245654